Universidade do Minho
Escola de Engenharia

Maria Margarida Fernandes Machado

A multibody approach to the contact dynamics: a knee joint application

Tese de Doutoramento
Doutoramento em Engenharia Biomédica

Trabalho realizado sob a orientação do
Professor Doutor João Paulo Flores Fernandes
Co-orientadores:
Professor Doutor Jorge Alberto Cadete Ambrósio
Professor Doutor António Manuel Godinho Completo

dezembro de 2012

Universidade do Minho, ____/____/_____

Assinatura:_____

Agradecimentos/Acknowledgments

Muitos foram os que cientificamente e/ou emocionalmente contribuíram para a realização desta tese e concretização deste desafio. É, por isso, com uma enorme satisfação que aqui expresso os meus sinceros agradecimentos a essas pessoas.

Ao Professor Paulo Flores, Professor Associado com Agregação na Universidade do Minho e meu orientador científico, quero agradecer a motivação, orientação e incansável apoio. Agradeço ainda a confiança que sempre depositou no meu trabalho e o rigor que sempre me exigiu. Mas, acima de tudo, agradeço a amizade sempre demonstrada e que, da minha parte, ficará para sempre. Foi para mim um prazer e honra trabalhar com um professor com as qualidades científicas e humanas do Professor Paulo Flores.

Ao Professor Jorge Ambrósio, Professor Catedrático na Universidade Técnica de Lisboa e meu co-orientador científico, quero expressar a minha gratidão pela coordenação e disponibilidade. Saliento ainda, o entusiasmo presente em todas as reuniões que constituiu um incentivo para meu trabalho. A co-orientação do Professor Jorge Ambrósio foi para mim uma grande responsabilidade e prestígio face às suas reconhecidas competências científicas. Para o futuro, ficará sempre o apreço e uma amizade verdadeira.

Ao Professor António Completo, Professor Auxiliar na Universidade de Aveiro e meu co-orientador científico, quero agradecer a coordenação e o alento que me concedeu durante o doutoramento. Agradeço ainda o apoio e a simpatia que sempre senti receber. Pelo conhecimento e experiência que me transmitiu, ficará sempre a admiração e o respeito.

Ao Professor Miguel Silva e aos investigadores João Pombo e Daniel Lopes da Universidade Técnica de Lisboa, expresso a minha gratidão pela disponibilidade, pelo conhecimento e partilha de ideias determinantes para a execução deste projecto. Agradeço também a amabilidade e as calorosas palavras de apoio que sempre me transmitiram. Ao Daniel, meu colega e companheiro de jornada, quero ainda agradecer a forte amizade e o espírito de entreajuda que sempre me concedeu durante todo o doutoramento.

À Fundação para a Ciência e Tecnologia (FCT), quero agradecer a concessão da Bolsa de Doutoramento SFRH/BD/40164/2007. Expresso também a minha gratidão pelo financiamento dos projetos ProPaFe (PTDC/EMEPME/ 67687/2006), DACHOR (MIT-Pt/BSHHMS/0042/ 2008) e BIOJOINTS (PTDC/EME-PME/099764/2008).

À Fundação Luso-Americana para o Desenvolvimento (FLAD), quero agradecer o financiamento de uma Bolsa de Mobilidade (Bolsa Papers Proj. 181/2011).

To all editors and authors that provided me a free permission to use their images in my thesis, I want to express my gratitude for this courtesy. Special thanks to University of Washington for the Musculoskeletal images published in "Musculoskeletal Atlas: A Musculoskeletal Atlas of the Human Body" by Carol Teitz and Dan Graney.

During my PhD, I visited the Computational Biomechanics Lab at University of Florida in Gainesville (FL) for a period of six months. I want to express my gratitude to my advisor there, Professor Benjamin Fregly, for his guidance, help and kindness. I would like to thank also my labmates for their friendship and support, namely Laura, Jonathan, Andrew, Jenifer, Ilan and Weston. Finally, I thank to Dr. Fregly's family (his wife Shirley and their kids Christopher and Rachel), Laura's family (her husband Stanley and their daughter Joana), Noel, Donna, Nance and all my friends at Creekside Community Church for taking good care of myself during my stay in Gainesville and making me feel at home.

To Professors Hamid Lankarani, Ayman Habib, Javier Cuadrado, Daniel Dopico and Josep M. Font Llagunes, I want to thank their assistance in the development of this work.

Ao Pedro Moreira e à Sara Tribuzi, quero agradecer as frutuosas trocas de ideias que contribuíram significativamente para o êxito deste trabalho. Agradeço ainda a todos os meus colegas da sala de investigadores, pelo apoio e boa-disposição diária que foram de grande alento nesta caminhada. Mas, acima de tudo, agradeço a forte amizade que nos une.

Estes agradecimentos não estariam completos sem dedicar uma palavra de carinho muito especial a toda a minha família e amigos. Em particular quero agradecer aos meus pais, à Mafalda, ao Zé e ao Simão pelo afeto, paciência e aconchego.

Porque tudo a Ele devo, agradeço por fim, a Deus.

Abstract

Title: A multibody approach to the contact dynamics: a knee joint application.

In this thesis, a general approach for dynamic analysis of multibody systems with contact is presented, being a special attention given to the articular contact at the human knee joint. Two methodologies, in two- and three-dimensions, for knee contact modeling are proposed under the framework of multibody systems using generalized Cartesian coordinates. The development of the planar multibody knee model encompasses four steps: (*i*) geometrical representation of contacting profiles by means of curve fitting techniques based on spline interpolation functions; (*ii*) location of contact points and evaluation of the contact indentation; (*iii*) calculation of the contact forces by using an appropriate constitutive law; (*iv*) description of the ligament behavior by a quadratic stress-strain relation. The motion of the tibia relative to the femur is modeled combining the action of the knee ligaments with the potential contacts between the bones. The contact forces, together with the forces produced by the ligaments, are introduced into the Newton-Euler equations of motion as external generalized forces. Within the three-dimensional methodology, the contact surfaces are described by means of point-clouds extracted from parametric representations. The spatial formulation presents a pre-processing unit. This preprocessor allows for a significantly reduction of the amount of memory required for data storage and an improvement of the computational efficiency of the contact detection process. Computational simulations were performed with the aim of validating both proposed approaches, two-dimensional and three-dimensional. The behavior of the planar knee model resultant of the application of different contact force laws was studied. Moreover, the influence of the geometric and material properties on the dynamic response of the knee joint model was investigated. In a broad sense, the proposed methodologies demonstrated to be suitable for the analysis of the dynamic behavior of multibody models

with contact, especially those biological systems such as the knee joint that involve complex geometries, a large range of motion and high dynamic loads.

Keywords: Biomechanics
Multibody dynamics
Contact detection
Contact force laws
Knee joint modeling
Computational efficiency

Resumo

Título: Uma abordagem baseada em sistemas de corpos múltiplos para a análise dinâmica de problemas de contacto: uma aplicação à articulação do joelho.

Nesta tese é proposta uma abordagem genérica para a análise dinâmica de sistemas de corpos múltiplos com contacto, dando um especial enfoque ao contacto articular no joelho humano. No âmbito da dinâmica de sistemas de corpos múltiplos são apresentadas duas metodologias, bidimensional e tridimensional, para a modelação do contacto no joelho usando coordenadas cartesianas generalizadas. O desenvolvimento do modelo bidimensional do joelho engloba quatro etapas: (*i*) representação geométrica dos perfis de contacto por meio de técnicas de ajuste de curva com base em funções de interpolação por splines, (*ii*) localização dos pontos de contacto e avaliação da indentação de contacto, (*iii*) cálculo das forças de contacto usando uma lei constitutiva apropriada, (*iv*) descrição do comportamento dos ligamentos através de uma relação quadrática de tensão-deformação. O movimento da tíbia em relação ao fémur é modelado como uma acção combinada entre os ligamentos do joelho e os potenciais contactos entre os ossos. As forças de contacto, juntamente com as forças produzidas pelos ligamentos, são introduzidas nas equações de movimento de Newton-Euler como forças externas generalizadas. Na metodologia tridimensional, as superfícies de contacto são descritas por meio de nuvens de pontos extraídas de representações paramétricas. No âmbito da formulação tridimensional é apresentada uma unidade de pré-processamento. Este pré-processador permite uma redução significativa da quantidade de memória necessária para o armazenamento de dados e, desta forma, melhora a eficiência computacional do algoritmo de deteção de contacto. Com o objetivo de validar as metodologias propostas, realizaram-se várias simulações computacionais. Os comportamentos do modelo bidimensional do joelho resultantes da aplicação de diferentes leis de força de contacto foram estudados. A influência das

propriedades geométricas e de material na resposta dinâmica do modelo bidimensional do joelho foi investigada. De uma forma geral, as metodologias propostas demonstraram ser adequadas para a análise do comportamento dinâmico de modelos de corpos múltiplos com contacto, especialmente sistema biológicos, como o joelho humano, que envolvem geometrias complexas, uma grande amplitude de movimentos e elevadas cargas dinâmicas.

Palavras-chave: Biomecânica
Dinâmica de corpos múltiplos
Detecção de contacto
Leis de força de contacto
Modelação da articulação do joelho
Eficiência computacional

Table of contents

Agradecimentos/Acknowledgments iii

Abstract v

Resumo vii

Table of contents ix

List of tables xiii

List of figures xvi

Nomenclature xxx

Latin symbols xxx

Greek symbols xxxiv

Subscripts xxxv

Superscripts xxxvi

Operators xxxvi

Abbreviations xxxvii

Software xl

CHAPTER 1 – Introduction **1**-1

1.1 Motivation **1**-2

1.2 Literature Review **1**-4

1.3 Scope and objectives **1**-44

1.4 Structure of the thesis **1**-45

1.5 Contributions of this work **1**-46

References **1**-48

CHAPTER 2 – Human knee joint: anatomy and function **2**-1

2.1 Basic terminology for human movement **2**-2

2.2 Structural anatomy **2**-4

2.3 Principal movements and its characteristics **2**-13

2.4 Mechanical response of knee surrounding tissues **2**-19

2.4.1. Bone: ultrastructure and mechanical behavior **2**-19

2.4.2. Cartilage and Menisci: ultrastructure and mechanical behavior **2**-20

2.4.3. Tendons and Ligaments: ultrastructure and mechanical behavior **2**-23

2.4.4. Muscles: ultrastructure and mechanical behavior **2**-25

2.5 Joint pathologies and replacement systems **2**-31

2.5.1. Overview of primary knee injuries **2**-31

2.5.2. Knee replacement systems: materials and design **2**-33

2.6 Summary and discussion **2**-35

References **2**-38

CHAPTER 3 – Multibody dynamics methodology for biomechanical modeling **3**-1

3.1 Multibody system concept and applications **3**-2

3.2 Types of coordinates and kinematic constraints **3**-5

3.3 Equations of motions for constrained systems **3**-18

3.4 Numerical solution of the equations of motion **3**-24

3.5 Demonstrative example of application **3**-31

3.6 Summary and discussion **3**-35

References **3**-36

CHAPTER 4 – Contact modeling and analysis **4**-1

4.1 Methods to deal with contact problems **4**-2

4.2 Geometric detection of contact **4**-5
4.2.1. Geometric representation **4**-6
4.2.2. Proximity queries **4**-8
4.2.3. Environmental simulation parameters **4**-9
4.3 Elastic contact force models **4**-13
4.4 Dissipative contact force models **4**-19
4.5 Demonstrative example of application **4**-28
4.6 Summary and discussion **4**-31
References **4**-32

CHAPTER 5 – A two-dimensional multibody model of the human knee joint **5**-1
5.1 Multibody knee model **5**-2
5.1.1. Geometric description **5**-4
5.1.2. Contact modeling formulation **5**-6
5.1.3. Physical models for ligaments and cartilage **5**-11
5.2 Global dynamic results **5**-14
5.3 Influence of the geometric conformality **5**-16
5.4 Influence of the constitutive contact force law **5**-21
5.5 Influence of the contact material properties **5**-23
5.6 Influence of the amplitude of the external applied force **5**-29
5.7 Summary and discussion **5**-33
References **5**-36

CHAPTER 6 – A three-dimensional multibody model of the human knee joint **6**-1
6.1 Fundamentals of spatial multibody modeling **6**-2
6.2 Geometric modeling of contacting surfaces **6**-5
6.2.1. Surface generation and representation **6**-7
6.2.2. Knee contact geometries **6**-12

6.3 Methodology for contact detection **6**-14
6.4 Computational algorithm for contact in multibody dynamics **6**-22
6.5 Dynamic simulations of 3D-contact problems **6**-23
6.5.1. Bouncing ball demonstration example **6**-24
6.5.2. Human knee model demonstration example **6**-28
6.6 Summary and discussion **6**-32
References **6**-34

CHAPTER 7 – Knee joint modeling using OpenSim software **7**-1
7.1 Overview of OpenSim software **7**-2
7.2 Development of a skeletal model of the knee joint **7**-3
7.3 Inverse kinematic analysis **7**-5
7.4 Muscle modeling **7**-7
7.5 Contact forces modeling and analysis **7**-11
7.5.1. Prediction of knee joint contact forces by inverse dynamics **7**-12
7.5.2. Study on the accuracy of OpenSim contact models **7**-15
7.6 Summary and discussion **7**-20
References **7**-22

CHAPTER 8 – Concluding remarks **8**-1
8.1 Conclusions **8**-1
8.2 Suggestions for future developments **8**-5

List of tables

CHAPTER 1

Table 1.1 Survey of knee joint models. Symbols appearing in this table are: P (planar), S (spatial), K (kinematic), QS (quasi-static), D (dynamic), O (optimization), MBS (multibody system), FEM (finite element method), E (experimental), H (hybrid), LL (lower-limb), NK (natural knee), AK (artificial knee), TF (tibiofemoral) and PF (patellofemoral). **1**-39

CHAPTER 2

Table 2.1 Muscles acting on the knee (Whittle, 2007). The meaning of the abbreviations is as follows: anterior (ant), posterior (post), superior (sup), inferior (inf), medial (med) and lateral (lat)..... **2**-10

Table 2.2 Range of tibiofemoral joint motion in the sagittal plane during common activities (Nordin and Frankel, 2001) **2**-16

CHAPTER 3

Table 3.1 Anthropometric data for each anatomical segment of the biomechanical human model..... **3**-33

CHAPTER 4

Table 4.1 Five proximity queries (Gottschalk, 2000) **4**-9

Table 4.2 Software packages for collision detection and proximity query..... **4**-12

Table 4.3 Geometric and inertial properties of the slider-crank mechanism and the free sliding block..... **4**-28

CHAPTER 5

Table 5.1 Absolute coordinates and inertia properties of the femur and tibia bodies.... ..... **5**-2

Table 5.2 Local coordinates of the insertion points and physical properties of the ligaments **5**-13

Table 5.3 Femur (R_i) and tibia (R_j) radii as well as the generalized stiffness parameter (K) used in each contact scenario, namely convex-convex spheres, convex-concave spheres and convex sphere-plane (Martelli *et al.*, 2006; Koo and Andriacchi, 2007) **5**-18

Table 5.4 Some contact force laws and its correspondent mathematical expressions..... ..... **5**-21

Table 5.5 Mechanical properties of the contact materials (Dickenson *et al.*, 1981; Piazza and Delp, 2001; Kurtz, 2004; Herman, 2007; Burgin and Aspen, 2008; Heijink *et al.*, 2008) **5**-24

CHAPTER 6

Table 6.1 Comparison between the geometrical properties of implicit and parametric surface functions (Campbell and Flynn, 2001)..... **6**-6

Table 6.2 Lookup table of the surface represented in Figure 6.4, which contains geometric data relative to the 3D-point sample extracted from the surface, namely parametric coordinates (u, v), Cartesian coordinates (x, y, z), Cartesian components of normal vector (n_x, n_y, n_z), Cartesian components of tangent vector (t_x, t_y, t_z), Cartesian components of binormal vector (b_x, b_y, b_z). This lookup table is presented in its sequential access form and the listed points are the ones bordered by a square in Figure 6.4..... **6**-11

Table 6.3 Dimensions of the storage windows and respective t_{CPU}^{w} and $\mathrm{ratio}_{\mathrm{CPU}}$ **6**-27

Table 6.4 Global coordinates and inertia properties of the femur and tibia bodies .. **6**-29

Table 6.5 Local attachment coordinates, strain at full extension and stiffness of the knee ligaments **6**-30

CHAPTER 7

Table 7.1 List of markers placed at the right knee for the leg extension trial..... **7**-5

Table 7.2 Analytical solution of the bouncing ball problem. This table includes the values of following variables: the ball energy at the initial instant of simulation (T^0), the first instant of contact for the first impact (t^-) and the relative indentation of the first instant of contact for the first impact (δ^-)..... ..... **7**-17

Table 7.3 Ball contact response obtained by using different contact models, namely Hertz law within MUBODYNA, Hunt and Crossley model within OpenSim and Elastic foundation model within OpenSim. This table includes the values of following variables: the first instant of contact for the first impact (t^-); the relative indentation of the first contact of the first impact (δ^-); the normal contact force of the first contact of the first impact (F^-); the instant of maximum indentation for the first impact (t_{max}); the maximum indentation for the first impact (δ_{max}); the maximum contact force for the first impact (F_{max}); the ball energy at instant of maximum indentation for the first impact (U^{max})..... **7**-18

Table 7.4 First instant of contact (t^-) of the seven impacts of the bouncing ball and impact duration (Δt_{impact}) using different contact models, namely Hertz law within MUBODYNA, Hunt and Crossley model within OpenSim and Elastic foundation model within OpenSim..... **7**-20

List of figures

CHAPTER 1

Figure 1.1 Schematic representation of the knee joint as a four-bar linkage, showing posterior displacement of the point of tibiofemoral contact point with flexion {Adapted from Smith *et al.* (2003) with Elsevier permission} **1**-5

Figure 1.2 Mechanical guidance of log-spiral and rack motion proposed by Freudenstein and Woo (1969) for modeling the knee joint {Adapted from Freudenstein and Woo (1969) with Springer permission} **1**-5

Figure 1.3 Forces and moment arms for knee flexion and extension considered in the analysis performed by Smidt (1973) {Adapted from Smidt (1973) with Elsevier permission} **1**-6

Figure 1.4 Position of ligaments adopted by Crowninshield *et al.* (1976): (a) Medial view; (b) Posterior view; (c) Lateral view. Twelve ligament fibers are represented in this scheme, namely deep (dMCL), oblique (oMCL), anterior (aMCL) and posterior fibers (pMCL) of the medial collateral ligament; medial (mPCL), lateral (lPCL), oblique (oPCL), anterior (aPCL) and posterior fibers (pPCL) of the posterior cruciate ligament; anterior (aACL) and posterior fibers (pACL) of the anterior cruciate ligament; lateral collateral ligament (LCL) {Adapted by Crowninshield *et al.* (1976) with Elsevier permission} **1**-7

Figure 1.5 Medial and lateral articular surfaces of the 3D-model of the knee joint proposed by Wismans *et al.* (1980) {Adapted from Wismans *et al.* (1980) with Elsevier permission} **1**-8

Figure 1.6 Schematic representation of the 2D-model of the knee joint developed by Moeinzadeh {Adapted from Moeinzadeh (1981) with author's permission} **1**-9

Figure 1.7 3D-model of the patellofemoral joint proposed by Van Eijden *et al.* (1986) {Adapted from van Eijden *et al.* (1986) with Elsevier permission} **1**-11

Figure 1.8 Knee joint model based on two four-bar linkages presented by Chittajallu and Kohrt (1996) {Adapted from Chittajallu and Kohrt (1996) with Elsevier permission} **1**-13

Figure 1.9 Knee joint model based on a four-bar linkage proposed by Farhat *et al.* (2010) {Adapted from Farhat *et al.* (2010) with Taylor & Francis permission} **1**-13

Figure 1.10 3D-model of the knee joint proposed by Abdel-Rahman and Hefzy (1998), showing the articular surfaces and 12 ligaments: (a) Anterior view; (b) Posterior view. The represented ligaments are: (1) anterior fibers of ACL, (2) posterior fibers of ACL, (3) anterior fibers of PCL, (4) posterior fibers of PCL, (5) anterior fibers of MCL, (6) oblique fibers of MCL, (7) deep fibers of MCL, (8) LCL, (9) medial fibers of posterior capsule, (10) lateral fibers of posterior capsule, (11) oblique popliteal ligament and (12) arcuate popliteal ligament {Adapted from Abdel-Rahman and Hefzy (1998) with Elsevier permission} **1**-15

Figure 1.11 Knee model proposed by Blankevoort *et al.* (1991). The coordinate axis (x_1, x_2, x_3) is associated with the tibia and is space-fixed, while the coordinate axis (x'_1, x'_2, x'_3) is related to the femur and is body-fixed. A material point P' is described by the vector **p**, relative to the space-fixed system, and by the vector **R**.**p'**, relative to body-frame. The vector **a** describes the translation of the body-fixed origin relative to the space-fixed origin {Adapted from Blankevoort *et al.* (1991) with Elsevier permission} **1**-16

Figure 1.12 Representation of the 3D-model of the knee joint proposed by Mommersteeg *et al.* (1995) {Adapted from Mommersteeg *et al.* (1995) with Elsevier permission} **1**-17

Figure 1.13 Patellofemoral joint model proposed by Hirokawa (1991): (a) Sagittal view at 90 degrees of knee flexion; (b) Close-up of the tendofemoral contact portion {Adapted from Hirokawa (1991) with Elsevier permission}..... **1**-17

Figure 1.14 Anterior view of the theoretical model of the right knee proposed by Loch *et al.* (1992) {Adapted from Loch *et al.* (1992) with Elsevier permission} **1**-18

Figure 1.15 Patellofemoral forces considered by Hefzy and Yang (1993): quadriceps tendon force (F_{Qt}), patellar ligament force (F_{Pl}), patellofemoral contact forces at the medial (F_{med}) and lateral (F_{lat}) side of the knee {Adapted from Hefzy and Yang (1993) with Elsevier permission} **1**-18

Figure 1.16 FE-mesh of 8-node solid elements proposed by Bendjaballah *et al.* (1995) for knee cartilage layers and menisci {Adapted from Bendjaballah *et al.* (1995) with Elsevier permission} **1**-19

Figure 1.17 Patellofemoral 3D-model proposed by Heegard *et al.* (1995) and its corresponding FE-mesh {Adapted from Heegard *et al.* (1995) with Elsevier permission} **1**-20

Figure 1.18 Knee joint model proposed by Gill and O'Connor (1996). The normal direction of the patellofemoral contact force (F_{Pf}) is depicted for 10, 90 and 140 degrees of knee flexion {Adapted from Gill and O'Connor (1996) with Elsevier permission} **1**-20

Figure 1.19 Frontal view of the parallel spatial mechanism model of the knee joint proposed by Wilson *et al.* (1998) {Adapted from Wilson *et al.* (1998) with Elsevier permission} **1**-21

Figure 1.20 The elastic foundation model used by Pandy *et al.* (1997) to calculate the pressure distributions at the tibiofemoral joint. The transverse section of the deformed elastic layer is assumed to be an ellipse. The pressure at any point within the contact area depends on the normal displacement (u_z). The stiffness of the contact layer is denoted as *h*. The profile of the pressure distribution is assumed to be paraboloidal {Adapted from Pandy *et al.* (1997) with Taylor & Francis permission} **1**-22

Figure 1.21 Schematic representation of the musculoskeletal knee model proposed by Shelburne and Pandy (1997) {Adapted from Shelburne and Pandy (1997) with Elsevier permission} **1**-23

Figure 1.22 Representation of the knee articular surfaces proposed by Kim (1998): (a) Tibiofemoral joint; (b) Patellofemoral joint {Adapted from Kim (1998) with Springer permission} **1**-24

Figure 1.23 Sagittal view of artificial knee model of Wimmer and Andriacchi (1997). The muscle groups crossing the knee are represented. Patellar ligament angle (β) changes with flexion angle (α) {Adapted from Wimmer and Andriacchi (1997) with Elsevier permission} **1**-25

Figure 1.24 Schematic diagram of the biomechanical model of Chen *et al.* (2001) during a walking simulation {Adapted from Zhu *et al.* (1999); Chen *et al.* (2001) with IEEE permission} **1**-26

Figure 1.25 Three-dimensional multibody model of a diarthrodial joint proposed by Kwak *et al.* (2000) {Adapted from Kwak *et al.* (2000) with Taylor & Francis permission} **1**-26

Figure 1.26 FEM-based model of a total knee replacement proposed by Halloran *et al.* (2005): (a) Solid model; (b) FEM mesh; (c) Transparent view showing contact pressures {Adapted from Halloran *et al.* (2005) with Elsevier permission} **1**-28

Figure 1.27 Patellofemoral joint model proposed by Besier *et al.* (2005). The surfaces of the bone and cartilage are fitted to (a) NURBS surfaces, which are used to generated (b) quadrilateral and hexahedral meshes of the bones and cartilage {Adapted from Besier *et al.* (2005) with Wolters Kluwer Health permission} **1**-29

Figure 1.28 Patellofemoral joint model proposed by Fernandez and Hunter (2005). The patella (a) is discretized with (b) contact points and defined as the slave surface. Each contact point on the slave (c) is projected to the closest target point on the master surface with a unit normal **n**. The interpenetration is

constrained by contact springs (d) placed between the patella and the femur. The master surface is defined as the shaded blue region (e) on the femoral condyles {Adapted from Fernandez and Hunter (2005) with Springer permission} **1**-30

Figure 1.29 (a) Multibody model of the knee joint with menisci proposed by Guess *et al.* (2010, 2011). (b) Virtual model of the human body performing a dual-limb squat task, including a multibody knee with menisci {Adapted from Guess (2012) with Springer permission} **1**-33

Figure 1.30 Contact surface preparation proposed by Bei and Fregly (2004) for an artificial knee model. (a) CAD model of the knee prosthesis; (b) Trimmed NURBS surfaces removed from the CAD model; (c) Untrimmed NURBS patches fitted to the contact surfaces and then merged into a single patch; (d) Reduced number of parametric B-spline curves used to represent the surface maintaining the level of surface accuracy {Adapted from Bei and Fregly (2004) with Elsevier permission} **1**-33

Figure 1.31 Planar model of the knee joint proposed by Küçük (2006). L_c represents the current length of the active cartilage layer, which is modeled by a set of linear springs {Adapted from Küçük (2006) with Elsevier permission}.. **1**-35

Figure 1.32 Mathematical 3D-model of the knee proposed by Akalan *et al.* (2008). The numbers denoted the knee ligaments: (1) LCL; (2) Anterior fiber of MCL; (3) Deep fiber of MCL; (4) Oblique fiber of MCL; (5) Medial capsule of popliteal ligament; (6) Lateral capsule of popliteal ligament; (7) Oblique popliteal ligament; (8) Arcuate popliteal ligament; (9) Anterior fiber of PCL; (10) Posterior fiber of PCL; (11) Anterior fiber of ACL; (12) Posterior fiber of ACL {Adapted from Akalan *et al.* (2008) with Elsevier permission} . **1**-36

Figure 1.33 Diagram presented by Lin *et al.* (2010) to illustrate the process of developing a surrogate contact model. This process entails 8 steps: (a) *n* points are sampled in the x, F_y, z, T_α, β, γ design space; (b) Static analyses are performed for the first *m* sample points using an elastic foundation model (EFM); (c) Coarse surrogate models are created based on static analysis results for these *m* sample points; (d) Coarse surrogate models are used to predict static analysis results for the remaining *n-m* sample points; (e) Sample points are screened and eliminated if their predicted outputs are outside the desirable ranges defined by one or more nominal dynamic simulations; (f) Additional static analyses are performed with the EFM for sample points that pass the screening process; (g) Final surrogate contact models are created using static analysis results from all retained sample points; (h) During a dynamic simulation, surrogate contact models calculate contact forces and torques applied to both bodies given the pose of the femoral component relative to the tibial insert{Adapted from Lin *et al.* (2010) with Elsevier permission} **1**-38

Figure 1.34 Simplified articular joint model presented by Li *et al.* (1997) {Adapted from Li *et al.* (1997) with Elsevier permission}. (a) A rigid ball covered by an elastic layer in contact with an elastic layer supported by a rigid foundation; (b) A ball in contact with a single elastic layer; (c) EFM model of the ball-socket joint; (d) An axisymmetric FEM-mesh for a non-conforming joint model..... **1**-42

Figure 1.35 Average radii in mm of femur and tibia articular surfaces: (a) Coronal view; (b) Lateral view; (c) Medial view {Adapted from Koo and Andriacchi (2007) with Elsevier permission} **1**-43

CHAPTER 2

Figure 2.1 The anatomical position, with three reference planes and six fundamental directions {Adapted from Whittle (2007) with Elsevier permission} **2**-2

Figure 2.2 Four anatomical directions: (a) Medial; (b) Lateral; (c) Proximal; (d) Distal {Adapted from Hannon (2005) with Elsevier permission} **2**-3

Figure 2.3 Movements about the knee joint: (a) Frontal view; (b) Lateral view {Adapted from Whittle (2007) with Elsevier permission} **2**-3

Figure 2.4 Three joints of the human knee articulation: (a) Tibiofemoral joint; (b) Patellofemoral joint; (c) Superior tibiofibular joint {Adapted from Hamill and Knutzen (2009) with Lippincott Williams & Wilkins permission}..... **2**-5

Figure 2.5 (a) Distal femur; (b) Proximal tibial {Adapted from Dargel *et al.* (2011) with Elsevier permission} **2**-6

Figure 2.6 Knee joint and its surrounding ligaments and intra-articular structures {Adapted from Kamekura *et al.* (2005) with Elsevier permission} **2**-7

Figure 2.7 Longitudinal cross-section view of the human knee joint {Adapted from Gerwin *et al.* (2006) with Elsevier permission} **2**-9

Figure 2.8 Principal muscles involved with the knee joint {Adapted from Teiz and Graney (2003) with the permission of University of Washington}..... **2**-9

Figure 2.9 Patella and its five facets {Adapted from Hamill and Knutzen (2009) Lippincott Williams & Wilkins permission} **2**-13

Figure 2.10 (a) Semicircular instant center pathway for the tibiofemoral joint in a 19-year-old man with a normal knee; (b) Abnormal instant center pathway for a 35-year-old man with a bucket-handle derangement {Adapted from Completo (2006) with Author's permission} **2**-14

Figure 2.11 Moment arm of the quadriceps muscles of a knee joint with: (a) Normal patella; (b) Patellectomy (Completo, 2006) **2**-17

Figure 2.12 Stress distribution in: (a) Normal knee; (b) Knee with the menisci removed {Adapted from Completo (2006) with Author's permission} **2**-18

Figure 2.13 Schematic representation of the main movements of the medial and lateral menisci from full extension to 90 degrees of knee flexion in a weight-bearing standing condition {Adapted from Completo (2006) with Author's permission} **2**-18

Figure 2.14 Longitudinal cross-section view of the proximal femur {Adapted from Boyle and Kim (2011) with Elsevier permission} **2**-20

Figure 2.15 Layered structure of cartilage collagen network showing four distinct zones: superficial tangential zone, middle zone, deep zone and calcified zone {Adapted from Mow and Ratcliffe (1997) with Lippincott Williams & Wilkins permission} **2**-21

Figure 2.16 Meniscus ultrastructure, showing the different fiber orientations {Adapted from Mow and Ratcliffe (1997) with Lippincott Williams & Wilkins permission} **2**-21

Figure 2.17 Hierarchical microarchitecture of tendons and ligaments (Herman, 2007) **2**-24

Figure 2.18 Level of complexity in the organization of a skeletal muscle {Adapted from Meiss (2003) with Lippincott Williams & Wilkins permission} **2**-25

Figure 2.19 Arrangement of the actin and myosin chains in the sarcomere within a muscle fiber {Adapted from Meiss (2003) with Lippincott Williams & Wilkins permission} **2**-27

Figure 2.20 Illustration of the different shapes of muscles with parallel fiber arrangements (fusiform, flat, circular, convergent and strap), and pennate fiber arrangements (unipennate, bipennate and multipennate) {Adapted from Hamill and Knutzen (2009) with Lippincott Williams & Wilkins permission; Adapted from Moore and Agur (2007) with Lippincott Williams & Wilkins permission} **2**-27

Figure 2.21 Force-length curve: (a) Individual fiber; (b) Whole muscle {Adapted from Mansour (2008) with Lippincott Williams & Wilkins permission} **2**-29

Figure 2.22 Muscle force relations: (a) Force-velocity curve; (b) Force-length-velocity curve {Adapted from Ackermann (2007); Adapted from Mansour (2008) with Lippincott Williams & Wilkins permission} **2**-29

Figure 2.23 (a) Hill type muscle model; (b) Modified Hill type muscle model {Adapted from Ackermann (2007) with Author's permission} **2**-30

Figure 2.24 Knee implants: (a) Total Knee Replacement {Adapted from Murnaghan and Hamer (2010) with Elsevier permission}; (b) Unicompartmental Knee Replacement {Adapted from Jung *et al.* (2008) with Elsevier permission}; (c) Patellofemoral Joint Replacement {Adapted from Donell and Glasgow (2007) with Elsevier permission}; (d) Bicompartmental Knee Replacement {Adapted from Palumbo *et al.* (2011) with Elsevier permission} **2**-33

Figure 2.25 Knee implants history {Adapted from Carr and Goswami (2009) with Elsevier permission} **2**-34

CHAPTER 3

Figure 3.1 Examples of application of multibody systems: (a) Vehicle dynamics; (b) Lumbar vertebrae model; (c) Railway dynamics; (d) slider-crank model with clearance revolute joint **3**-4

Figure 3.2 Types of coordinates frequently used in multibody systems **3**-6

Figure 3.3 Examples of human body models: (a) AnyBody modeling system^{TM}; (b) OpenSim; (c) APOLLO {Adapted from Silva (2003) with Author's permission} **3**-8

Figure 3.4 Transition from (a) absolute coordinates to (b) natural coordinates **3**-9

Figure 3.5 Global and local components of a point P_i on body i **3**-10

Figure 3.6 Flowchart of computational procedure for kinematic analysis of a multibody system **3**-14

Figure 3.7 Revolute joint connecting bodies i and j **3**-14

Figure 3.8 Human arm multibody model composed by three bodies: hand (1), forearm (2) and arm (3). The motions of forearm and arm are prescribed by the trajectories $t_2(t)$ and $t_3(t)$, respectively **3**-17

Figure 3.9 Different types of forces that can be present in a biomechanical multibody system **3**-19

Figure 3.10 Open loop and closed loop control systems **3**-23

Figure 3.11 Flowchart of computational algorithm for dynamic analysis of multibody systems based on the direct integration method **3**-26

Figure 3.12 Geometric interpretation of the Euler integration method **3**-28

Figure 3.13 Geometric interpretation of the fourth-order Runge-Kutta method..... **3**-29

Figure 3.14 Biomechanical multibody model of a human body on the sagittal plane **3**-32

Figure 3.15 Influence of the Baumgarte parameters, α and β, on the y-position of the four bodies of the human body model: (a) HAT; (b) Thigh; (c) Shank; (d) Foot ... **3**-35

CHAPTER 4

Figure 4.1 Taxonomy of geometric models (Lin and Gottschalk, 1998) **4**-6

Figure 4.2 Four steps to generate a BSP tree (van den Bergen, 2004)..... **4**-10

Figure 4.3 Bounding volumes: (a) Sphere; (b) AABB; (c) OBB; (d) 8-DOP..... **4**-11

Figure 4.4 Schematic representation of two externally colliding spheres..... **4**-14

Figure 4.5 Externally colliding spheres modeled by Hooke's contact law: (a) Normal contact force and indentation *versus* time; (b) Normal contact force-indentation relation **4**-14

Figure 4.6 Externally colliding spheres modeled by Hertz contact law: (a) Normal contact force and indentation *versus* time; (b) Normal contact force-indentation relation; (c) Phase portrait..... **4**-16

Figure 4.7 Elastic foundation model or Winkler foundation model..... **4**-17

Figure 4.8 Schematic diagram of a normal contact force-indentation relation for: (a) Spring-dashpot model (e.g., Kelvin and Voight law); (b) Nonlinear damping model (e.g., Hunt and Crossley law)..... **4**-20

Figure 4.9 Externally colliding spheres modeled by Hunt and Crossley force law: (a) Normal contact force and indentation *versus* time; (b) Normal force-indentation relation; (c) Phase portrait..... **4**-21

Figure 4.10 Externally colliding spheres modeled by Hertz, Hunt and Crossley, Herbert and McWhannell, and Lee and Wang contact force laws: (a) Normal contact force-indentation relation; (b) Phase portrait..... **4**-23

Figure 4.11 Externally colliding spheres modeled by Hertz, Hunt and Crossley, Lankarani and Nikravesh, Gonthier *et al.*, Zhiying and Qishao, and Flores *et al.* force models: (a) Normal contact force-indentation relation; (b) Phase portrait..... **4**-27

Figure 4.12 Evolution of the hysteresis damping factor as function of the coefficient of restitution **4**-28

Figure 4.13 Multibody system composed by a slider-crank mechanism and a free sliding block..... **4**-28

Figure 4.14 (a) Position of the free sliding block; (b) Velocity of the constrained slider... ..... **4**-30

Figure 4.15 Normal contact force-indentation relation for the two impacts: (a) First impact; (b) Second impact **4**-30

CHAPTER 5

Figure 5.1 Two-dimensional multibody model of the human knee joint..... **5**-3

Figure 5.2 Knee contact profiles within a: (a) MRI at the sagittal plane; (b) Knee joint model..... **5**-4

Figure 5.3 Two contacting bodies, in which the distance between them is exaggerated with the purpose to represent all the necessary vectors **5**-6

Figure 5.4 Two possible contact scenarios: (a) Contact at a single point without indentation; (b) Contact at a multiple points with indentation **5**-8

Figure 5.5 Flowchart of the developed algorithm for contact dynamics of planar multibody systems, which was implemented in a multibody code named MUBODYNA (Flores, 2010) **5**-11

Figure 5.6 Typical ligament stress-strain relationship (Butler *et al.*, 1978)..... **5**-12

Figure 5.7 *xy*-Coordinates of the Tibia obtained using different spline interpolation techniques: (a) Tibia center of mass; (b) Tibia contact points..... **5**-15

Figure 5.8 Knee contact response using shape preserving splines: (a) Indentation *versus* knee flexion angle; (b) Velocity of indentation *versus* knee flexion angle; (c) Normal contact force *versus* knee flexion angle; (d) Force-indentation relation **5**-15

Figure 5.9 Knee MRI images: (a) lateral, (b) medial and (c) intercondylar views {Adapted from Koo *et al.*, (2005) with Elsevier permission} **5**-17

Figure 5.10 Representation of the different contact scenarios: (a) convex-convex spheres, (b) convex-concave spheres and (c) convex sphere-plane..... **5**-17

Figure 5.11 (a) Indentation *versus* knee flexion angle using three different geometric models; (b) Normal contact force *versus* knee flexion angle using three different geometric models **5**-19

Figure 5.12 Normal contact force *versus* indentation using three different geometric models: (a) First impact; (b) Whole simulation **5**-20

Figure 5.13 Indentation *versus* knee flexion angle of a healthy knee model analyzed by different contact force laws: (a) First impact; (b) Whole simulation..... **5**-21

Figure 5.14 Normal contact force *versus* knee flexion angle of a healthy knee model analyzed by different contact force laws: (a) First impact; (b) Whole simulation..... **5**-22

Figure 5.15 Force-indentation relation of a healthy knee model analyzed by different contact force laws: (a) First impact; (b) Whole simulation **5**-22

Figure 5.16 Force-indentation relation of the five knee models: (a) First impact; (b) Whole simulation..... **5**-26

Figure 5.17 Contact response of the five knee models along the knee flexion angle during the first contact (from 27.5 to 22.5 degrees of flexion): (a) Indentation; (b) Normal contact force..... **5**-26

Figure 5.18 Contact response of the five knee models along the knee flexion angle during the whole contact period (from 28 to -5 degrees of flexion): (a) Indentation; (b) Normal contact force..... **5**-27

Figure 5.19 Dynamic response of the five knee models during the knee hyperextension (from 0 to -5 degrees of flexion): (a) Indentation *versus* knee flexion angle; (b) Normal contact force *versus* knee flexion angle **5**-27

Figure 5.20 Force-indentation relations for the pathologic model (100%OA+OP knee) analyzed by different contact force laws: (a) first impact; (b) whole simulation..... **5**-29

Figure 5.21 Force-indentation relations for the artificial knee model analyzed by different contact force laws: (a) first impact; (b) whole simulation **5**-29

Figure 5.22 Ligament forces along flexion angle for an amplitude of external force equal to 50 N, when the contact forces are computed by: (a) Hertz law; (b) Flores *et al.* model..... **5**-30

Figure 5.23 Ligament forces along flexion angle for an amplitude of external force equal to 150 N, when the contact forces are computed by: (a) Hertz law; (b) Flores *et al.* model..... **5**-30

Figure 5.24 Indentation along flexion angle for two different values of amplitude of external force, when the contact forces are computed by: (a) Hertz law; (b) Flores *et al.* model..... **5**-31

Figure 5.25 Velocity of indentation along flexion angle for two different values of amplitude of external force, when the contact forces are computed by: (a) Hertz law; (b) Flores *et al.* model..... **5**-32

Figure 5.26 Normal contact forces along flexion angle for two different values of amplitude of external force, when the contact forces are calculated by: (a) Hertz law; (b) Flores *et al.* model..... **5**-32

Figure 5.27 Tibia contact points for two different values of amplitude of external force, when the contact forces are computed by: (a) Hertz contact law; (b) Flores *et al.* model..... **5**-32

Figure 5.28 Normal contact force *versus* indentation for two different values of amplitude of external force using the Flores *et al*. contact force model: (a) First impact; (b) Whole simulation..... **5**-32

CHAPTER 6

Figure 6.1 Schematic representation of a rigid body: (a) 2D-space; (b) 3D-space. In the 2D-space, 3 independent coordinates are needed to define the location of the body, while in the 3D-space it is required six independent coordinates (Nikravesh, 1988)..... **6**-2

Figure 6.2 Schematic representation of an orientational axis of rotation $\vec{w}$ (Nikravesh, 1988)..... **6**-3

Figure 6.3 Representation of one eighth of a spherical surface using the parametric method..... **6**-8

Figure 6.4 Schematic representation of the regular surface sampling..... **6**-10

Figure 6.5 Schematic representation of the lookup table reshuffle of a surface defined with 100 points that is stored in 25 equal-sized records..... **6**-11

Figure 6.6 Representation of the contact surfaces and ligaments included within the 3D-knee model..... **6**-13

Figure 6.7 Examples of CAD models of knee contact surfaces: (a) femoral articular cartilage; (b) tibial articular cartilage; (c) tibiofemoral articular cartilage; (d) femoral component; (e) tibial insert; (f) tibiofemoral artificial joint (Fregly *et al.*, 2012)..... **6**-14

Figure 6.8 Representation of two generalized contact surfaces (Glocker, 1999)..... **6**-15

Figure 6.9 Graphical representation of the bilinear interpolation for a surface described by four points **6**-16

Figure 6.10 Illustration of the main differences between a sequential access file and a direct access file **6**-18

Figure 6.11 Structure of the direct access file of a parametric representation of a surface with 100 points **6**-19

Figure 6.12 Schematic representation of an update of a storage window **6**-20

Figure 6.13 Schematic representation of a contact surface with a storage window: (a) Eight impacts without needing a window update; (b) Update of the storage window in the ninth impact **6**-21

Figure 6.14 Algorithm proposed to deal with 3D-contact problems in multibody systems **6**-23

Figure 6.15 Schematic representation of the bouncing ball model **6**-24

Figure 6.16 Bouncing ball response using different contact approaches: (a) ball position on *zOy* plane; (b) normal contact force *versus* contact indentation; (c) contact indentation *versus* time; (d) contact indentation *versus* time for the first impact **6**-25

Figure 6.17 Schematic representation of four models of spheres discretized in: (a) 81 points; (b) 1089 points; (c) 110889 points; (d) 998001 points **6**-26

Figure 6.18 Bouncing ball response using different levels of surface discretization: (a) contact indentation for whole simulation; (b) contact indentation for the first impact **6**-26

Figure 6.19 Illustration of the update of the storage window during a bouncing ball simulation **6**-28

Figure 6.20 Initial configuration of the three-dimensional model of the knee joint **6**-28

Figure 6.21 Representation of the eight ligament fibers on the knee joint model **6**-29

Figure 6.22 Contact response of the 3D-model of the knee joint using the Hertz contact law: (a) indentation *versus* knee flexion angle; (b) normal contact force *versus* knee flexion angle **6**-31

Figure 6.23 Kinematic response of the 3D-model of the knee joint using the Hertz contact law: (a) 3D-Position of tibia center-of-mass (in mm); (b) Femur contact points for 9 different positions of the tibia, namely 0, 10, 20, 30, 40, 50, 60, 70 and 80 degrees of knee flexion **6**-31

Figure 6.24 Dynamic response of the knee ligaments using the Hertz contact law: (a) Ligament force *versus* knee flexion angle; (b) Ligament force *versus* ligament strain **6**-32

CHAPTER 7

Figure 7.1 OpenSim organization and hierarchy structure {adapted from Seth *et al.*, 2011} **7**-3

Figure 7.2 Representation of the skeletal model of a knee joint with a prosthesis developed within OpenSim GUI: (a) lateral view; (b) anterior view 7-4

Figure 7.3 Placement of the markers on the knee: (a) OpenSim model; (b) Leg extension trial. The meaning of the marker's acronyms is listed in Table 7.1 ..... **7**-5

Figure 7.4 Knee flexion angle *versus* time obtained in OpenSim by inverse kinematic analysis **7**-6

Figure 7.5 Schematic representation of the knee model with fourteen muscle actuators: (a) anterior view; (b) medial view; (c) posterior view; (d) lateral view. The fourteen muscle actuators represented in this figure are numbered from 1 to 14, representing: (1) Sartorius, (2) Gracilis, (3) Biceps femoris long head, (4) Biceps femoris short head, (5) Gastrocnemius lateral, (6) Gastrocnemius medial, (7) Semimembranosus, (8) Semitendinosus, (9) Tensor fascia lata, (10) Vastus medialis, (11) Vastus intermedius, (12) Vastus lateralis, (13) Rectus femoris, (14) Patellar tendon **7**-8

Figure 7.6 Muscle properties: (a) force-length relation; (b) force-velocity relation **7**-9

Figure 7.7 Schematic representation of the CMC algorithm **7**-10

Figure 7.8 Geometrical models used to model knee contact surfaces: (a) sphere-plane contact; (b) two sphere-ellipsoid contacts (medial and lateral); (c) contact between meshes of CAD files **7**-12

Figure 7.9 Triangular mesh volumes generated by CAD files of knee prosthesis: (a) Medial contact meshes, (b) Lateral contact meshes **7**-12

Figure 7.10 Components of the tibiofemoral contact force on *x*-, *y*- and *z*- directions for the sphere-plane geometric model **7**-13

Figure 7.11 Components of the tibiofemoral contact force on *x*-, *y*- and *z*- directions for ellipsoid-sphere geometric model: (a) medial forces; (b) lateral forces. .. **7**-13

Figure 7.12 Components of the tibiofemoral contact forces on *x*-, *y*- and *z*- directions for CAD-based models: (a) medial forces; (b) lateral forces **7**-13

Figure 7.13 Components of the tibiofemoral contact force on *x*-, *y*- and *z*- directions for the plane-sphere geometric model computed by the use of the Elastic foundation model (EFM) and the Hunt and Crossley model (HCM). **7**-15

Figure 7.14 Bouncing ball model used in OpenSim simulations **7**-16

Figure 7.15 Ball contact response using different contact force laws, namely Hertz contact law within MUBODYNA, Hunt and Crossley model (HCM) within OpenSim and Elastic foundation model (EFM) within OpenSim: (a) *y*-position of the ball *versus* time; (b) normal contact forces *versus* time **7**-17

Figure 7.16 Vertical position of the ball using different contact force laws, namely Hertz contact law within MUBODYNA, Hunt and Crossley model (HCM) within OpenSim and Elastic foundation model (EFM) within OpenSim: (a) First impact; (b) Last impact (7^{th} impact) **7**-18

Figure 7.17 Normal contact forces of the ball using different contact laws, namely Hertz contact law within MUBODYNA, Hunt and Crossley model (HCM) within OpenSim and Elastic foundation model (EFM) within OpenSim: (a) First impact; (b) Last impact (7^{th} impact) **7**-19

Nomenclature

All matrices and vectors are written in boldface.

All scalars are written in italic face.

LATIN SYMBOLS

Symbol	SI-Unit	Eq.	Description
$\mathbf{A}$	-	3.6	Rotational transformation matrix
A	-	-	Auxiliary point
A	N	5.1	Amplitude of sinusoidal pulsed force applied to the knee model
a	m	4.32	Distance between the body center of mass and its contact profile
a_0, a_1, a_2, a_3	-	5.2	Cubic spline polynomial coefficients of s_i
a_i	-	7.2	Activation level of muscle at a discrete time step
A_s	m^2	4.10	Area of the spring element on normal direction
a_y	m/s^2	7.7	Vertical acceleration (*i.e.*, gravitational acceleration)
$\mathbf{b}$	-	6.13	Binormal vector
B	-	-	Auxiliary point
b_0, b_1, b_2, b_3	-	5.3	Cubic spline polynomial coefficients of s_j
C	-	-	Auxiliary point
c_r	-	4.13	Coefficient of restitution
D	Ns/m	4.11	Damping coefficient
$\mathbf{d}$	-	5.14	Distance vector
d	m	5.21	Magnitude of distance vector
d_m	-	4.24	Dimensionless factor
ΔE	J	4.19	Dissipated energy
E	N/m^2	4.4	Young's modulus of elasticity
e_0, e_1, e_2, e_3	-	6.1	Euler parameters
E_w	N/m^2	4.6	Winkler modulus of an elastic layer
f	-	3.47	Integration function
F_1	N	5.32	Normal contact force resultant from a partial indentation of the first contact layer

LATIN SYMBOLS (*continued*)

Symbol	SI-Unit	Eq.	Description
F_1^{max}	N	5.32	Normal contact force resultant from a total indentation of the first contact layer
F_2	N	5.32	Normal contact force at the second contact layer
F_e	N	5.1	External applied force
F_i^0	N	7.2	Maximum isometric force
F_l	N	5.23	Ligament force
F_N	N	4.1	Normal contact force
$f\left(F_i^0, l_i, v_i\right)$	-	7.3	Force-length-velocity surface
$\mathbf{g}$	N, Nm	3.33	Generalized force vector
g	-	3.46	Integration function
$\mathbf{g}^{(c)}$	N, Nm	3.34	Vector of constraint reaction equation
h	-	3.45	Integration step size
h_s	m	4.6	Thickness of a contact layer
h_{s_1}	m	5.32	Thickness of the first contact layer
$\boldsymbol{I}$	kgm^2	-	Moment of Inertia
J	-	7.4	Objective function of static optimization
k	N/m	4.1	Linear stiffness parameter
K	$N/m^{1.5}$	4.2	Generalized stiffness parameter
K_1	$N/m^{1.5}$	5.33	Generalized stiffness of the first contact layer
K_2	$N/m^{1.5}$	5.33	Generalized stiffness of the second contact layer
k_l	N/m^2	5.23	Ligament stiffness
k_p	-	7.5	Feedback gain on the position error
k_v	-	7.5	Feedback gain on the velocity error
$\mathbf{L}$	-	6.5	Auxiliary 3×4 matrix that is function of Euler parameters
l	m	5.23	Current ligament length
l^0	m	5.23	Unstrained ligament length
l_i	m	7.3	Muscle fiber length
l_i^0	m	-	Optimal muscle fiber length
l_{record}	-	6.23	Record length
l_i^0	m	-	Tendon slack length
$\mathbf{M}$	kg, kgm^2	3.33	System mass matrix

LATIN SYMBOLS (*continued*)

Symbol	SI-Unit	Eq.	Description
m	kg	7.8	Mass
$\mathbf{n}$	-	5.12	Normal unit vector
n_b	-	-	Number of rigid bodies in a multibody system
n_c	-	-	Number of generalized Cartesian coordinates
n_{bit}	-	6.23	Memory space required to store each value in a record
n_d	-	6.23	Number of surface data associated with a point that is stored into the lookup table
n_i	-	7.2	Number of muscles included into the model
n_{pr}	-	6.23	Number of points per record
O	-	-	Auxiliary point
$\mathbf{p}$	-	6.1	Euler parameter vector
P	-	-	Auxiliary point
$\dot{\mathbf{p}}$	-	6.5	Vector of time derivatives of Euler parameter
p_s	N/m^2	4.6	Spring contact pressure
$\mathbf{q}$	-	3.1	Vector that contains the state of positions, or vector of generalized coordinates
Q	-	-	Auxiliary point
$\dot{\mathbf{q}}$	-	3.14	Vector that contains the state of velocities
$\ddot{\mathbf{q}}$	-	3.15	Vector that contains the state of accelerations
$\ddot{\mathbf{q}}^*$	-	7.5	Desired acceleration
$\mathbf{q}^{exp}$	-	7.5	Experimentally-derived coordinates
$\mathbf{q}_j^{\exp}$	-	7.1	Experimental value for coordinate j
$\mathbf{r}$	-	3.8	Global position vector
R	m	4.3	Radius
$r_{i,k}$	m	7.2	Muscle i moment arm about the k-th joint axis
$ratio_{CPU}$	-	6.25	Ratio between t_{CPU}^w and t_{CPU}
$\mathbf{s}$	-	3.8	Local position vector
$\mathbf{s}(u,v)$	-	6.10	Parametric position vector of a surface
s_i	-	5.2	Spline function of profile of body i
s_j	-	5.3	Spline function of profile of body j
$\dot{s}_i$	-	5.4	First time derivative of spline function of profile of body i
$\dot{s}_j$	-	5.5	First time derivative of spline function of profile of body j

LATIN SYMBOLS (*continued*)

Symbol	SI-Unit	Eq.	Description
$\ddot{s}_i$	-	5.6	Second time derivative of spline function of profile of body *i*
$\ddot{s}_j$	-	5.7	Second time derivative of spline function of profile of body *j*
$\mathbf{s}''^{P}_{k}$	-	6.17	Local component of P_k with respect to the surface reference frame $\xi_k^Q \eta_k^Q \zeta_k^Q$
$\mathbf{t}$	-	5.13	Tangential unit vector
t	s	3.13	Time
T	J	7.9	Ball energy at the instant of maximum indentation
t^-	s	7.7	Instant of time when a ball hits the ground for the first time
T^0	J	7.8	Ball energy at the initial instant of simulation
t_{CPU}	s	6.25	Computational time consumed without surface window
t_{CPU}^w	s	6.25	Computational time consumed with surface window
t_d	s	5.1	Duration of sinusoidal pulsed force applied to the knee model
T^{max}	J	7.9	Kinetic energy of the system at the end of the compression phase
$t_k(t)$	-	3.29	Trajectory of a guiding constraint of body *k* as a function of time
$\mathbf{u}$	-	3.3	Unit vector
U^{max}	J	7.9	Maximum elastic strain energy stored
u, v	-	6.10	Parametric coordinates
$\mathbf{v}$	-	-	Velocity vector
$\mathbf{v_a}$, $\mathbf{v_b}$, $\mathbf{v_c}$	-	-	Auxiliary vectors
v_b	-	5.30	Magnitude of vector $\mathbf{v_b}$
v_i	m/s	7.3	Muscle shortening velocity
v_N	m/s	5.12	Normal velocity
v_T	m/s	5.13	Tangential velocity
$\boldsymbol{w}$	-	-	Arbitrary axis
w_i	-	7.1	Weighting factors of markers *i*
x	m	3.2	*x*-Cartesian coordinate
$\mathbf{x}_i(\mathbf{q})$	-	7.1	Position of marker *i* on the model
$\mathbf{x}_i^{exp}$	-	7.1	Experimental position of marker *i*
x_{max}	m	6.15	Edge size of the plane on *x*-direction
XY, *xy*	-	-	2D-global coordinate system

LATIN SYMBOLS (*continued*)

Symbol	SI-Unit	Eq.	Description
XYZ, *xyz*	-	-	3D-global coordinate system
y	m	3.2	*y*-Cartesian coordinate
$\mathbf{y}$	m, m/s	3.39	System position and velocity
$\dot{\mathbf{y}}$	m/s, m/s^2	3.39	System velocity and acceleration
y_0	m	7.7	Initial *y*-coordinate of the ball center of mass
y_b	m	7.6	*y*-coordinate of the ball center of mass
$y_{\max}$	m	6.15	Edge size of the plane on *y*-direction

GREEK SYMBOLS

Symbol	SI-Unit	Eq.	Description
α	-	3.37	Baumgarte stabilization coefficient
α_i	-	-	Pennation angle
β	-	3.37	Baumgarte stabilization coefficient
χ	Ns/m$^{2.5}$	4.12	Hysteretic damping factor
δ	m	4.1	Contact indentation
$\dot{\delta}$	m/s	4.11	Relative normal contact velocity
$\dot{\delta}^{(-)}$	m/s	4.13	Initial impact velocity
δ_{max}	m$^{2.5}$	4.29	Maximal contact indentation
ε_g	-	3.43	Global error
ε_l	-	-	Ligament strain
ϕ	rad	3.2	Angular coordinate
$\mathbf{\Phi}$	-	3.13	Vector of kinematic constraints
$\dot{\mathbf{\Phi}}$	-	3.37	Constraint velocity equation
$\ddot{\mathbf{\Phi}}$	-	3.37	Constraint acceleration equation
$\mathbf{\Phi_q}$	-	3.14	Jacobian matrix of the kinematic constraint equations
$\mathbf{\Phi_{qt}}$	-	3.15	Time derivative of Jacobian matrix
$\mathbf{\Phi_t}$	-	3.14	Time derivative of kinematic constraint equations
$\mathbf{\Phi_{tt}}$	-	3.15	Double time derivative of kinematic constraint equations

GREEK SYMBOLS (*continued*)

Symbol	SI-Unit	Eq.	Description
$\boldsymbol{\gamma}$	-	3.15	Right hand side vector of acceleration equations, or vector of quadratic velocity terms
$\boldsymbol{\lambda}$	-	3.34	Vector of Lagrange multipliers associated with constraints
ν	-	4.4	Poisson's ratio
θ	rad	-	Knee flexion angle
θ_A	rad	5.30	Angle between vector $\mathbf{v_b}$ and $\mathbf{v_c}$
θ_i	rad	5.2	Polar parameter that define spline function s_i
θ_j	rad	5.3	Polar parameters that define spline function s_j
σ	m^2/N	4.3	Material parameter
τ_k	N, Nm	7.2	Generalized force acting about the *k*-th joint axis
$\boldsymbol{\upsilon}$	-	3.14	Right hand side vector of velocity equations
ω	rad/s	6.5	Angular velocity
$\dot{\omega}$	rad/s^2	6.8	Angular acceleration
ω_j	-	7.1	Weighting factors of coordinates *j*
$\xi\eta$	-	-	2D Body-fixed coordinate system
$\xi\eta\zeta$	-	-	3D Body-fixed coordinate system

SUBSCRIPTS

Symbol	Description
i	Relative to element *i*
j	Relative to element *j*
k	Relative to element *k*
l	ligament
n	Relative to *n* elements
n, N	Normal direction
P	Relative to point *P*
t	Time
t, T	Tangential direction
u	Parametric *u*-direction
v	Parametric *v*-direction

SUBSCRIPTS (*continued*)

Symbol	Description
x	global x-direction
y	global y-direction
z	global z-direction
ξ	local ξ-direction
η	local η-direction
ζ	local ζ-direction

SUPERSCRIPTS

Symbol	Description
0	Initial conditions
C, O, P, Q	Relative to points C, O, P, Q
(g)	Guiding constraint
i	Index
n	Nonlinear power exponent
p	Power exponent defined by the user
(r)	Revolute joint
u	parametric u-direction
v	parametric v-direction
x	global x-direction
y	global y-direction
z	global z-direction
ϕ	Angular direction

OPERATORS

Symbol	Description
$( )^T$	Matrix or vector transpose
$(')$	Components of a vector in a body-fixed coordinate system
$(\dot{})$	First derivative with respect to time

OPERATORS (*continued*)

Symbol	Description
$(\ddot{})$	Second derivative with respect to time
$(.)$	Scalar or internal product
$(\times)$	Cross or external product
(∂)	Partial derivative
$(\sim)$	Skew-symmetric matrix or vector
Δ	Increment

ABBREVIATIONS

Symbol	Description
2D	**Two**-**D**imensional
3D	**Three**-**D**imensional
AABBs	**A**xis-**a**ligned **B**ounding **B**oxe**s**
ACL	**A**nterior **C**ruciate **L**igament
ADAMS	**A**utomatic **D**ynamic **A**nalysis of **M**echanical **S**ystems
AK	**A**rtificial **K**nee
AP	**A**nterior-**P**osterior
API	**A**pplication **P**rogramming **I**nterface
BSP	**B**inary **S**pace **P**artitioning
CAD	**C**omputer-**a**ided **D**esign
CAM	**C**omputer-**a**ided **M**anufacturing
CE	**C**ontractile **E**lement
CMC	**C**omputed **M**uscle **C**ontrol
COMPAMM	**Comp**uter **A**nalysis of **M**achines and **M**echanisms
CPU	**C**entral **P**rocessing **U**nit
CSG	**C**onstructive **S**olid **G**eometry
CT	**C**omputed **T**omography
CULLIDE	Interactive **Colli**sion **De**tection between Complex Models in Large Environments Using Graphics Hardware
D	**D**ynamic
DADS	**D**ynamic **A**nalysis and **D**esign **S**ystem

ABBREVIATIONS (*continued*)

Symbol	Description
DAE	**D**ifferential **A**lgebraic **E**quation
DAP	**D**ynamic **A**nalysis **P**rogram
DE	**D**amping **E**lement
DEEP	**D**ual-space **E**xpansion for **E**stimating **P**enetration Depth
DEFORMCD	**C**ollision **D**etection for **Deform**ing Objects
DICOM	**D**igital **I**maging and **Co**mmunications in **M**edicine
DIM	**D**irect **I**ntegration **M**ethod
DOF	**D**egrees-**o**f-**f**reedom
DOPs	**D**iscrete **O**rientation **P**olytope**s**
DVD	**D**iscrete **V**oronoi **D**iagrams
E	**E**xperimental
EFM	**E**lastic **F**oundation **M**odel
EMG	**E**lectro**m**yo**g**raphy
FD	**F**orward **D**ynamics
FEM	**F**inite **E**lement **M**ethod
FFD	**F**ree**f**orm **D**eformation
FORTRAN	**For**mula **Tran**slation
GPUs	**G**raphics **P**rocessing **U**nits
GRF	**G**round **R**eaction **F**orces
GUI	**G**raphical **U**ser **I**nterface
HAT	**H**ead-**A**rms-**T**runk
HCM	**H**unt and **C**rossley **M**odel
H-COLLIDE	Framework for Fast and Accurate **Colli**sion **De**tection for **H**aptic Interaction
HM	**H**ertz **M**odel
HYB	**H**ybrid
IC	**I**nstant **C**enter or **I**nstantaneous **C**enter of **R**otation
I-COLLIDE	**I**nteractive and Exact **Colli**sion **De**tection for Large-Scaled Environments
ID	**I**nverse **D**ynamics
IGES	**I**nitial **G**raphics **E**xchange **S**pecification
IK	**I**nverse **K**inematics
IMMPACT	**I**nteractive **M**assive **M**odel **P**roximity **a**nd **C**ollision **T**ester
K	**K**inematic

ABBREVIATIONS (*continued*)

Symbol	Description
LCL	**L**ateral **C**ollateral **L**igament
LCP	**L**inear **C**omplementarity **P**roblem
LL	**L**ower **L**imb
MADYMO	**Ma**thematical **Dy**namical **Mo**dels
MBS	**M**ulti**b**ody **S**ystem
MCL	**M**edial **C**ollateral **L**igament
mEFM	**m**odified **E**lastic **F**oundation **M**odel
mH	**m**odified **H**ertzian **T**heory
ML	**M**edial-**L**ateral
MRI	**M**agnetic **R**esonance **I**maging
MSC	**M**acNeal-**S**chwendler **C**orporation
MUBODYNA	**Mu**ltibody **Dyn**amic **A**nalysis
NEWEUL / NEWEUL-M^2	Software package for the dynamic analysis of mechanical systems
NK	**N**atural **K**nee
NURBS	**N**on-**U**niform **R**ational **B**-**S**plines
OA	**O**steo**a**rthristis
OBBs	**O**riented **B**ounding **B**oxe**s**
OP	**O**steo**p**orosis
OPCODE	**Op**timized **Co**llision **De**tection
OPT	**Opt**imization
P	**P**lanar
PCL	**P**osterior **C**ruciate **L**igament
PCM	**P**olygonal **C**ontact **M**odel
PD	**P**roportional **D**erivative
PE	**P**arallel Elastic **E**lement
PF	**P**atello**f**emoral joint
PGs	**P**roteo**g**lycan**s**
PIVOT	**P**roximity **I**nformation from **Vo**ronoi **T**echniques
PQP	**P**roximity **Q**uery **P**ackage
QS	**Q**uasi-**S**tatic
RAPID	**R**obust and **A**ccurate **P**olygon **I**nterference **D**etection

ABBREVIATIONS (*continued*)

Symbol	Description
S	**S**patial
SE	**S**eries Elastic **E**lement
SELF-CCD	**C**ontinuous **C**ollision **D**etection for Deforming Objects
SES	**S**implified **E**lastic **S**olution
SIMM	**S**oftware for **I**nteractive **M**usculoskeletal **M**odeling
SO	**S**tatic **O**ptimization
SOLID	**So**ftware **L**ibrary for **I**nterference **D**etection
SPG	**S**tereo**p**hoto**g**rammetric
STEP	**S**tandard for **t**he **E**xchange of **P**roduct
STL	**St**ereo**l**ithography
SWIFT	**S**peedy **W**alking Via **I**mproved **F**eature **T**esting
SWIFT^{++}	**S**peedy **W**alking Via **I**mproved **F**eature **T**esting for Non-convex Objects
TF	**T**ibio**f**emoral joint
TKR	**T**otal **K**nee **R**eplacement
UHMWPE	**U**ltra-**H**igh **M**olecular **W**eight **P**olyethylene
V-Clip	**V**oronoi **Clip**
V-COLLIDE	Accelerated **Colli**sion **De**tection for **V**RML

SOFTWARE

Application Field	Software
Finite Element Analysis	ABAQUS, Inc.; ANSYS, Inc.
Musculoskeletal Modeling	AnyBody Modeling System™; APOLLO; LifeModeler™; OpenSim; SIMM
Computer Graphics and Geometric Modeling	Autodesk®; Blender; Geomagic Studio®; Maya®; Rhinoceros®
Multibody System Simulation	COMPAMM; DAP; LMS® DADS; MADYMO®; MSC Software™ ADAMS; MUBODYNA; NEWEUL/NEWEUL-M^2; PC Crash™; SIMPACK
Collision Detection	CULLIDE; DEEP; DVD; DEFORMCD; H-COLLIDE; I-COLLIDE; IMMPACT; OPCODE; PIVOT; PQP; RAPID; SELF-CCD; SOLID; SWIFT/ SWIFT++; V-Clip; V-COLLIDE
Medical Image Analysis	sliceOmatic™

1

Introduction

1.1 *Motivation* **1**-2

1.2 *Literature review* **1**-4

1.3 *Scope and objectives* **1**-44

1.4 *Structure of the thesis* **1**-45

1.5 *Contributions of this work* **1**-46

References **1**-48

Multibody-based methodologies have been developed in such a way that, besides the representation of mechanical systems made only of rigid bodies, they also allow for the description of deformable bodies. Along with the theoretical developments in recent years, several powerful and reliable multibody commercial programs have been put on the market allowing for the study of human body motion as a multibody system (MBS) to undergo significant developments. Among others, these computational tools allow for the geometrical and physical properties of soft-tissue structures that constitute the biomechanical models to be taken into account in their full detail. Under the framework of multibody dynamics, the treatment of contact-impact is of particular importance and, so, it is introduced into the equations of motion either by using unilateral constraints or by applying a continuous contact force law (Ambrósio, 2005). By introducing the ability to handle contact in the internal structures of the biomechanical models quite a good number of physiological issues can be addressed with a better physical insight.

Within this study, a multibody approach to the contact dynamics is proposed, aiming to contribute for the efficiency of the computational methods dealing with 3D-contact events between freeform surfaces. The present work focuses on the analysis of biomechanical models, such as the human knee, which can undergo moderate and

high loading forces, depending on its dynamic condition. This approach allows for the prediction of intra-joint forces during daily activities, which serves as one of the basis for the design of implants and prosthetic devices (Machado *et al.*, 2010).

In this Chapter, the motivation for this work is presented and an extensive literature review on the biomechanical models of the knee joint is provided. The scope and objectives of this study are described, being the structure and organization of this thesis also explained. To finish, the main contributions of this work are emphasized.

1.1 Motivation

Knee joint pain is a very common musculoskeletal pathological condition that affects 6 percent and 25 percent of population over the age of 30 and 55, respectively (Howe *et al.*, 2012). According to World Health Organization (2003), 40 percent of the population over the age of 70 suffers from osteoarthritis of the knee. Among patients with osteoarthritis, 80 percent have some degree of limitation of movement, and 25 percent cannot perform major daily activities of life (World Health Organization, 2003). The prevalence of knee osteoarthritis is projected to increase due to population ageing and rising obesity rates (Bennell and Hinman, 2011).

Osteoarthritis is a chronic localized joint disease characterized by progressive deterioration and loss of articular cartilage and by reactive bone changes at the margins of the joints and in the subchondral bone (Felson, 2006). Clinical manifestations are characterized by slowly developing joint pain, stiffness, and joint enlargement with limitations of motion (Bennell and Hinman, 2011). Treatments such as weight loss, braces, orthotics, steroid injections, and physical therapy may also help to alleviate pain and to restore function. If the pain or immobility becomes too severe and other therapies do not alleviate the symptoms, a joint replacement becomes necessary (Sarzi-Puttini *et al.*, 2005). The etiology of knee osteoarthritis is not entirely clear. Nonetheless, its progression has been associated with multiple factors including: (*i*) age and gender, (*ii*) genetics, (*iii*) hormonal and metabolic factors, (*iv*) obesity, (*v*) acute joint injury and joint deformity, (*vi*) occupational factors and sports, (*vii*) muscle weakness and physical disability (Sarzi-Puttini *et al.*, 2005). Among these, it is believed that the mechanical factors play a major role in the development and progression of knee osteoarthritis (Bei and Fregly, 2004; Andriacchi and Mündermann, 2006). For instance, large external knee adduction moments during walking may increase the proportion of the load

sustained by the medial compartment, and may be large enough to completely unload the lateral compartment (Winby *et al.*, 2009).

Identifying and quantifying the joint loads placed on the surrounding structures of the knee is of paramount importance for understanding and studying realistic knee mechanics and to evaluate the true efficacy of any biomechanical intervention (Yang *et al.*, 2010). The knowledge of *in vivo* forces acting at the human knee and *in vivo* torques acting across the tibiofemoral joint is of great value to clinicians, researchers and implant designers (Komistek *et al.*, 2005; Lanovaz and Ellis, 2009). The value of determining *in vivo* forces and torques could lead to three key outcomes: (*i*) prediction of how new designs will perform; (*ii*) simulation of orthopedic surgery procedures and prediction/optimization of clinical outcome based on surgical parameters under consideration; and (*iii*) investigation of loading mechanisms that contribute to degenerative joint disease, as well as movement modifications or clinical interventions to reduce these effects (Komistek *et al.*, 2005). While dynamic X-ray imaging advances permit accurate measurement of *in vivo* knee joint motion (Lu *et al.*, 2008), a non-invasive and clinically feasible approach for experimental measuring *in vivo* knee joint loading does not exist. Thus, joint contact loads must be predicted by computational models (Lin *et al.*, 2010).

Computational models are becoming an important tool for investigating biomechanical variables that are difficult to address experimentally (Lanovaz and Ellis, 2009). In a broad sense, there are two main computational approaches to model the human body, or a subsystem of it, as a biomechanical system. These methods are either based on the finite element analysis, or the multibody systems methodologies. The finite element methods (FEM) provide the system state of stress and deformation at any time. Although FEM are most accurate and versatile they tend to be very time consuming and require a high level of information on the system, which may not be accessible to the common analyst or designer, and hence remain confined to research and development. Based on simplifying premises, engineers and designers prefer to use simpler and, still, accurate methods, such as those based on the formulation of multibody systems.

By and large, finite element models are applied in cases where localized structural deformations or soft tissues need to be described and analyzed in detail, while multibody models are usually applied in cases where gross-motions are involved and when complex interactions with the surrounding environment are expected (Machado *et*

al., 2010). For instance, finite element analyses have been performed to predict with accuracy surface and subsurface implant stresses under quasi-static loading conditions (Halloran *et al.*, 2005). In turn, the human gait as a gross-motion simulation has been studied by means of MBS formulations. Moreover, when a modeling system is under dynamic loading conditions, MBS methodologies are also usually employed due to its simplicity and computationally efficiency (Landon *et al.*, 2009).

The knee joint has the key role of promoting movement between thigh and calf in order to allow the human subject to walk. It presents a large amplitude of motion, in the range 0-67 degrees during level walking. The knee joint, being the intermediate joint of the lower limb, has to bear the majority of the body weight and to provide stability to the whole body (Nordin and Frankel, 2001). Thus, physiologic loads, produced by muscles, ligaments, articular contact and external forces, have to be taken into account during dynamic simulations, because they may affect the motion characteristics of the knee, as well as the integrity of its surrounding biologic structures (Landon *et al.*, 2009). Multibody-based models are useful and reliable to represent natural and artificial knee joints under realistic dynamic loads.

The current demand and interest in developing mathematical models of the knee joint for studying the dynamic behavior of this biomechanical system, mainly in what concerns with its articular contact response, have motivated this research work. Being the contact-impact problem common in several dynamic systems besides the knee joint, a general methodology for contact analysis is proposed throughout this thesis.

1.2 Literature review

Over the last decades, a number of theoretical and experimental works have been devoted to the simulation of human knee joint. As a rough classification, these knee joint models can be divided into kinematic and dynamic. The purely kinematic models try to describe the motions between femur and tibia, without considering the forces and the torques which act during these motions. Dynamic models have been developed for estimating the forces on ligaments and muscles and between the articular surfaces.

The work of Strasser (1917) was a pioneer in the field of knee joint modeling. The knee model presented by Strasser was a purely kinematic model based on a four-bar linkage, in which two links represent the cruciate ligaments, while the other links

represent the femur and tibia bones. Figure 1.1 shows a schematic representation of the knee joint modeled as a four-bar linkage. Afterwards, this modeling concept introduced by Strasser (1917) was improved by Menschik (1974), who included two curves representing the femur and tibia articular surfaces and investigated the location of the insertion areas of the collateral ligaments.

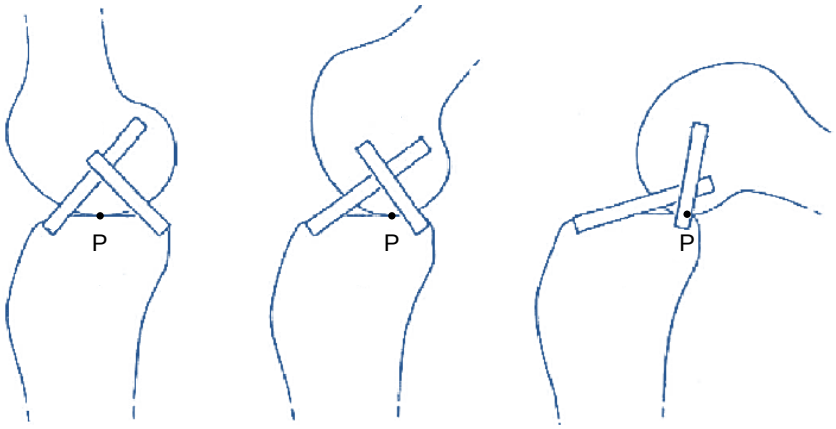

Figure 1.1 Schematic representation of the knee joint as a four-bar linkage, showing posterior displacement of the point of tibiofemoral contact point with flexion {Adapted from Smith *et al.* (2003) with Elsevier permission}.

Freudenstein and Woo (1969) proposed a knee joint model based on a planar mechanism alternative to the classical four-bar linkage, which is illustrated in Figure 1.2. In this work, the relative motion between upper and lower legs at the knee joint has been analyzed as a planar motion, and logarithmic-spiral centrodes have been proposed as representative of this motion.

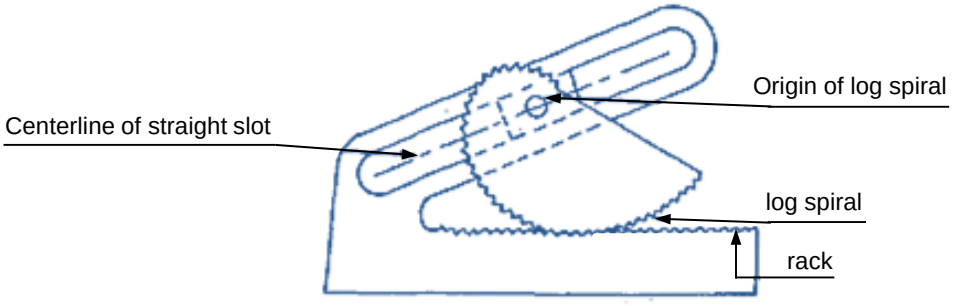

Figure 1.2 Mechanical guidance of log-spiral and rack motion proposed by Freudenstein and Woo (1969) for modeling the knee joint {Adapted from Freudenstein and Woo (1969) with Springer permission}.

Mathematical models with the aim to determine the forces and torques at the knee joint were developed by Morrison (1969, 1970), Kettelkamp and Chao (1972), Smidt (1973), Perry *et al.* (1975), Seedhom and Terayama (1976) and Crowninshield *et al.* (1976). Morrison (1969, 1970) developed a synthetic model analysis incorporated with several experiments that dealt with force actions transmitted by the knee joint during

several activities, such as level walking, walking up and down a ramp, and walking up and down stairs. In this study, the human knee is modeled as a simple hinge joint for sake of simplicity. Kettelkamp and Chao (1972) described a method of determining force distribution on the tibial plateaus of a standing subject and studied the effect of the angle of the tibiofemoral mechanical axes on force distribution. Smidt (1973) performed mathematical analyses for the sagittal plane using data obtained from roentgenograms and a load cell. Within this study, the displacement of the axis of rotation for the human knee joint was evaluated, as well as the moment arm of the knee extensors and knee flexors. Figure 1.3 illustrates the free-body diagram of the human knee joint adopted by Smidt (1973) in his analysis.

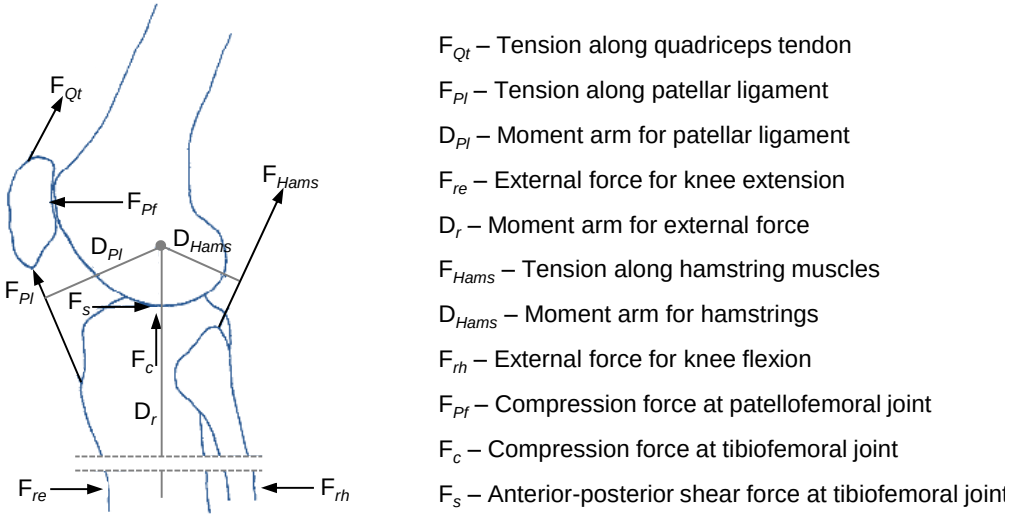

Figure 1.3 Forces and moment arms for knee flexion and extension considered in the analysis performed by Smidt (1973) {Adapted from Smidt (1973) with Elsevier permission}.

Perry *et al.* (1975) measured the forces in the quadriceps, patella and tibia during knee stance flexion by using an instrumented cadaver lower limb. Seedhom and Terayama (1976) performed preliminary analysis of the knee joint forces during the activity of raising from a chair, with and without the aid of arms, by utilizing a planar quasi-static model of the knee joint. Crowninshield *et al.* (1976) presented an analytical model to study the biomechanics of the knee that accounts for the geometry, characteristics of motion and material properties of this joint. In this work, the so-called inverse method was considered, in which the ligament forces caused by a set of translations and rotations in specific directions are determined by comparing the geometries of the initial and displaced configurations of the knee joint. Within this model, the main ligaments of the knee are represented by spring elements that interconnect rigid bodies, which represent the femur and tibia. Figure 1.4 depicts the

locations of ligaments adopted by Crowninshield *et al.* (1976). The internal spring forces were calculated by displacing the femur or tibia about a fixed axis and computing the resulting force in the ligament. The relative effect of a given ligament was also investigated by eliminating it in the model and comparing the result to an actual test where the ligament was transected. The knee model proposed by Crowninshield *et al.* does not account for viscoelastic nature of the knee and, thus is valid only for short-term quasi-static analyses. To overcome this limitation, the model was extended by Pope, Crowninshield and co-workers (1976). This updated version was a rheological model that uses linear viscoelasticity theory to model the knee joint using a Kelvin body idealization. Within this model, Pope *et al.* (1976) studied the behavior of the human knee by means of dynamic, static and creep tests.

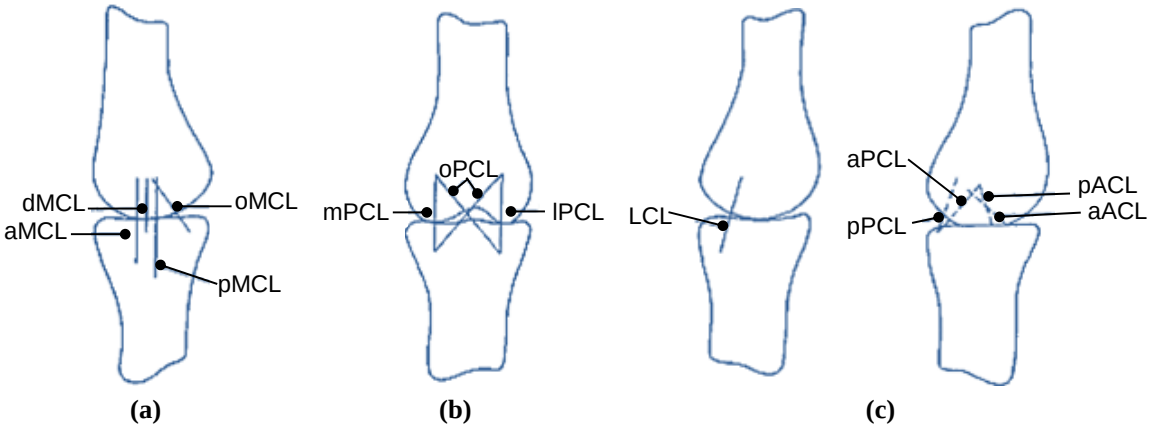

Figure 1.4 Position of ligaments adopted by Crowninshield *et al.* (1976): (a) Medial view; (b) Posterior view; (c) Lateral view. Twelve ligament fibers are represented in this scheme, namely deep (dMCL), oblique (oMCL), anterior (aMCL) and posterior fibers (pMCL) of the medial collateral ligament; medial (mPCL), lateral (lPCL), oblique (oPCL), anterior (aPCL) and posterior fibers (pPCL) of the posterior cruciate ligament; anterior (aACL) and posterior fibers (pACL) of the anterior cruciate ligament; lateral collateral ligament (LCL) {Adapted by Crowninshield *et al.* (1976) with Elsevier permission}.

The first models of the knee joint that can describe forces as well as motions have been presented by Andriacchi *et al.* (1977) and Wismans (1980). Andriacchi *et al.* developed a knee joint model by employing finite element methods. This model is quasi-static and comprises a representation of the proximal tibia, the distal femur, soft tissue structures and contacting surfaces of the medial and lateral condyles. The ligaments and capsule are represented by nonlinear springs, while the joint surfaces are modeled by a number of flat surfaces. Later, Andriacchi *et al.* (1983) proposed an updated version of this model, which includes a representation of the menisci. Within this study, the contact surfaces were modeled by ten hydrostatic elements, while the menisci were represented by using shear beam elements.

Figure 1.5 depicts the knee joint model proposed by Wismans *et al.* (1980). This model is a 3D-representation that takes into account the geometry of the joint surfaces as well as the geometry and material properties of the ligaments and capsule. In this study, the geometry of joint surfaces was fitted to polynomials in space with a least-squares method. The ligaments and capsule are represented by seven nonlinear springs and their mechanical behavior is approximated by a quadratic force-elongation function. The solution method proposed by Wismans (1980) is quasi-static and, hence, a particular flexion angle and an arbitrary system of external forces must be prescribed. Knee sagittal activity is simulated as a series of flexion steps. After each step, the equilibrium positions of the bones are determined from the quasi-static equilibrium equations and the equations describing the contact conditions between the condyles. Thus, for a given loading at various flexion-extension angles, the location of contact points, magnitude and direction of contact forces, magnitude of ligament elongation and ligament forces can be calculated. It is worth noting that the artificial restrictions of the quasi-static inverse method, such as the necessity to specify the preferred configuration, can be eliminated if the dynamic parameters of the problem were included into the model, as it is in the case proposed by Machado *et al.* (2010).

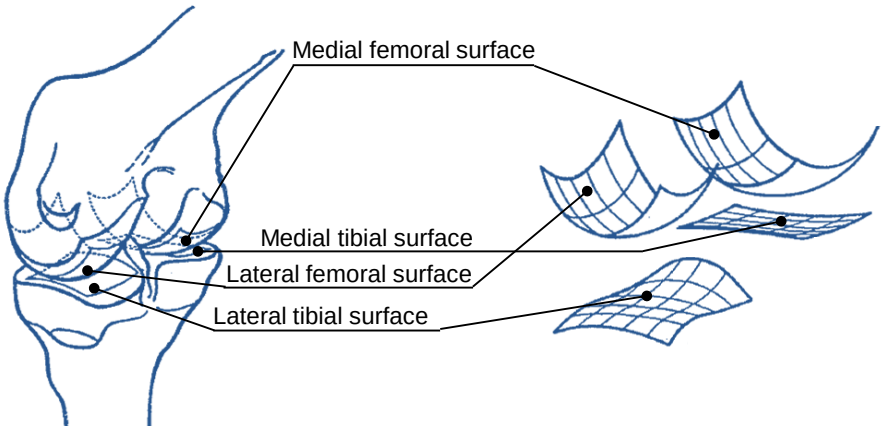

Figure 1.5 Medial and lateral articular surfaces of the 3D-model of the knee joint proposed by Wismans *et al.* (1980) {Adapted from Wismans *et al.* (1980) with Elsevier permission}.

Besides the models presented by Andriacchi *et al.* (1977) and Wismans (1980), other relevant knee models were proposed between 1977 and 1980. Menschik (1977) extended his previous work (1974) by combining the crossed four-bar linkage with a Burmester curve, which is used to define the collateral ligaments. Later, Goodfellow and O'Connor (1978) utilized the idea of the four-bar cruciate linkage to explain the movements of the meniscal bearings in knee prostheses and to justify the use of spherical femoral components for tibiofemoral articulation.

Using static optimization techniques, Hardt (1978) addressed the problem of obtaining individual force histories of all important muscles of the lower limb during normal level walking. The biomechanical model utilized by Hardt, which is composed by the pelvis and the lower limb system. The hip and ankle joints are represented by spherical joints, while the knee is modeled as a simple revolute joint. Wahrenberg *et al.* (1978a, 1978b) utilized also revolute joint models for predicting impulsive reaction forces and moments into the knee joint at the sagittal plane. Within these studies, a theoretical model regarding the lower limb as a double pendulum was used and the kicking motion was studied (Wahrenberg *et al.*, 1978a, 1978b).

Moeinzadeh and Engin dedicated some of their research on the dynamic modeling of human joint structures with special focus on the knee joint (Moeinzadeh, 1981; Engin and Moeinzadeh, 1983; Moeinzadeh and Engin, 1983; Moeinzadeh *et al.*, 1983). Within these studies, a mathematical 2D-model of the human knee joint was developed. Figure 1.6 illustrates this model of the knee joint, which comprises two rigid bodies (femur and tibia) connected by nonlinear springs that represent the ligaments. The contact profiles were described by polynomial functions. Within this model, numerical analyses were performed in order to estimate ligament and contact forces when two kinds of dynamic loads were applied on the tibia, namely a rectangular pulse and an exponentially decaying sinusoidal pulse (Moeinzadeh, 1981; Moeinzadeh and Engin, 1983; Moeinzadeh *et al.*, 1983; Moeinzadeh and Engin, 1988). Moeinzadeh and Engin (1988) extended this dynamic model to the 3D-space, although the dynamic calculations were performed relative only to the sagittal plane (Huiskes, 1992). Numerical solutions for differential algebraic equations (DAE) were employed in both approaches (2D and 3D).

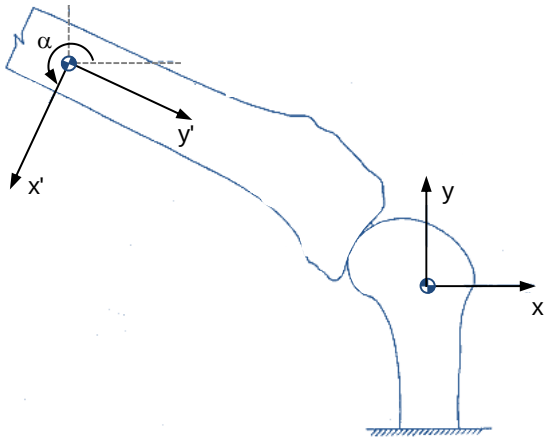

Figure 1.6 Schematic representation of the 2D-model of the knee joint developed by Moeinzadeh {Adapted from Moeinzadeh (1981) with author's permission}.

Grood and Suntay (1983) proposed a convenient coordinate system for describing 3D-joint position with special application to the knee joint. This work was of paramount importance as still is adopted for joint modeling purposes. Other relevant work was performed by Hefzy and Grood (1983) on the dynamic response of the knee ligaments. In this study, the ligaments are modeled as tensile bands running in a straight line and two forms of geometric nonlinearities are introduced and analyzed: ligaments wrapping around bone surfaces and wrapping of ligaments around each other.

Wongchaisuwat *et al.* (1984a, 1984b) demonstrated the key role of the ligaments on the stability of the knee joint throughout their investigation. These authors studied the motion of the human knee in the sagittal plane through an analytical model, which accounts for the geometry of the joint surface, ligaments and some muscle groups. Within these studies, the reaction forces at the contact point between the tibia and the femur were considered to be constraint forces due to three different surface motions, namely gliding, rolling and combined gliding and rolling.

In order to obtain accurate geometrical representations of the joint surfaces, Huiskes *et al.* (1985) introduced an analytical stereophotogrammetric (SPG) technique to measure the 3D-geometry of articular surfaces *in vitro*. This procedure uses a set of two cameras and a slide projector that projects a regular grid on the articular surface to be measured. Later, Ateshian *et al.* (1991) enhanced this method in accuracy and efficiency by proposing an approach to map the cartilage thickness over the entire articular surface. Kurosawa *et al.* (1985) also focused their research on knee geometry and its relation to joint motion. These authors studied the 3D-knee motion by using the center of the posterior femoral condyles as reference points and by analyzing sections of distal femurs in the computer. Within their study, Kurosawa *et al.* (1985) depicted that the posterior femoral condyles can be closely fitted to spherical surfaces.

The work of van Eijden and co-workers (1986) was one of the pioneer studies on dynamic modeling of the patellofemoral joint. They proposed a mathematical model of the patellofemoral joint taking into account movements and forces in the sagittal plane. Figure 1.7 shows this patellofemoral joint model, which enables the calculation of the relative position of the patella, patellar ligament and quadriceps tendon, the location of the patellofemoral contact point and the magnitude of the patellofemoral compression force and the force in the patellar ligament. Within this study, van Eijden *et al.* (1986)

investigated the ratio between patellar ligament force (F_{Pl}) and quadriceps tendon force (F_{Qt}) as a function of knee flexion angle.

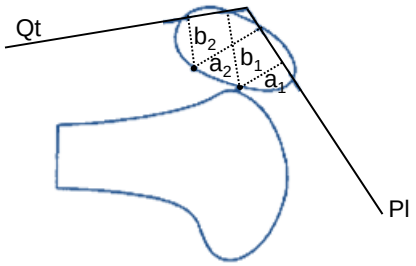

Figure 1.7 3D-model of the patellofemoral joint proposed by Van Eijden *et al.* (1986) {Adapted from van Eijden *et al.* (1986) with Elsevier permission}.

Mikosz *et al.* (1988) developed a mathematical muscle model of the knee joint, which comprises the proximal tibia, the distal femur, the patellar mechanism and 13 muscles crossing the knee joint. This 3D-model accounts for the rolling and gliding movement of the tibiofemoral articulation. The computational technique involves equilibrating three components of external moments at the knee joint to the internal moments generated by muscular forces and soft tissue. In this work, the variables contained in the moment equilibrium equation are randomly chosen based on the choice of the tibiofemoral contact point.

An extensive review of mathematical models of the knee joint was published by Hefzy and Grood in 1988 and, later, updated by Hefzy and Cooke (1996). These authors classified the mathematical knee models into two types: phenomenological and anatomically based models. The phenomenological models are gross models, describing the overall response of the knee without considering its real substructures, such as articular surfaces and ligaments. These models are further categorized into simple hinge models and rheological models (*i.e.*, knee is modeled as a viscoelastic joint). Examples of simple hinge models are the ones proposed by Morrison (1969, 1970), Hardt (1978) and Wahrenberg *et al.* (1978a, 1978b). The models presented by Crowninshield *et al.* (1976) and Pope *et al.* (1976) are examples of rheological models. In turn, anatomically based models are developed to study the behaviors of the various structures forming the knee joint. These models require accurate description of the geometry and material properties of knee components. Hefzy and Grood (1988) classified the anatomically based models into kinematic and kinetic models. Kinematic models describe and establish relations between motion parameters of the knee joint. They do not relate these motion parameters to the loading conditions. Since the knee is a highly compliant

structure, the relations between motion parameters are heavily dependent on loading conditions making each of these models valid only under a specific loading condition. Kinetic models relate the motion parameters to the joint loading condition. These models fall into two groups: quasi-static and dynamic. Quasi-static models determine forces and motion parameters of the knee joint through solution of the equilibrium equations, subject to appropriate constraints, at a specific knee position. This procedure is repeated at other positions to cover the range of motion of the knee joint. Quasi-static models are unable to predict the effects of dynamic inertial loads which occur in many locomotion activities. Examples of quasi-static models are the ones proposed by Andriacchi *et al.* (1977, 1983) and Wismans (1980). In turn, dynamic models solve the differential equations of motion, subject to relevant constraints, to obtain the forces and motion parameters of the knee joint under dynamic loading conditions (Hefzy and Abdel-Rahman, 2000). An example of a dynamic formulation used to model the knee joint is the one proposed by Moeinzadeh and his co-workers (Moeinzadeh, 1981; Moeinzadeh *et al.*, 1983; Moeinzadeh and Engin, 1988).

Huson *et al.* (1989) described a kinematic model of the human knee by using a four-bar linkage, giving emphasis to the functional relation between several morphological characteristics concerning the shape of the articular surfaces and the constellation of the cruciate ligaments. Six combined configurations of the ligaments and articular surfaces were investigated by Huson *et al.* (1989). Zavatsky and O'Connor (1992a, 1992b) presented a mathematical model of the knee ligaments in the sagittal plane, where the cruciate ligament fibers were represented as isometric links in a kinematic mechanism that controls passive knee flexion. The proposed model was used to analyze the shape and fiber length changes of the cruciate and collateral ligaments in response to passive motion of the knee.

Chittajallu and Kohrt (1996) described also a planar model of passive knee motion that includes the four major ligaments of the knee, namely anterior cruciate ligament (ACL), posterior cruciate ligament (PCL), medial collateral ligament (MCL) and lateral collateral ligament (LCL). This model comprised two four-bar linkages as Figure 1.8 depicts. The ACL and PCL formed one four-bar linkage while the MCL and LCL formed the second one. Tibia and femur were the ground and coupler links, respectively, in both linkages.

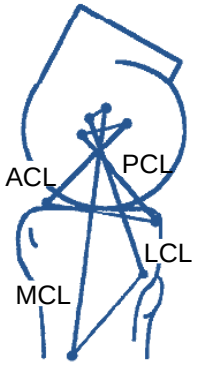

Figure 1.8 Knee joint model based on two four-bar linkages presented by Chittajallu and Kohrt (1996) {Adapted from Chittajallu and Kohrt (1996) with Elsevier permission}.

Lu and Lu (2006) described also the mobility of the tibiofemoral joint by means of a four-bar linkage, formed by the isometric fibers of the ACL and PCL and the lines joining their attachments on the femur and tibia. In this study, the forces transmitted by the force-bearing structures of the knee joint during normal stair ascent and descent were analyzed and their mechanical differences were evaluated. The 2D-model of the human locomotor system proposed by Lu *et al.* (1998) was adopted in this work, which is comprised by four rigid bodies, namely the pelvis, thigh, shank and foot. Eight muscles were incorporated into the lower limb model. A knee extensor mechanism composed of the patellofemoral joint, patellar ligament and quadriceps tendons was also included into the model (Gill and O'Connor, 1996).

Farhat *et al.* (2010) proposed a dynamic model for the lower extremity capable of estimating forces in the cruciate and collateral ligaments and those normal to the articular cartilage generated in the knee. Within this study, the knee is modeled, once again, as a four-bar linkage. The pelvis is represented by a spherical joint, while the ankle is approximated to a revolute joint. Figure 1.9 shows the four-bar linkage used by Farhat *et al.* (2010) to simulate the knee joint motion, which was obtained by a kinematic synthesis process. This model includes also the main knee muscles, being their forces estimated by static optimization.

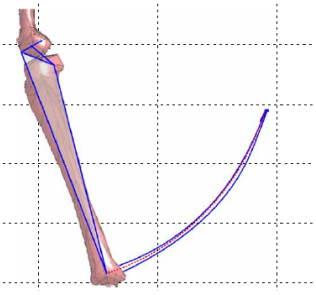

Figure 1.9 Knee joint model based on a four-bar linkage proposed by Farhat *et al.* (2010) {Adapted from Farhat *et al.* (2010) with Taylor & Francis permission}.

As far as the prosthetic knees are concerned, Essinger *et al.* (1989) developed a quasi-static knee model to evaluate the mechanical behavior during flexion of knee prosthesis. The tibial and femoral surfaces are defined as deformable and rigid, respectively. The model includes also a simplified patellofemoral joint. In this work, the 3D-shape of the articular surfaces is mathematically described, as well as the ligaments and capsule structures. Later, Garg and Walker (1990) focused their study on the geometry of the knee prosthesis and investigated the influence of the congruency of the contact surface on the dynamic response of the knee. Therefore, a mathematical model of the knee joint is utilized to quantify the effect of tibia surface geometry and prosthetic component placement on ligament length change and maximum achievable range of motion. In this work, three configurations for the surfaces of total knee replacements (TKR) are considered, namely flat, laxity and conforming.

The contributions of Abdel-Rahman and Hefzy on the development of mathematical models of the knee joint for dynamic analysis are worthy to highlight. As a first step, Abdel-Rahman and Hefzy (1991) presented a 2D-dynamic model of the knee joint similar to the work proposed by Moeinzadeh *et al.* (1983). This model comprised two rigid bodies, namely a fixed femur and a moving tibia, connected by ten nonlinear springs, which represent the different fibers of the ACL, PCL, MCL, LCL, and the posterior part of the knee capsule. Within this formulation, part of a circle is used to represent the profile of the femur and, the tibia is described by means of a parabolic polynomial function. Abdel-Rahman and Hefzy (1991) evaluated the dynamic response of the knee joint undern a sudden impact, which was simulated by a posterior forcing pulse in the form of a rectangular step function applied to the tibial center of gravity. Later, this planar model of the knee joint was updated (Abdel-Rahman and Hefzy, 1993). In the new version of the model, the joint profiles are described by polynomial functions and a single point contact is assumed to exist at all times. As in the previous work (Abdel-Rahman and Hefzy, 1991), the knee response was determined under sudden rectangular pulsing posterior forces applied to tibia, being considered different amplitudes and durations (Abdel-Rahman and Hefzy, 1993).

Abdel-Rahman *et al.* (1996) proposed a 3D-dynamic model of the knee joint, which was later enhanced by Abdel-Rahman and Hefzy (1998). This model is composed by two body segments in contact, the femur and the tibia, performing a general spatial motion within the constraints of the ligamentous structures, which are

modeled as nonlinear elastic springs. The femoral articular surfaces are approximated by spherical surfaces, while the tibial plateaus are considered to be planar surfaces. These articular surfaces are depicted in Figure 1.10. In this work, the dynamic response of the tibiofemoral joint when subjected to sudden external loads was analyzed. Afterwards, Caruntu and Hefzy (2004) included the patellofemoral joint into this model. Instead of modeling the articular surfaces as spheres or planes, Caruntu and Hefzy used Coons' bicubic surfaces. Two joint coordinate frames were applied to describe the six degrees-of-freedom motions of the tibiofemoral and patellofemoral joints using twelve kinematic parameters. The contact forces were evaluated using a linear elastic foundation model, which was formerly used on knee by Blankevoort *et al.* (1991).

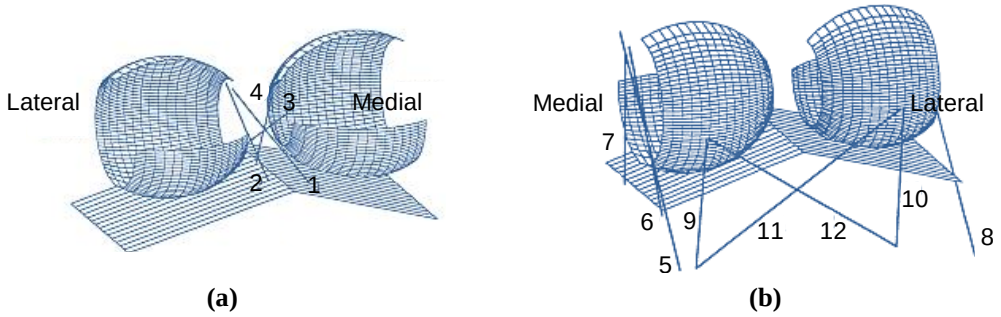

Figure 1.10 3D-model of the knee joint proposed by Abdel-Rahman and Hefzy (1998), showing the articular surfaces and 12 ligaments: (a) Anterior view; (b) Posterior view. The represented ligaments are: (1) anterior fibers of ACL, (2) posterior fibers of ACL, (3) anterior fibers of PCL, (4) posterior fibers of PCL, (5) anterior fibers of MCL, (6) oblique fibers of MCL, (7) deep fibers of MCL, (8) LCL, (9) medial fibers of posterior capsule, (10) lateral fibers of posterior capsule, (11) oblique popliteal ligament and (12) arcuate popliteal ligament {Adapted from Abdel-Rahman and Hefzy (1998) with Elsevier permission}.

Blankevoort *et al.* (1991) focused their study on the effect of articular contact on the passive motion characteristics of the knee joint by using a mathematical 3D-model, which is illustrated in Figure 1.11. In this analysis, two distinct mathematical contact descriptions are compared, namely rigid and deformable contact approaches. The methodology adopted for deformable contact is based on the simplified theory of contact developed by Kalker (1990) for thin layers of isotropic and linear-elastic material bonded to a rigid foundation. Blankevoort *et al.* (1991) investigated the consequences of a deformable contact formulation in their model by varying cartilage stiffness values in both linear and nonlinear elastic models. The ligament properties are described as nonlinear and time-dependent. Blankevoort *et al.* (1991) depicted that the incorporation of deformable contact did not alter the motion characteristics in a qualitative sense, and that the quantitative changes were small. Moreover, it was also concluded that the deformable contact is a valid approach when aiming to study of the

passive motion characteristics of the knee joint under moderate loading conditions. Blankevoort and Huiskes (1991) proposed a model for wrapping of a ligament around bone within a mathematical 3D-model of the human knee. The bony edge is described by a curved line in which the contact point of the line element representing a ligament is located. Five years later, this formulation was updated by the same authors (Blankevoort and Huiskes, 1996). This enhanced version includes a geometrical description of the articular surfaces, which are covered by a thin layer of deformable cartilage and connected by an arbitrary number of nonlinear elastic elements that represent the ligaments. The femur is assumed to move relative to the tibia and the constraint forces and moments respond to the prescribed degrees-of-freedom. This quasi-static model relies upon the equilibrium of forces and moments on the knee joint from externally applied loads, ligament forces, contact forces and/or constraint loads.

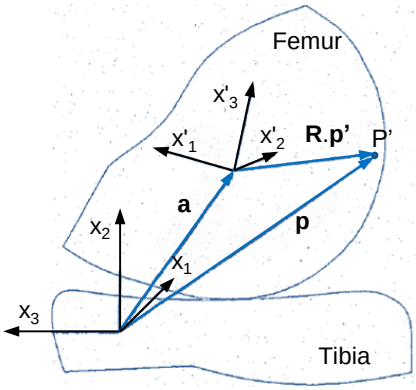

Figure 1.11 Knee model proposed by Blankevoort *et al.* (1991). The coordinate axis (x_1, x_2, x_3) is associated with the tibia and is space-fixed, while the coordinate axis (x'_1, x'_2, x'_3) is related to the femur and is body-fixed. A material point P' is described by the vector **p**, relative to the space-fixed system, and by the vector **R.p'**, relative to body-frame. The vector **a** describes the translation of the body-fixed origin relative to the space-fixed origin {Adapted from Blankevoort *et al.* (1991) with Elsevier permission}.

In 1995, Blankevoort and Huiskes collaborated also with Mommersteeg and other three co-workers on the development of a novel concept for modeling the ligaments as multi-bundle structures with non-uniform mechanical properties and zero force lengths. The proposed novel concept for modeling the ligaments was validated within a 3D-model of the human knee joint, which is illustrated in Figure 1.12. This model describes the position of the femur relative to the tibia for a given configuration of external loads and kinematic constraints (Mommersteeg *et al.*, 1995).

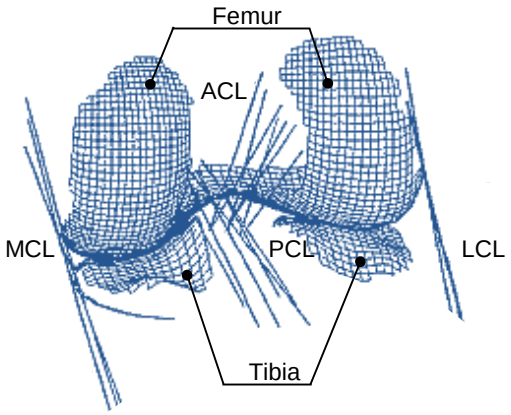

Figure 1.12 Representation of the 3D-model of the knee joint proposed by Mommersteeg *et al.* (1995) {Adapted from Mommersteeg *et al.* (1995) with Elsevier permission}.

Following the work of van Eijden *et al.* (1986), Hirokawa (1991) presented one of the first three-dimensional models of the patellofemoral joint. Figure 1.13 illustrates this model, which takes into account the geometry of the articular surfaces and the mechanical properties of the patellar ligament. Within this study, several variables, such as patellofemoral contact force and tensile force of the patellar ligament, were computed for various knee flexion angles. The patellar contact stress was evaluated by using the Hertz contact law. In 1993, this author published a comprehensive literature survey concerning kinematic and kinetic studies on the knee joint (Hirokawa, 1993).

Loch *et al.* (1992) developed a mathematical 3D-model of the human knee joint in order to examine the role of single ligaments on joint motion and tissue forces. The proposed model relies on a linear approach and is valid for the analysis of small motions about an equilibrium position. Figure 1.14 illustrates this model, which comprises two rigid bodies (femur and tibia) interconnected by deformable structures, including ligaments and articular cartilage.

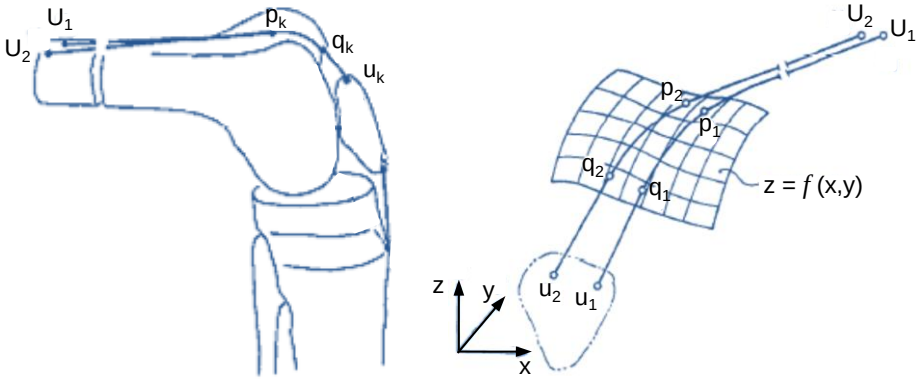

Figure 1.13 Patellofemoral joint model proposed by Hirokawa (1991): (a) Sagittal view at 90 degrees of knee flexion; (b) Close-up of the tendofemoral contact portion {Adapted from Hirokawa (1991) with Elsevier permission}.

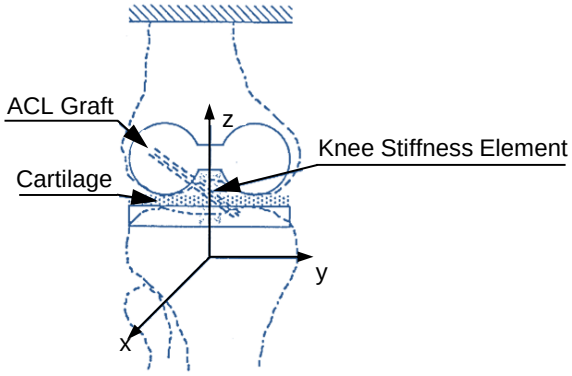

Figure 1.14 Anterior view of the theoretical model of the right knee proposed by Loch *et al.* (1992) {Adapted from Loch *et al.* (1992) with Elsevier permission}.

Hefzy *et al.* (1992) carried out a study with the purpose of to determine the effect of tibial rotations on the patellofemoral motion and contact areas during a physiological loading condition. In this work, a commercially available device, named the 3-SPACE digitizer and tracker system, was used to collect the motion data, utilizing cadaveric human lower limbs, and the geometric measurements describing the articular surfaces of the patellofemoral joint. The articular surfaces are mathematically represented by piecewise continuous parametric Coons' bicubic surface patches. Later, Hefzy and Yang (1993) presented a mathematical 3D-model of the patellofemoral joint, which comprises two rigid bodies representing a moving patella and a fixed femur, as Figure 1.15 depicts. The femoral and patellar surfaces are mathematically represented using Coons bicubic surface patches, as in author previous work (Hefzy *et al.*, 1992). The model included eleven constraints, namely six contact conditions, four geometric conditions, and the condition of a rigid patellar ligament. The forces acting on the patella comprise the medial and lateral patellofemoral contact and the patellar ligament force, all of which were represented as ratios to the quadriceps tendon force.

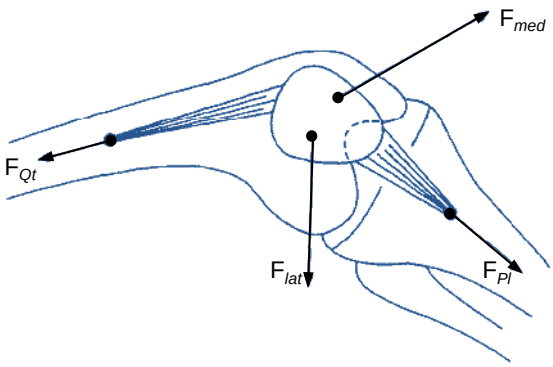

Figure 1.15 Patellofemoral forces considered by Hefzy and Yang (1993): quadriceps tendon force (F_{Qt}), patellar ligament force (F_{Pl}), patellofemoral contact forces at the medial (F_{med}) and lateral (F_{lat}) side of the knee {Adapted from Hefzy and Yang (1993) with Elsevier permission}.

Tümer and Engin (1993) introduced a 2D-dynamic model of the human knee, comprising three body segments: femur, tibia and patella. These rigid bodies are connected by five ligaments, namely ACL, PCL, MCL, LCL, and patellar ligament. Both knee articulations, tibiofemoral and patellofemoral, are considered. According to Tümer and Engin (1993), this model permits to analyze the dynamic response of the knee for any one or combination of quadriceps femoris, hamstrings, and gastrocnemius muscle actions, as well as any externally applied forces on the lower leg. Within this study, dynamic simulations were performed for knee extension under the impulsive action of the quadriceps femoris group in order to simulate a lower limb activity such as kicking motion. Patellofemoral contact force was also evaluated in this work.

Bendjaballah *et al.* (1995) developed a 3D-nonlinear FEM model of the knee, which is shown in Figure 1.16. This model is composed by three bony structures (tibia, femur and patella) and corresponding cartilage layers, medial and lateral menisci, and five principal ligaments (ACL, PCL, MCL, LCL and patellar ligament). The menisci are represented as a non-homogeneous composite of a solid matrix reinforced by radial and circumferential collagen fibers. The articular cartilage is modeled as a frictionless contact material. For simulation purposes, the tibia is considered to be fixed while the femur is set free to translate in medial-lateral, anterior-posterior, and proximal-distal directions. Also, scenarios of knee total meniscetomy were considered for simulation.

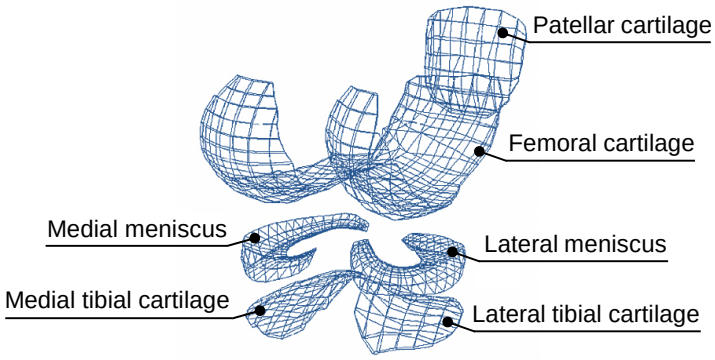

Figure 1.16 FE-mesh of 8-node solid elements proposed by Bendjaballah *et al.* (1995) for knee cartilage layers and menisci {Adapted from Bendjaballah *et al.* (1995) with Elsevier permission}.

Heegard *et al.* (1995) performed a study oriented toward an accurate and reliable determination of the human patella biomechanics during passive knee flexion. For this purpose, a FEM-based model of this joint was developed, which is depicted in Figure 1.17. This model is able to compute simultaneously joint kinematics, ligament forces and articular contact pressures and stresses. The knee joint components (bone, cartilage, tendons) are modeled using objective forms of nonlinear elastic material laws. Within

this study, a unilateral contact law allowing for large slip between the patella and the femur was implemented using an augmented Lagrangian formulation.

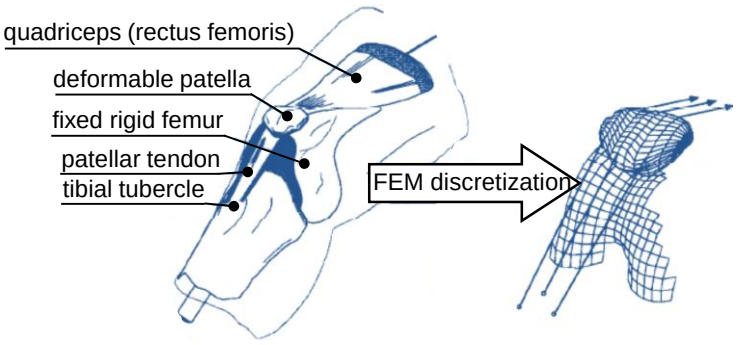

Figure 1.17 Patellofemoral 3D-model proposed by Heegard *et al.* (1995) and its corresponding FE-mesh {Adapted from Heegard *et al.* (1995) with Elsevier permission}.

O'Connor and co-workers dedicated some of their research on knee modeling based upon multibody system methodologies (Gill and O'Connor, 1996; Wilson and O'Connor, 1997; Wilson *et al.*, 1998). Gill and O'Connor (1996) proposed a biarticulating 2D-model of the patellofemoral joint for estimating the proximal rolling of the patella on the femur during flexion. This model included two separate articulations on the patella, representing the medial ridge and lateral facets, in order to allow for the prediction of transfer of contact from the trochlea to the femoral condyles at high knee flexion angles. Within this study, Gill and O'Connor (1996) related the kinematics and mechanics of the patella to the geometry and mechanics of the cruciate ligaments and the tibiofemoral joint. Furthermore, the incongruity of the patella is explained by the necessity of the patella to roll on the femur to ensure the mechanical equilibrium of the joint. Figure 1.18 shows the biarticulating 2D-model of the knee joint proposed by Gill and O'Connor (1996), where it is represented the normal direction of the patellofemoral contact force for 10, 90 and 140 degrees of knee flexion.

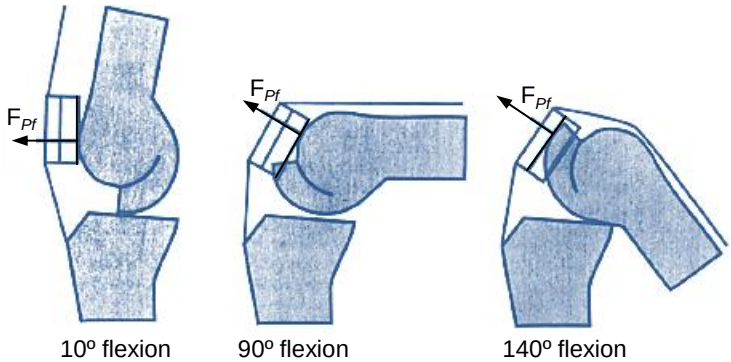

Figure 1.18 Knee joint model proposed by Gill and O'Connor (1996). The normal direction of the patellofemoral contact force (F_{Pf}) is depicted for 10, 90 and 140 degrees of knee flexion {Adapted from Gill and O'Connor (1996) with Elsevier permission}.

Wilson and O'Connor (1997) proposed a model for the human knee with two main purposes: (*i*) to estimate the lines of action of the forces through the ACL, PCL, MCL and at articular contact in the medial and lateral compartments; (*ii*) to predict the changing position and orientation of the axis of rotation of the knee. In this model, the ligaments act as constraints to the motion between tibia and femur, which are considered as rigid bodies. Also, it is assumed that there is an isometric fascicle in the ACL, in the PCL and in the MCL, but that there is no isometric fascicle in the LCL. Each isometric fascicle is represented as an inextensible constraint on the motion between the tibia and the femur. The posterior femoral condyles are modeled as spherical surfaces, while the tibial condyles are considered to be flat. The articular surfaces in both compartments are assumed to remain in contact through the range of flexion of the knee. Wilson *et al.* (1998) extended their previous work (Wilson and O'Connor, 1997) and investigated the hypothesis that the coupled features of passive knee flexion are guided by articular contact and by the ACL, PCL and MCL. Therefore, a mathematical 3D-model of the knee was developed, in which the articular surfaces in the lateral and medial compartments and the ACL, PCL and MCL are represented as five constraints in a one DOF parallel spatial mechanism. The femur and tibia are modeled as rigid bodies and a single point contact is assumed to exist at all times in both compartments. Medial and lateral articular constraints are each represented by a spherical pair at the center of the femoral condyle connected by a rod to a planar pair at the point of contact on the tibial plateau, as Figure 1.19 shows. Each ligament is represented by a rod connecting a spherical joint on the tibia to a spherical joint on the femur. The resulting configuration is a parallel spatial mechanism similar to a Stewart platform robotic manipulator that allows for rolling and sliding at the contact point.

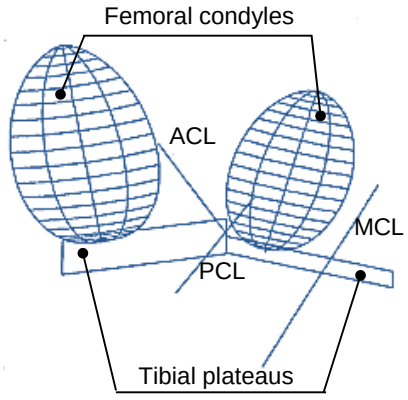

Figure 1.19 Frontal view of the parallel spatial mechanism model of the knee joint proposed by Wilson *et al.* (1998) {Adapted from Wilson *et al.* (1998) with Elsevier permission}.

Ling *et al.* (1997) used a planar model of the knee joint in the sagittal plane to investigate some biomechanical features of knee mechanics, such as the joint surface contact point, ligament forces, instantaneous center and slide/roll ratio between the femur and tibia. In this study, the profile of the femur is described with two segments, namely a four-order polynomial and other analytical function. A second-order polynomial is also generated to describe the 2D-profile of the tibia in the sagittal plane. The articular surfaces are considered frictionless and five knee ligaments are included in the model, namely ACL, PCL, MCL, LCL and patellar ligament (Ling *et al.*, 1997).

Pandy and co-workers devoted some of their research to knee and muscle modeling (Pandy *et al.*, 1997; Shelburne and Pandy, 1997; Pandy and Sasaki, 1998). Pandy *et al.* (1997) developed a 3D-model of the knee joint to study the interactions between the muscles, ligaments, and bones during physical activity. Elastic elements are used to describe the geometry and mechanical properties of the cruciate ligaments, the collateral ligaments, and the posterior capsule. The model is actuated by musculotendinous units, being each of them composed by a Hill-type contractile element, a series-elastic element, and a parallel-elastic element. The tendons are assumed to be elastic. The femoral condyles are described by high-order polynomials and the tibial plateaus and patellar facets are fitted to flat surfaces. The contacting surfaces of the femur and tibia are modeled as deformable, while those of the femur and patella are assumed to be rigid. Tibiofemoral indentation is determined by modeling cartilage as a thin, linear elastic layer, mounted on rigid bone, as Figure 1.20 shows.

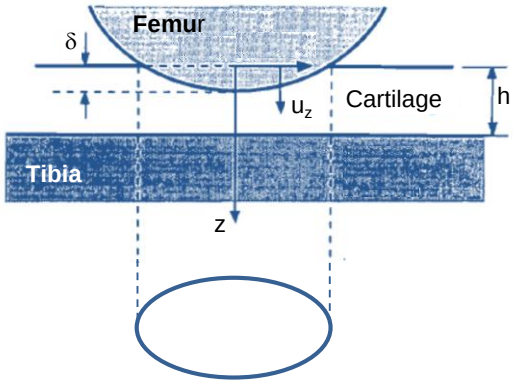

Figure 1.20 The elastic foundation model used by Pandy *et al.* (1997) to calculate the pressure distributions at the tibiofemoral joint. The transverse section of the deformed elastic layer is assumed to be an ellipse. The pressure at any point within the contact area depends on the normal displacement (u_z). The stiffness of the contact layer is denoted as *h*. The profile of the pressure distribution is assumed to be paraboloidal {Adapted from Pandy *et al.* (1997) with Taylor & Francis permission}.

Shelburne and Pandy (1997) analyzed the forces in the ligaments induced by isometric contractions of the extensor and flexor muscles within a 3D-knee model. Figure 1.21 illustrates the knee joint model utilized by Shelburne and Pandy (1997), which is an updated version of the model presented by Pandy *et al.* (1997). In this enhanced version, the patella is included and assumed to be rectangular. Furthermore, 2D-splines are considered to describe the lateral femoral condyle and the femoral groove, while the tibial plateau is modeled as a flat surface sloped 8 degrees posteriorly in the sagittal plane (Shelburne and Pandy, 1997).

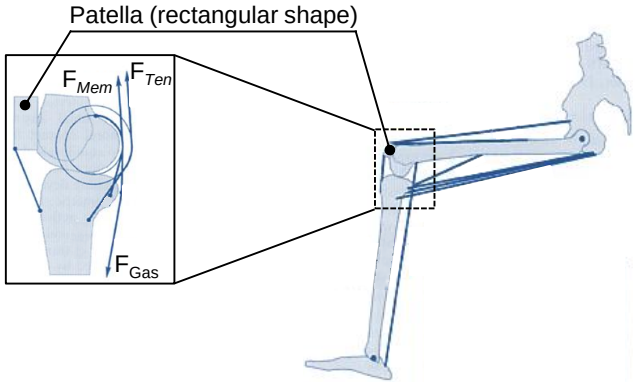

Figure 1.21 Schematic representation of the musculoskeletal knee model proposed by Shelburne and Pandy (1997) {Adapted from Shelburne and Pandy (1997) with Elsevier permission}.

After his contribution on the development of the 3D-model of the knee presented by Pandy *et al.* (1997), Kim (1998) utilized this model to study the interactions between the articular surfaces and the geometrical and mechanical properties of the ligaments. Figure 1.22 illustrates the eight contact surfaces considered in this knee joint model. The tibial plateaux and the surface of each patellar facet were approximated as flat surfaces, while the femoral condyles and the surfaces of the femoral groove were modeled by fitting polynomials to cadaver data. Within this model, the common normal concept is applied to detect contact, while the elastic foundation model is used to calculate the contact forces at the medial and lateral compartments of the knee joint. Twelve elastic elements are used to describe the function of the ligamentous and capsular structures of the knee. In order to assess the accuracy of the model calculations, some cadaveric experiments were carried out. An experimental setup was used to perform leg raise tasks by means of cadaveric knee specimens. In these experiments, the intact knee was extended by a known force applied to the quadriceps tendon, with and without weights attached to the ankle. The response of the model to both anterior-posterior drawer and axial rotation suggested that the geometrical and mechanical properties of the model ligaments approximate the behavior of real

ligaments in the intact knee. By comparing this response with experimental data obtained from cadaveric knee extension, it was concluded that the 3D-model reproduces the response of the real knee during movement.

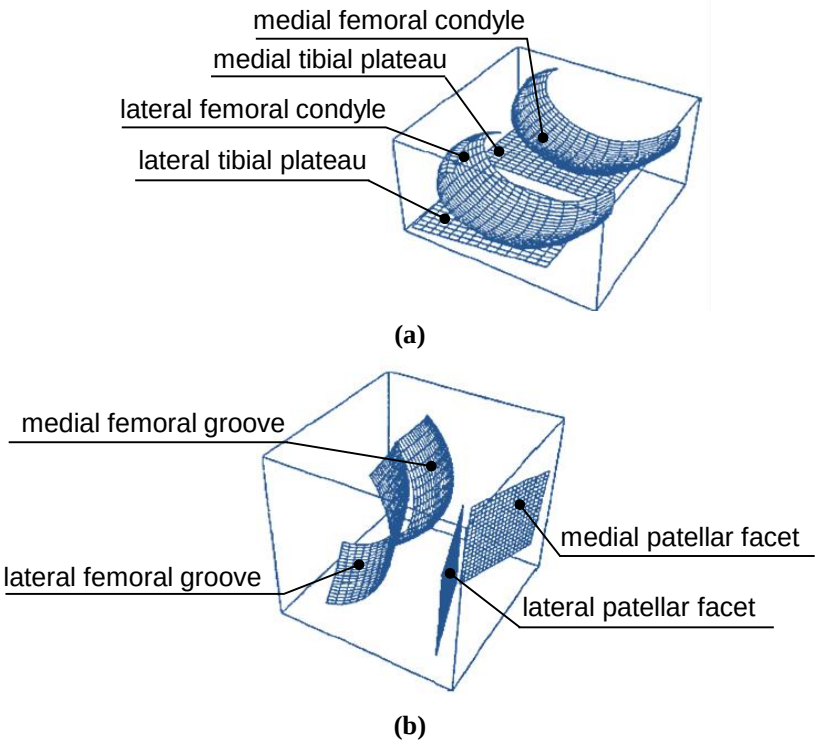

Figure 1.22 Representation of the knee articular surfaces proposed by Kim (1998): (a) Tibiofemoral joint; (b) Patellofemoral joint {Adapted from Kim (1998) with Springer permission}.

Regarding TKR systems, the studies of Sathasivam and Walker (1997) and Wimmer and Andriacchi (1997) should be highlighted. Sathasivam and Walker (1997) introduced a TKR model that could determine the displacements and rotations as a function of condylar geometry, compressive force, soft tissue restraints and surface friction. The validity of this model was determined by comparing the results with experimental data from a knee simulator machine. The model was used to investigate the effect of friction and soft tissue restraint on the motion and contact point locations for a range of input forces and moments. In turn, Wimmer and Andriacchi (1997) analyzed the tractive forces during the rolling motion at the knee joint in order to determine which factors cause these forces to increase in TKR systems. With the aim of calculating these traction forces, Wimmer and Andriacchi (1997) utilized the knee joint model that is illustrated in Figure 1.23. The curvature of the femoral condyle is modeled as a cylinder, with a radius of 55 mm, while the tibial component is considered to be planar with a 10 degrees slope. The inputs for this model are: the shape of the articulating surface, coefficient of friction, contact path, muscle anatomy and gait

kinetics common to patients with a TKR. Within this model, the effects of variations in the coefficient of friction, gait characteristics, antagonistic muscle contraction and patellofemoral mechanics were evaluated. Furthermore, the implications of the tractive forces to polyethylene wear were investigated.

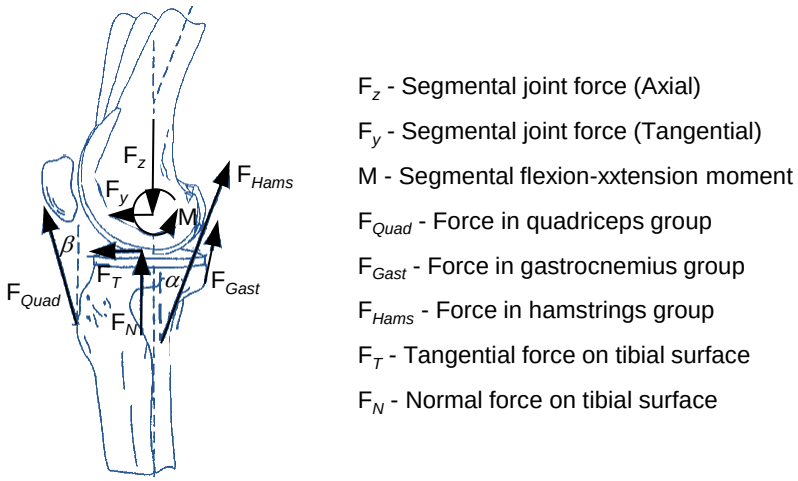

Figure 1.23 Sagittal view of artificial knee model of Wimmer and Andriacchi (1997). The muscle groups crossing the knee are represented. Patellar ligament angle (β) changes with flexion angle (α) {Adapted from Wimmer and Andriacchi (1997) with Elsevier permission}.

Zhu *et al.* (1999) proposed a framework for modeling subject-specific knee joint systems. This framework is divided in four steps: (*i*) development of a subject-specific 3D-model of the knee joint; (*ii*) calculation of contact stresses; (*iii*) integration of knee kinematics and pressure distribution within a human gait model; (*iv*) virtual examination with interactive visualization. Within this work, surface fitting methods are used to find accurate mathematical representations of the articular surfaces, while the contact forces are computed by using Hertz contact law (Zhu *et al.*, 1999). In 2001, Chen *et al.* applied this modeling framework to develop a biomechanical model of the knee joint. This model comprises two rigid bodies (femur and tibia), ligaments, articular surfaces and menisci. Ligaments and capsule are modeled by seven nonlinear springs, while the tibiofemoral contact areas are reduced to contact points. The articular surfaces are described by fitting a parametric surface (a *n*-degree bivariable parametric polynomial surface) to the points of the tibial plateau and the femoral condyle in the 3D polygon mesh of the knee model. The menisci are modeled by elastic springs, being Hook's law applied to calculate the forces generated by these springs. Figure 1.24 depicts the biomechanical model presented by Chen *et al.* (2001). Later, Zhu and Chen (2004) proposed a new method for simulating and visualizing femur-menisci contact in human knee joint using computer generated 3D-models. The development of these 3D-models followed the framework proposed in author's previous work (Zhu *et al.*, 1999). Femur

and tibia are considered to be rigid and continuously in contact at one or two points. In this work, the deformation of menisci was explained throughout four steps: (*i*) acquisition of the feature curves; (*ii*) definition of the internal forces on each feature point; (*iii*) deformation of the feature curves by using a physically-based deformation method; (*iv*) deformation of the remaining points of the model by using a spatial deformation method. Within this study, the contact area between menisci and femur is computed by applying the collision detection library RAPID (Zhu and Chen, 2004).

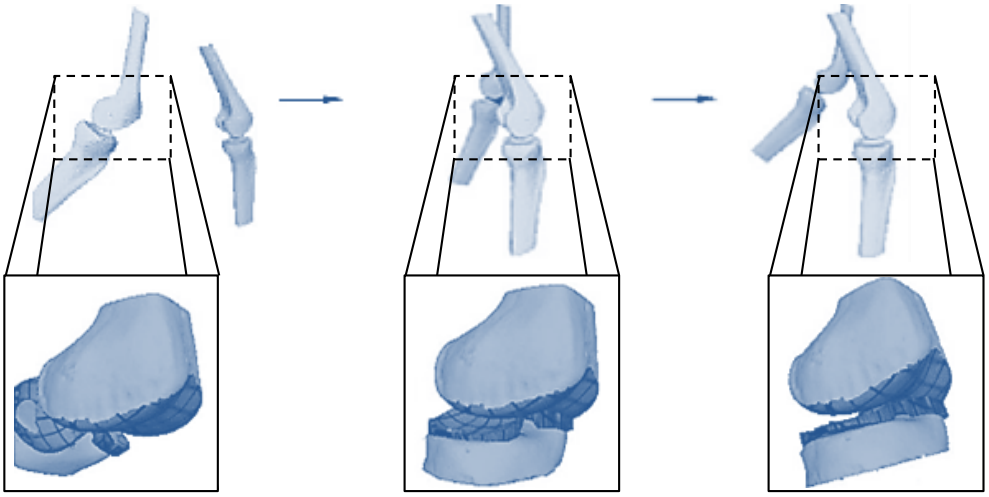

Figure 1.24 Schematic diagram of the biomechanical model of Chen *et al.* (2001) during a walking simulation {Adapted from Zhu *et al.* (1999); Chen *et al.* (2001) with IEEE permission}.

A quasi-static formulation for modeling diarthrodial joints using MBS methodologies was presented by Kwak *et al.* (2000). Figure 1.25 represents a general 3D-model of diarthrodial joint that allows for the inclusion of articular surfaces, muscles, tendons, ligaments, and the wrapping of soft tissues around bone and cartilage. The geometry of the articular surfaces is represented by parametric functions. Within this model, the computational efficiency is enhanced by the use of analytical Jacobians.

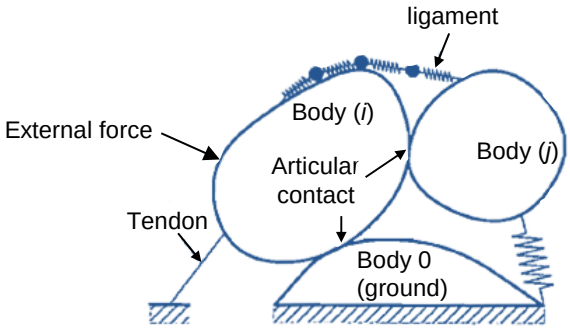

Figure 1.25 Three-dimensional multibody model of a diarthrodial joint proposed by Kwak *et al.* (2000) {Adapted from Kwak *et al.* (2000) with Taylor & Francis permission}.

Piazza and Delp (2001) develop a six-segment model of the human body for use in a forward dynamic simulation of a step-up task. It is worth noting that this is one of the first models of whole body that did not consider the knee as a hinge joint. In this study, the knee is modeled as two free articular systems: the tibiofemoral and patellofemoral joints. This model is utilized to predict the motions of knee implants by means of the action of thirteen muscles crossing the joint. The collateral and patellar ligaments are modeled as purely elastic tensile springs with quadratic force-strain relations. The femoral, tibial, and patellar components are represented by 3D-polyhedral meshes. The locations of contact points are determined using RAPID, while implant contact forces are computed as a solution of a linear complementarity problem (LCP).

A similar work to the published by Piazza and Delp (2001) was performed by McLean *et al.* (2003), who presented also a subject-specific 3D-model of the lower limb. The aim of this work was to predict neuromuscular control effects on knee joint loading during movements that can potentially cause injury to the ACL. The inputs of the forward dynamic model were the initial position and velocity of the skeletal elements, and the muscle stimulation patterns, while the outputs were movement and ground reaction forces (GRF), as well as resultant forces and moments acting across the knee joint. An optimization method was utilized to find muscle stimulation patterns that best reproduced the subject's movement and GRF during a sidestepping task.

Donahue *et al.* (2002) investigated how the variables associated with a meniscal replacement affect tibiofemoral contact by utilizing a 3D-finite element model of the knee joint. This model includes the cortical and trabecular bone of the femur and tibia, articular cartilage of the femoral condyles and tibial plateaus, the medial and lateral menisci with their horn attachments, the transverse ligament, the ACL, and the MCL. The main goals of this study were: (*i*) to determine to what extent bony deformations affect contact behavior; and (*ii*) to verify whether constraining rotations affect the contact behavior of the joint during compressive loading (Donahue *et al.*, 2002). Penrose *et al.* (2002) presented also a detailed FEM model of the human knee. These authors utilized the FEM model to validate the gross kinematic response of the human knee. For this purpose, four scenarios of daily activities were considered, namely gait cycle, stair descent, frontal car crash and pedestrian impact. Godest *et al.* (2002) utilized finite element methodologies to study both the knee kinematics and its internal stresses. In this work, a wear analysis of a TKR within a knee simulator machine was performed

for a single gait cycle. Later, Halloran *et al.* (2005) presented and experimentally validated an explicit FEM-model of a TKR that incorporates tibiofemoral and patellofemoral articulations, as Figure 1.26 shows. For computational efficiency, Halloran *et al.* (2005) developed rigid body analyses that can reasonably reproduce the kinematics, contact pressure distribution, and contact area of a fully deformable system. Results from the deformable model showed that the patellofemoral and tibiofemoral kinematics were in good agreement with experimental measurements. Moreover, kinematic results from the rigid body analyses were nearly identical to those from the fully deformable model, and the contact pressure and contact area correlation was acceptable given the great reduction in analysis time (Halloran *et al.*, 2005).

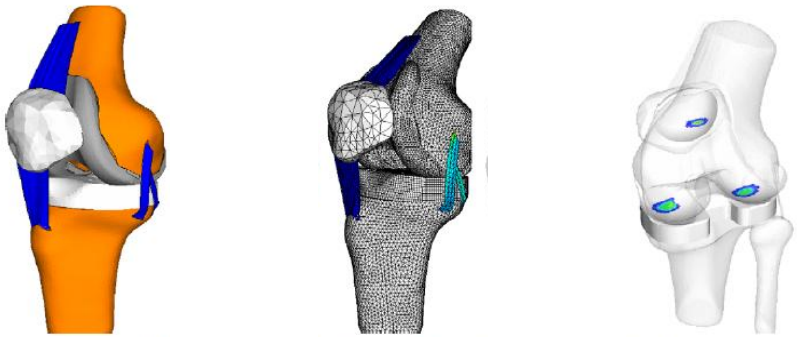

(a) **(b)** **(c)**

Figure 1.26 FEM-based model of a total knee replacement proposed by Halloran *et al.* (2005): (a) Solid model; (b) FEM mesh; (c) Transparent view showing contact pressures {Adapted from Halloran *et al.* (2005) with Elsevier permission}.

Dhaher and Kahn (2002) proposed a 3D-mathematical model of the patellofemoral joint, which includes soft tissues and bone surfaces. In this study, a basis-function based method was used to model the articular surfaces. Cohen *et al.* (2003) presented twenty subject-specific MBS models of the patellofemoral joint based on MRI data with the intent to demonstrate that these patient-specific computer models can be generated in a routine fashion and, can be utilized to support clinical choices and, hence, to improve clinical outcomes of patellofemoral joint reconstructions.

Elias *et al.* (2004) utilized a computational model to determine how loading variations alter the patellofemoral force and pressure distributions for individual knees. Triangular elements are used to describe each articular surface. Compression-only springs are placed at each element centroid to model the cartilage, while tension-only springs are positioned between the patella and the femur to represent the remaining joint capsule. Using a discrete element analysis technique, the motion of the patella with respect to the femur was determined by minimizing the potential energy stored within

the springs. The force and pressure distributions were quantified based on the deformation of each spring. Later, Elias and Cosgarea (2007) extended this work by introducing a method for simulating knee function in computational models representing patients with patellofemoral disorders.

Besier *et al.* (2005) presented a modeling pipeline to estimate *in vivo* cartilage stress in the patellofemoral joint. This modeling pipeline can be described in three steps: (*i*) to create subject-specific geometry and finite element mesh; (*ii*) to obtain subject-specific joint orientation and muscle forces; and (*iii*) to perform simulations and to test the model. NURBS surfaces are used to create a uniform mesh of quadrilateral elements for the bone of the patella, femur, and tibia, as Figure 1.27 depicts. The femoral and patellar cartilage is represented by 3D-hexahedral elements. Quasi-static loading simulations were performed using a nonlinear FEM solver (ABAQUS, Inc.).

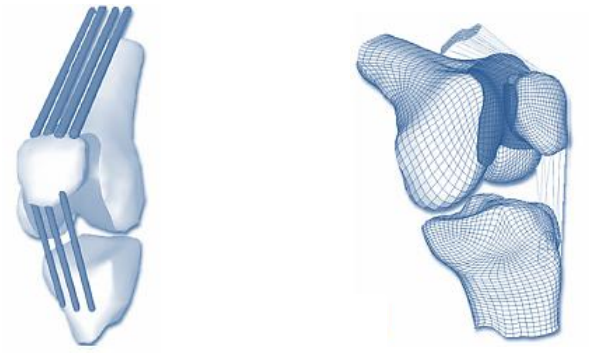

(a) **(b)**

Figure 1.27 Patellofemoral joint model proposed by Besier *et al.* (2005). The surfaces of the bone and cartilage are fitted to (a) NURBS surfaces, which are used to generated (b) quadrilateral and hexahedral meshes of the bones and cartilage {Adapted from Besier *et al.* (2005) with Wolters Kluwer Health permission}.

Fernandez and Hunter (2005) published an important work on patellofemoral modeling. Within this study, a quasi-static analysis of the patellofemoral joint was carried out in order to examine the main features of patella biomechanics, namely patella tracking, quadriceps extensor forces, surface contact and internal patella stresses. For this purpose, a 3D-anatomically FEM-based model of patellofemoral articulation using high-order cubic Hermite elements was developed, which is illustrated in Figure 1.28. This model is customized to patient MRI using a variant of freeform deformation (FFD), called 'host-mesh' fitting. The contact problem is addressed by constraining the three primary constraints of frictionless contact known as Signorini conditions, which describe a standard linear complementary problem.

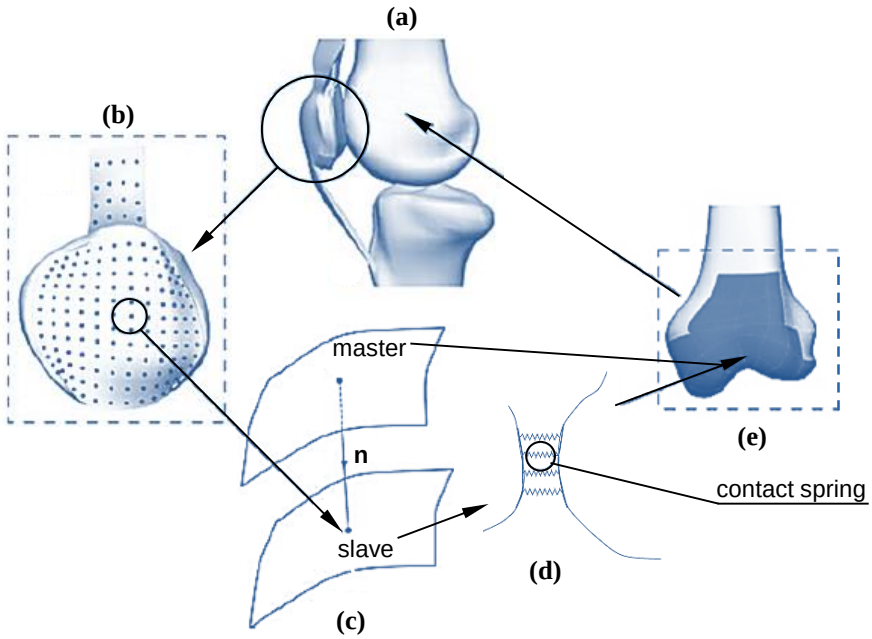

Figure 1.28 Patellofemoral joint model proposed by Fernandez and Hunter (2005). The patella (a) is discretized with (b) contact points and defined as the slave surface. Each contact point on the slave (c) is projected to the closest target point on the master surface with a unit normal **n**. The interpenetration is constrained by contact springs (d) placed between the patella and the femur. The master surface is defined as the shaded blue region (e) on the femoral condyles {Adapted from Fernandez and Hunter (2005) with Springer permission}.

With the intent of reproducing desired 3D-knee net loading or motion on a dynamic knee simulator, Guess and Maletsky (2005) developed a 3D-computational model that translates 3D-knee net loading estimated in a gait lab into control profiles that drive the actuators of the dynamic simulator. The main goals of this study were: (*i*) construct a constrained and simplified analog knee instrumented to measure joint forces; (*ii*) develop a 3D-computational model of a dynamic knee simulator and the analog knee; (*iii*) verify the capability of the computational model to predict knee loading by comparing predicted and measured analog knee forces through squat and laxity tests performed on the simulator; (*iv*) verify the capability of the model to generate control profiles to the controllable axes of the simulator by reproducing the loading and motion of a 3D-walking profile on the analog knee. This work was later extended by Guess and his collaborators (Guess *et al.*, 2010; Mishra *et al.*, 2011; Guess *et al.*, 2011; Stylianou *et al.*, 2012; Guess, 2012).

Guess *et al.* (2010) included a multibody model of the menisci into a subject-specific computational model of the knee joint. In this work, meniscus geometries are divided into 61 discrete elements, being 29 medial and 32 lateral, that are connected through 6×6 stiffness matrices. An optimization and design of experiments approach was used to determine parameters for the 6×6 stiffness matrices. Similarly,

parameters for compliant contact models of tibio-menisco-femoral articulations were derived from FEM solutions. As a final step, a multibody knee model was developed and placed within a dynamic knee simulator model and the tibiofemoral and patellofemoral kinematics compared to an identically loaded cadaver knee. The main goal of this work was to develop dynamic anatomical knee models with a computational efficiency sufficient for incorporation in 3D-movement simulations. This work revealed that menisci have a significant effect on the distribution of tibiofemoral contact forces and a beneficial, but statistically insignificant, effect on tibiofemoral kinematics during the walk cycle simulated in the dynamic knee simulator.

Guess *et al.* (2011) presented a method for modeling the tibiofemoral cartilage contact mechanics within a dynamic 3D-multibody framework for use in musculoskeletal simulations. This method is computationally efficient, capable of modeling contact friction and predicting cartilage shear forces, and allows inclusion of multiple articulating surfaces required for inclusion of menisci. The effects of contact model parameters on kinematics, contact pressure prediction and shear forces were explored throughout this work. The knee model utilized in this project is based on author's previous work (Guess *et al.*, 2010) and is represented in Figure 1.29a. This model includes a representation of the tibial plateau cartilage as discrete bodies, which are fixed to the tibia bone. The tibial cartilage is related to the femoral cartilage via deformable contacts. Parameters for the compliant contact law defined between each tibia cartilage element and the femur were derived using three methods: simplified Hertzian contact theory, simplified elastic foundation contact theory and parameter optimization from a FEM solution. Likewise in Guess *et al.* (2010), the predicted kinematics from different model formulations were compared to measured kinematics from the identically loaded cadaver knee during a simulated gait. By means of this work, Guess *et al.* (2011) proved that the developed multibody knee model is computationally efficient and 283 times faster than a FEM simulation using the same geometries and boundary conditions. With the intent of to optimize the computationally efficiency of 3D-multibody models, Mishra *et al.* (2011) introduced data-driven surrogate models that could successfully capture realistic and complex 3D-behavior of tibiofemoral joint interactions, while maintaining a reduced computational time. Training, validation, and test datasets were obtained from the experimentally validated multibody model of a cadaver knee previously developed by Guess *et al.* (2010). Inputs to the surrogate models are positions and orientations of the tibia relative to the femur,

while the outputs are resulting forces and torques at the tibia with respect to the femur. Three different nonlinear dynamic families of models (Hammerstein–Wiener, nonlinear autoregressive, and time delay neural network models) were identified, and variations of their structures were ranked using normalized mean squared error on validation and test data. Within this work, Mishra *et al.* (2011) observed that individually, time delay neural network models performed better than other models.

Stylianou *et al.* (2012) developed an anatomically correct canine stifle joint model with discrete cartilage and menisci under a multibody framework, and validate it against experimental measurements. The effect of including discrete representation of the cartilage and menisci structures on the accuracy of the model was investigated throughout this work. At the same year, Guess (2012) combined some of his previous works and performed a study that associates a cadaver-based validated natural multibody knee model with a muscle driven forward dynamics simulation from a subject of similar height and weight for prediction of joint contact mechanics. The knee joint model was constructed within a previously developed MBS computational model of the dynamic knee simulator (Guess and Maletsky, 2005). The ligaments are represented by nonlinear spring-damper elements, while the cartilage on the medial tibia plateau is sectioned into discrete hexahedral elements (71 elements) because of the major incidence of osteoarthritis in the medial compartment. The menisci are modeled as 17 discrete elements each, being its geometry elements connected to neighboring elements by 6×6 stiffness matrices (Guess *et al.*, 2010). The contact model used for all articulating surfaces in the knee is based on a nonlinear damping approach defined by default in the software MSC Software™ ADAMS (MSC Software Corporation, Santa Ana, CA). A total of 248 deformable contacts are defined at the knee: (*i*) femur bone/cartilage and patella bone/cartilage, (*ii*) femur bone/cartilage and lateral tibia cartilage, (*iii*) femur bone/cartilage and all 71 medial tibia cartilage elements, (*iv*) femur bone/cartilage and all 17 lateral meniscus elements, (*v*) femur bone/cartilage and all 17 medial meniscus elements, (*vi*) lateral tibia cartilage and all 17 lateral meniscus elements, and (*vii*) each medial meniscus elements and all medial tibia plateau elements that may come in contact with it. To validate the subject-specific multibody knee model, walking and dual-limb squat profiles were simulated on both the cadaver knee and virtual knee and the resulting bone kinematics compared. Figure 1.29b shows the virtual knee model performing a dual-limb squat task. The resulting tibiofemoral contact forces were compared to versions of knee joint model with and without menisci (Guess, 2012).

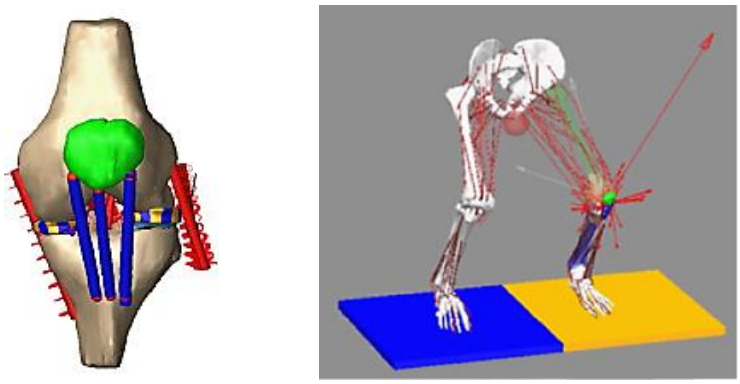

(a) **(b)**

Figure 1.29 (a) Multibody model of the knee joint with menisci proposed by Guess *et al.* (2010, 2011). (b) Virtual model of the human body performing a dual-limb squat task, including a multibody knee with menisci {Adapted from Guess (2012) with Springer permission}.

The knee contact problem has been studied for a long time (Wismans, 1980). Nonetheless, a special emphasis is given to this research topic in the last decade, in particular in what concerns with the efficiency of the computational approaches developed to predict joint loading response. Bei and Fregly (2004) is one of the most cited papers on the issue of knee contact mechanics. This paper consists in a technical note, in which a four-step methodology for incorporating deformable contact models of the tibiofemoral joint into a multibody dynamics framework is proposed. These four steps entail: (*i*) the preparation of the articular surface geometry, which is illustrated in Figure 1.30; (*ii*) the development of efficient methods to calculate distances between contact surfaces; (*iii*) the implementation of an efficient contact solver that accounts for the unique characteristics of human joints; and (*iv*) the specification of an application programming interface (API) that will work within any multibody dynamic simulation environment. The articular surfaces are fitted to NURBS surfaces, while the contact forces are evaluated by applying the elastic foundation model. This implementation accommodates natural or artificial tibiofemoral joint models, small or large strain contact models, and linear or nonlinear material models.

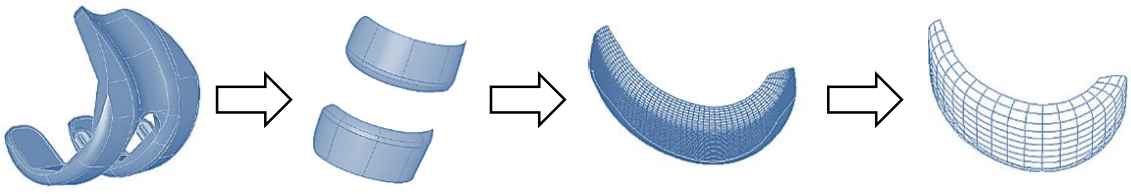

(a) **(b)** **(c)** **(d)**

Figure 1.30 Contact surface preparation proposed by Bei and Fregly (2004) for an artificial knee model. (a) CAD model of the knee prosthesis; (b) Trimmed NURBS surfaces removed from the CAD model; (c) Untrimmed NURBS patches fitted to the contact surfaces and then merged into a single patch; (d) Reduced number of parametric B-spline curves used to represent the surface maintaining the level of surface accuracy {Adapted from Bei and Fregly (2004) with Elsevier permission}.

Regarding the distance calculations, Bei and Fregly (2004) presented four strategies to minimize the number of distance calculations. The first strategy is to perform a geometry initialization in a pre-processing phase prior to beginning the simulation. This includes reading the contact surfaces of the tibia and femur, detecting connectivity between the NURBS patches of each contact surface, constructing contact pairs and associated data structures, and determining whether the surfaces are from a natural or artificial knee. A second strategy is to calculate distances from one contact surface directly to the other. For any element on a fixed-body contact surface, the distance to the corresponding moving-body contact surface is calculated directly and then corrected, cutting the number of distance evaluations in half. The correction uses trigonometry to approximate the distance along the local midsurface normal regardless of the method used for calculating distances. If minimum distance is used, *i.e.*, the distance vector is perpendicular to the point found on the moving body, the correction grows the distance slightly. If ray firing is used, *i.e.*, the distance vector is perpendicular to the starting point on the fixed body, it shrinks the distance slightly. Another strategy for minimizing distance calculations is to copy previous contact solutions whenever the relative kinematics changes little. A final strategy for minimizing distance calculations is to use the previous contact solution as an initial guess for the current solution.

Mun and Lee (2004) proposed a 3D-knee model, which comprises two rigid bodies, namely femur and tibia, and twelve ligaments represented by nonlinear spring elements. The articular geometry is represented using two cam profiles obtained from the extrusion of the sagittal plain view of a representative computed tomography (CT) image of the knee. The curves of the condyles represent a spiral of a spiral and are defined using cubic interpolation spline functions. Within this model, the ligaments carry load only when they are in tension and exhibit two-piece force-elongation relation: a nonlinear relation in the initial stage of ligament strain and a linear relation in later stages. This model allows for sliding and rolling motions and utilizes inverse dynamics and least-square methods for computing the lateral and medial contact forces.

Likewise Stylianou *et al*. (2012), Shahar and Banks-Sills (2004) presented a 3D-mathematical model of a canine knee. The aim of this study was to determine the forces in the knee ligaments and the knee joint reaction forces during the stance phase of a slow walk. This quasi-static model considers two articulations, namely tibiofemoral and patellofemoral. Bones are modeled as rigid bodies, while the ligaments are

represented by nonlinear springs. The patellar ligament is considered inextensible, since it is much stiffer and thicker than the other knee ligaments. The patella is assumed to rotate in the sagittal plane only. Fourth-order polynomials are used to describe the articular surfaces. Three pairs of contact are considered, namely medial tibiofemoral, lateral tibiofemoral and patellofemoral. Muscle forces acting on the femur and the hip joint reaction force were determined by numerical optimization. The effects of the menisci and friction were ignored (Shahar and Banks-Sills, 2004).

Küçük (2006) utilized the software Working Model 2D^{TM} to perform dynamic simulation within a knee joint model. Figure 1.31 shows this model, which comprises two rigid bodies, femur and tibia, undergoing general planar motion in the sagittal plane. The femur is considered to be fixed while the tibia glides and rolls over femur without losing contact. The femoral profile is described by a circular arc polynomial as Abdel-Rahman and Hefzy (1993) suggested. In turn, the tibia profile is represented as a parabolic curve as that of employed by Moeinzadeh *et al.* (1983). The ligaments and the posterior capsule are approximated by ten bundles of nonlinear springs, while the deformable cartilage layer is modeled by eighteen linear springs (Küçük, 2006).

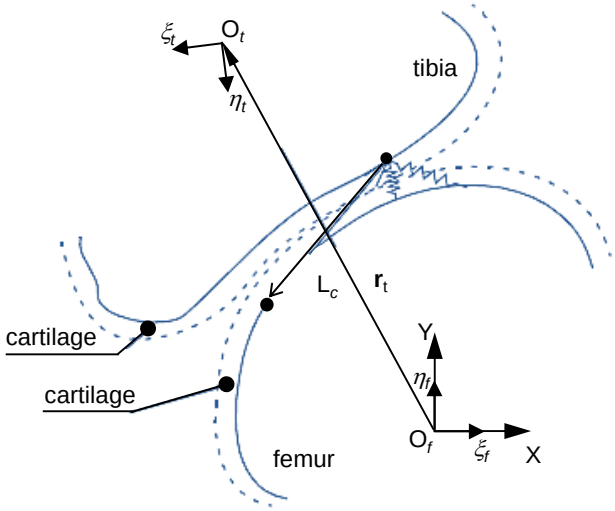

Figure 1.31 Planar model of the knee joint proposed by Küçük (2006). L_c represents the current length of the active cartilage layer, which is modeled by a set of linear springs {Adapted from Küçük (2006) with Elsevier permission}.

Fukunaga *et al.* (2008) proposed a 3D-model of the knee joint for analyzing the kinetics and kinematics of knee prosthesis during deep flexion. Both knee articulations, tibiofemoral and patellofemoral, are incorporated into the model. The femur is described with the fixed coordinate system, while the tibia and patella are modeled as moving systems. This model includes three muscles groups (quadriceps, hamstrings and

gastrocnemius) and three ligaments (MCL, LCL and patellar ligament). The shapes of prosthetic articular surfaces are represented by parametric polynomial functions.

Akalan *et al.* (2008) presented a knee joint model comprising ligament bundles and contact surfaces for simulation of passive knee motion. It is worth noting that these authors adopted a different strategy to model the articular surfaces. Instead of assuming a spherical shape for the femur condyles, experimentally obtained contact points were included into the model, as it can be observed in Figure 1.32. The output rotations, translations and contact forces are compared to a reference model (Abdel-Rahman and Hefzy, 1998), showing a close accordance. Within this study, Akalan *et al.* (2008) demonstrated that isometric ligament bundles play an important role in understanding the femur shape from contact points on tibia.

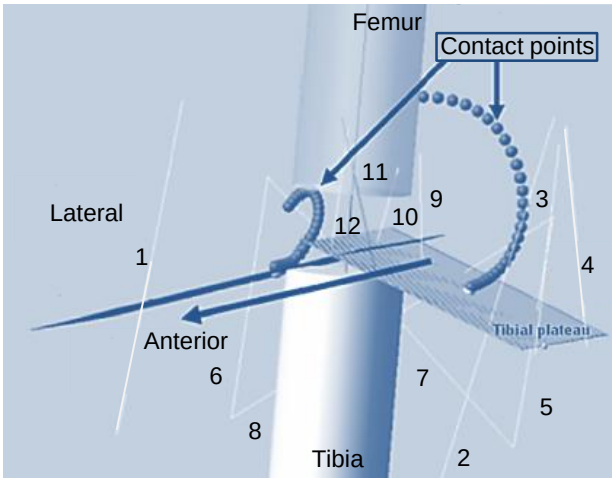

Figure 1.32 Mathematical 3D-model of the knee proposed by Akalan *et al.* (2008). The numbers denoted the knee ligaments: (1) LCL; (2) Anterior fiber of MCL; (3) Deep fiber of MCL; (4) Oblique fiber of MCL; (5) Medial capsule of popliteal ligament; (6) Lateral capsule of popliteal ligament; (7) Oblique popliteal ligament; (8) Arcuate popliteal ligament; (9) Anterior fiber of PCL; (10) Posterior fiber of PCL; (11) Anterior fiber of ACL; (12) Posterior fiber of ACL {Adapted from Akalan *et al.* (2008) with Elsevier permission}.

Yao *et al.* (2008) studied the sensitivities of tibio-menisco-femoral joint contact behavior to variations in knee kinematics using a FEM model. Cartilage and menisci were smoothed using thin-plate splines imported into HyperMesh 7.0 software. Furthermore, Lu *et al.* (2008) measured the *in vivo* 3D-motion and surface kinematics of normal knee during active knee extension under unloaded and loaded conditions by using single-plane fluoroscopy with a voxel-based 2D to 3D registration method.

Guo *et al.* (2009) presented spatial FEM-based model of the human knee joint. Hexahedral block-structures meshes of the bones and soft tissues were used to construct

the FEM model at software ANSYS, Inc. Bones are assumed to be a linear elastic and isotropic material, while cartilage, menisci and ligaments are considered viscoelastic tissues. Contacts are assumed to be frictionless and nonlinear. Within this model, nineteen potential contact zones are defined: two at the medial zone, namely the femoral cartilage-medial meniscus and medial meniscus-tibia cartilage; two at the lateral zone, namely the femoral cartilage-lateral meniscus and lateral meniscus-tibia cartilage; five between femur and ligaments, which are ACL, PCL, MCL, LCL and quadriceps tendon; five between tibia and ligaments, which are ACL, PCL, MCL, LCL and quadriceps tendon; one between cruciate ligaments; two between patella and ligaments, which are quadriceps tendon and patellar ligament; one between femoral cartilage and the retropatellar articular cartilage; one between tibial cartilage and fibular cartilage.

Lin *et al.* (2010) introduced a novel surrogate modeling approach for performing computationally efficient 3D-contact analyses within multibody dynamic simulations. This approach fits a computationally cheap surrogate contact model to data points sampled from a computationally expensive elastic contact model (e.g., finite element model or elastic foundation model). An overview of the process of creating this surrogate contact models is presented in Figure 1.33. The proposed methodology was applied to dynamic wear simulation of a commercial knee implant tested in a Stanmore knee simulator machine. Dynamic simulations performed with the surrogate contact models were highly accurate compared with simulations performed with the elastic foundation contact model used to create the surrogates. Even including the 6 h of computational time required for surrogate model creation, computational time required to perform five Monte Carlo analyses, taking about 13 h, was over 100 times less than if an elastic foundation approach has been used, taking about 1420 h. Despite of its computational benefits, the surrogate contact approach presented by Lin *et al.* (2010) possesses at least five limitations: (*i*) the determination of sensitive directions is influenced by how coordinate systems are embedded in the master and slave bodies; (*ii*) sensitive directions could change with model pose for some shapes; (*iii*) a new surrogate contact model must be generated any time the geometries or material properties of the contacting bodies are changed; (*iv*) the evaluation of surrogate contact model accuracy currently requires performing the same dynamic simulation with the computationally expensive contact model; (*v*) the proposed approach does not account for friction forces.

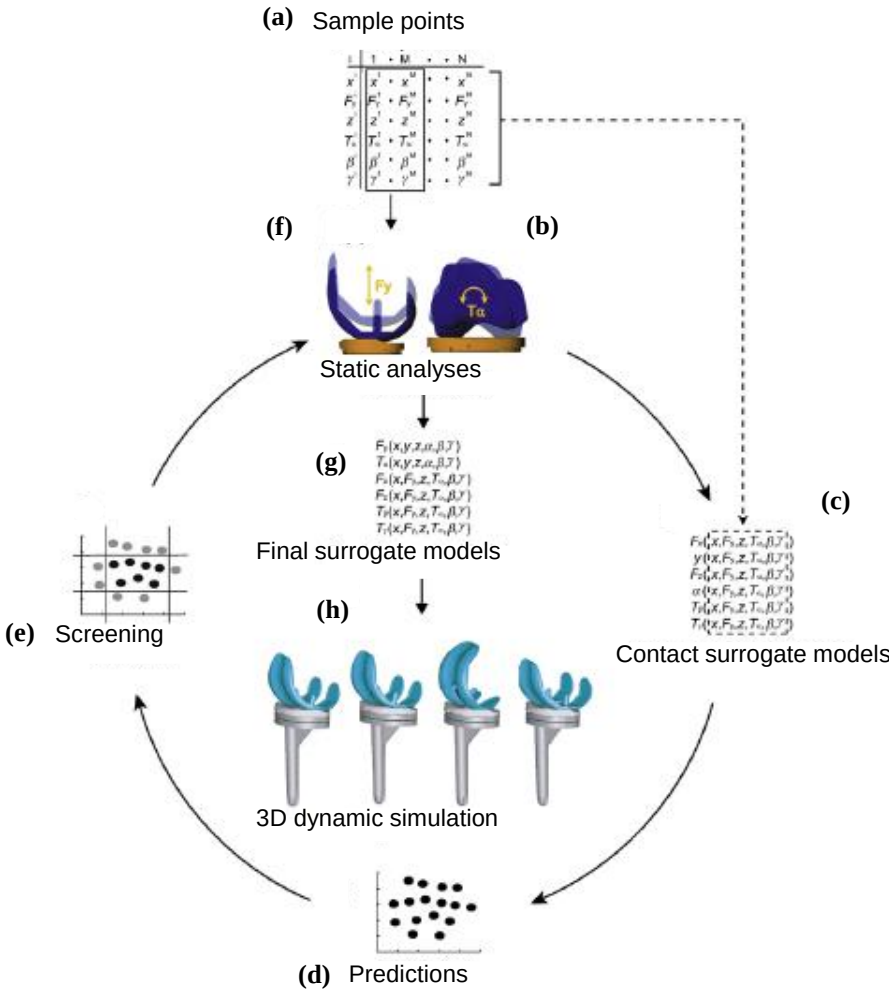

Figure 1.33 Diagram presented by Lin *et al.* (2010) to illustrate the process of developing a surrogate contact model. This process entails 8 steps: (a) *n* points are sampled in the *x*, F_y, *z*, T_α, β, γ design space; (b) Static analyses are performed for the first *m* sample points using an elastic foundation model (EFM); (c) Coarse surrogate models are created based on static analysis results for these *m* sample points; (d) Coarse surrogate models are used to predict static analysis results for the remaining *n-m* sample points; (e) Sample points are screened and eliminated if their predicted outputs are outside the desirable ranges defined by one or more nominal dynamic simulations; (f) Additional static analyses are performed with the EFM for sample points that pass the screening process; (g) Final surrogate contact models are created using static analysis results from all retained sample points; (h) During a dynamic simulation, surrogate contact models calculate contact forces and torques applied to both bodies given the pose of the femoral component relative to the tibial insert{Adapted from Lin *et al.* (2010) with Elsevier permission}.

Machado *et al.* (2010) presented a dynamic model of the human knee for contact analysis. This multibody model comprises two rigid bodies: the fixed femur and the moving tibia. The tibia is connected to the femur by four ligaments, which are ACL, PCL, MCL and LCL, modeled as nonlinear springs. The mechanical behavior of the ligaments is described by a quadratic stress-strain relation that is a function of the ligament stiffness and its unstrained length. The cartilage is characterized as a deformable structure with specific material properties. The motion of the tibia relative

to the femur is not modeled with conventional kinematic joint, but rather in terms of the action of the ligaments and potential contact between the condyles. Based on medical images of the human knee, the geometry of the articular profiles is fitted to spline interpolation functions. Within this model, constitutive laws based on the Hertzian theory augmented with a dissipative term are used to compute knee contact forces.

Argatov (2012) proposed a new methodology for modeling tibiofemoral contact based on asymptotic model of frictionless elliptical contact interaction between thin biphasic cartilage layers. This approach requires smooth contact geometries and efficient contact detection methods. Within this study, the tibia is considered to be rigidly fixed, while the articular surfaces are modeled using polynomial functions.

In order to get an overview of the survey of knee models described above, the most relevant knee models and their characteristics were summarized in Table 1.1. Each knee model is described as planar or spatial, being the type of analysis utilized in each simulation characterized as kinematic (K), quasi-static (QS) or dynamic (D). Within Table 1.1, the model approach is distinguished between multibody system (MBS), finite element method (FEM), optimization (OPT) or hybrid (HYB). The modeling joints are also indicated in Table 1.1; some models represent only the tibiofemoral joint (TF), others authors focused their research on modeling the patellofemoral joint (PF); besides, there are works that account for both joints (TF and PF). Three types of biomodels were considered, namely natural knee (NK), artificial knee (AK) and lower limb (LL). The presence of ligaments, tendons, muscles, menisci and cartilage is reported in Table 1.1. The geometrical representation of the articular surfaces and the evaluation of the contact forces were completed in some of these studies, which is also point out in Table 1.1.

Table 1.1 Survey of knee joint models. Symbols appearing in this table are: P (planar), S (spatial), K (kinematic), QS (quasi-static), D (dynamic), O (optimization), MBS (multibody system), FEM (finite element method), E (experimental), H (hybrid), LL (lower-limb), NK (natural knee), AK (artificial knee), TF (tibiofemoral) and PF (patellofemoral).

Study	Planar/Spatial	Analysis type	Approach	Biomodel type	Modeling joints	Ligaments	Tendons	Muscles	Menisci	Cartilage	Contact Analysis	Articular geometry
Strasser (1917)	P	K	MBS	NK	TF	✓	✗	✗	✗	✗	✗	✗
Freudenstein and Woo (1969)	P	K	MBS	NK	TF	✓	✗	✗	✗	✗	✗	✓
Smidt (1973)	P	QS	MBS	NK	TF, PF	✗	✓	✓	✗	✗	✓	✗
Menschik (1974)	P	K	MBS	NK	TF	✓	✗	✗	✗	✗	✗	✓

Table 1.1 (*continued*)

Study	Planar/Spatial	Analysis type	Approach	Biomodel type	Modeling joints	Ligaments	Tendons	Muscles	Menisci	Cartilage	Contact Analysis	Articular geometry
Crowninshield *et al.* (1976)	S	QS	MBS	NK	TF	✓	✗	✗	✗	✗	✗	✓
Andriacchi *et al.* (1983)	S	QS	FEM	NK	TF	✓	✗	✗	✓	✓	✓	✓
Goodfellow and O'Connor (1978)	P	K	MBS	NK	TF	✓	✗	✗	✓	✗	✗	✓
Hardt (1978)	S	D	OPT	LL	TK	✗	✗	✓	✗	✗	✗	✗
Wismans (1980)	S	QS	MBS	NK	TF	✓	✗	✗	✗	✓	✓	✓
Moeinzadeh (1981) Moeinzadeh and Engin (1988)	P S	D	MBS	NK	TF	✓	✗	✗	✗	✓	✓	✓
Van Eijden *et al.* (1986)	P	D	MBS	NK	PF	✗	✓	✗	✗	✓	✓	✓
Huson *et al.* (1989)	P	K	MBS	NK	TF	✓	✗	✗	✗	✗	✗	✓
Essinger *et al.* (1989)	S	QS	MBS	AK	TF, PF	✓	✓	✗	✗	✓	✓	✓
Garg and Walker (1990)	P	K	MBS	AK	TF	✓	✗	✗	✗	✗	✗	✓
Blankevoort *et al.* (1991) Blankevoort and Huiskes (1991)	S	QS	MBS	NK	TF	✓	✗	✗	✗	✓	✓	✓
Hirokawa (1991)	S	D	MBS	NK	PF	✓	✓	✗	✗	✓	✓	✓
Abdel-Rahman and Hefzy (1993)	P	D	MBS	NK	TF	✓	✗	✗	✗	✓	✓	✓
Loch *et al.* (1992)	S	QS	MBS	NK	TF	✓	✗	✗	✗	✓	✓	✓
Hefzy and Yang (1993)	S	QS	MBS	NK	PF	✓	✓	✗	✗	✓	✓	✓
Tümer and Engin (1993)	P	D	MBS	NK	TF, PF	✓	✓	✓	✗	✓	✓	✓
Bendjaballah *et al.* (1995)	S	QS	FEM	NK	TF, PF	✓	✓	✗	✓	✓	✓	✓
Heegard *et al.* (1995)	S	QS	FEM	NK	PF	✓	✓	✗	✗	✓	✓	✓
Mommersteeg *et al.* (1995)	S	QS	MBS	NK	TF	✓	✗	✗	✗	✓	✓	✓
Gill and O'Connor (1996)	P	D	MBS	NK	TF, PF	✓	✓	✗	✗	✓	✓	✓
Blankevoort and Huiskes (1996)	S	QS	MBS	NK	TF	✓	✗	✗	✗	✓	✓	✓
Chittajallu and Kohrt (1996)	P	D	MBS	NK	TF	✓	✗	✗	✗	✓	✓	✓
Abdel-Rahman *et al.* (1996) Abdel-Rahman and Hefzy (1998)	S	D	MBS	NK	TF	✓	✗	✗	✗	✓	✓	✓
Ling *et al.* (1997)	P	D	MBS	NK	TF	✓	✗	✗	✗	✓	✓	✓
Pandy *et al.* (1997)	S	D	MBS	NK	TF, PF	✓	✓	✓	✗	✓	✓	✓
Wimmer and Andriacchi (1997)	P	D	MBS	AK	TF	✗	✓	✓	✗	✓	✓	✓
Sathasivam and Walker (1997)	S	QS	EXP	AK	TK	✗	✗	✗	✗	✓	✓	✓
Shelburne and Pandy (1997)	P	QS	MBS	NK	TF, PF	✓	✓	✓	✗	✓	✓	✓
Wilson and O'Connor (1997) Wilson *et al.* (1998)	P S	QS	MBS	NK	TF	✓	✗	✗	✗	✓	✓	✓
Kim (1998)	S	QS	MBS	NK	TF, PF	✓	✓	✗	✗	✓	✓	✓
Zhu *et al.* (1999) Chen *et al.* (2001) Zhu and Chen (2004)	S	QS	MBS	NK	TF	✗ ✓ ✓	✗	✗	✗ ✓ ✓	✓	✓	✓
Kwak *et al.* (2000)	S	QS	MBS	NK	TF	✓	✓	✗	✗	✓	✓	✓

Table 1.1 (*continued*)

Study	Planar/Spatial	Analysis type	Approach	Biomodel type	Modeling joints	Ligaments	Tendons	Muscles	Menisci	Cartilage	Contact Analysis	Articular geometry
Piazza and Delp (2001)	S	D	MBS	LL	TF, PF	✓	✓	✓	✗	✗	✓	✓
Donahue *et al.* (2002)	S	QS	FEM	NK	TF	✓	✗	✗	✓	✓	✓	✓
Dhaher and Kahn (2002)	S	QS	MBS	NK	TF, PF	✗	✓	✓	✗	✓	✓	✓
McLean *et al.* (2003)	S	D	MBS	LL	TF	✗	✓	✓	✗	✗	✗	✗
Bei and Fregly (2004)	S	D	MBS	NK, AK	TF	✗	✗	✗	✗	✓	✓	✓
Caruntu and Hefzy (2004)	S	D	MBS	NK	TF, PF	✓	✗	✗	✗	✓	✓	✓
Mun and Lee (2004)	S	D	MBS	NK	TF	✓	✗	✗	✗	✓	✓	✓
Elias *et al.* (2004) Elias and Cosgarea (2007)	S	QS	FEM	NK	PF	✗	✓	✓	✗	✓	✓	✓
Fernandez and Hunter (2005)	S	QS	FEM	NK	PF	✗	✓	✓	✗	✓	✓	✓
Halloran *et al.* (2005)	S	QS	FEM	AK	TF, PF	✓	✓	✗	✗	✓	✓	✓
Besier *et al.* (2005)	S	QS	FEM	NK	PF	✗	✓	✓	✗	✓	✓	✓
Küçük (2006)	P	D	MBS	NK	TF	✓	✗	✗	✗	✓	✓	✓
Fukunaga *et al.* (2008)	S	D	MBS	AK	TF, PF	✓	✓	✓	✗	✓	✓	✓
Akalan *et al.* (2008)	S	D	MBS	NK	TF	✓	✗	✗	✗	✗	✓	✗
Guo *et al.* (2009)	S	QS	FEM	NK	TF, PF	✓	✓	✗	✓	✓	✓	✓
Farhat *et al.* (2010)	S	D	OPT	LL	TF	✓	✓	✓	✓	✗	✗	✓
Lin *et al.* (2010)	S	D	MBS	AK	TK	✗	✗	✗	✗	✓	✓	✓
Machado *et al.* (2010)	P	D	MBS	NK	TK	✓	✗	✗	✗	✓	✓	✓
Guess *et al.* (2010, 2011); Guess (2012); Stylianou *et al.* (2012).	S	D	HYB	NK	TF, PF	✓	✓	✓	✓	✓	✓	✓

It is worth noting that some researchers dedicated their investigation on comparing and/or validating existing models and modeling approaches, instead of developing new models of the knee joint. Some examples of these studies are the works by Li *et al.* (1997), Koo and Andriacchi (2007), Halloran *et al.* (2008), Pérez-González *et al.* (2008) and Machado *et al.* (2011). Li *et al.* (1997) performed a comparative study, where the pressure distribution along the contact surface of an articulating joint model was analyzed using different numerical and analytical methods, namely (*i*) the rigid body spring model (also known as EFM); (*ii*) the finite element method; (*iii*) the simplified elasticity solution (SES); and (*iv)* the modified Hertz model (mHM). Figure 1.34 shows a simplified articular joint model introduced by Li *et al.* (1997), in which it is visible the differences on articular joint model when this system is modeled with distinct contact approaches. The FEM and mHM methods model an articular joint as

interposing elastic layers, while the EFM and SES methods assume a simplified joint with a rigid convex indenter on an elastic concave surface. Within this study, Li *et al.* (1997) concluded that the EFM, in comparison with the other three methods, is relatively simple and effective in predicting joint contact pressure under symmetric and non-symmetric loading, and is also computationally efficient.

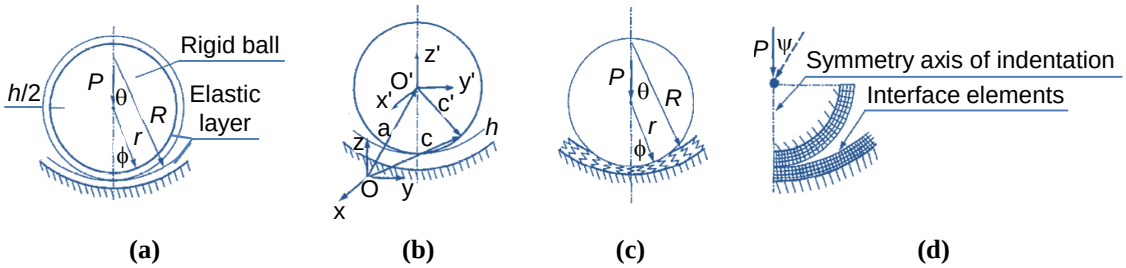

Figure 1.34 Simplified articular joint model presented by Li *et al.* (1997) {Adapted from Li *et al.* (1997) with Elsevier permission}. (a) A rigid ball covered by an elastic layer in contact with an elastic layer supported by a rigid foundation; (b) A ball in contact with a single elastic layer; (c) EFM model of the ball-socket joint; (d) An axisymmetric FEM-mesh for a non-conforming joint model.

Koo and Andriacchi (2007) developed a comparative study to evaluate the influence of the global functional loads and the local contact anatomy on articular cartilage thickness at the knee. In this study, the articular surfaces are modeled as two semi-ellipsoids and the medial/lateral contact pressure ratio was calculated using elliptical Hertzian contact stress theory. The results reported by Koo and Andriacchi (2007) revealed that contact pressure is higher in the lateral than medial compartments and cartilage thicker in the lateral than medial compartments. Within this work, Koo and Andriacchi (2007) measured the radii of femoral and tibial surface of medial and lateral compartments in a weight-bearing position by means of 3D-models, which were built based on bilateral knee MRI obtained from eleven young healthy adults with no history of knee injury. Figure 1.35 depicts the average radii in mm, of femoral and tibial cartilage in the medial-lateral (ML) and anterior-posterior (AP) direction in the lateral and medial compartments. In this study, Koo and Andriacchi (2007) concluded that the femoral cartilage had convex surfaces in the medial and lateral compartments in both AP and ML directions, while the tibial cartilage had mostly concave surfaces, except for the AP direction in the lateral compartment. According to these authors, tibiofemoral contact surfaces conformed best (convex-concave surfaces contact with similar radii) in the ML direction in the medial compartment and worst (convex-convex surfaces contact) in the AL direction in the lateral compartment.

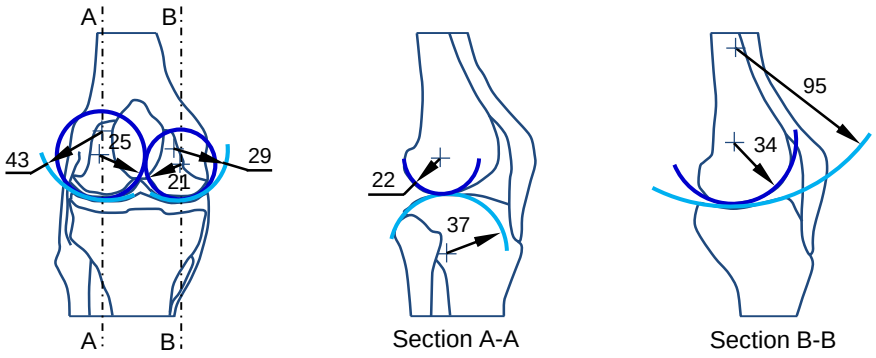

Figure 1.35 Average radii in mm of femur and tibia articular surfaces: (a) Coronal view; (b) Lateral view; (c) Medial view {Adapted from Koo and Andriacchi (2007) with Elsevier permission}.

Also in 2008, Pérez-González *et al.* realized that different models have been used in the literature for the simulation of articular contact in knee joint models, but that there was a lack of systematic comparisons of the models applied to simulate a common contact scenario. According to Pérez-González *et al.* (2008), these kinds of studies are of paramount importance and provide relevant information about the accuracy and suitability of the contact approaches for application in models of the artificial knee. Therefore, these authors performed a comparative study using the Herz model (HM), the EFM, and the FEM models to evaluate the contact forces at an artificial knee. In this work, it was concluded that EFM offers some advantages when compared with that of the HM for its application to realistic prosthetic surfaces and when compared with the FEM in computational time. Nonetheless, Pérez-González *et al.* (2008) proved also that EFM-based predictions can differ from FEM-based estimations in certain circumstances. To overcome this issue a new modified elastic foundation model (mEFM) was proposed. This novel approach maintains basically the simplicity of the original model while producing much more accurate results. According to Pérez-González *et al.* (2008), mEFM offered a good settlement between computation time and accuracy for applications where FEM models become cumbersome as a consequence of the preprocessing or computation times.

Machado *et al.* (2011) presented other comparative study with the purpose to evaluate the influence of the contact approach on the dynamic response of the knee joint. For this purpose, a multibody knee model was utilized, which was previously developed by the same research group (Machado *et al.*, 2010). Hertz, Hunt and Crossley, and Lankarani and Nikravesh force models were compared for equivalent contact conditions. Later, Machado *et al.* (2012) extended this comparative study by

simulating the dynamic response of the same knee model with a different contact force law proposed by Flores *et al*. (2011). In their work, Machado *et al.* (2011) did not consider only the contact force law as a study variable, but also the contact geometry and material properties. Regarding the contact geometry, since the tibial plateaus do not exhibit the same conformality in both knee compartments, three contact scenarios were tested, namely convex-convex contact, convex-concave contact, and convex sphere-plane contact. Furthermore, in order to examine healthy, pathological, and artificial knee response to the same contact loads, the contact material properties and surfaces thickness were considered as variables (Machado *et al.*, 2011).

1.3 Scope and objectives

The main objective of this work is to develop a computational multibody model able to describe how the biologic structures of the knee joint interact to generate movement and, at the same time, provide stability to the whole body. For this purpose, specific goals related to the process of modeling biologic systems for multibody dynamics have been established. These specific goals are listed as follows:

(*i*) To study the multibody system formulation, especially the issues associated with the dynamic simulation of human motion;

(*ii*) To understand the general issues on contact modeling and analysis, in particular the geometrical features and the constitutive force laws;

(*iii*) To develop a multibody 2D-model of the human knee for dynamic analysis, giving special attention to the process of modeling the ligaments and the articular contacts.

(i*v*) To investigate the influence of contact modeling features on the dynamic response of the knee multibody model;

(*v*) To develop an efficient computational algorithm for contact analysis of general multibody system with contact, such as the human knee joint.

1.4 Structure of the thesis

The present thesis is organized in eight Chapters: (1) Introduction; (2) Human knee joint: anatomy and function; (3) Multibody dynamics methodology for biomechanical modeling; (4) Contact modeling and analysis; (5) A multibody 2D-model of the human knee joint; (6) A multibody 3D-model of the human knee joint; (7) Knee joint modeling using OpenSim software; (8) Concluding remarks. It is important noting that each Chapter comprises its own references.

In Chapter One, the general motivation for this research work is presented and a literature review of the biomechanical models of the knee joint is provided. The objectives and contributions of the present study are also offered.

Chapter Two focuses on the human knee joint, starting with an overview of the terminology used for human movement. The structural anatomy of the human knee joint is widely described in this Chapter, as well as the principal movements of this human articulation. Chapter Two provides a brief explanation of the ultrastructure and mechanical behavior of the principal biologic tissues that surround the knee, namely bone, articular cartilage, menisci, ligaments, tendons and muscles. Knee joint pathologies and replacement systems are also revised in this Chapter.

In the third Chapter, the multibody system formulation used for biomechanical modeling is described. First of all, the concept of multibody system and its applications is presented. Then, the different types of coordinates that can be employed in multibody system approaches are summarized. The kinematic constraints that compose a multibody system are revised throughout this Chapter. Within Chapter Three, the overall mathematical formulation associated with constrained multibody system is provided, namely the equations of motion and their numerical solutions. In this Chapter, a human multibody model is considered as a demonstrative example of application. Using this biomechanical model, the influence of the Baumgarte stabilization method on keeping the constraint violations under control is considered.

Chapter Four deals with the contact-impact phenomena and the methodologies utilized in multibody dynamics to solve and analyze these problems. An overview of the existing techniques for geometric detection of contact events is provided throughout this Chapter. The most common elastic and dissipative laws used to evaluate normal contact

forces are also revised. Within this Chapter, a slider-crank mechanism experiencing two frictionless impacts with an external free sliding block is used as application example.

In the fifth Chapter, a multibody 2D-model of the knee joint is proposed. Firstly, the techniques utilized to define the geometric features of the knee joint are presented. The contact methodologies adopted to develop this model are explained. The mathematical formulation utilized to characterize the nonlinear behavior of the ligaments is also described. Computational simulations were performed using the proposed knee model, being the obtained results included in this Chapter. Within Chapter Five, a study about the influence of contact modeling features on knee dynamics is also presented.

Chapter Six describes a multibody 3D-model of the human knee joint for contact dynamics. Firstly, a generic methodology to represent and generate freeform contact surfaces is offered. Then, the process of geometric modeling of the knee articular surfaces is explained. An efficient methodology to deal with spatial contact problems is proposed throughout this Chapter. Some computational simulations using this methodology were performed and some of the results are discussed.

Chapter Seven presents a modeling framework explaining how to build a knee joint model in OpenSim software. The limitations of using this software to contact modeling and analysis are highlighted throughout Chapter Seven.

Finally, the main conclusions of the present work and some suggestions for future research are offered in Chapter Eight.

1.5 Contributions of this work

Within this work, a multibody approach to the contact dynamics is presented and applied to the knee joint. Two models of the human knee are developed: a 2-D and a 3-D model. Moreover, specific formulations are implemented into the multibody dynamics algorithm in order to account for all relevant physical phenomena inherent to biomechanical systems with contact problems, such as the human knee.

In what concerns with 2D-model, it can be highlighted five modeling procedures: (*i*) geometrical representation of contacting outlines by the use of curve fitting techniques; (*ii*) development of a methodology for locate the contact points between

two contacting bodies with freeform convex profiles; (*iii*) mathematical description of the nonlinear behavior of ligaments (*iv*) application of distinct formulations for the contact detection between two spherical bodies with conformal and non-conformal configurations; (*v*) implementation of a double layer-based contact model that permits force calculations on the contacting surface and subsurface.

Regarding the 3D-model, some novel formulations can be pointed out: (*i*) geometrical description of contacting surfaces by means of parametric functions; (*ii*) organization of the geometric data into a lookup table for improving the contact point searching and computational efficiency; (*iii*) development of a contact approach that allows keeping and updating the small part of the geometric data that stores in memory, reducing thereby the amount of computational memory utilized and, enhancing the efficiency of the contact detection.

In a broad sense, the main features that characterize and distinguish the proposed model of the knee joint are: (*i*) the system is a dynamic one, since it relates the body forces with the motion produced, and hence it is more appropriate for studying human daily activities compared with quasi-static models; (*ii*) it does not contain any conventional kinematic joint and, hence, is capable of representing all modes of knee motion; (*iii*) the model explicitly relates the knee mechanical properties and the contact forces produced; (*iv*) the system is simple and easy to implement in other types of biomechanisms, such as those that consider whole-body gross motion. Furthermore, the procedure for defining contact geometries and detecting contacts is rather general and could be used for modeling any MBS system encountering a contact. It is worth noting that throughout this work several modeling features associated with contact-impact events are investigated, namely the constitutive contact law used to evaluate the contact forces, the convexity of the contact geometries, and the presence of a second contact layer. The study of the influence of these modeling variables on the dynamic response of the knee joint model is an original contribution of this thesis. The developed coding strategies to enhance the computational efficiency of the proposed methodologies represent also an added value of this work.

References

Abdel-Rahman, E., Hefzy, M.S. (1991) Two-dimensional dynamic model of the tibio-femoral joint. *Advances in Bioengineering*, 20, pp. 413.

Abdel-Rahman, E., Hefzy, M.S. (1993) A two-dimensional dynamic anatomical model of the human knee joint. *Journal of Biomechanical Engineering*, 115(4A), pp. 357-365.

Abdel-Rahman, E., Hefzy, M.S., Cooke, T.D.V. (1996) Determination of the ligamentous and contact forces in the human tibio-femoral joint using a three-dimensional dynamic anatomical model. *Proceedings of the 1996 15th Southern Biomedical Engineering Conference* (pp. 372-376), Dayton (OH).

Abdel-Rahman, E., Hefzy, M.S. (1998) Three-dimensional dynamic behaviour of the human knee joint under impact loading. *Medical Engineering & Physics*, 20(4), pp. 276-290.

Akalan, N.E, Özkan, M., Temelli, Y. (2008) Three-dimensional knee model: constrained by isometric ligament bundles and experimentally obtained tibio-femoral contacts. *Journal of Biomechanics*, 41(4), pp. 890-896.

Ambrósio, J.A.C. (2005) Multibody dynamics: bridging for multidiscipliary applications. In: W. Gutkowski, T.A. Kowalewski (Eds.) *Mechanics of the 21st Century* (pp. 61–88). Springer: Dordrecht, Netherlands.

Andriacchi, T.P., Mikosz, R.P., Hampton, S.J., Galante, J.O. (1977) A statically indeterminate model of the human knee joint. *Proceedings of the Biomechanics Symposium AMD* (23, pp. 227-239), New Haven (CT).

Andriacchi, T.P., Mikosz, R.P., Hampton, S.J., Galante, J.O. (1983) Model studies of the stiffness characteristics of the human knee joint. *Journal of Biomechanics*, 16(1), pp. 23-29.

Andriacchi, T.P., Mündermann, A. (2006) The role of ambulatory mechanics in the initiation and progression of knee osteoarthritis. *Current Opinion in Rheumatology*, 18(5), pp. 514-518.

Argatov, I. (2012) Development of an asymptotic modeling methodology for tibio-femoral contact in multibody dynamic simulations of the human knee joint. *Multibody System Dynamics*, 28(1-2), pp. 3-20.

Ateshian, G.A., Soslowsky, L.J., Mow, V.C. (1991) Quantitation of articular surface topography and cartilage thickness in knee joints using stereophotogrammetry. *Journal of Biomechanics*, 24(8), pp. 761-776.

Bei, Y., Fregly, B.J. (2004) Multibody dynamic simulation of the knee contact mechanics. *Medical Engineering & Physics*, 26(9), pp. 777-789.

Bendjaballah, M.Z., Shirazi-Adl, A., Zukor, D.J. (1995) Biomechanics of the human knee joint in compression: reconstruction, mesh generation and finite element analysis. *The Knee*, 2(2), pp. 69-79.

Bennell, K.L., Hinman, R.S. (2011) A review of the clinical evidence for exercise in osteoarthritis of the hip and knee. *Journal of Science and Medicine in Sport*, 14(1), pp. 4-9.

Besier, T.F., Gold, G.E., Beaupre, G.S., Delp, S.L. (2005) A modeling framework to estimate patellofemoral joint cartilage stress in vivo. *Medicine & Science in Sports & Exercise*, 37(11), pp. 1924-1930.

Blankevoort, L., Huiskes, R. (1991) Ligament-bone interaction in a three-dimensional model of the knee. *Journal of Biomechanical Engineering*, 113(3), pp. 263-269.

Blankevoort, L., Huiskes, R. (1996) Validation of a three-dimensional model of the knee. *Journal of Biomechanics*, 29(7), pp. 955-961.

Blankevoort, L., Kuiper, J.H., Huiskes, R., Grootenboer, H.J. (1991) Articular contact in a three-dimensional model of the knee. *Journal of Biomechanics*, 24(11), pp. 1019-1031.

Caruntu, D.I., Hefzy, M.S. (2004) 3-D Anatomically based dynamic modeling of the human knee to include tibio-femoral and patello-femoral joints. *Journal of Biomechanical Engineering*, 126(1), pp. 44-53.

Chen, J.X., Wechsler, H., Pullen, J.M., Zhu, Y., MacMahon, E.B. (2001) Knee surgery assistance: patient model construction, motion simulation, and biomechanical visualization. *IEEE Transactions on Biomedical Engineering*, 48(9), pp. 1042-1052.

Chittajallu, S.K., Kohrt, K.G. (1996) FORM2D - A mathematical model of the knee. *Mathematical and Computer Modelling*, 24(9), pp. 91-101.

Cohen, Z.A., Henry, J.H., McCarthy, D.M., Mow, V.C., Ateshian, G.A. (2003) Computer simulations of patellofemoral joint surgery. *The American Journal of Sports Medicine*, 31(1), pp. 87-98.

Crowninshield, R., Pope, M.H., Johnson, R.J. (1976) An analytical model of the knee. *Journal of Biomechanics*, 9(6), pp. 397–405.

Dhaher, Y.Y., Kahn, L.E. (2002) The effect of vastus medialis forces on patello-femoral contact: a model-based study. *Journal of Biomechanical Engineering*, 124(6), pp. 758-767.

Donahue, T.L.H., Hull, M.L., Rashid, M.M., Jacobs, C.R. (2002) A finite element model of the human knee joint for the study of tibio-femoral contact. *Journal of Biomechanical Engineering*, 124(3), pp. 273-280.

Elias, J.J., Cosgarea, A.J. (2007) Computational modeling: an alternative approach for investigating patellofemoral mechanics. *Sports medicine and arthroscopy review*, 15(2), pp. 89-94.

Elias, J.J., Wilson, D.R., Adamson, R., Cosgarea, A.J. (2004) Evaluation of a computational model used to predict the patellofemoral contact pressure distribution. *Journal of Biomechanics*, 37(3), pp. 295-302.

Engin, A.E., Moeinzadeh, M.H. (1983) Dynamic modelling of human articulating joints. *Mathematical modelling*, 4(2), pp. 117-141.

Essinger, J.R., Leyvraz, P.F., Heegard, J.H., Robertson, D.D. (1989) A mathematical model for the evaluation of the behaviour during flexion of condylar-type knee prostheses. *Journal of Biomechanics*, 22(11-12), pp. 1229-1241.

Farhat, N., Mata, V., Rosa, D., Fayos, J. (2010) A procedure for estimating the relevant forces in the human knee using a four-bar mechanism. *Computer Methods in Biomechanics and Biomedical Engineering*, 13(5), pp. 577-587.

Felson, D. (2006) Osteoarthritis of the knee. *The New England Journal of Medicine*, 354(8), pp. 841-848.

Fernandez, J.W., Hunter, P.J. (2005) An anatomically based patient-specific finite element model of patella articulation: towards a diagnostic tool. *Biomechanics and modeling in mechanobiology*, 4(1), pp. 20-38.

Flores, P., Machado, M., Silva, M.T., Martins, J.M. (2011) On the continuous contact force models for soft materials in multibody dynamics. *Multibody System Dynamics*, 25(3), pp. 357-375.

Freudenstein, F., Woo, L. S. (1969) Kinematics of the human knee joint. *Bulletin of Mathematical Biology*, 31(2), pp. 215-232.

Fukunaga, M., Katsuhara, T., Hirokawa, S. (2008) A 3D model analysis of artificial knee joint during passive deep flexion. *Memoirs of the Faculty of Engineering, Kyushu University*, 68(1), pp. 11-18.

Garg, A., Walker, P.S. (1990) Prediction of total knee motion using a three-dimensional computer-graphics model. *Journal of Biomechanics*, 23(1), pp. 45-53.

Gill, H.S., O'Connor, J.J. (1996) Biarticulating two-dimensional computer model of the human patellofemoral joint. *Clinical Biomechanics*, 11(2), pp. 81-89.

Godest, A.C., Beaugonin, M., Haug, E., Taylor, M., Gregson, P.J. (2002) Simulation of a knee joint replacement during a gait cycle using explicit finite element analysis. *Journal of Biomechanics*, 35(2), pp. 267-275.

Goodfellow, J., O'Connor, J. (1978) The mechanics of the knee and prosthesis design. *The Journal of Bone & Joint Surgery - B*, 60(3), pp. 358-369.

Grood, E.S., Suntay, W.J. (1983) A joint coordinate system for the clinical description of three-dimensional motions: application to the knee. *Journal of Biomechanical Engineering*, 105, 136-144.

Guess, T.M. (2012) Forward dynamics simulation using a natural knee with menisci in the multibody framework. *Multibody System Dynamics*, 28(1-2), pp. 37-53.

Guess, T.M., Liu, H., Bhashyam, S., Thiagarajan, G. (2011) A multibody knee model with discrete cartilage prediction of tibio-femoral contact mechanics. *Computer Methods in Biomechanics and Biomedical Engineering*, pp. 1-15, (DOI: 10.1080/10255842.2011.617004).

Guess, T.M., Maletsky, L.P. (2005) Computational modeling of a dynamic knee simulator for reproduction of knee loading. *Journal of Biomechanical Engineering*, 127, pp. 1216-1221.

Guess, T.M., Thiagarajan, G., Kia, M., Mishra, M. (2010) A subject specific multibody model of the knee with menisci. *Medical Engineering & Physics*, 32(5), pp. 505-515.

Guo, Y., Zhang, X., Chen, W. (2009) Three-dimensional finite element simulation of total knee joint in gait cycle. *Acta Mechanica Solida Sinica*, 22(4), pp. 347-351.

Halloran, J.P., Easley, S.K., Petrella, A.J., Rullkoetter, P.J. (2008) Comparison of deformable and elastic foundation finite element simulations for predicting knee replacement mechanics. *Journal of Biomechanical Engineering*, 127(5), pp. 813-818.

Halloran, J.P., Petrella, A.J., Rullkoetter, P.J. (2005) Explicit finite element modeling of total knee replacement mechanics. *Journal of Biomechanics*, 38(2), pp. 323-331.

Hardt, D.E. (1978) Determining muscle forces in the leg during normal human walking - an application and evaluation of optimization methods. *Journal of Biomechanical Engineering*, 100(2), pp. 72-78.

Heegard, J., Leyvraz, P.F., Curnier, A., Rakotomanana, L., Huiskes, R. (1995) The biomechanics of the human patella during passive knee flexion. *Journal of Biomechanics*, 28(11), pp. 1265-1279.

Hefzy, M.S., Abdel-Rahman, E. (2000) Three-dimensional dynamic anatomical modeling of the human knee joint. In: L. Cornelius (Ed.) *Musculoskeletal Models and Techniques, Biomechanical Systems Techniques and Applications*. CRC Press: Boca Raton (FL).

Hefzy, M.S., Cooke, T.D.V. (1996) Review of knee models: 1996 update. *Applied Mechanics Reviews*, 49(10), pp. 187-193.

Hefzy, M.S., Grood, E.S. (1983) An analytical technique for modeling knee joint stiffness - Part II: Ligamentous geometric nonlinearities. *Journal of Biomechanical Engineering*, 105(2), pp. 145-153.

Hefzy, M.S., Grood, E.S. (1988) Review of knee models. *Applied Mechanics Reviews*, 41(1), pp. 1-13.

Hefzy, M.S., Jackson, W.T., Saddemi, S.R., Hsieh, Y.F. (1992) Effects of tibial rotations on patellar tracking and patello-femoral contact areas. *Journal of Biomedical Engineering*, 14(4), pp. 329-343.

Hefzy, M.S., Yang, H. (1993) A three-dimensional anatomical model of the human patello-femoral joint, for the determination of patello-femoral motions and contact characteristics. *Journal of Biomedical Engineering*, 15(4), pp. 289-302.

Hirokawa, S. (1991) Three-dimensional mathematical model analysis of the patellofemoral joint. *Journal of Biomechanics*, 24(8), pp. 659-671.

Hirokawa, S. (1993) Biomechanics of the knee joint: a critical review. *Critical Reviews in Biomedical Engineering*, 21(2), pp. 79-135.

Howe, T.E., Dawson, L.J., Syme, G., Duncan, L., Reid, J. (2012) Evaluation of outcome measures for use in clinical practice for adults with musculoskeletal conditions of the knee: a systematic review. *Manual Therapy*, 17(2), pp. 100-118.

Huiskes, R. (1992) Mathematical Modeling of the Knee. In: G. Finerman, F.R. Noyes (Eds.) *Biology and biomechanics of the traumatized synovial joint: the knee as a model* (21, pp. 419-439). American Academy of Orthopaedic Surgeons: Rosemont (IL).

Huiskes, R., Kremers, J., de Lange, A., Woltring, H.J., Selvik, G., van Rens, T.J.(1985) Analytical stereophotogrammetric determination of three-dimensional knee-joint geometry. *Journal of Biomechanics*, 18(8), pp. 559-570.

Huson, A., Spoor, C.W., Verbout, A.J. (1989) A model of the human knee, derived from kinematic principles and its relevance for endoprosthesis design. *Acta Morphol Neerl Scand*, 27(1-2), pp. 45-62.

Kalker, J.J. (1990) *Three-dimensional elastic bodies in rolling contact*. Kluwer Academic Publishers: Dordrecht.

Kettelkamp, D.B., Chao, E.Y. (1972) A method for quantitative analysis of medial and lateral compression forces at the knee during standing. *Clinical Orthopaedics and Related Research*, 83, pp. 202-213.

Kim, S. (1998) Three-dimensional dynamic model of the knee. *Journal of Mechanical Science and Technology*, 12(6), pp. 1041-1063.

Komistek, R.D., Kane, T.R., Mahfouz, M., Ochoa, J.A., Dennis, D.A. (2005) Knee mechanics: a review of past and present techniques to determine in vivo loads. *Journal of Biomechanics*, 38(2), pp. 215-228.

Koo, S., Andriacchi, T.P. (2007) A comparison of the influence of global functional loads vs. local contact anatomy on articular cartilage thickness at the knee. *Journal of Biomechanics*, 40(13), pp. 2961-2966.

Küçük, H. (2006) The effect of modeling cartilage on predicted ligament and contact forces at the knee. *Computers in Biology and Medicine*, 36(4), pp. 363-375.

Kurosawa, H., Walker, P.S., Abe, S., Garg, A., Hunter, T. (1985) Geometry and motion of the knee for implant and orthotic design. *Journal of Biomechanics*, 18(7), pp. 487-491.

Kwak, S.D., Blankevoort, L., Ateshian, G.A. (2000) A mathematical formulation for 3D quasi-static multibody models of diarthrodial joints. *Computer Methods in Biomechanics and Biomedical Engineering*, 3(1), pp. 41-64.

Landon, R.L., Hast, M.W., Piazza, S.J. (2009) Robust contact modeling using trimmed NURBS surfaces for dynamic simulations of articular contact. *Computer Methods in Applied Mechanics and Engineering*, 198(30-32), pp. 2339-2346.

Lanovaz, J.L., Ellis, R.E. (2009) A cadaverically evaluated dynamic FEM model of closed-chain TKR mechanics. *Journal of Biomechanical Engineering*, 131(5), 051002, 11p.

Li, G., Sakamoto, M., Chao, E. (1997) A comparison of different methods in predicting static pressure distribution in articulating joints. *Journal of Biomechanics*, 30(6), pp. 635-638.

Lin, Y-C., Haftka, R.T., Queipo, N.V., Fregly, B.J. (2010) Surrogate articular contact models for computationally efficient multibody dynamic simulations. *Medical Engineering & Physics*, 32(6), pp 584-594.

Ling, Z-K., Guo, H-Q., Boersma, S. (1997) Analytical study on the kinematic and dynamic behaviors of a knee joint. *Medical Engineering & Physics*, 19(1), pp. 29-36.

Loch, D.A., Luo, Z.P., Lewis, J.L., Stewart, N.J. (1992) A theoretical model of the knee and ACL: theory and experimental verification. *Journal of Biomechanics*, 25(1), pp. 81-90.

Lu, T-W., Lu, C.H. (2006) Forces transmitted in the knee joint during stair ascent and descent. *Journal of Mechanics*, 22(4), pp. 289-297.

Lu, T-W., O'Connor, J.J., Taylor, S.J.G., Walker, P.S. (1998) Validation of a lower limb model with in vivo femoral forces telemetered from two subjects. *Journal of Biomechanics*, 31(1), pp. 63-69.

Lu, T-W., Tsai, T-Y., Kuo, M-Y., Hsu, H-C., Chen, H-L. (2008) In vivo three-dimensional kinematics of the normal knee during active extension under unloaded and loaded conditions using single-plane fluoroscopy. *Medical Engineering & Physics*, 30(8), pp. 1004-1012.

Machado, M., Flores, P., Ambrósio, J., Completo, A. (2011) Influence of the contact model on the dynamic response of the human knee joint. *Proceedings of the Institution of Mechanical Engineers, Part K: Journal of Multi-body Dynamics*, 225(4), pp. 344-358.

Machado, M., Flores, P., Claro, J.C.P., Ambrósio, J., Silva, M., Completo, A., Lankarani, H.M. (2010) Development of a planar multibody model of the human knee joint. *Nonlinear Dynamics*, 60(3), pp. 459-478.

Machado, M., Moreira, P., Flores, P., Lankarani, H.M. (2012) Compliant contact force models in multibody dynamics: Evolution of the Hertz contact theory. *Mechanism and Machine Theory*, 53, pp. 99-121.

McLean, S.G., Su, A., van den Bogert, A.J. (2003) Development and validation of a 3-D model to predict knee joint loading during dynamic movement. *Journal of Biomechanical Engineering*, 125, pp. 864-874.

Menschik, A. (1974) Mechanik des kniegelenkes *Teil 1. Z. Orthoped*, 112, pp. 481-495.

Menschik, A. (1977) The basic kinematic principle of the collateral ligaments, demonstrated on the knee joint. In G. Chapchal (Ed.), *Injuries of the ligaments and their repair*. George Thieme Publishers: Stuttgart, Germany.

Mikosz, R.P., Andriacchi, T.P., Andersson, G.B.J. (1988) Model analysis of factors influencing the prediction of muscle forces at the knee. *Journal of Orthopaedic Research*, 6(2), pp. 205-214.

Mishra, M., Derakhshani, R., Paiva, G.C., Guess, T.M. (2011) Nonlinear surrogate modeling of tibio-femoral joint interactions. *Biomedical Signal Processing and Control*, 6(2), pp.164-174.

Moeinzadeh, M.H. (1981) *Two and three-dimensional dynamic modeling of human joint structures with special application to the knee joint*. PhD Thesis, Ohio State University, Columbus (OH).

Moeinzadeh, M.H., Engin, A.E. (1983) Response of a two-dimensional dynamic model of the human knee to the externally applied forces and moments. *Journal of Biomedical Engineering*, 5(4), pp. 281-291.

Moeinzadeh, M.H., Engin, A.E. (1988) Dynamic modeling of the human knee joint. *Computational Methods in Bioengineering*, 9, pp. 145-156.

Moeinzadeh, M.H., Engin, A.E., Akkas, N. (1983) Two-dimensional dynamic modelling of human knee joint. *Journal of Biomechanics*, 16(4), pp. 253–264.

Mommersteeg, T.J.A., Blankevoort, L., Huiskes, R., Kooloos, J.G.M., Kauer, J.M.G., Hendriks, J.C.M. (1995) The effect of variable relative insertion orientation of human knee bone-ligament-bone complexes on the tensile stiffness. *Journal of Biomechanics*, 28(6), pp. 745-752.

Morrison, J.B. (1969) Function of the knee joint in various activities. *Biomedical Engineering*, 4(12), pp. 573-580.

Morrison, J.B. (1970) The mechanics of the knee joint in relation to normal walking. *Journal of Biomechanics*, 3(1), pp. 51-61.

Mun, J.H., Lee, D.W. (2004) Three-dimensional contact dynamic model of the human knee joint during walking. *Journal of Mechanical Science and Technology*, 18(2), pp. 211-220.

Nordin, M., Frankel, V.H. (2001) Biomechanics of the knee. In M. Nordin, V.H. Frankel (Eds.), *Basic Biomechanics of the Musculoskeletal System* (pp. 176-201). Lippincott Williams & Wilkins: Philadelphia (PA).

Pandy, M.G., Sasaki, K. (1998) A three-dimensional musculoskeletal model of the human knee joint. Part 2: analysis of ligament function. *Computer Methods in Biomechanics and Biomedical Engineering*, 1(4), pp. 265-283.

Pandy, M.G., Sasaki, K., Kim, S. (1997) A three-dimensional musculoskeletal model of the human knee joint. Part 1: theoretical construction. *Computer Methods in Biomechanics and Biomedical Engineering*, 1(2), pp. 87-108.

Penrose, J.M.T., Holt, G.M., Beaugonin, M., Hose, D.R. (2002) Development of an accurate three-dimensional finite element knee model. *Computer Methods in Biomechanics and Biomedical Engineering*, 5(4), pp. 291-300.

Pérez-González, A., Fenollosa-Esteve, C., Sancho-Bru, J.L., Sánchez-Marín, F.T., Vergara, M., Rodríguez-Cervantes, P.J. (2008) A modified elastic foundation contact model for application in 3D models of the prosthetic knee. *Medical Engineering & Physics*, 30(3), pp. 387–398.

Perry, J., Antonelli, D., Ford, W. (1975) Analysis of knee-joint forces during flexed-knee stance. *The Journal of Bone & Joint Surgery* - A, 57(7), pp. 961-967.

Piazza, S.J., Delp, S.L. (2001) Three-dimensional dynamic simulation of total knee replacement motion during a step-up task. *Journal of Biomechanical Engineering*, 123(6), pp. 599–606.

Pope, M.H., Crowninshield, R., Miller, R., Johnson, R. (1976) The static and dynamic behavior of the human knee in vivo. *Journal of Biomechanics*, 9(7), pp. 449-452.

Sarzi-Puttini, P., Cimmino, M.A., Scarpa, R., Caporali, R., Parazzini, F., Zaninelli, A., Atzeni, F., Canesi, B. (2005) Osteoarthritis: an overview of the disease and its treatment strategies. *Seminars in Arthritis and Rheumatism*, 35(1), pp. 1-10.

Sathasivam, S., Walker, P.S. (1997) A Computer model with surface friction for the prediction of the total knee kinematics. *Journal of Biomechanics*, 30(2), pp. 177-184.

Seedhom, B.B., Terayama, K. (1976) Knee forces during the activity of getting out of a chair with and without the aid of arms. *Biomedical Engineering*, 11(8), pp. 278-282.

Shahar, R., Banks-Sills, L. (2004) A quasi-static three-dimensional, mathematical, three-body segment model of the canine knee. *Journal of Biomechanics*, 37(12), pp. 1849-1859.

Shelburne, K.B., Pandy, M.G. (1997) A musculoskeletal model of the knee for evaluating ligament forces during isometric contractions. *Journal of Biomechanics*, 30(2), pp. 163-176.

Smidt, G.L. (1973) Biomechanical analysis of knee flexion and extension. *Journal of Biomechanics*, 6(1), pp. 79-92.

Smith, P.N., Refshauge, K.M., Scarvell, J.M. (2003) Development of the concepts of knee kinematics. *Archives of physical medicine and rehabilitation*, 84(12), pp. 1895-1902.

Strasser, H. (1917) *Lehrbuch der Muskel und Gelenkmechanik*. Springer: Berlin.

Stylianou, A.P., Guess, T.M., Cook, J.L. (2012) Development and validation of a multi-body model of the canine stifle joint. *Computer Methods in Biomechanics and Biomedical Engineering* (DOI: 10.1080/10255842.2012.684243).

Tümer, S.T., Engin, A.E. (1993) Three-body segment dynamic model of the human knee. *Journal of Biomechanical Engineering*, 115(4A), pp. 350-356.

van Eijden, T., Kouwenhoven, E., Verburg, J., Weijs, W.A. (1986) A mathematical model of the patellofemoral joint. *Journal of Biomechanics*, 19(3), pp. 219-223.

Wahrenberg, H., Lindbeck, L., Ekholm, J. (1978a) Knee muscular moment, tendon tension force and EMG during a vigorous movement in man. *Scandinavian Journal of Rehabilitation Medicine*, 10(2), pp. 99-106.

Wahrenberg, H., Lindbeck, L., Ekholm, J. (1978b) Dynamic load in the human knee joint during voluntary active impact to the lower leg. *Scandinavian Journal of Rehabilitation Medicine*, 10(2), pp. 93-98.

Wilson, D.R., Feikes, J.D., O'Connor, J.J. (1998) Ligaments and articular contact guide passive knee flexion. *Journal of Biomechanics*, 31(12), pp. 1127-1136.

Wilson, D.R., O'Connor, J.J. (1997) A three-dimensional geometric model of the knee for the study of joint forces in gait. *Gait & Posture*, 5(2), pp. 108-115.

Wimmer, M.A., Andriacchi, T.P. (1997) Tractive forces during rolling motion of the knee: implications for wear in total knee replacement. *Journal of Biomechanics*, 30(2), pp. 131-137.

Winby, C.R., Lloyd, D.G., Besier, T.F., Kirk, T.B. (2009) Muscle and external load contribution to knee joint contact loads during normal gait. *Journal of Biomechanics*, 42(14), pp. 2294-2300.

Wismans, J. (1980) *A three-dimensional mathematical model of the human knee joint*. PhD Thesis, Eindhoven University of Technology, Eindhoven, Netherlands.

Wismans, J., Veldpaus, F., Janssen, J., Huson, A., Struben, P. (1980) A three-dimensional mathematical model of the knee-joint. *Journal of Biomechanics*, 13(8), pp. 677-685.

Wongchaisuwat, C., Hemami, H., Buchner, HJ (1984a) Control of sliding and rolling at natural joints. *Journal of Biomechanical Engineering*, 106(4), pp. 368-375.

Wongchaisuwat, C., Hemami, H., Hines, M.J. (1984b) Control exerted by ligaments. *Journal of Biomechanics*, 17(7), pp. 525-532.

World Health Organization (2003) *The burden of musculoskeletal conditions at the start of the new millennium*. Report of a WHO scientific group, Geneva, Switzerland.

Yang, N.H., Canavan, P.K., Nayeb-Hashemi, H., Najafi, B., Vaziri, A. (2010) Protocol for constructing subject-specific biomechanical models of knee joint. *Computer Methods in Biomechanics and Biomedical Engineering*, 13(5), pp. 589-603.

Yao, J., Salo, A.D., Lee, J., Lerner, A.L. (2008) Sensitivity of tibio-menisco-femoral joint contact behavior to variations in knee kinematics. *Journal of Biomechanics*, 41(2), pp. 390-398.

Zavatsky, A.B., O'Connor, J.J. (1992a) A model of human knee ligaments in the sagittal plane: Part 1 - response to passive flexion. *Proceedings of the Institution of Mechanical Engineers, Part H: Journal of Engineering in Medicine*, 206(3), pp. 125-134.

Zavatsky, A.B., O'Connor, J.J. (1992b) A model of human knee ligaments in the sagittal plane: Part 2 - fibre recruitment under load. *Proceedings of the Institution of Mechanical Engineers, Part H: Journal of Engineering in Medicine*, 206(3), pp. 135-145.

Zhu, Y., Chen, J.X. (2004) Simulation and visualization of knee joint contact using deformable model. *Proceedings of the 4th International Conference on Computer and Information Technology* (pp. 708-715), Wuhan, China.

Zhu, Y., Chen, J.X., Xiao, S., MacMahon, E. (1999) 3D knee modeling and biomechanical simulation. *Computing in Science & Engineering*, 1(4), pp. 82-87.

2

Human knee joint: anatomy and function

2.1 *Basic terminology for human movement* **2**-2
2.2 *Structural anatomy* **2**-4
2.3 *Principal movements and its characteristics* **2**-13
2.4 *Mechanical response of knee surrounding tissues* **2**-19
2.5 *Joint pathologies and replacement systems* **2**-31
2.6 *Summary and discussion* **2**-35
References **2**-38

The knee joint (latin: articulatio genus) is the largest synovial joint in the human body, and of all joints possesses the most voluminous synovial cavity. It is a complicated system that interconnects four bones with ligaments, muscles and intra-articular structures, such as menisci and hyaline cartilage. These elements are generally capable of bearing and transferring load during various physical activities. Being the intermediate joint of the lower limb, the knee has to support the body weight and to provide stability to the whole body. Nevertheless, the knee joint has also to promote movement between thigh and shank in order to allow the human subject to walk. From a mechanical viewpoint, the knee ensures two almost mutually exclusive conditions: stability and mobility (Wismans, 1980; Hirokawa, 1993; Yang *et al.*, 2010).

The present Chapter includes an overview of concepts and terms used in biomechanics, as well as a description of knee anatomy. The principal movements of this articulation and some biomechanical features are revised. The mechanical behavior of human knee joint and its surrounding tissues are also presented. Finally, some attention is given to the knee joint pathologies and to knee implant models.

2.1 Basic terminology for human movement

In biomechanics, specific terms are employed to describe spatial relations between different parts of the body. This terminology is based on the anatomical position in which a person is standing upright, with the feet together and the arms by the sides of the body with the palms forward. Figure 2.1 illustrates this standing configuration, as well as the three primary planes and the terms describing relations between different parts of the body. The sagittal plane is the only plane of symmetry. This plane divides the human body into left- and right-hand sides. As it can be observed in Figure 2.1, the transverse plane passes through the hip bone, dividing it into superior and inferior sections. The frontal plane, also called coronal plane, divides the human body into anterior and posterior sections (Tözeren, 2000; Whittle, 2007). Within a single part of the body, four additional terms are utilized to describe relations, which are depicted in Figure 2.2. Medial means towards the midline of the body, while lateral means away from the midline of the body. Proximal means towards the rest of the body, while distal means away from the rest of the body (Whittle, 2007).

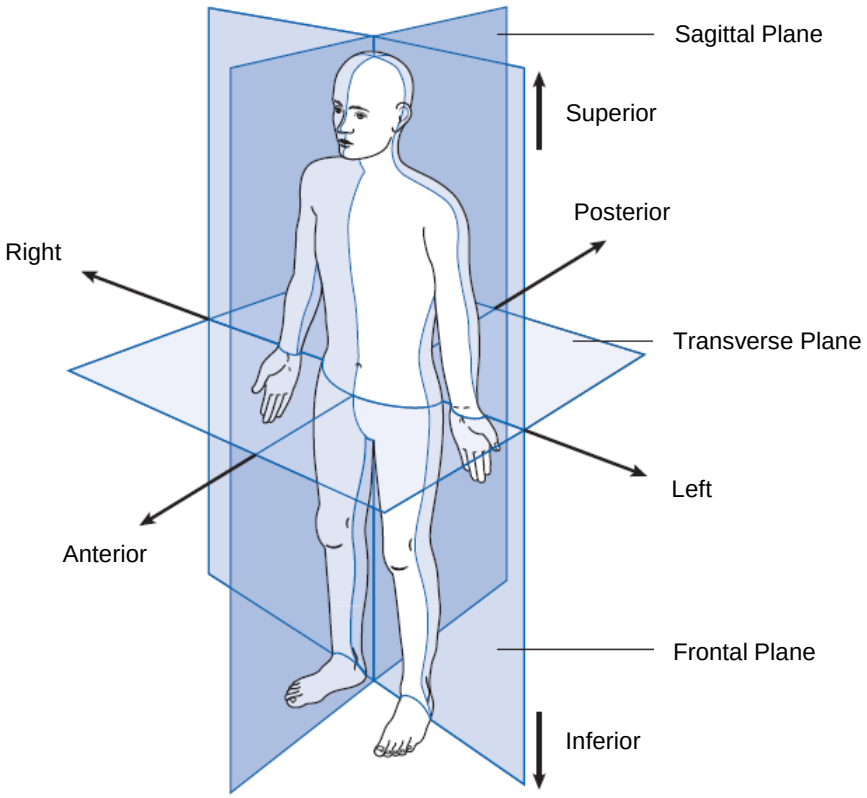

Figure 2.1 The anatomical position, with three reference planes and six fundamental directions {Adapted from Whittle (2007) with Elsevier permission}.

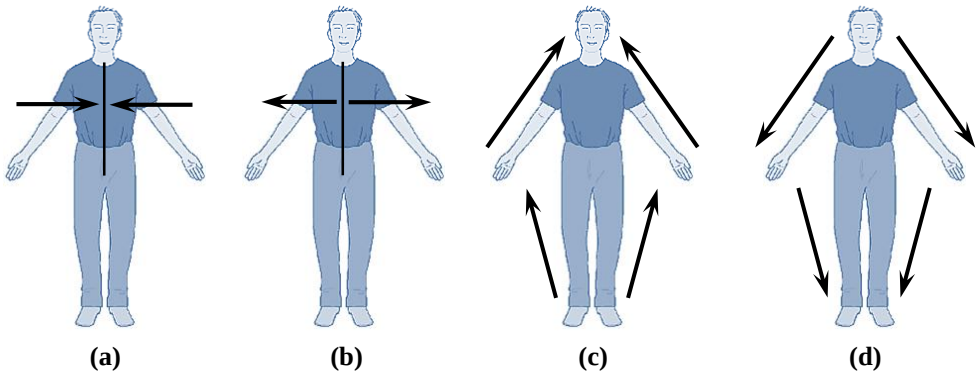

Figure 2.2 Four anatomical directions: (a) Medial; (b) Lateral; (c) Proximal; (d) Distal {Adapted from Hannon (2005) with Elsevier permission}.

Standard terminology is also used to classify movement configurations of the various parts of the human body. Most joints can only move in one or two of the three primary planes. The directions of these motions for the knee are shown in Figure 2.3. According to Evans (1986), the movements of the human joints can be described as active, conjunct or passive. The active joint motion is voluntary, while the conjunct movements are the consequence of other movements and are due to the geometry of the articulating surfaces and the presence of surrounding ligamentous structures. The passive movements are those that are performed by an examiner with the purpose of evaluating the laxity of the joint.

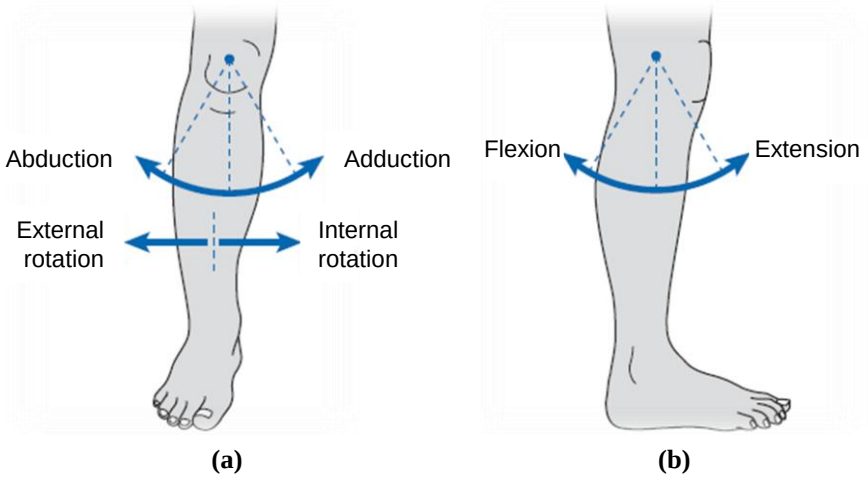

Figure 2.3 Movements about the knee joint: (a) Frontal view; (b) Lateral view {Adapted from Whittle (2007) with Elsevier permission}.

Flexion and extension movements are considered active movements that take place in the sagittal plane. Flexion is a rotational motion that brings two adjoining long bones closer to each other, such as occurs in the flexion of the leg. Extension denotes rotation in the opposite direction of flexion. If the movement of extension continues past the anatomical position, it is called hyperextension (Tözeren, 2000; Whittle, 2007).

Internal-external rotation takes place in the transverse plane and are also called medial and lateral rotation, respectively. These movements are influenced by the position of the joint in the sagittal plane and generally can occur only with the joint in some amount of flexion (Tözeren, 2000; Mader, 2005; Whittle, 2007).

Abduction and adduction are the movements of the limbs in the frontal plane, which are similarly affected by the amount of joint flexion. Abduction is movement away from the longitudinal axis of the body whereas adduction is moving the limb back, as Figure 2.3 depicts (Tözeren, 2000; Whittle, 2007).

Furthermore, other terms are used to describe the motions of the joints or body segments, namely pronation-supination, varus-valgus, among others. The pronation and supination movements correspond to the rotations about the long axis of the forearm or foot. The pronation of both hands brings the thumbs together, while the supination brings the little fingers together (Whittle, 2007). In turn, the varus-valgus describes an angulation of a joint towards or away from the midline of the body, respectively. Varus-valgus is an example of a passive movement. For more information on the anatomical classification of human movement, the interested reader is referred to the work by Mader (2005) and Whittle (2007).

2.2 Structural anatomy

Human body has different types of articular joints, which according to its mobility can be divided in three main groups: synarthroses (or fibrous joints), amphiarthroses (or cartilaginous joints) and diarthroses (or synovial joints). The synarthroses, such as the skull sutures, are immovable. The amphiarthroses are connected by fibrocartilage, as in the intervertebral discs, or by hyaline cartilage, as in the costal cartilages that join the ribs to the sternum. These joints are slightly movable. Finally, the diarthroses are separated by a cavity and are freely movable. The joint cavity or capsule is lined by a synovial membrane, which produces synovial fluid, a lubricant for the joint. The knee joint is an example of a diarthrose or synovial joint. The synovial joints can be also classified in subcategories based on the architecture and topology of the surfaces involved, and on the types of movement permitted. These subcategories of synovial joints include ball and socket joints, ellipsoidal joints, pivot joints, hinge joints, saddle joints, planar joints and condyloid joints (Mader, 2005).

The knee is a synovial joint composed by four bones, namely femur, tibia, patella and fibula. The femur is the thigh bone and is the longest bone of the human body. The tibia is the second longest bone of the human body and is a shank bone, as well as the fibula. The tibia is located medially and the fibula is situated in the lateral side. The patella, also called kneecap, has a triangular shape and is the largest sesamoid bone in the human body. It is supported superiorly by the quadriceps tendon and inferiorly by the patella ligament. The patella is located anteriorly to the trochlear groove of the femur with the apex oriented inferiorly (Mason *et al.*, 2008). The four bones articulate with each other forming three joints: the tibiofemoral, the patellofemoral and the superior tibiofibular. These three articulations are illustrated in Figure 2.4.

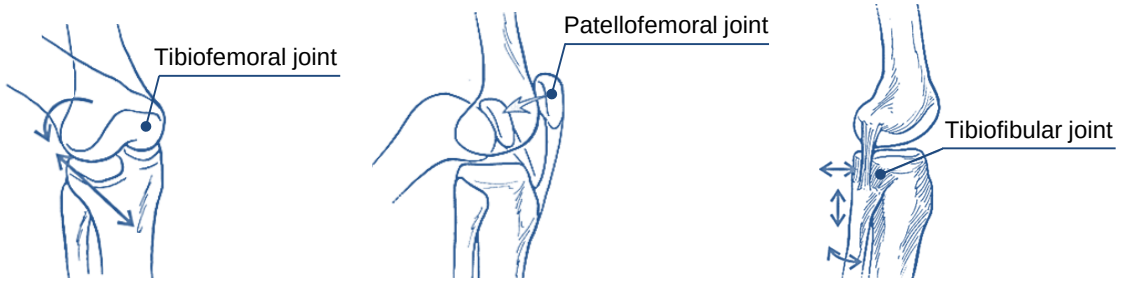

Figure 2.4 Three joints of the human knee articulation: (a) Tibiofemoral joint; (b) Patellofemoral joint; (c) Superior tibiofibular joint {Adapted from Hamill and Knutzen (2009) with Lippincott Williams & Wilkins permission}.

Figure 2.5a shows the distal end of the femur that composes the tibiofemoral joint. This bony structure exhibits two large convex surfaces named condyles. The medial and lateral condyles are separated by the trochlear (or patellar) groove and the intercondylar notch (or fossa) in the anterior and posterior sides, respectively. The femoral condyles are asymmetric and present some geometrical differences. The lateral condyle has a larger surface area and projects more posteriorly. This condyle is flatter and more prominent in the anterior direction in order to hold the patella in the right place. The medial condyle is longer in the anterior-posterior direction and projects more distally and medially. Instead of being aligned with the femur as the lateral condyle, the medial condyle is in alignment with the tibia (Hamill and Knutzen, 2009).

The femoral condyles lie on the tibial plateaus, which are divided by a ridge of bone named the intercondylar eminence, as Figure 2.5b illustrates. The intercondylar eminence has a key role of centering the joint and stabilizing the bones during the weight bearing (*i.e.*, when a single lower limb supports all the body weight). The tibial plateaus are distinct in shape and conformality. On one hand, the lateral tibial plateau

exhibits a circular and convex surface. On the other hand, the medial tibial plateau is slightly concave being therefore conformal with the convex medial condyle of the femur. Moreover, the medial plateau presents an elliptical shape, larger and longer in the anterior-posterior direction as the medial femoral condyle. Thus, the medial tibia and femur fit perfectly together and the lateral tibia and femur do not. These geometrical differences are some of the features that make the knee articulation a unique joint, hard to model and replace. For example, the non-conformality of the lateral femur and tibia is one of the determinants of rotation because it lets the lateral condyle to undergo a greater excursion (*i.e.* movement from and back to the midline) with the flexion and extension motion (Hamill and Knutzen, 2009).

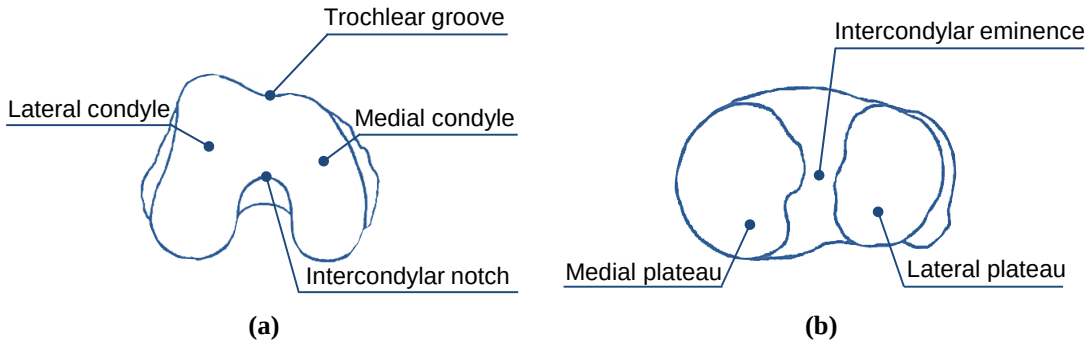

Figure 2.5 (a) Distal femur; (b) Proximal tibial {Adapted from Dargel *et al.* (2011) with Elsevier permission}.

Similarly to other articulating bone ends of diarthroses, the distal femur and the proximal tibia are covered by a thin (1-6 mm) dense, translucent, white connective tissue designated hyaline articular cartilage. The articular cartilage is a very specialized tissue precisely suited for withstanding high joint loads without failure during an average individual's lifetime. In synovial joints, articular cartilage has two primary functions: (*i*) to distribute joint loads over a wide area, thus decreasing the stresses sustained by the contacting joint surfaces, and (*ii*) to allow relative movement of the opposing joint surfaces with minimal friction and wear (Nordin and Frankel, 2001).

Besides the hyaline articular cartilage, two c-shaped structures lie between the tibia and the femur, as depicted in Figure 2.6. These structures are named menisci and are composed by fibriocartilage. The lateral meniscus occupies a larger percentage of area than the medial meniscus and is capable of moving more than twice the distance of the medial meniscus in the anterior-posterior direction (Hamill and Knutzen, 2009). The primary functions of the menisci are: (*i*) to improve joint stability by extending the contact surface on the tibia, (*ii*) to participate in shock absorption by transmitting half of

the weight-bearing load in full extension and a significant portion of the load in flexion, (*iii*) to protect the underlying hyaline articular cartilage and subchondral bone, (*iv*) to reduce the stresses on the contact sites, and (*v*) to enhance lubrication of the joint by acting as a space-filling mechanism and allowing dispersal of more synovial fluid to the surface of the tibia and the femur bones (Hamill and Knutzen, 2009).

The distal femur and the proximal tibia are connected by ligaments, which prevent the excessive motion and augment the mechanical stability of the joint (Nordin and Frankel, 2001). These ligaments guide the knee motion by maintaining the relative position of the tibia and femur so that contact is appropriate and at the right time. The ligaments support the joint passively as they are loaded in tension only, and serve as a backup to muscles (Hamill and Knutzen, 2009). In Figure 2.6a, the primary ligaments of the tibiofemoral joint are represented, namely the anterior cruciate ligament (ACL), the posterior cruciate ligament (PCL), the medial collateral ligament (MCL) and the lateral collateral ligament (LCL). It is important to mention that the MCL and the LCL are also named as tibial collateral ligament and fibular collateral ligament, respectively.

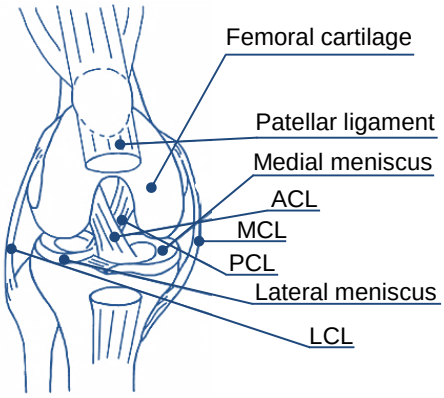

Figure 2.6 Knee joint and its surrounding ligaments and intra-articular structures {Adapted from Kamekura *et al.* (2005) with Elsevier permission}.

The collateral ligaments run along the sides of the knee and limit the sideways motion of the knee. MCL support the knee against any valgus force providing 78 percent of total valgus restraint, while LCL offers the main resistance to varus force, about 69 percent of the varus restraint. Both collateral ligaments are taut in full extension even though the anterior portion of the MCL is also stretched in flexion. In full flexion, MCL and LCL reduce their lengths by approximately 17 and 25 percent, respectively. Furthermore, MCL offers some resistance to both internal and external rotation (Woo *et al*., 1999; Hamill and Knutzen, 2009).

The cruciate ligaments are intrinsic, lying inside the joint in the intercondylar space. These ligaments control both anterior-posterior and rotational motions of the human knee. The ACL is 40 percent longer than the PCL. Both cruciate ligaments stabilize, limit rotation, and cause sliding of the condyles over the tibia in flexion. They both also offer some stabilization against varus and valgus forces. The cruciate ligaments offer the main resistance to the movement of the tibia relative to the femur on the sagittal plane. The ACL restrains 85 percent of the anterior movement of the tibia. The PCL limits 95 percent the movement of the tibia on the posterior direction (Woo *et al*., 1999; Hamill and Knutzen, 2009).

As far as the ACL length is concerned, it elongates by about 7 percent as the knee moves from extension to 90 degrees of flexion and maintains the same length up through maximum flexion. If the joint is internally rotated, the insertion of the ACL moves anteriorly, elongating the ligament slightly more. Different parts of the ACL are taut in different knee positions. Nonetheless, as a whole, the ACL is considered to be taut in the extended position (Woo *et al*., 1999; Hamill and Knutzen, 2009).

The PCL decreases in length and slackens by 10 percent at 30 degrees of knee flexion and then maintains that length throughout flexion. The PCL increases in length by about 5 percent with internal rotation of the joint up to 60 degrees of flexion and then decreases in length by 5 to 10 percent as flexion continues. The ligament is not affected by external rotation in the joint, maintaining a fairly constant length. It is maximally strained through 45 to 60 degrees of flexion. As with the ACL, the fibers of the PCL participate in different functions. However, as a whole, the PCL is taut in maximum knee flexion (Woo *et al*., 1999; Hamill and Knutzen, 2009).

Another important support structure surrounding the knee is the joint capsule, which is present in all human diarthroses. The joint capsule of the knee joint, also designated as capsular ligament, consists of an external fibrous layer, or fibrous capsule, and an internal synovial membrane or synovium, separated by fatty deposits anteriorly and posteriorly. The femur, the tibia and the patella are kept together by the fibrous capsule, which enclose a single, large joint cavity between the bones, as depicted in Figure 2.7. The synovial membrane, which lines inside of the joint capsule, produces an oily fluid named synovial fluid.

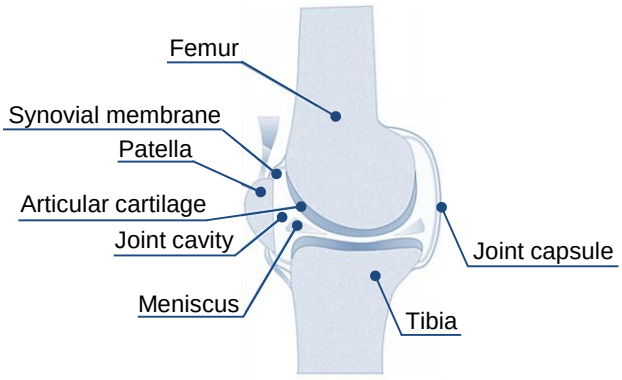

Figure 2.7 Longitudinal cross-section view of the human knee joint {Adapted from Gerwin *et al.* (2006) with Elsevier permission}.

The synovial fluid plays as a lubricant in order to keep the articular surfaces as frictionless as possible. This fluid is normally pale yellow and viscous and is only present in small amounts, being its composition similar to blood plasma. The synovial membrane is attached to the margins of the articular surfaces and to the superior and inferior outer margins of the menisci. The cruciate ligaments, which are attached to the intercondylar region of the tibia below and the intercondylar fossa of the femur above, are outside the joint cavity, but enclosed within the fibrous capsule (Mader, 2005).

The muscles that surround the knee are responsible for the movements and stability of the joint. These muscles are illustrated in Figure 2.8 and listed in Table 2.1.

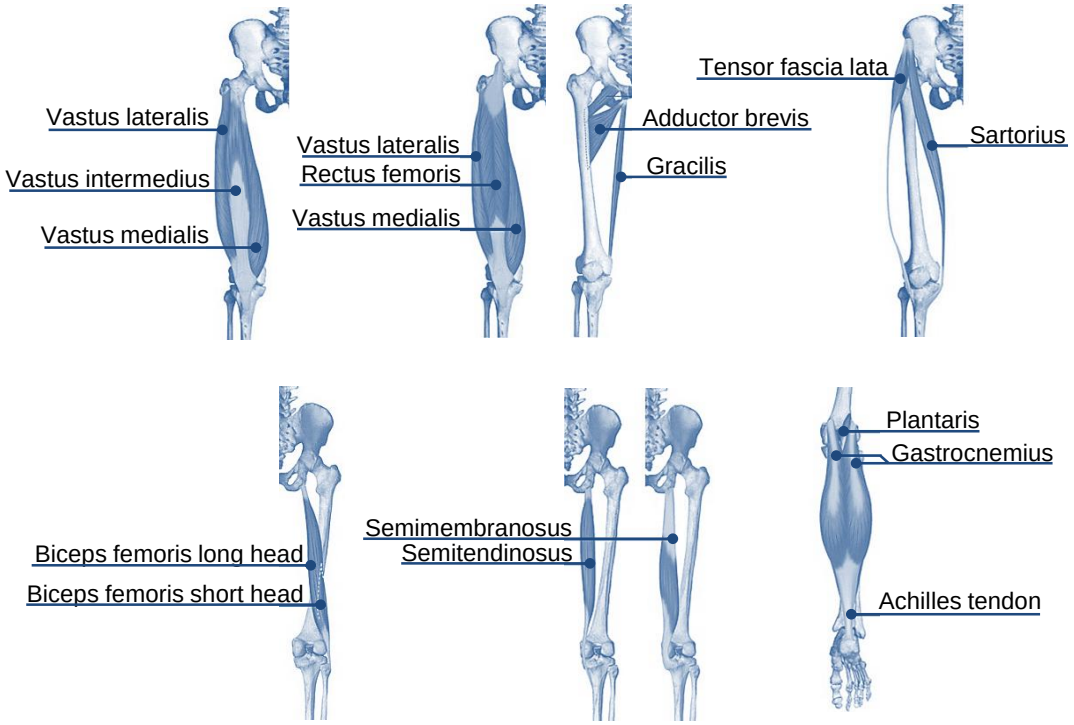

Figure 2.8 Principal muscles involved with the knee joint {Adapted from Teiz and Graney (2003) with the permission of University of Washington}.

Most muscles are attached to different bones at their two ends and cross over one joint, the monarticular muscles, or two joints, the biarticular muscles, or even several joints, the polyarticular muscles. In many cases, the attachment to one of the bones covers a broad area, whereas at the other end it narrows into a tendon. Ligaments and tendons are similar and frequently confused. As a general rule, ligaments connect two bones together, whereas tendons connect muscles to bones (Whittle, 2007).

Table 2.1 Muscles acting on the knee (Whittle, 2007). The meaning of the abbreviations is as follows: anterior (ant), posterior (post), superior (sup), inferior (inf), medial (med) and lateral (lat).

	Muscles	**Origin**	**Insertion**	**Functions**
	Tensor fascia lata (biarticular)	Pelvis close to the ant. sup. iliac spine.	Iliotibial tract	Hip and Knee abductor.
Quadriceps (knee extensors)	Rectus femoris (biarticular)	Ant. inf. iliac spine of the pelvis.	Quadriceps tendon	Hip flexor; Knee extensor.
	Vastus medialis (monoarticular)	Upper part of the femur on the med. side.	Quadriceps tendon	Knee extensor.
	Vastus intermedius (monoarticular)	Upper part of the femur on the ant. side.	Quadriceps tendon	Knee extensor.
	Vastus lateralis (monoarticular)	Upper part of the femur on the lat. side.	Quadriceps tendon	Knee extensor.
Hamstrings (knee flexors)	Biceps femoris (biarticular)	Long head – ischial tuberosity; Short head – middle of the femur shaft.	Lat. tibial plateau	Hip extensor; Knee flexor.
	Semitendinosus (biarticular)	Ischial tuberosity of the pelvis.	Med. tibial plateau	Hip extensor; Knee flexor.
	Semimembranosus (biarticular)	Ischial tuberosity of the pelvis.	Med. tibial plateau	Hip extensor; Knee flexor.
Pes anserinus (knee medial stabilizers)	Gracilis (biarticular)	Pubis at the med. side of the thigh.	Back of the tibia on its med. side.	Hip adductor; Knee flexor.
	Sartoris (biarticular)	Ant. sup. iliac spine of the pelvis and winding around the front of the thigh.	Front of the tibia on its med. side.	Hip flexor.
	Popliteus	Lat. condyle of femur and lat. meniscus.	Post. surface of tibia, sup. to soleal line.	Unlock the knee by internally rotating.
	Gastrocnemius (biarticular)	Back of the med. and lat. condyles of the femur.	Achiles tendon	Knee flexor; Plantarflexor.

At the knee joint, three muscle groups can be distinguished: the quadriceps, the hamstrings and the pes anserinus. The quadriceps comprises four distinct muscles, namely the rectus femoris, vastus medialis, vastus lateralis and vastus intermedius, being responsible for the knee extension. The muscle group that contributes to knee flexion is the hamstrings, consisting of the biceps femoris, semimembranosus and semitendinosus. In turn, the pes anserinus muscles, that is, the sartorius, gracilis and semimembranosus are dynamic medial stabilizers, which contribute for knee flexion and internal rotation (Margo *et. al.*, 2010).

The quadriceps muscle group is one of the strongest muscle groups in the human body, being three times stronger than its antagonistic muscle group, the hamstrings. The quadriceps femoris contributes to the stability of the patella via the patellar tendon. Furthermore, the quadriceps muscle group pulls the menisci anteriorly in extension via the meniscopatellar ligament. When the quadriceps muscles contract, they reduce the strain in the MCL and work with the PCL to prevent posterior displacement of the tibia. The quadriceps muscles are antagonistic to the ACL (Hamill and Knutzen, 2009).

The only biarticular muscle of the quadriceps group is the rectus femoris. This muscle does not significantly contribute to knee extension force unless the hip joint is in a favorable position. It is limited as an extensor of the knee if the hip is flexed and is facilitated as a knee extensor if the hip joint is extended. In walking and running, the rectus femoris contributes to the extension force in the toe-off phase when the thigh is extended. Likewise, in kicking, the rectus femoris activity is maximized in the preparatory phase as the thigh is brought back into hyperextension with the leg in flexion (Hamill and Knutzen, 2009; Margo *et. al.*, 2010).

The vastus lateralis is the largest and strongest muscle of the quadriceps group. It applies a lateral force to the patella and pulls medially the vastus medialis. The vastus medialis may be divided into the vastus medialis obliquus and the vastus medialis longus. The vastus medialis obliquus fibers arise more distally and are more oblique in orientation, varying from 55 to 70 degrees relative to the longus fibers (Margo *et. al.*, 2010). Although the vastus medialis as a whole is an extensor of the knee, the vastus medialis obliquus is also a medial stabilizer of the patella (Hamill and Knutzen, 2009).

The action of the hamstrings can be quite complex because they are biarticular muscles that work to flex the knee and to extend the hip as well. The hamstrings operate

most effectively as knee flexors from a position of hip flexion by increasing the length and tension in the muscle group. Therefore, the hamstring group is very active with the limb off the ground, working frequently to slow a rapidly extending leg. The greatest force of the hamstrings is generated at 90 degrees of flexion. The hamstrings work with the ACL to restraint anterior tibial displacement. These muscles are also knee rotators because of their insertions on the sides of the knee joint (Hamill and Knutzen, 2009).

The biceps femoris has two heads connecting on the lateral side of the knee, namely the long head and the short head. This muscle offers lateral support to the joint and also produces external rotation of the lower leg. In turn, the semimembranosus pulls the meniscus posteriorly in flexion and also contributes to the production of internal rotation in the joint (Hamill and Knutzen, 2009).

The other medial hamstring, the semitendinosus, is part of the pes anserinus muscular attachment on the medial surface of the tibia. It is the most effective flexor of the pes anserinus muscle group, contributing 47 percent to the flexion force. The semitendinosus works with both the ACL and the MCL in supporting the knee joint and also contributes to the generation of internal rotation (Hamill and Knutzen, 2009).

The two remaining pes anserinus muscles, the sartorius and the gracilis, contribute in 19 and 34 percent to the flexion strength, respectively. The popliteus is a weak flexor that supports the PCL in deep flexion and draws the meniscus posteriorly. Finally, the two-joint gastrocnemius contributes to knee flexion, especially when the foot is in the neutral or dorsiflexed position. The pes anserinus muscles, along with the semimembranosus and the popliteus, contribute also for the internal rotation of the tibia. Only one muscle, the biceps femoris, contributes significantly to the generation of external rotation of the tibia. Both internal and external rotations are necessary movements associated with function of the knee joint (Hamill and Knutzen, 2009).

Figure 2.4b shows the patellofemoral joint, which corresponds to the articulation of the posterior patella with the trochlear groove of the distal femur, and is considered a saddle joint. As depicted in Figure 2.9, the patella is held in place by the quadriceps tendon that continues as a ligament, *i.e.* the patellar ligament, which attaches to the tibial tuberosity. A vertical ridge of bone separates the underside of the patella into medial and lateral facets, each of which can be further divided into superior and inferior facets. A fifth facet, the odd facet, lies on the far medial side of the patella, as Figure 2.9

illustrates. The main functions of the patella are: (*i*) to improve the efficiency of the extensor forces through the entire knee flexion range, (*ii*) to centralize the forces of the different quadriceps muscle bellies, and (*iii*) to provide a smooth sliding mechanism for the quadriceps muscle with little friction due to its cartilage cover. The patella offers also a protecting shield to the knee (Heegaard *et al.*, 1995; Hamill and Knutzen, 2009).

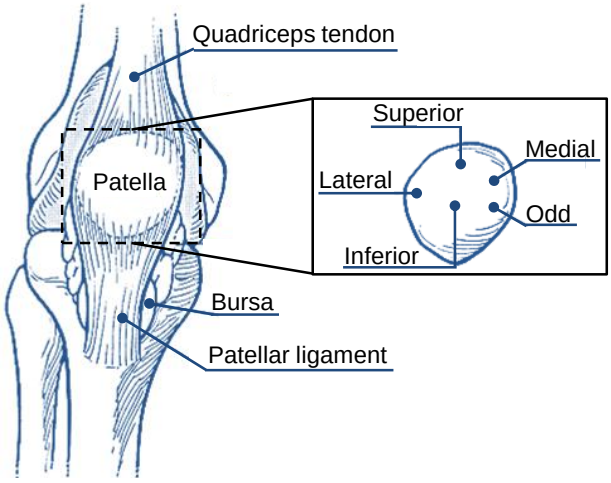

Figure 2.9 Patella and its five facets {Adapted from Hamill and Knutzen (2009) Lippincott Williams & Wilkins permission}.

The third articulation of the knee is the superior tibiofibular joint, represented in Figure 2.4c, which is a small joint between the head of the fibula and the lateral tibial plateau. Radakovich and Malone (1982) referred to this joint as "the forgotten joint", because it had been ignored by clinicians and anatomist for a long time. According to these authors, flexion and extension of the knee do not occur without tibial rotation and this motion is quite restricted. Therefore, to accommodate internal and external rotatory movements of the tibia, the superior tibiofibular joint provides a compensatory motion (Radakovich and Malone, 1982). The superior tibiofibular articulation is a gliding joint that moves anterior-posteriorly, inferior-superiorly, and rotates in response to movements of the tibia or the foot. The primary functions of this joint are: (*i*) to dissipate the torsional stresses applied at the ankle joint and (*ii*) to dissipate the lateral tibial bending movements (Radakovich and Malone, 1982; Hamill and Knutzen, 2009).

2.3 Principal movements and its characteristics

Knee joint motion is a result of the bony geometry, the soft-tissue structures (such as ligaments and menisci), the joint loading and the muscle activation. The intrinsic anatomy of the human knee provides for movement with six degrees-of-freedom.

Normal knee function is achieved in various combinations of rotation and translation of the femur with respect to the tibia. The primary motions of the knee are the flexion and extension movements on the sagittal plane. The knee joint describes also secondary motions, including internal-external rotation and abduction-adduction, which play an key role in overall function (Dyrby and Andriacchi, 2004). The flexion and extension movements at the knee joint involve a combination of rolling and sliding called "femoral roll back". The full extension generally occurs at 0 degrees, full flexion at 140 degrees and the average limit of hyperextension is 5 degrees. In full flexion, the posterior, more curved surfaces of the femoral condyles are located towards the posterior periphery of the tibial plateaus. As the joint moves from flexion to extension, the femoral condyles roll forwards or slide in the menisci as the menisci themselves slide across the tibial plateaus until full extension is reached (Ramson, 1995).

The instant center technique is a simpler method that can be utilized to analyze planar joint motions. As a body rotates about other body, at any instant there is a point that does not have relative motion, that is, a point that has zero relative velocity. This point constitutes an instantaneous center of rotation, or instant center (IC). The instant center technique can be applied to the tibiofemoral joint in order to determine the pathway of the IC in the sagittal plane at this articulation. The normal pathway of the IC at the tibiofemoral joint during flexion-extension movement is a semi-circle trajectory, as Figure 2.10a depicts. Nonetheless, any internal derangement may influence the IC trajectory and, hence, it will be easily identified by the instant center technique. An abnormal IC pathway for a 35-year-old man with a bucket-handle derangement is illustrated in Figure 2.10b (Nordin and Frankel, 2001; Completo, 2006).

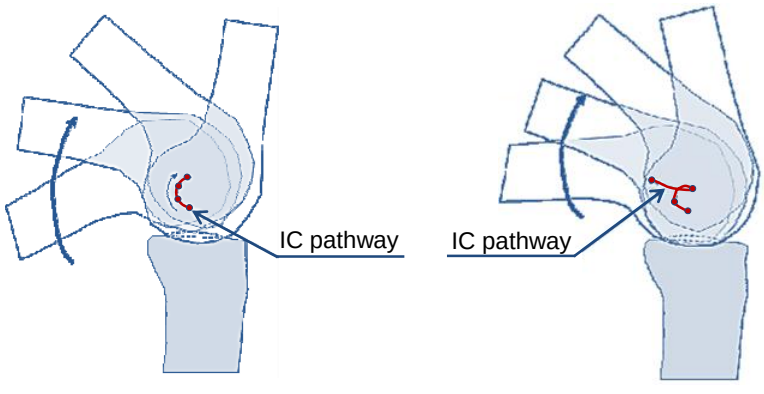

Figure 2.10 (a) Semicircular instant center pathway for the tibiofemoral joint in a 19-year-old man with a normal knee; (b) Abnormal instant center pathway for a 35-year-old man with a bucket-handle derangement {Adapted from Completo (2006) with Author's permission}.

The knee motion in the sagittal plane during level walking is ranged from 0 to approximately 67 degrees. At the beginning of the stance phase, *i.e.* at heel strike, the knee is in full or nearly full extension, as well as at the end of this phase of the gait cycle, that is, before the toe-off. The maximum knee flexion is observed during the middle of the swing phase (Nordin and Frankel, 2001).

With the knee in full extension, rotation is almost completely restricted by the interlocking of the femoral and tibial condyles. The range of rotation increases as the knee is flexed, reaching a maximum at 90 degrees of flexion. With the knee in this position, external rotation ranges from 0 to approximately 45 degrees and internal rotation ranges from 0 to approximately 30 degrees. During gait, total rotation of the tibia with respect to the femur ranged from approximately 4 to 13 degrees. External rotation began during knee extension in the stance phase and reached a peak value at the end of the swing phase just before heel strike. In turn, internal rotation is reported during flexion in the swing phase (Nordin and Frankel, 2001; Completo, 2006).

Beyond 90 degrees of flexion, the range of internal and external rotation decreases, mainly because the soft tissues restrict rotation (Ramson, 1995). The rotation occurring in the last 20 degrees of extension has been termed the "screw-home mechanism". The screw-home mechanism is the point at which the medial and lateral condyles are locked to form the close-packed position for the knee joint. The screw-home mechanism moves the tibial tuberosity laterally and produces a medial shift at the knee. Some of the hypothetical causes of the screw-home movement are that the lateral condyle surface is covered first and a rotation occurs to accommodate the larger surface of the medial condyle or that the ACL becomes taut just before rotation, forcing rotation of the femur on the tibia. Finally, it is speculated that the cruciate ligaments become taut in early extension and pull the condyles in opposite directions, causing the rotation (Nordin and Frankel, 2001; Hamill and Knutzen, 2009).

When the knee is in full extension, almost all motions in the frontal plane are precluded. Passive abduction and adduction increase with knee flexion up to 30 degrees, but each reaches a maximum of only a few degrees. With the knee flexed beyond 30 degrees, motion in the frontal plane again decreases because of the limiting function of the soft tissues. During gait, the maximal abduction of the tibia is observed at heel strike and at the beginning of the stance phase, while maximal adduction occurs when the knee is flexed during the swing phase (Nordin and Frankel, 2001).

Values for the range of motion of the tibiofemoral joint in the sagittal plane during several common activities are presented in Table 2.2. It is worth noting that any restriction of knee motion can be compensated for by increases motion in other joints. An increased speed of movement requires a greater range of motion in the tibiofemoral joint. As the pace accelerates from walking slowly to running, progressively more knee flexion is needed during the stance phase (Nordin and Frankel, 2001; Completo, 2006).

Table 2.2 Range of tibiofemoral joint motion in the sagittal plane during common activities (Nordin and Frankel, 2001).

Activity	**Range of motion (knee flexion angle in degrees)**
Walking	0-67
Climbing stairs	0-83
Descending stairs	0-90
Sitting down	0-93
Tying a shoe	0-106
Lifting an object	0-117

The patellofemoral joint presents a gliding motion. From full extension to full flexion of the knee, the patella glides caudally approximately 7 cm on the femoral condyles. The medial and lateral condyles of the femur articulate with the patella from full extension to 140 degrees of flexion. Beyond 90 degrees of flexion, the patella rotates externally, and only the medial femoral condyle articulates with the patella. At full flexion, the patella sinks into the intercondylar groove (Nordin and Frankel, 2001). The patella is free to move in the extended position and can be shifted in multiple directions. Patellar movement is restricted in the flexed position because of the increased contact with the femur (Hamill and Knutzen, 2009).

The patella enhances the effects of the quadriceps muscles regarding knee extension by increasing the moment arm of the quadriceps, as Figure 2.11a shows, especially in the earlier degree of flexion, from 30 percent near extension to 15 percent at 30 degrees of flexion (Grelsamer and Weinstein, 2001). Therefore, the patella is of paramount importance for the extensor apparatus because its presence minimizes the force differential generated by the quadriceps (Grelsamer and Weinstein, 2001). Also, the patella contributes indirectly to the global stability of the knee. If the patella is surgically removed (*i.e.*, patellectomy), the patellar ligament lies closer to the center of motion of the tibiofemoral joint, as can be observed in Figure 2.11b. Acting with a shorter moment arm, the quadriceps muscles must produce even more force than is normally required. This increase in force may be beyond the capacity of the quadriceps

muscles in some patients, particularly those who have intra-articular disease or are advanced in age. Thus, a patellectomy leads to quadriceps atrophy and loss of extension force in proportions (Heegaard *et al.*, 1995).

The forces and moments acting on the knee rely on the body-weight, the muscle action, the soft-tissue restriction, the externally applied loads, the physical activity of the human subject and the health condition of the articular joint. The flexion-extension moments during stance phase are approximately 20 to 30 times larger than the moments produced in the frontal (abduction-adduction) and transverse (internal-external) planes. During the gait cycle, the joint reaction force shifts from the medial to the lateral tibial plateau. In the stance phase, when the force reaches its peak value, it is sustained mainly by the medial plateau (adduction moment). In the swing phase, when the force is minimal, it is sustained primarily by the lateral plateau (Nordin and Frankel, 2001).

(a) **(b)**

Figure 2.11 Moment arm of the quadriceps muscles of a knee joint with: (a) Normal patella; (b) Patellectomy (Completo, 2006).

In a normal knee, joint reaction forces are sustained by the menisci as well as by the articular cartilage, which allow for a stress distribution over a wide area of the tibial plateau. The menisci restrain the motion of the knee joint. In flexion and extension, the menisci move with the femoral condyles. As the knee flexes, the menisci move posteriorly because of the rolling of the femur and the action of the muscles. At the end of flexion, the menisci fill up the posterior portion of the joint, acting as a space-filling buffer. The reverse occurs in extension (Hamill and Knutzen, 2009).

The menisci are of paramount importance for the human knee joint and their absence increases the susceptibility to injury and lesion. For example, the menisci removal (*i.e.* meniscectomy) reduces the contact area in two thirds, increasing the pressure on the contacting surfaces (Hamill and Knutzen, 2009). Hence, the stresses are no longer distributed over a wide area but instead are limited to a contact area in the center of the plateau as Figure 2.12 depicts. Moreover, a meniscectomy not only

increases the magnitude of the stresses on the cartilage and subchondral bone at the center of the tibial plateau, but also diminishes the size and changes the location of the contact area and increases 20 percent the joint friction. Over the long term, the high stresses placed on the smaller contact area may be harmful to the exposed cartilage (Nordin and Frankel, 2001; Completo, 2006).

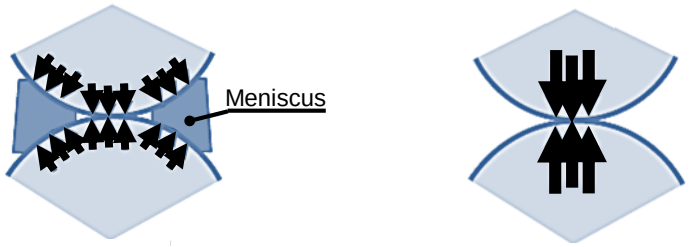

Figure 2.12 Stress distribution in: (a) Normal knee; (b) Knee with the menisci removed {Adapted from Completo (2006) with Author's permission}.

The menisci are thought to carry up to 70 percent of the load across the knee. Movement during knee flexion of the menisci would therefore protect the articulating surfaces while avoiding injury to it. Figure 2.13 shows the movements in the transverse plane of the medial and lateral menisci from full extension to 90 degrees of flexion.

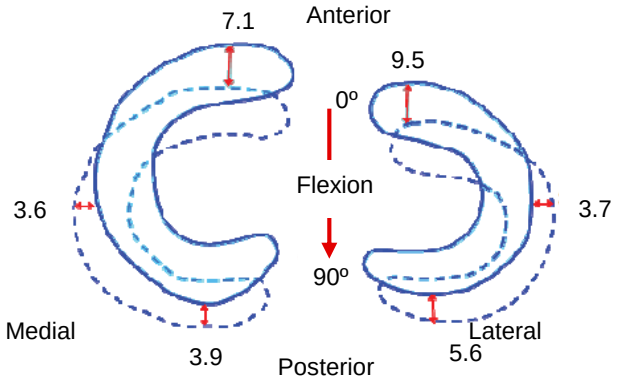

Figure 2.13 Schematic representation of the main movements of the medial and lateral menisci from full extension to 90 degrees of knee flexion in a weight-bearing standing condition {Adapted from Completo (2006) with Author's permission}.

The menisci movements are significantly greater in weight-bearing that in non-weight bearing for both lateral and medial menisci. Therefore, it can be concluded that the menisci not only protect the articular cartilage and subchondral bone, but also they contribute actively to knee joint stability (Nordin and Frankel, 2001). The absence of the lateral meniscus is more critical than the medial meniscus, because the lateral meniscus carries a greater percentage of the load (Englund *et al.*, 2001).

2.4 Mechanical response of knee surrounding tissues

The human knee presents a bony structure enclosed by biological soft tissues, namely cartilage, ligaments and muscles. The bone offers sustenance and resistance to compressive loads and the cartilage works as a binder or a bearing surface between bones (Mansour, 2008). The ligaments support the joint passively as they are loaded in tension only, while the muscles support the joint actively. Thus, the functional stability of the knee joint relies on the passive restraint of the ligaments, the joint geometry, the active muscles and the compressive forces pushing the bones together (Lieber and Burkholder, 2008; Hamill and Knutzen, 2009). Indeed, either to provide joint mobility or to ensure the static stability, the tissues surrounding the knee joint are continuously withstanding and transferring high loading forces. Therefore, the knowledge of the mechanical behavior of these tissues is crucial for the understanding of the realistic knee mechanics, and also for the biomechanical modeling of the knee, as a natural or an artificial joint (Yang *et al.*, 2010).

2.4.1 Bone: ultrastructure and mechanical behavior

Bone is a hard tissue composed by a matrix of collagen and inorganic salts. The inorganic minerals, calcium and phosphate, along with the organic collagen fibers, make up approximately 60 to 70 percent of bone tissue. Water constitutes approximately 25 to 30 percent of the weight of bone tissue. Collagen fibers offer bone tensile strength and flexibility, while bone minerals provide compressive strength and rigidity (Hamill and Knutzen, 2009). Bone is an anisotropic, heterogeneous, inhomogeneous, nonlinear, thermorheologically complex viscoelastic material. According to Currey (1984), the most relevant material property of the bone tissue is its stiffness that makes it ideal for its biological role of body sustenance under static and dynamic conditions (Katz, 2008).

Two tissue layers can be distinguished from a typical long bone as the femur, as Figure 2.14 shows. The hard outer layer is the cortical bone, also referred as compact or dense bone, and is the responsible for bone strength. The internal layer consists in a porous mesh of trabeculae that can absorb shock and is denominated as trabecular bone, cancellous bone or spongy bone (Herman, 2007).

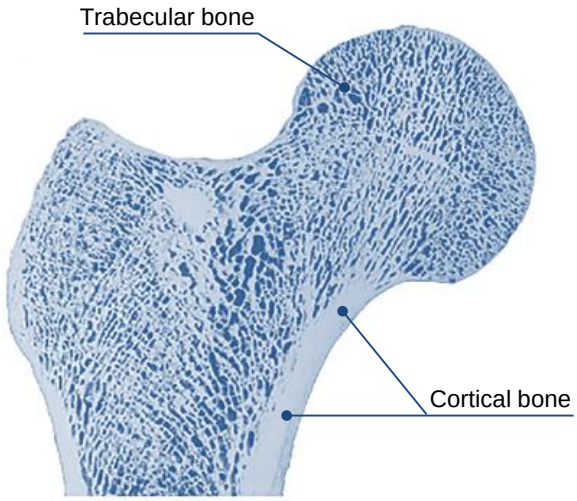

Figure 2.14 Longitudinal cross-section view of the proximal femur {Adapted from Boyle and Kim (2011) with Elsevier permission}.

The cortical bone and the trabecular bone have different porosity, as well as very different properties. On one hand, compact bone has a large Young's modulus, about 17.9 GPa, and it can withstand more stress in compression than in tension, despite it has a fairly large ultimate tensile stress, in the order of 120 MPa. On the other hand, trabecular bone is more porous and has a very small Young's modulus of 76 MPa. It is worth noting that the bone is a tissue that is continuously being modified, reshaped, remodeled, and overhauled (Herman, 2007; Hamill and Knutzen, 2009).

2.4.2 Cartilage and Menisci: ultrastructure and mechanical behavior

At the human body, there are three types of cartilage: elastic cartilage, hyaline cartilage, also known as articular cartilage, and fibrocartilage. Hyaline cartilage is the most common cartilage in adults and is found in the ventral ends of ribs and covering the joint surfaces of long and sesamoid bones. This type of cartilage is glassy smooth, glistening, and bluish-white in appearance. The meniscus is an example of a biological structure composed by fibriocartilage (Mansour, 2008; Mow and Ratcliffe, 1997).

Articular cartilage and menisci can be characterized as multiphasic materials with two major phases: the freely movable interstitial fluid composed of water and electrolytes and a porous-permeable solid matrix composed of collagen, proteoglycans (PGs), and other proteins (Mow and Ratcliffe, 1997). Figure 2.15 represents the ultrastructure of articular cartilage in terms of four zones between the articular surface and the subchondral bone: the surface or superficial tangential zone, the intermediate or middle zone, the deep or radiate zone, and the calcified zone (Ateshian and Hung, 2006;

Mansour, 2008). The interested reader in the details on these four zones of the cartilage is referred to the works by Mow and Hung (2001) and Lieber and Burkholder (2008).

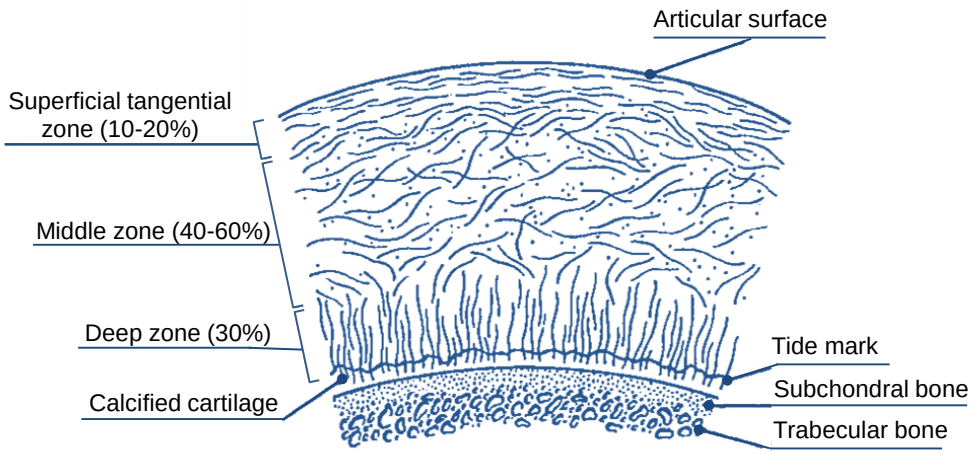

Figure 2.15 Layered structure of cartilage collagen network showing four distinct zones: superficial tangential zone, middle zone, deep zone and calcified zone {Adapted from Mow and Ratcliffe (1997) with Lippincott Williams & Wilkins permission}.

The fibrous structure of the meniscus also has a layered appearance, as Figure 2.16 shows, but it differs from that of articular cartilage. The meniscus is composed of fine fibrils in a random mesh-like woven matrix. The interested reader in the details on this ultrastructure is referred to the works by Mow and Ratcliffe (1997).

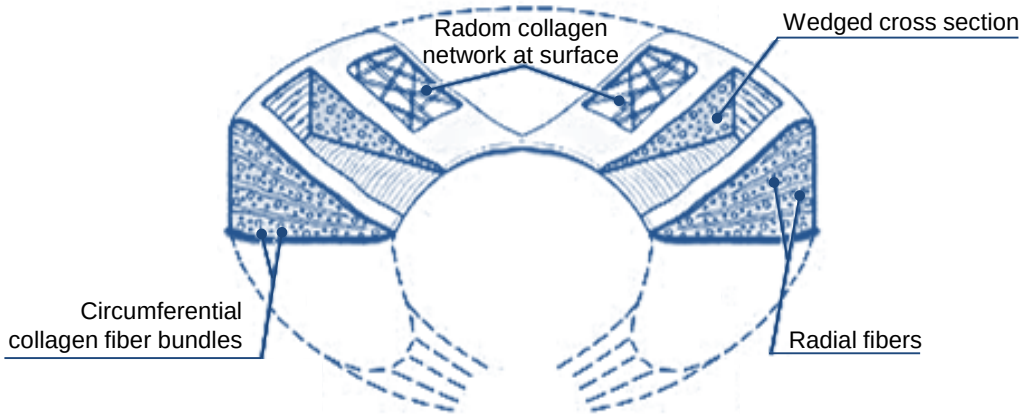

Figure 2.16 Meniscus ultrastructure, showing the different fiber orientations {Adapted from Mow and Ratcliffe (1997) with Lippincott Williams & Wilkins permission}.

The layered morphology of the collagen network and the preferred orientation of collagen fibers are of paramount importance for distributing the stress more uniformly across the loaded regions of the joint tissue. Also, the articular cartilage and the menisci compose a smooth, wear-resistant bearing surface with low friction. Regarding mechanical properties, both articular and meniscal cartilages are anisotropic and nonhomogeneous. Tensile properties of both tissues are nonlinear and their shear

properties are viscoelastic. Therefore, Poisson's ratio of the solid matrix of cartilage takes values from 0 to 0.4 (Mow and Ratcliffe, 1997).

The Young's modulus of articular cartilage is a strain-rate sensitive ranging from 0.3 to 1.5 MPa, under static conditions, to 18 MPa, during dynamic loading. This apparent mismatch can be explained by the relatively low permeability of cartilage typically around 10×10^{-15} m^4/Ns. Interstitial water cannot be squeezed out from the tissue during dynamic loading but is pressurized and therefore supports the high physiological stresses. Under long-term loading conditions, fluid flow through the porous matrix takes place and causes creep or stress–relaxation phenomenon. This process is controlled by the cartilage permeability, which is strain dependent. The pressurization and flow mechanisms protect articular cartilage against excessive strains and mechanical failure (Laasanen *et al.*, 2003; Ateshian and Hung, 2006).

Various theoretical models have been developed to explain the mechanical behavior of articular cartilage (Laasanen *et al.*, 2003). The first models were isotropic and linearly elastic and could be applied only to characterize the instantaneous or equilibrium responses of cartilage after step-load application (Hayes *et al.*, 1972). Afterwards, various viscoelastic models, based on springs and dashpots, were proposed to account for creep and stress-relaxation behaviors (Mow *et al.*, 1980; Mak *et al.*, 1987). Later, advanced solutions were proposed for predicting the dynamic response of articular cartilage, such as transversely isotropic biphasic models (Mow *et al.*, 2000), poroviscoelastic models (Suh and Bai, 1998), and fibril reinforced poroelastic models (Soulhat *et al.*, 1999). In general, the biphasic models are more accurate than the simple spring models, since these approaches describe the motion of the hydrating fluid relative to the organic matrix (Lieber and Burkholder, 2008).

The minimal wear of articular cartilage at the knee joint indicates that sophisticated lubrication processes are played within the joint and within and on the surface of the tissue. These processes have been associated with a lubricating fluid-film forming between the articular cartilage surface and to an adsorbed boundary lubricant on the surface during motion and loading. Joint lubrication is out of the scope of this work, nonetheless the interested reader is referred to the works by Wright and Dowson (1976), Mow and Hung (2001) and Furey (2008).

2.4.3 Tendons and Ligaments: ultrastructure and mechanical behavior

Tendons and ligaments are passive structures, *i.e.*, they do not actively produce motion, that closely surround, connect, and stabilize the knee articulation. Tendons and ligaments are dense connective tissues known as parallel-fibered collagenous tissues. These tissues are biological composites consisting of a ground substance matrix reinforced by collagen and elastin. The ground substance matrix is composed of PGs, glycolipids, and fibroblasts and holds large amounts of water. About two-thirds of the weight of normal tissue is water, and 70 to 80 percent of the remaining weight is made up by collagen (Nordin and Frankel, 2001; Weiss and Gardiner, 2001). Collagen is the main load carrying component in these tissues and its content is somewhat larger in tendons than in ligaments. The great mechanical stability of collagen gives the tendons and ligaments their typical strength and flexibility (De Vita and Slaughter, 2007).

Ligaments connect bone to bone, whereas tendons connect bone to muscle. The myotendinous junction and the bony attachments are complex and vary considerably. Tendons generally have large parallel fibers that insert uniformly into bone. Ligaments have smaller-diameter fibers that can be either parallel, as in the collateral ligaments of the knee, or branching and interwoven, as in the knee cruciate ligaments. There are two types of tendon- and ligament-bone insertions: direct and indirect. For direct insertions, such as femoral insertion of MCL, fibers attach directly into the bone and the transition of ligament to bone occurs in four zones: ligament, fibrocartilage, mineralized fibrocartilage and bone. For an indirect insertion, such as tibial insertion of MCL, superficial fibers are attached to periosteum while the deeper fibers are directly attached to the bone at acute angles (Woo *et al.*, 1999; Weiss and Gardiner, 2001).

In parallel-fibered tissues, such as tendons and ligaments, collagen is characterized by a hierarchal structure, as illustrates Figure 2.17. Collagen molecules are packed together to form collagen fibrils, collagen fibrils aggregate to form collagen fibers, and collagen fibers are arranged in fascicles that run parallel to the ligament loading direction (De Vita and Slaughter, 2007). The parallel fiber arrangement of tendons and ligaments allows early tensile resistance once the "crimp pattern" is straightened (Woo *et al.*, 1999).

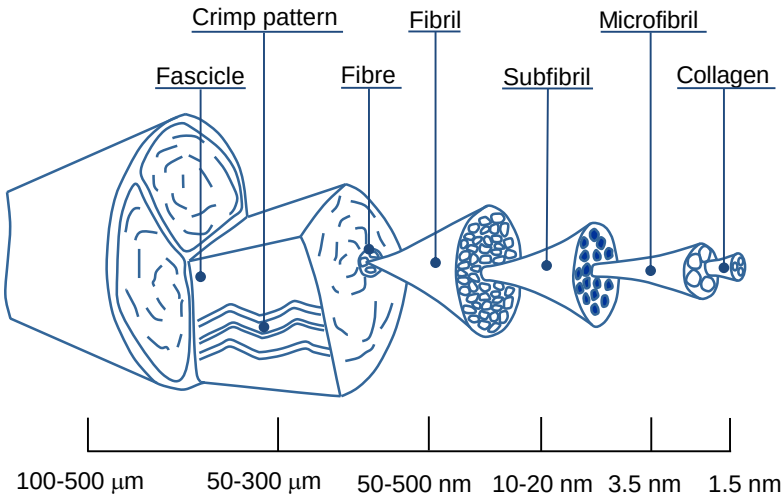

Figure 2.17 Hierarchical microarchitecture of tendons and ligaments (Herman, 2007).

Tendons and ligaments are well suited to the physiological functions that they perform. They are pliant and flexible, allowing natural movements of the bones to which they attach, but are strong and inextensible to offer suitable resistance to applied forces. Both structures, tendons and ligaments, sustain chiefly tensile loads during normal and excessive loading. Their load-deformation or stress-strain behaviors are anisotropic, oriented primarily for the resistance of tensile loads (Woo *et al.*, 1999; Nordin and Frankel, 2001). Indeed, collagen provides the primary resistance to tensile loading but offers negligible resistance to compression. Also, tendons and ligaments offer little resistance to bending. The parameters describing the structural properties of the bone–tendon and bone-ligament complexes include stiffness, ultimate load, ultimate elongation, and energy absorbed at failure (Weiss and Gardiner, 2001).

Tendons and ligaments display time- and history-dependent viscoelastic properties (Weiss and Gardiner, 2001). As a result of internal energy dissipation, the tendon or ligament fibers allow the material to return to its original shape and size after being deformed during loading and unloading between two limits of elongation. Meanwhile part of the energy is stored and what is left represents the energy loss during the cycle and is called hysteresis. The loading and unloading curves of these tissues do not follow the same path but instead form a loop. The area enclosed by the hysteresis loop represents the energy dissipated (Nordin and Frankel, 2001).

Other important features associated with the viscoelastic properties of tendons and ligaments are creep and stress relaxation (Woo *et al.*, 1999). The creep rate depends on the applied stress, while the relaxation rate depends on the applied stretch (Peña *et al.*,

2008). The viscoelastic behavior of tendons and ligaments has an important clinical significance. During walking, the applied strains and strain rates are nearly constant. Cyclic stress relaxation will effectively soften tissue substance with continuous decreases in peak stress as cycling proceeds. This phenomenon may help to prevent fatigue failure of ligaments and tendons. Similarly, deformation increases slightly during cycles to a constant load demonstrating creep behavior of tendons and ligaments. These changes have been noted clinically with temporary softening of all these tissues and thus increase of test excursion, *i.e.*, laxity, in exercised joints. After a short recovery period, there is a return to normal joint stiffness and apparent length (Woo *et al.*, 1999).

2.4.4 Muscles: ultrastructure and mechanical behavior

The functional unit that produces motion at the knee joint consists of two discrete components: the muscle belly and the tendon. The muscle belly consists of muscle fibers and connective tissues that surround the fibers (Mansour, 2008). The level of complexity in the organization of the skeletal muscle is illustrated in Figure 2.18.

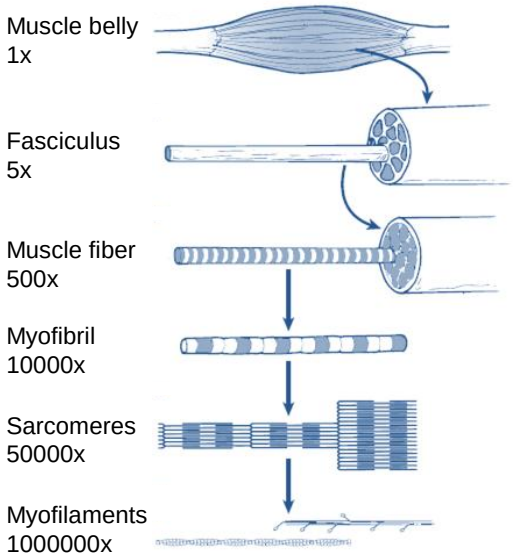

Figure 2.18 Level of complexity in the organization of a skeletal muscle {Adapted from Meiss (2003) with Lippincott Williams & Wilkins permission}.

The muscle fiber is a long cylindrical cell that is encompassed by a loose connective tissue called the endomysium. The endomysium is a very fine sheath carrying the capillaries and nerves that nourish and innervate each muscle fiber. Directly underneath the endomysium is the sarcolemma, which is a thin plasma membrane surface that branches into the muscle. The muscle fibers are organized into

various-sized bundles, or fascicles, which are in turn encased in a dense connective tissue sheath known as the perimysium. The perimysium protects the muscle fibers and provides pathways for the nerves and blood vessels (Hamill and Knutzen, 2009). The muscle is composed of several fascicles surrounded by a fascia of fibrous connective tissue called the epimysium. The epimysium plays a vital role in the transfer of muscular tension to the bone. The endomysium, sarcolemma, perimysium and epimysium act as parallel elastic components (Nordin *et al.*, 2001).

A muscle fiber is composed by a set of myofibrils, which are aligned in order to create a band pattern. Each repeat of this pattern is called sarcomere. The sarcomere is the smallest contractile unit of a myofibril, and the events that take place in one sarcomere are duplicated in the others. Various sarcomeres build a myofibril, various myofibrils build the muscle fiber and various muscle fibers build the muscle. The myofibril are composed of thin filaments of the protein actin and thick filaments of the protein myosin, and the intramyofibrillar cytoskeleton is composed of the elastic filaments of titin and the inelastic filaments of nebulin. The sarcomere, illustrated in Figure 2.19, is a nearly crystalline structure, composed of a dark *A*-band and two adjacent *I*-bands. Myosin filaments are rigidly fixed at the *M*-line and are the principal constituents of the *A*-band (anisotropic, light bending). Actin filaments are rigidly fixed at the *Z*-line, comprising the *I*-band (isotropic, light transmitting). In the center of the *A*-band, in the gap between the ends of the actin filaments, is the *H*-zone, a light band containing only myosin filaments and that part of titin that is integrated in the myosin filaments (Nordin *et al.*, 2001; Lieber and Burkholder, 2008).

Concerning the arrangement of the muscle fibers, it varies significantly among muscles and has marked effects on a muscle's ability to produce movement and to generate force. Fiber arrangements have different names but fall into two major categories: parallel and pennate (Mansour, 2008). In the parallel fiber arrangement, the fascicles are parallel to the long axis of the muscle and all the fibers contract the same amount (Herman, 2007). During muscular contraction, these muscles get shorter and, hence, the diameter of the muscle belly increases in order to keep the muscle volume constant (Tözeren, 2000). Figure 2.20 illustrates the five different shapes of parallel fiber arrangements, namely flat, fusiform, strap, convergent, and circular.

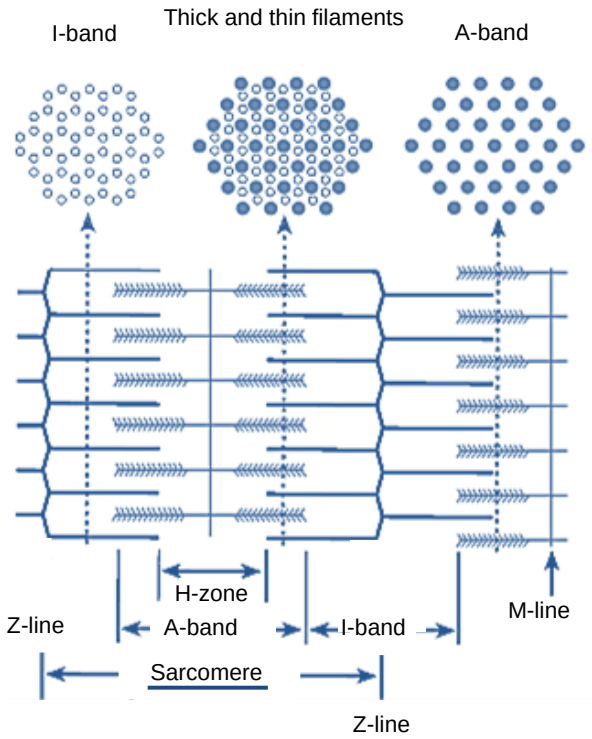

Figure 2.19 Arrangement of the actin and myosin chains in the sarcomere within a muscle fiber {Adapted from Meiss (2003) with Lippincott Williams & Wilkins permission}.

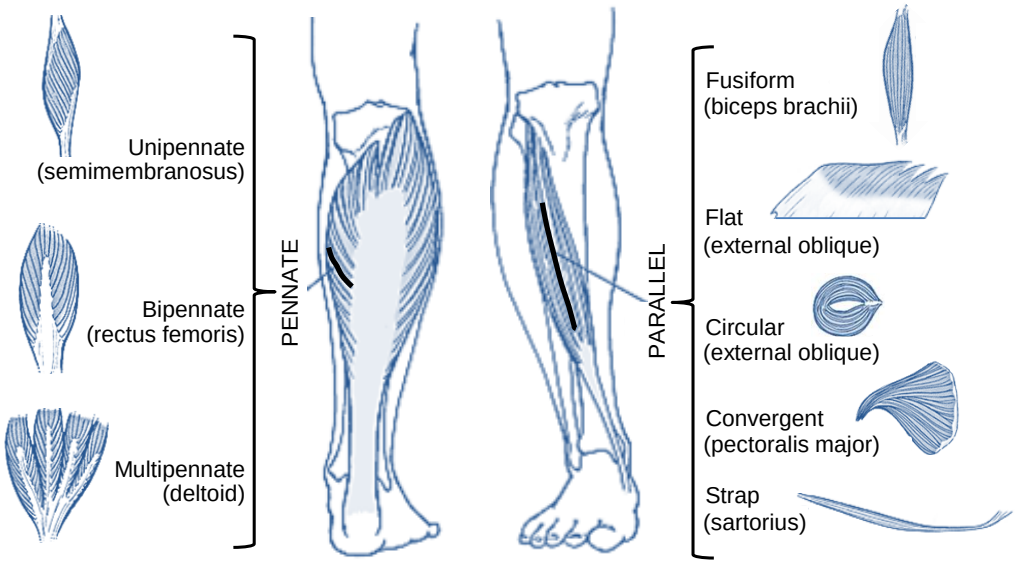

Figure 2.20 Illustration of the different shapes of muscles with parallel fiber arrangements (fusiform, flat, circular, convergent and strap), and pennate fiber arrangements (unipennate, bipennate and multipennate) {Adapted from Hamill and Knutzen (2009) with Lippincott Williams & Wilkins permission; Adapted from Moore and Agur (2007) with Lippincott Williams & Wilkins permission}.

In a pennate muscle, one or more tendons run through the body of the muscle, with fibers attached to them at an angle (Tözeren, 2000). This angle is referred as pennation angle. Pennate muscles fall into subcategories according to the number of tendons penetrating the muscle. There are unipennate, bipennate, and multipennate muscles, as Figure 2.20 depicts. Fibers of unipennate muscles run parallel to each other,

but at an angle to the muscle axis. Bipennate muscle fibers run in two distinct directions. Multipennate muscles have one distinct attachment and one broad attachment, and the pennation angle is different for every fiber (Lieber and Burkholder, 2008; Mansour, 2008). In contrast to the parallel muscles in which all the force of the fibers is transmitted through the tendon, in the pennate muscles the fibers are attached to the tendon at a pennation angle, and so only part of the force of each fiber is effectively transmitted. While this is a distinct disadvantage of the pennate design, it has other relative advantages. Because the geometry allows fibers to attach along part of the length of the tendon, many more fibers can be attached to the tendon. Also, this geometry allows the central tendon to move a longer distance than in the parallel scheme, so the bones attached to the tendon can move more (Herman, 2007).

Muscles may contract concentrically, eccentrically, or isometrically depending on the relationship between the muscle tension and the resistance to be overcome. Concentric and eccentric contractions involve dynamic work, in which the muscle moves a joint or controls its movement, respectively. The isometric muscle contraction is used to stabilize a segment (Hamill and Knutzen, 2009; Nordin *et al.*, 2001). Besides muscle length, other parameters may influence the contraction conditions. When the velocity of contraction and also the angular speed of the joint are constant, the contraction is referred as isokinetic. When a tension is constant throughout a range of joint motion, the contraction scenario are defined as isotonic (Herman, 2007).

The total force that a muscle can produce is influenced by its mechanical properties, which can be described by examining the force-length and the force-velocity relationships of the muscle and the skeletal muscle architecture (Nordin *et al.*, 2001). The relation between the maximal fiber force and its length is described by a force-length curve. Figure 2.21a shows the force-length relationship illustrated for an individual muscle fiber. If this relationship is measured in a whole muscle contracting isometrically and tetanically, the force produced by both active components and passive components must be taken into account and the force-length relationship will be as illustrated in Figure 2.21b (Nordin *et al.*, 2001). The curve labeled “active tension” represents the tension developed by the contractile elements of the muscle, and it resembles the curve for the individual fiber (Figure 2.14a). The curve labeled “passive tension” reflects the tension developed when the muscle surpasses its resting length and the non-contractile muscle belly is stretched (Nordin *et al.*, 2001). Under conditions of

constant load, the relationship between force and velocity is nearly hyperbolic, as Figure 2.22a shows (Lieber and Burkholder, 2008). The velocity of shortening of a muscle contracting concentrically is inversely related to the external load applied. The velocity of shortening is greatest when the external load is zero, but as the load increases the muscle shortens more and more slowly. When the external load equals the maximal isometric force that the muscle can exert, the velocity of shortening becomes zero and the muscle contracts isometrically. When the load is increased still further, the muscle contracts eccentrically (Nordin *et al.*, 2001). Muscles usually do not maintain a zero speed or a constant length and therefore, its response depends both on its length and the velocity of contraction. The combination of these two relations results in the force-length-velocity relationship illustrated in Figure 2.22.

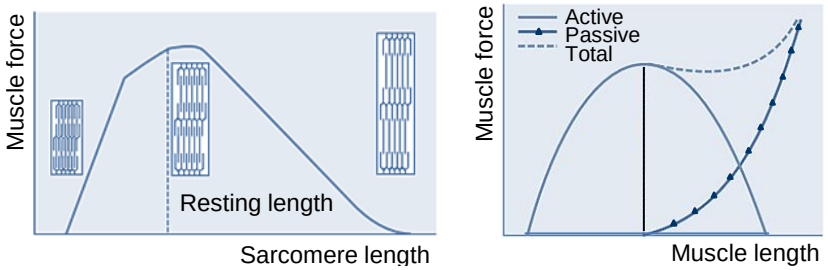

Figure 2.21 Force-length curve: (a) Individual fiber; (b) Whole muscle {Adapted from Mansour (2008) with Lippincott Williams & Wilkins permission}.

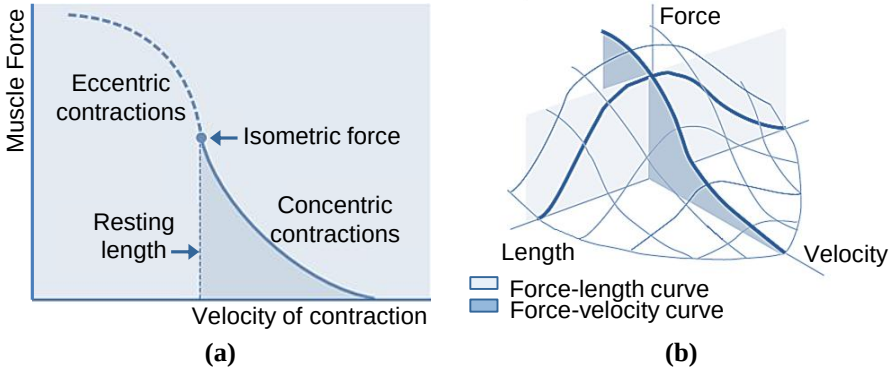

Figure 2.22 Muscle force relations: (a) Force-velocity curve; (b) Force-length-velocity curve {Adapted from Ackermann (2007); Adapted from Mansour (2008) with Lippincott Williams & Wilkins permission}.

From a biomechanical point of view, skeletal muscle exhibits a very complex mechanical behavior which is active, incompressible, transversely isotropic, and hyperelastic. A number of mathematical skeletal muscle models have been developed over the past two decades and they can be classified as belonging to one of two categories: Huxley-type and Hill-type muscle models. Huxley-type or crossbridge models describe the muscle behavior at the molecular level and are mainly used to

understand the properties of the microscopic contractile element. Thus, the Huxley-type models are frequently utilized to interpret mechanical and biochemical outcomes of experiments with isolated muscles. However, these models are inadequate to studies of muscle coordination tasks involving many muscles, since their high complexity compromises the interpretation and computational tractability. Moreover, these models require a series of parameters that are difficult to assess accurately. Hence, these models are rarely used to study muscle coordination (Ackermann, 2007). In turn, Hill-type muscle models are phenomenological models based on the interpretation of the input-output behavior of muscles obtained experimentally. There are many different levels of complexity, but in movement simulation the three-component Hill-type muscle model is almost exclusively used. The three-component Hill-type muscle model, illustrated in Figure 2.23a, is composed by a contractile component representing the muscle fibers, a parallel elastic element (PE) representing the nonlinear stiffness of connective tissue in parallel to the contractile elements, and a series elastic element (SE), representing the nonlinear stiffness of tissue in series with the contractile elements. The contractile element (CE) proposed by Hill consists in a force generator working in parallel with a velocity dependent damping element (DE), as Figure 2.23 shows.

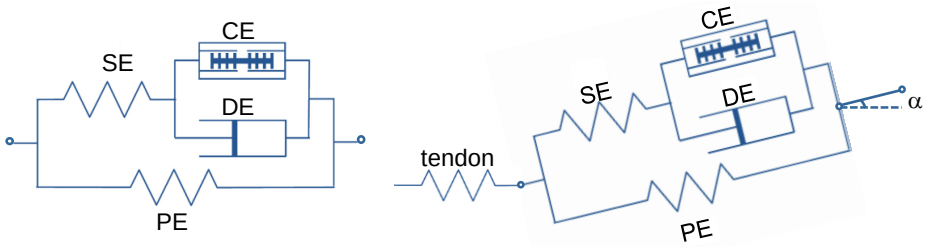

Figure 2.23 (a) Hill type muscle model; (b) Modified Hill type muscle model {Adapted from Ackermann (2007) with Author's permission}.

The DE must be placed in parallel with the CE so that the velocities of the CE and the DE maintain the same direction. The contractile element is described by independent isometric force–length (Figure 2.21a) and isotonic force–velocity relations (Figure 2.22a) and its force is modulated by an activation state (Lieber and Burkholder, 2008). Thus, the contractile component is the one responsible for to convert the stimulation of the nervous system into a force, and to reflect the shortening of the muscle through the actin and myosin structures. The elasticity inherent in muscle is represented by the SE and the PE. Because the SE is in series with the CE, any force produced by the CE is also applied to the SE. The SE is a highly nonlinearly elastic structure. Muscle displays elastic behavior even when the CE is not producing force. An

external force applied to a muscle causes the muscle to resist, but the muscle also stretches. This passive elastic response is produced by structures that must be in parallel with the CE rather than in series. The PE is highly nonlinear and increases in stiffness as the muscle lengthens. SE and PE also behave like springs when acting quickly (Hamill and Knutzen, 2009). In some model variations, the inclusion of tendon as an elastic element distinctly separate from the SE of the muscle model has been shown to be important for physiologically realistic models of muscles crossing the knee and ankle (Hoy *et al.*, 1990; Zajac, 1989). This modified Hill type is illustrated in Figure 2.23b.

2.5 Joint pathologies and replacement systems

The knee is the largest and possibly the most complex synovial joint in the body as it comprises a combination of three articulations. Furthermore, the knee joint is located between the two longest lever arms of the body and bears a majority of body weight. These issues make the human knee vulnerable to trauma and overuse injuries that can lead to significant functional limitations and disability (McGinty *et al.*, 2000).

2.5.1 Overview of primary knee injuries

The cause of an injury to the knee can often be related to poor conditioning or training or to an alignment problem in the lower extremity. Injuries in the knee have been attributable to hindfoot and forefoot varus-valgus, tibial or femoral varus-valgus, limb length differences, deficits in flexibility, strength imbalances between agonists and antagonists muscles, and improper technique or training (Hamill and Knutzen, 2009). Whenever a patient has a painful or swollen knee, the first diagnosis step is to evaluate whether there is trauma or not. In case there is trauma, it can happen that the pain is recognized as a mechanical disorder (Silva, 2007). In this situation, the most likely diagnosis in population over the age of 40 is Osteoarthritis (OA), with or without meniscal or ligamentous pathology (Hamill and Knutzen, 2009).

Osteoarthritis, or degenerative joint disease, is characterized by the breakdown of articular cartilage. Particles of articular cartilage may break off and cause pain or inflammation in the joint. Over time, the cartilage may wear away entirely, resulting in bone-on-bone contact. Since bones, unlike cartilage, have many nerve cells, direct bone contact can be very painful to the OA patient. In addition to the pain and swelling, the OA sufferer can experience a progressive loss of mobility (*i.e.*, stiffness) at the knee

joint. This is due to loss of the joint space, where the articular cartilage has completely worn away. The exact cause of OA is unknown. It is a progressive disease that is due to cartilaginous, bony, synovial, mechanical, and other factors operating independently, as well as in combination. Treatments such as weight loss, braces, orthotics, steroid injections, and physical therapy may also help alleviate pain and restore function. However, since articular cartilage is avascular, or lacks a blood supply, repair and growth of adult cartilage is minimal. If the pain or immobility becomes too severe and other therapies do not alleviate the symptoms, a joint replacement becomes necessary (Altman, 1987; Nordin and Frankel, 2001; Sarzi-Puttini *et al.*, 2005, Felson, 2006).

Traumatic injuries to the knee usually involve the ligaments. Ligaments are injured as a result of application of a force causing a twisting action of the knee. High-friction or uneven surfaces are usually associated with increased ligamentous injury. Any movement fixing the foot while the body continues to move forward, such as often occurs in skiing will likely produce a ligament sprain or tear. Simply, any turn on a weight-bearing limb leaves the knee vulnerable to ligamentous injury. Likewise ligaments, menisci can be torn through compression associated with a twisting action in a weight-bearing position, as well as in kicking and other violent extension actions. Tearing the meniscus by compression is a result of the femur grinding into the tibia and ripping the menisci (Hamill and Knutzen, 2009).

Patellofemoral pain syndrome is pain around the patella and is often seen in individuals who exhibit valgum alignments or femoral anteversion in the extremity. Patellofemoral pain is aggravated by going down hills or stairs or squatting. Stress on the patella is related to a greater *Q*-angle because of increased stress on the patella. Some patellofemoral pain is associated with cartilage destruction, in which the cartilage underneath the patella becomes soft and fibrillated (Hamill and Knutzen, 2009). This pathological condition is also known as chondromalacia patellae.

In a broad sense, knee surgical treatments include tissue-repair approaches, arthroscopic lavage and debridement, and arthroplasty (Silva, 2007). An arthroplasty, *i.e.*, joint replacement, is a surgical orthopedical procedure in which the arthritic or dysfunctional joint surface is replaced with something better or by remodeling or realigning the joint by osteotomy or by some other approach. The main objective of an arthroplasty is to expand the envelope of function of symptomatic arthritic joint as safely and predictably as possible. An arthroplasty is capable of substantial increases in

the functional capacity of a given arthritic joint, but it is not designed to restore the full physiological function of a normal, uninjured adult joint. Whenever there is a joint replacement, the primary mechanical factor that limits its long-term outcome is the implant wear, which is critically influenced by the joint kinematics. Therefore, a special attention has been given to knee wear analysis in the last decade with the intent to find and/or develop the best solutions in terms of materials and processes that can lead to the construction of optimized prosthesis (Fregly *et al.*, 2005; Li *et al.*, 2011; Sawyer *et al.*, 2008). Furthermore, knowledge of the flexion angle, the anterior-posterior sliding distance, and the angle of tibial rotation is also crucial in replicating normal human activities in total knee replacement systems (TKR) and TKR materials wear testing.

2.5.2 Knee replacement systems: materials and design

Knee implants are designed to replace biological materials that have been damaged. In most cases, cartilage and bone are removed from the articulating surfaces of the joint and synthetic materials are used. When only one compartment of the knee is affected, a unicompartmental (or partial) knee arthroplasty can be performed. In cases where two or three knee compartments are affected, a total knee arthroplasty is indicated. There are three types of uni-compartmental knee implants, namely medial unicondylar implants, lateral unicondylar implants and patellofemoral implants. Moreover, when the medial and patellar compartments are compromised and a TKR is not required or desired, bi-compartmental knee implant can be utilized. These solutions replace the medial and patellar compartments and allows for the ACL and PCL to be retained. Figure 2.24 displays different types of knee implants, namely a TKR, a medial unicondylar implant, a patellofemoral implant and a bi-compartmental knee implant.

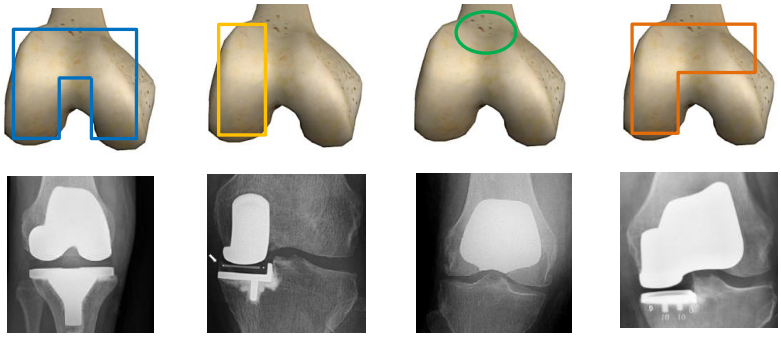

Figure 2.24 Knee implants: (a) Total Knee Replacement {Adapted from Murnaghan and Hamer (2010) with Elsevier permission}; (b) Unicompartmental Knee Replacement {Adapted from Jung *et al.* (2008) with Elsevier permission}; (c) Patellofemoral Joint Replacement {Adapted from Donell and Glasgow (2007) with Elsevier permission}; (d) Bicompartmental Knee Replacement {Adapted from Palumbo *et al.* (2011) with Elsevier permission}.

The earliest model of knee implant, named tibial plateau prosthesis, was developed by McKeever, in the late 1950s, consisting in a single metal component. Afterwards, several new designs of knee implants were proposed. Figure 2.25 gives a historical perspective of the progression of knee implant designs. Currently there are more than 150 different knee implants. These designs comprise multiple components made of polymer, ceramic and metal, that attempt to mimic the natural knee. The tibial articulating surface and the patellar component tend to be made of polymers such as ultra-high molecular weight polyethylene (UHMWPE) or cross-linked polyethylene. The femoral component and the tibial tray are usually made of titanium alloys, cobalt-chromium-molybdenum (CoCrMo) or stainless steel (Carr and Goswami, 2009).

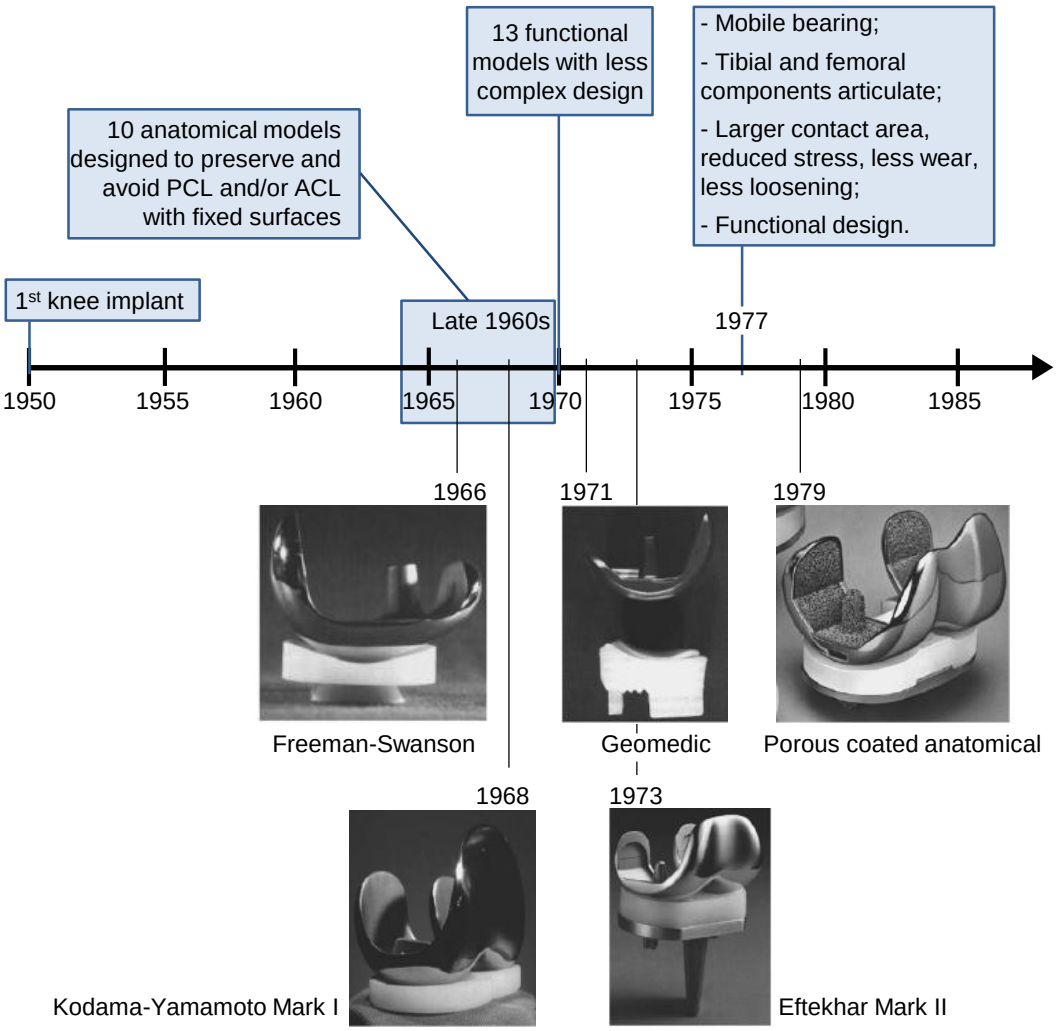

Figure 2.25 Knee implants history {Adapted from Carr and Goswami (2009) with Elsevier permission}.

In order to assess the performance of the knee implant models, some biomechanical factors are analyzed throughout experimental and numerical studies. These biomechanical factors include: (*i*) contact stresses, (*ii*) kinematics for different

degrees of congruency and (*iii*) fatigue to validate the quality of knee implants under specific loading conditions. The interested reader in the details on these biomechanical studies is referred to the work by Carr and Goswami (2009) and Grupp *et al.* (2009). The materials used for knee implants are selected with the purpose to balance strength requirements with biocompatibility needs. While use of materials such as titanium alloys, cobalt-chrome and UHMWPE have led to improved implant designs, wear, loosening and other factors continue to limit the performance of knee implants (Carr and Goswami, 2009). Indeed, the main type of failure observed clinically is due to UHMWPE (Collier *et al.*, 1991). The UHMWPE wear is of considerable concern because it can lead to the generation of debris that may cause synovitis (*i.e.*, joint swelling) and osteolysis (*i.e.*, bone resorption) of the surrounding bone (McEwen *et al.*, 2005). In extreme cases, wear debris migration can cause bone necrosis (*i.e.*, bone death) and loosening of the tibial tray. Wear can also lead to misalignment or instability of the joint and can initiate fracture of the tibial component (Walker *et al.*, 2000).

Implant failure often leads to revision surgery. In cases of absence of osteolysis or implant loosening, only the UHWMPE needs be replaced. Unfortunately, aseptic (*i.e.*, non-toxic) loosening is the most common reason for revision, in which case, an entirely new TKR must be implanted. In these revisions, more bone must be removed from the patient and a larger TKR is inserted. Revision surgery is much more complex and technically more difficult than the first-time knee replacement. Furthermore, with this surgical intervention the range of motion in the knee is generally compromised, decreasing greatly in comparison with the initial replacement (Lavernia *et al.*, 1995).

2.6 Summary and discussion

An overview of the knee joint, namely its anatomy, mechanobiology, kinematics and biomechanics, was presented throughout this Chapter. The human knee is a synovial joint composed by four bones, which articulate with each other forming three joints: the tibiofemoral, the patellofemoral and the superior tibiofibular. The understanding of the knee structure and function is fundamental not only for the construction of meaningful biomechanical models but also for the design of corrective or replacement measures.

The tibiofemoral joint is the principal knee articulation as it is responsible for the flexion and extension movements of the knee in the sagittal plane. The tibiofemoral

joint comprises the distal end of the femur with the proximal tibia. The distal femur exhibits two large convex surfaces, namely the medial and lateral condyles. The femoral condyles lie on the tibial plateaus that are distinct in shape and conformality. The lateral plateau exhibits a convex surface, while the medial plateau is slightly concave. The patellofemoral joint corresponds to the articulation of the posterior patella with the trochlear groove of the distal femur. This joint improves the efficiency of the extensor forces through the entire knee flexion range by increasing the moment arm of the quadriceps. Also, the patella provides a smooth sliding mechanism and plays as a protecting shield to the knee joint. The third articulation of the knee is the superior tibiofibular joint, which is a small joint between the head of the fibula and the lateral tibial plateau. The primary functions of this joint are the dissipation of lateral tibial bending movements and torsional stresses applied at the ankle joint.

Besides the flexion and extension movements, the knee joint describes also secondary motions, namely internal-external rotation and abduction-adduction. The flexion-extension motion ranges from 0 to 140 degrees, being the average limit of hyperextension 5 degrees. Regarding the secondary motions, the range of rotation increases as the knee is flexed, reaching a maximum at 90 degrees of flexion. Passive abduction and adduction increase with knee flexion up to 30 degrees, but each reaches a maximum of only a few degrees. In what concerns with the patellofemoral joint, it presents a gliding motion. The medial and lateral femoral condyles articulate with the patella from full extension to 140 degrees of flexion.

The human knee presents a bony structure enclosed by biological soft tissues. The bone is a hard tissue that presents two tissue layers. The outer layer is named cortical bone is the responsible for bone strength. The internal layer consists in a porous mesh of trabeculae that can absorb shock. Bone tissue is an anisotropic, heterogeneous, inhomogeneous, nonlinear, viscoelastic material. At the human knee, the primary function of the bone is to offer sustenance and resistance to compressive loads.

The femoral condyles and tibial plateau are covered by articular cartilage. Besides the hyaline articular cartilage, two c-shaped structures lie between the tibia and the femur, namely the menisci. These structures extend the contact surface on the tibia and participate in shock absorption. Articular cartilage and menisci can be characterized as multiphasic materials with two major phases: the freely movable interstitial fluid and a porous-permeable solid matrix. Regarding mechanical properties, both are anisotropic

and nonhomogeneous, being their tensile and shear properties are nonlinear viscoelastic. The joint capsule is also an important structure that surrounds the knee joint. It consists in an external fibrous layer and an internal synovial membrane. The synovial membrane produces the synovial fluid that plays as a lubricant and, hence, contributes for a minimal wear of articular cartilage.

Femur and tibia are connected by ligaments that prevent excessive motion. The four main ligaments are: anterior cruciate ligament, posterior cruciate ligament, medial collateral ligament and lateral collateral ligament. Ligaments connect bone to bone, whereas tendons connect bone to muscle. Tendons and ligaments are dense connective tissues known as parallel-fibered collagenous tissues. These tissues are pliant and flexible, allowing natural movements of the bones to which they attach, but are strong and inextensible so as to offer suitable resistance to applied forces. Their stress-strain behaviors are anisotropic, oriented mostly for the resistance of tensile loads. Tendons and ligaments display time- and history-dependent viscoelastic properties.

The muscles that are responsible for the movements and the stability of the knee fall into three groups: quadriceps, hamstrings and pes anserinus. The quadriceps is responsible for the knee extension, while the hamstrings assist knee flexion. The pes anserinus contributes for knee flexion and internal rotation.

Muscles may present two types of fiber arrangements: parallel and pennate. In the parallel fiber arrangement, the fascicles are parallel to the long axis and all the fibers contract the same amount. In contrast to the parallel muscles in which all the force of the fibers is transmitted through the tendon, in the pennate muscles the fibers are attached to the tendon at a pennation angle, and so only part of the force of each fiber is effectively transmitted. Muscles usually do not maintain a zero speed or a constant length and thus, its response depends both on its length and the velocity of contraction. The combination of these two relations results in the force-length-velocity relationship. From a mechanical point of view, skeletal muscle exhibits a very complex behavior which is active, incompressible, transversely isotropic, and hyperelastic.

Mathematical muscle models fall into two categories: Huxley-type and Hill-type. Huxley-type models describe the muscle behavior at a molecular level, while Hill-type muscle models are phenomenological models. The three-component Hill-type model is almost exclusively used and is composed by a contractile component, a parallel elastic

element and a series elastic element. The contractile component consists in a force generator working in parallel with a velocity dependent damping element.

The human knee is quite susceptible to trauma and overuse injuries as it has to bear the majority of body weight. Ligaments and menisci are frequently damaged by traumatic injuries as result of application of a force causing a twisting action of the knee. In turn, Osteoarthritis is the most likely diagnosis at the knee in population over the age of 40. This is a degenerative joint disease characterized by the breakdown of articular cartilage. It is a progressive disease and in severe clinical scenarios, an arthroplasty (*i.e.* joint replacement) becomes necessary. Some patellofemoral pain is also associated with cartilage destruction, and in these cases, an arthroplasty of the patellofemoral joint may be also performed. Presently there are more than 150 different knee implants. Regarding the geometrical configuration, there are uni-comparmental, bi-compartmental and total replacement systems. As far as the material is concerned, the current designs of knee implants comprise multiple components made of polymer, ceramic and metal. Whenever there is a joint replacement, the primary mechanical factor that limits its long-term outcome is the implant wear. An implant failure leads to revision surgery, which generally decreases even more the range of motion.

References

Ackermann, M. (2007) *Dynamics and energetics of walking with prostheses*. PhD Thesis, University of Stuttgart, Stuttgart, Germany.

Altman, R.D. (1987) Overview of osteoarthritis. *The American Journal of Medicine*, 84(4B), pp. 65-69.

Ateshian, G., Hung, C.T. (2006) The natural synovial joint: properties of cartilage. *Proceedings of the Institution of Mechanical Engineers, Part J: Journal of Engineering Tribology*, 220(8), pp. 657-670.

Boyle, C., Kim, I.Y. (2011) Three-dimensional micro-level computational study of Wolff's law via trabecular bone remodeling in the human proximal femur using design space topology optimization. *Journal of Biomechanics*, 44(5), pp. 935-942.

Carr, B.C., Goswami, T. (2009) Knee implants - review of models and biomechanics. *Materials and Design*, 30(2), pp. 398-413.

Chai, H.-M. (2004) *The Knee Complex*. (URL: http://www.pt.ntu.edu.tw/hmchai/kines04/kinlower/Knee.htm, accessed on 11th January).

Collier, J.P., Mayor, M.B., McNamara, J.L., Surprenant, V.A., Jensen, R.E. (1991) Analysis of the failure of 122 polyethylene inserts from uncemented tibial knee components. *Clinical Orthopaedics & Related Research*, 273, pp. 232-242.

Completo, A. (2006) *Estudo numérico e experimental da biomecânica da prótese do joelho*. PhD Thesis, University of Aveiro, Aveiro, Portugal.

Currey, J.D. (1984) *The mechanical adaptations of bones.* Princeton University Press. New Jersey (NJ).

Dargel, J., Michael, J.W.P., Feiser, J., Ivo, R., Koebke, J. (2011) Human knee joint anatomy revisited: morphometry in the light of sex-specific total knee arthroplasty. *The Journal of Arthroplasty*, 26(3), pp. 346-353.

De Vita, R., Slaughter, W.S. (2007) A constitutive law for the failure behavior of medical collateral ligament. *Biomechanics and Modeling in Mechanobiology*, 6(3), pp. 189-197.

Donell, S.T., Glasgow, M.M.S. (2007) Isolated patellofemoral osteoarthritis. *The Knee*, 14(3), pp. 169-176.

Dyrby, C.O., Andriacchi, T.P. (2004) Secondary motions of the knee during weight bearing and non-weight bearing activities. *Journal of Orthopaedic Research*, 22(4), pp. 794-800.

Englund, M., Roos, E.M., Roos, H.P., Lohmander, L.S. (2001) Patient-relevant outcomes fourteen years after meniscectomy: influence of type of meniscal tear and size of resection. *Rheumatology*, 40(6), pp. 631-639.

Evans, P. (1986) *The Knee Joint: A Clinical Guide*. Churchill Livingstone: Edinburgh (NY).

Felson, D. (2006) Osteoarthritis of the knee. *The New England Journal of Medicine*, 354(8), pp. 841-848.

Fregly, B.J., Sawyer, W.G., Harman, M.K., Banks, S.A. (2005) Computational wear prediction of a total knee replacement from in vivo kinematics. *Journal of Biomechanics*, 28(2), pp. 305-314.

Furey, M.J. (2008). Joint lubrication. In D. Peterson, J. Bronzino (Eds.), *Biomechanics: Principles and Applications*. Taylor & Francis: Boca Raton (FL).

Gerwin, N., Hops, C., Lucke, A. (2006) Intraarticular drug delivery in osteoarthritis. *Advanced Drug Delivery Reviews*, 58(2), pp. 226-242.

Grelsamer, R.P., Weinstein, C.H. (2001) Applied biomechanics of the patella. *Clinical Orthopaedics & Related Research*, 389, pp. 9-14.

Grupp, T.M., Stulberg, D., Kaddick, C., Maas, A., Fritz, B. (2009) Fixed bearing knee congruency - influence on contact mechanics, abrasive wear and kinematics. *The International Journal of Artificial Organs*, 32(4), pp. 213-223.

Hamill, J., Knutzen, K.M. (2009) *Biomechanical Basis of Human Movement*. Lippincott Williams & Wilkins: Philadelphia (PA).

Hannon, J.C. (2005) A review of Aston Patterning®. *Journal of Bodywork and Movement Therapies*, 9(4), pp. 260-269.

Hayes, W.C., Keer, L.M., Herrmann, G., Mockros, L.F. (1972) A mathematical analysis for indentation tests of articular cartilage. *Journal of Biomechanics*, 5(5), pp. 541-551.

Heegaard, J., Leyvraz, P.F., Curnier, A., Rakotomanana, L., Huiskes, R. (1995) The biomechanics of the human patella during passive knee flexion. *Journal of Biomechanics*, 28(11), pp. 1265-1279.

Herman, I.P. (2007) *Physics of the human body*. Springer-Verlag: New York (NY).

Hirokawa, S. (1993) Biomechanics of the knee joint: a critical review. *Critical Reviews in Biomedical Engineering*, 21(2), pp. 79-135.

Hoy, M.G., Zajac, F.E., Gordon, M.E. (1990) A musculoskeletal model of the human lower extremity: The effect of muscle, tendon, and moment arm on the moment-angle relationship of musculotendon actuators at the hip, knee and ankle. *Journal of Biomechanics*, 23(2), pp. 157-169.

Jung, K.A., Lee, S.C., Song, M.B. (2008) Lateral meniscus and lateral femoral condyle cartilage injury by retained cement after medial unicondylar knee arthroplasty. *The Journal of Arthroplasty*, 23(7), pp. 1086-1089.

Kamekura, S., Hoshi, K., Shimoaka, T., Chung, U., Chikuda, H., Yamada, T., Uchida, M., Ogata, N., Seichi, A., Nakamura, K., Kawaguchi, H. (2005) Osteoarthritis development in novel experimental mouse models induced by knee joint instability. *Osteoarthritis Cartilage*, 13(7), pp. 632-41.

Katz, J.L. (2008) Mechanics of hard tissue. In D. Peterson, J. Bronzino (Eds.), *Biomechanics: Principles and Applications*. Taylor & Francis: Boca Raton (FL).

Laasanen, M.S., Töyräs, J., Korhonen, R.K., Rieppo, J., Saarakkala, S., Nieminen, M.T., Hirvonen, J., Jurvelin, J.S. (2003) Biomechanical properties of knee articular cartilage. *Biorheology*, 40(1-3), pp. 133-40.

Lavernia, C.J., Drakeford, M.K., Tsao, A.K., Gittelsohn, A., Krackow, K.A., Hungerford, D.S. (1995) Revision and primary hip and knee arthroplasty. *Clinical Orthopaedics and Related Research*, 311, pp. 136-141.

Li, L., Patil, S., Steklov, N., Bae, W., Temple-Wong, M., D'Lima, D.D., Sah, R.L., Fregly, B.J. (2011) Computational wear simulation of patellofemoral articular cartilage during in vitro testing. *Journal of Biomechanics*, 44(8), pp. 1507-1513.

Lieber, R.L., Burkholder, T.J. (2008) Musculoskeletal soft tissue mechanics. In D. Peterson, J. Bronzino (Eds.), *Biomechanics: Principles and Applications*. Taylor & Francis: Boca Raton (FL).

Machado, M., Flores, P., Claro, J.C.P., Ambrósio, J., Silva, M., Completo, A., Lankarani, H.M. (2010) Development of a planar multibody model of the human knee joint. *Nonlinear Dynamics*, 60(3), pp. 459-478.

Mader, S.S. (2005) *Understanding Human Anatomy & Physiology*. McGraw-Hill Higher Education: Tampa (FL).

Mak, A.F., Lai, W.M., Mow, V.C. (1987) Biphasic indentation of articular cartilage: I. Theoretical analysis. *Journal of Biomechanics*, 20(7), pp. 703-714.

Mansour, J.M. (2008) Biomechanics of cartilage. In C. Oatis (Ed.), *Kinesiology: The Mechanics and Pathomechanics of Human Movement* (pp. 66-79). Lippincott Williams & Wilkins: Philadelphia (PA).

Margo, B.J., Radnay, C.S., Scuderi, G.R. (2010) Anatomy of the knee. In G. Scuderi, A. Tria Jr. (Eds.), *The Knee: a comprehensive review* (pp. 1-17). World Scientific Publishing: Singapore.

Mason, J.J., Leszko, F., Johnson, T., Komistek, R.D. (2008) Patellofemoral joint forces. *Journal of Biomechanics*, 41(11), pp. 2337-2348.

McEwen, H.M.J., Barnett, P.I., Bell, C.J., Farrar, R.,Auger, D.D., Stone, M.H., Fisher, J. (2005) The influence of design, materials and kinematics on the in vitro wear of total knee replacements. *Journal of Biomechanics*, 38(2), pp. 357-365.

McGinty, G., Irrgang, J.J., Pezzullo, D. (2000) Biomechanical considerations for rehabilitation of the knee. *Clinical Biomechanics*, 15(3), pp. 160-166.

Meiss, R.A. (2003) Contractile Properties of Muscle Cells. In R.A. Rhoades, D. Bell (Eds.), *Medical Physiology* (pp. 137-151). Lippincott Williams & Wilkins: Philadelphia (PA).

Moore, K.L., Agur, A.M.R. (2007) *Essential Clinical Anatomy*. Lippincott Williams & Wilkins: Philadelphia (PA).

Mow, V.C., Good, P.M., Gardner, T.R. (2000) A new method to determine the tensile properties of articular cartilage using the indentation test. *Transactions of the 46th Annual Meeting of the Orthopaedic Research Society*, 25, pp. 103.

Mow, V.C., Hung, C.T. (2001) Biomechanics of cartilage. In M. Nordin, V. Frankel (Eds.), *Basic Biomechanics of the Musculoskeletal System* (pp. 60-101). Lippincott Williams & Wilkins: Philadelphia (PA).

Mow, V.C., Kuei, S.C., Lai, W.M., Armstrong, C.G. (1980) Biphasic creep and stress relaxation of articular cartilage in compression: theory and experiments. *Journal of Biomechanical Engineering*, 102(1), pp. 73-84.

Mow, V.C., Ratcliffe, A. (1997) Structure and function of articular cartilage and meniscus. In V.C. Mow, W.C. Hayes (Eds.), *Basic Orthopaedic Biomechanics* (pp. 113-177). Lippincott-Raven Publishers: Philadelphia.

Murnaghan, J.M., Hamer, A.J. (2010) Hip and knee replacement. *Surgery (Oxford)*, 28(10), pp. 508-513.

Nordin, M., Frankel, V.H. (2001) Biomechanics of the knee. In M. Nordin, V.H. Frankel (Eds.), *Basic Biomechanics of the Musculoskeletal System* (pp. 176-201). Lippincott Williams & Wilkins: Philadelphia (PA).

Nordin, M., Lorenz, T., Campello, M. (2001) Biomechanics of Tendons and Ligaments. In M. Nordin, V.H. Frankel (Eds.), *Basic Biomechanics of the Musculoskeletal System* (pp. 102-125). Lippincott Williams & Wilkins: Philadelphia (PA).

Palumbo, B.T., Henderson, E.R., Edwards, P.K., Burris, R.B., Gutiérrez, S., Raterman, S.J. (2011) Initial experience of the journey-deuce bicompartmental knee prosthesis: a review of 36 cases. *The Journal of Arthroplasty*, 26(6), supplement, pp. 40-45.

Peña, E., Peña, J.A., Doblaré, M. (2008) On modelling nonlinear viscoelastic effects in ligaments. *Journal of Biomechanics*, 41(12), pp. 2659-2666.

Radakovich, M., Malone, T. (1982) The superior tibiofibular joint : the forgotten joint. *Journal of Orthopaedic & Sports Physical Therapy*, 3(3), pp. 129-132.

Ramson, A. (1995) *Towards a biomechanical simulator of the fundamental behaviour of the human knee joint*. First year report, University of Hull, Hull, United Kingdom.

Sarzi-Puttini, P., Cimmino, M.A., Scarpa, R., Caporali, R., Parazzini, F., Zaninelli, A., Atzeni, F., Canesi, B. (2005) Osteoarthritis: an overview of the disease and its treatment strategies. *Seminars in Arthritis and Rheumatism*, 35(1), pp. 1-10.

Sawyer, W.G., Banks, S.A., Fregly, B.J. (2008) Predicting knee replacement damage in a simulator machine using a computational model with a consistent wear factor. *Journal of Biomechanical Engineering*, 130(1), 011004, 10p.

Silva, J.F. (2007) *Dynamic modeling and analysis of the knee joint*. MSc Thesis, University of Minho, Guimarães, Portugal.

Soulhat, J., Buschmann, M.D., Shirazi-Adl, A. (1999) A fibril-network-reinforced biphasic model of cartilage in unconfined compression. *Journal of Biomechanical Engineering*, 121(3), 340-347.

Suh, J.K., Bai, S. (1998) Finite element formulation of biphasic poroviscoelastic model for articular cartilage. *Journal of Biomechanical Engineering*, 120(2), pp. 195-201.

Teiz, C., Graney, D. (2003) *Musculoskeletal Atlas: A Musculoskeletal Atlas of the Human Body*. University of Washington, Seattle (WA).

Tözeren, A. (2000) *Human Body Dynamics: Classical Mechanics and Human Movement*. Springer-Verlag: New York (NY).

Walker, P.S., Blunn, G.W., Perry, J.P., Bell, C.J., Sathasivam, S., Andriacchi, T.P., Paul, J.P., Haider, H., Campbell, P.A. (2000) Methodology for long-term wear testing of total knee replacements. *Clinical Orthopaedics & Related Research*, 372, pp. 290-301.

Weiss, J.A., Gardiner, J.C. (2001) Computational modeling of ligament mechanics. *Critical Reviews in Biomedical Engineering*, 29(4), pp. 1-70.

Whittle, M.W. (2007) *Gait Analysis - An Introduction*. Elsevier: Philadelphia (PA).

Wismans, J. (1980) *A three-dimensional mathematical model of the human knee joint*. PhD Thesis, Eindhoven University of Technology, Eindhoven, Netherlands.

Woo, S.L-Y., Debski, R.E., Withrow, J.D., Janaushek, M.A. (1999) Biomechanics of knee ligaments. *The American Journal of Sports Medicine*, 27(4), pp. 533-543.

Wright, V., Dowson, D. (1976) Lubrication and cartilage. *Journal of Anatomy*, 121(1), pp. 107-118.

Yang, N.H., Canavan, P.K., Nayeb-Hashemi, H., Najafi, B., Vaziri, A. (2010) Protocol for constructing subject-specific biomechanical models of knee joint. *Computer Methods in Biomechanics and Biomedical Engineering*, 13(5), pp. 589-603.

Zajac, F.E. (1989) Muscle and tendon: properties, models, scaling, and application to biomechanics and motor control. *Critical Reviews in Biomedical Engineering*, 17(4), pp. 359-411.

3

Multibody dynamics methodology for biomechanical modeling

3.1 *Multibody system concept and applications* **3**-2

3.2 *Types of coordinates and kinematic constraints* **3**-5

3.3 *Equations of motions for constrained systems* **3**-18

3.4 *Numerical solution of the equations of motion* **3**-24

3.5 *Demonstrative example of application* **3**-31

3.6 *Summary and discussion* **3**-35

References **3**-36

The dynamic analysis of the human body motion and of the interactions among its skeletal structures can provide relevant information on the mechanical behavior of this system (Machado *et al.*, 2010). The biomechanical studies of the human body motion are mostly carried out using computational methods, due to the complexity and non-linearity of the equations typically involved in dynamic simulations of human activities (Silva, 2003). The computational approaches utilized in biomechanics have been enhanced along with the advances of faster computers and currently it is possible to efficiently evaluate the kinematics and dynamics of complex biomechanical systems by modeling those as multibody systems (Ferreira, 2008). In a broad sense, a multibody system (MBS) is a set of interconnected bodies that may undergo large displacements and/or rotations (Nikravesh, 1988). The multibody system methodologies comprise the study of a multibody system as a function of a set of initial conditions, external applied forces and/or prescribed motion. This mathematical formulation enables the simulation and analysis of system motion, as well as the evaluation of the internal and interaction forces that develop during the period of simulation (Pombo, 2004).

In this Chapter, the fundamental issues of the multibody system formulation used to support the methodologies developed here are revised. The equations of motion for multibody systems are derived using the Newton-Euler approach together with an augmentation method. The Newton-Euler equations represent the translational and rotational motions of the bodies, while the augmentation method is used to adjoin the constraint equations of the multibody system. The kinematic constraints and force elements that compose a multibody system are also discussed in the framework of their application to the development of biomechanical models suitable to the study of human mobility tasks. Additionally, the equations of motion are solved using the Baumgarte stabilization technique with the intent of keeping the constraint violations under control. Finally, a human body model is considered as a demonstrative example of application.

3.1 Multibody system concept and applications

In a broad sense, a multibody system (MBS) embraces two main features, namely: (*i*) physical components that describe large translational and rotational displacements and (*ii*) kinematic joints that impose some restrictions on the relative motion of the bodies. In other words, a multibody system encompasses a collection of bodies interconnected by kinematic joints and possibly acted by some force elements (Nikravesh, 1988; Haug, 1989). The kinematic joints constrain the relative motion between the bodies connected by them, while the force elements represent the internal forces that are produced in the system. Driving elements and prescribed trajectories for given points of the system components, often called guiding constraints, can also be represented under this general concept of MBS (Silva, 2003; Flores *et al.*, 2008).

The bodies that belong to a multibody system can be considered as rigid or flexible. A body is said to be rigid when the distance between any two points belonging to the body remain unchanged regardless of its motion. In practice, the rigidity assumption is accepted when its deformations are so small that they can be neglected. In the two-dimensional space, the motion of a free or unconstrained rigid body can be fully described using three generalized coordinates associated with the three degrees-of-freedom (DOF). In turn, when a body has some amount of flexibility, it has three rigid degrees-of-freedom plus the number of generalized coordinates necessary to describe the deformations (Shabana, 1989). The expression flexible multibody system

refers to a system holding deformable bodies with internal dynamics. In fact, rigid bodies are a representation of reality because bodies are not absolutely rigid in nature. However, in a good number of common applications, the bodies are soft enough to experience significant local deformations during contact events and at the same time they are significantly stiff to behave as rigid and, consequently, their flexibility can be neglected. Within the scope of this work, only rigid bodies are considered. The interested reader in the details on flexible multibody systems is referred to the works by Shabana (1997b), Ambrósio and Nikravesh (1992), Dias and Pereira (1995), Wasfy and Noor (2003), Ambrósio *et al.* (2007), Gerstmayr *et al.* (2008) and Tian *et al.* (2011).

Multibody system dynamics was identified with its own particularities as a branch of mechanics in 1977 during the IUTAM symposium on multibody dynamics organized by Magnus (1978). In a simple manner, multibody systems methodologies include the following two phases: (*i*) development of mathematical models of systems experiencing large motions and (*ii*) implementation of computational procedures to perform the analysis of the global motion produced. The equations of motion of a multibody system can be solved using either forward or inverse methods, depending on the purpose of the dynamic analysis. The forward dynamics analysis is aimed at predicting the dynamic response of the system when subjected to external forces, while the inverse dynamics approach is intended to estimate the internal and external forces that are claimed to produce an observed dynamic behavior (Silva, 2003; Meireles *et al.*, 2009).

The multibody methodologies enable the study of the kinematics and dynamics of a wide range of systems in a large number of engineering fields of application, such as (*i*) robotics and control (Zhu *et al.*, 2006; Kecskeméthy *et al.*, 2009), (*ii*) heavy machinery and mechanisms (Sugiyama and Suda, 2009; Flores, 2009), (*iii*) vehicles and railway dynamics (Sharp *et al.*, 2004; Pombo and Ambrósio, 2008), (*iv*) space systems (Ambrósio *et al.*, 2007), (*v*) efficient methods and real-time applications (Cuadrado *et al.*, 2004), (*vi*) contact mechanics (Dopico *et al.*, 2011), (*vii*) biomechanics (Silva and Ambrósio, 2002), just to mention a few. Figure 3.1 illustrates some multibody system applications, which result from the association of structural and mechanical subsystems with the purpose to transmit or transform a given motion.

There are different coordinates and formalisms that lead to suitable descriptions of multibody systems, each of them presenting relative advantages and drawbacks (Wittenburg, 1977; Nikravesh, 1988; Haug, 1989; Huston, 1990; Schiehlen, 1990b). The fundamental methodologies of analytical and recursive dynamics for rigid and flexible bodies have been summarized and discussed in several review papers published over the last two decades, such as those by Schiehlen (1990a; 2006), Shabana (1997b), Eberhard and Schiehlen (2006), Jálon (2007) and Nikravesh (2008b). In turn, many multibody computational programs capable of automatic generation and integration of the differential equations of motion have been developed, namely NEWEUL/ NEWEUL-M^2 (Schiehlen and Kreuzer, 1978; Kurz *et al.*, 2010), DAP (Nikravesh, 1988), MSC Software™ ADAMS (MSC Software Corporation, Santa Ana, CA), LMS® DADS (LMS International, Leuven, Belgium), COMPAMM (Jiménez *et al.*, 1990), SIMPACK (Rulka, 1990), AnyBody Modeling System™ (AnyBody Technology, Aalborg, Denmark), MADYMO® (Tass, Rijswijk, Netherlands), PC Crash™ (MEA Forensic, Vancouver, Canada), LifeModeler™ (LifeModeler, Inc., San Clemente, CA), SIMM (Delp *et al.*, 1990), APOLLO (Silva, 2003) and MUBODYNA (Flores, 2010). The various formulations of multibody systems used in these programs differ in the principle used, types of coordinates adopted and the method selected for handling constraints in systems characterized by closed loop topology.

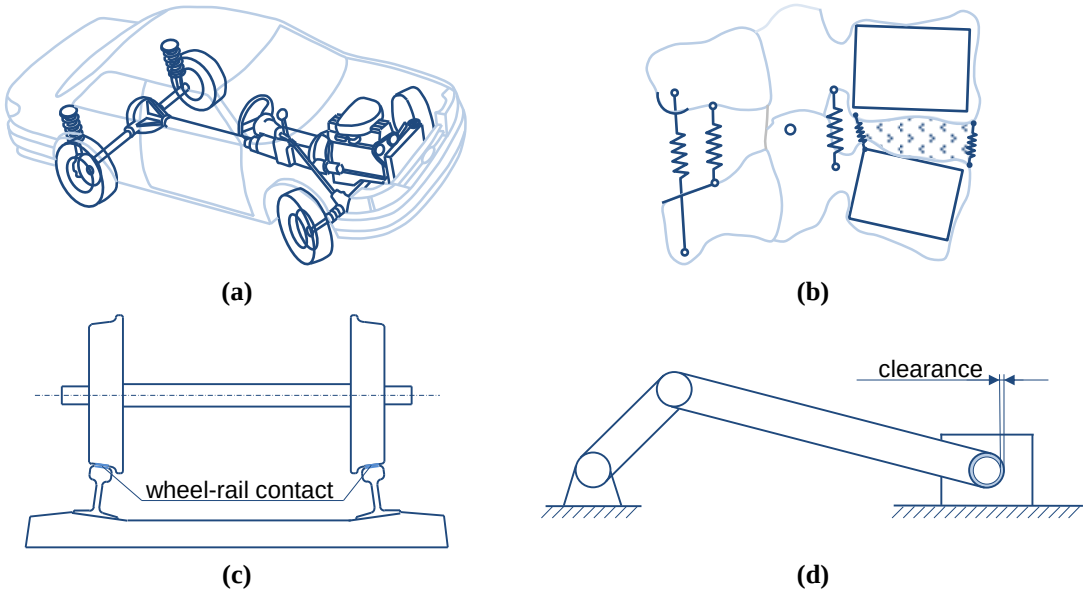

Figure 3.1 Examples of application of multibody systems: (a) Vehicle dynamics; (b) Lumbar vertebrae model; (c) Railway dynamics; (d) slider-crank model with clearance revolute joint.

Multibody models are usually used in cases where gross-motions are involved and when complex interactions with surrounding environment are expected. For instance, the human gait as a gross-motion can be described using multibody system formulations. In the field of biomechanics, the multibody system methodologies have been extensively used in the analysis of the human body motion as well as in the study of the interaction of its structures with the surroundings for several physical activities. Biomechanical studies based on multibody formulations are performed to achieve a variety of purposes: (*i*) to identify and quantify the loads placed on the biological tissues that surround the human articulations with the intention of to understand joint disorders and associated pathologies (Bei and Fregly, 2004; Guess *et al.*, 2010; Li *et al.*, 2011; Machado *et al.*, 2011); (*ii*) to investigate how the musculoskeletal structures work together to generate motion in order to help in the diagnosis and clinical treatments (Pandy, 2001; García-Vallejo and Schiehlen, 2011; Gonçalves *et al.*, 2011); (*iii*) to analyze the actions of top athletes to improve different sporting performances (Fintelman *et al.*, 2011); (*iv*) to optimize the design of sportive equipment (Hoyos and Martínez, 1999); (*v*) to assess operating and labor conditions in an ergonomic perspective (Rasmussen *et al.*, 2002; Barroso *et al.*, 2005; Castellucci *et al.*, 2010); (*vi*) to improve the design and analysis of medical and orthotic devices (Silva *et al.*, 2010; Moreira *et al.*, 2010; Cuadrado *et al.*, 2011; Font-Llagunes *et al.*, 2011); (*vii*) to analyze the occupant dynamics for crashworthiness and vehicle safety related research and design (Ma and Lankarani, 1997; Carvalho and Ambrósio, 2011).

3.2 Types of coordinates and kinematic constraints

Prior to establishing the equations of motion that govern the dynamic behavior of MBS, it is first necessary to select the way how to describe them. The description variables must be able to characterize the system configuration, that is, the position of the material points of the bodies. The description variables, also called generalized coordinates, must uniquely define the position of the system components at any instant of time during the multibody system analysis. The expression generalized coordinates is employed to include both linear and angular coordinates (Huston, 1990).

The minimum number of variables necessary to fully describe the configuration of a system is named as degrees-of-freedom of the system, or simply mobility (Müller, 2009). Different sets of coordinates may be chosen to describe the configuration of the bodies. A general and broad embracing rule to group the different sets of coordinates is to divide them into independent and dependent coordinates (Wehage and Haug, 1982). The independent coordinates are free to vary arbitrarily, while the dependent coordinates are required to satisfy the equations of constraints. Additionally, the dependent coordinates can be classified as absolute coordinates (Orlandea *et al.*, 1977), relative coordinates (Chace, 1967) and natural coordinates (Jálon and Bayo, 1994). Figure 3.2 summarizes the different types of coordinates most frequently used to describe the configuration of multibody systems. Another possible manner to classify the coordinates is to split them into Lagrangian and Eulerian coordinates. According to Nikravesh (1988), the general distinction between Lagrangian and Eulerian coordinates is that the former allows the definition of the body position relative to a moving coordinate system, whereas the later normally requires that the position of each rigid body in space be defined relative to a fixed global coordinate system. In view of that, the Eulerian formulation requires the definition of a larger number of coordinates in order to specify the position of each rigid body of a multibody system.

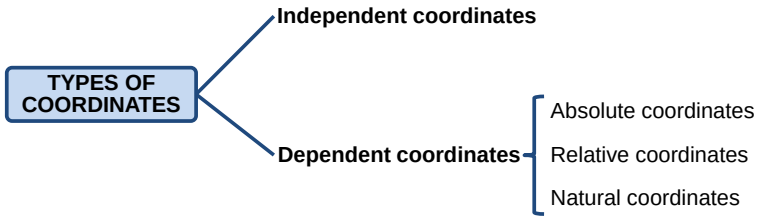

Figure 3.2 Types of coordinates frequently used in multibody systems.

For the case in which a multibody system is modeled with independent coordinates, the number of variables used to describe the system configuration is equal to the number of DOF. Furthermore, the use of independent coordinates produces constraint equations with a high degree of nonlinearity that require a complex computational implementation. Moreover, in some cases, the independent coordinates do not define the system configuration in a univocal manner. For the dependent coordinates, besides the variables associated with the system degrees-of-freedom, it is also required to consider other set of coordinates and the necessary constraint equations that relate the independent and dependent coordinates (Nikravesh, 2008a).

In the absolute coordinates, also called reference point coordinates or Cartesian coordinates, the generalized coordinates define the position of each body, typically the location of the center of mass, and the orientation of the body in the system. In the planar case, this situation corresponds to three variables, namely two Cartesian coordinates, x and y, and one angle, ϕ, all defined with respect to a global coordinate system. The formulation of multibody systems with absolute coordinates has a simple and straightforward computer implementation and handless naturally the existence of closed-loop systems. Additionally, the constraint equations necessary to describe the system constraints are generally easy to obtain and implement computationally. Furthermore, this approach exhibits good computational efficiency and the degree of nonlinearity of the resulting equations is lower than that exhibited when using independent coordinates. In addition, with absolute coordinates, the configurations of the systems are defined in a univocal manner. The major drawback associated with the absolute coordinates formulation is the large number of variables and constraint equations involved (Nikravesh, 1988; Shabana, 1989; Jálon and Bayo, 1994; Nikravesh, 2008a). Figure 3.3a illustrates a human body model developed in the AnyBody Modeling System™, which is an example of a MBS code that utilize absolute coordinates to model and simulate biomechanical systems (Rasmussen *et al.*, 2003).

The relative coordinates, also referred as joint coordinates or state variables, define the position and orientation of a body with respect to a preceding body in a multibody system. In general, this type of coordinates is directly related to the relative degrees-of-freedom allowed by joints that connect bodies. The relative coordinates are used to formulate a minimum number of equations of motion of multibody systems. When the system is an open kinematic chain, the number of relative coordinates is equal to the number of DOF. In these circumstances, the relative coordinates are, in fact, the independent variables used to define the configuration of the system. For closed kinematic chains a preprocessing analysis of the system is required to deal with the assembling constraints, and then the system topology has to be analyzed to find how to write them properly. Therefore, it can be said that relative coordinates are not convenient when the system topology can be changed during the global motion produced. In sharp contrast to the absolute coordinates, the incorporation of general force functions, constraint equations and prescribed trajectories in the system

formulation are not trivial tasks when relative coordinates are utilized. Another disadvantage associated with this type of coordinates is that they generate equations of high level of nonlinearity and, hence, their computational implementation is hard. Nevertheless, the use of relative coordinates presents a good computational efficiency and defines the system in a univocal manner. The free and open-source software OpenSim, which enables the construction of musculoskeletal models and the visualization of their motion, is an example of a computational code, developed under the framework of multibody systems, that utilizes relative coordinates in its formulation (Delp *et al.*, 2007; Seth *et al.*, 2011). An example of a musculoskeletal model developed using OpenSim is shown in Figure 3.3b.

Finally, the natural coordinates, also designated as point coordinates or fully Cartesian coordinates, are an interesting alternative to absolute or relative coordinates when describing multibody systems (Jálon, 2007). The natural coordinates are composed by the Cartesian coordinates of some points and by the Cartesian coordinates of some unit vectors distributed on the different bodies of the system. The points are typically located in relevant positions of the system components, such as joints and extremities of the bodies. In turn, the vectors are generally used to define rotational and direction axes for kinematic joints. The code APOLLO is an example of a dynamic computational program that uses natural coordinates to model biomechanical multibody systems has been developed by Silva (2003). A biomechanical model developed in the APOLLO code is depicted in Figure 3.3c.

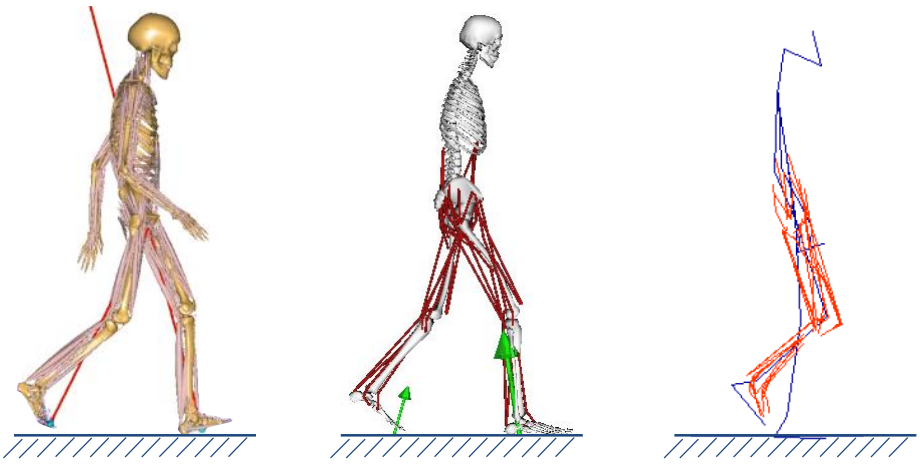

(a) **(b)** **(c)**

Figure 3.3 Examples of human body models: (a) AnyBody modeling system^{TM}; (b) OpenSim; (c) APOLLO {Adapted from Silva (2003) with Author's permission}.

The natural coordinates have the great advantage that there is no need for any angular variables (Jálon and Bayo, 1994), as it is the case of absolute and relative coordinates. In two-dimensional space, the natural coordinates can be seen as an extension of the absolute coordinates when the reference points are moved to relevant points of the multibody system, in which they represent important features. Thus, the configuration of each body is described by at least two points properly located. Figure 3.4 shows a schematic representation of the transition from absolute to natural coordinates. Natural coordinates are especially appropriate to sensitive analysis and optimization procedures, because the lengths, for instance, appear explicitly in the constraint equations. Furthermore, when using natural coordinates there is no need for preprocessing, as in the case of the closed kinematic chain systems described by relative coordinates. The natural coordinates are not independent but they are related by the natural rigid body conditions, that is, the condition of keeping constant distances and angles. Thus, the constraint equations can be formulated by the scalar product of the vectors, leading to quadratic constraint equations and constant or linear terms in the Jacobian matrix (Jálon, 2007).

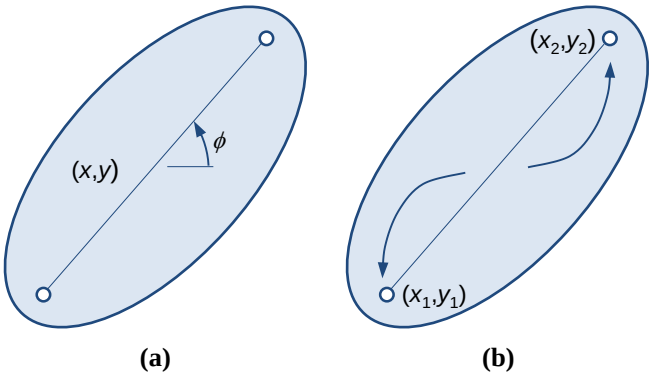

Figure 3.4 Transition from (a) absolute coordinates to (b) natural coordinates.

The process of selecting a type of coordinates to describe a multibody system is not a minor task, because the use of either type of coordinates brings a few associated limitations that will restrict the applications or will demand additional efforts of computation and/or implementation. Hence, the type of coordinates to be used must focus on the type of problem to be analyzed and should be a tradeoff between the advantages and drawbacks of each type of coordinates. In the present study, due to their simplicity and computational implementation easiness, absolute coordinates are employed to formulate the equations of motion of multibody systems. It is worth noting

that the absolute coordinates have the great merit to be straightforward, even for systems with high level of complexity.

When a multibody system is made of n_b rigid bodies, the vector of generalized coordinates can be written as

$$\mathbf{q} = \left\{ \mathbf{q}_1^T \quad \mathbf{q}_2^T \quad \cdots \quad \mathbf{q}_{nb}^T \right\}^T \tag{3.1}$$

When absolute coordinates are used, the position and orientation of the body i are defined by a set of translational and rotational coordinates. Figure 3.5 shows that body i is uniquely located in the plane by specifying the global position, $\mathbf{r}_i$, of the body-fixed coordinate system origin, O_i, and the angle ϕ_i of rotation of this system of coordinates with respect to the x-axis of the global coordinate system.

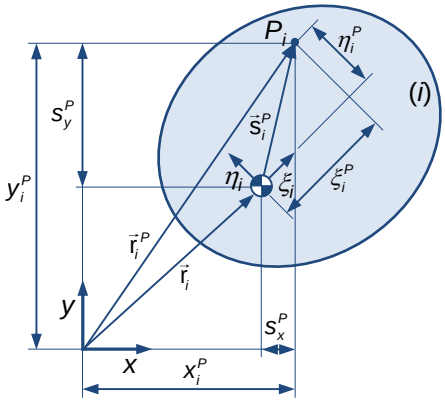

Figure 3.5 Global and local components of a point P_i on body i.

The vector of coordinates of the body i is denoted by

$$\mathbf{q}_i = \left\{ x_i \quad y_i \quad \phi_i \right\}^T \tag{3.2}$$

Let $\mathbf{u}_x$ and $\mathbf{u}_y$ be unit vectors along the global x and y-axes, respectively, and let $\mathbf{u}_{\xi_i}$ and $\mathbf{u}_{\eta_i}$ be unit vectors along the body-fixed axes ξ_i and η_i, respectively. With regard to Figure 3.5, the unit vector components $\mathbf{u}_x$ and $\mathbf{u}_y$ of vector $\mathbf{u}$ can be written as

$$\mathbf{u}_x = \mathbf{u}_{\xi_i} \cos\phi_i - \mathbf{u}_{\eta_i} \sin\phi_i \tag{3.3}$$

$$\mathbf{u}_y = \mathbf{u}_{\xi_i} \sin\phi_i + \mathbf{u}_{\eta_i} \cos\phi_i \tag{3.4}$$

In matrix form, Equations (3.3) and (3.4) take the form of

$$\begin{Bmatrix} \mathbf{u}_x \\ \mathbf{u}_y \end{Bmatrix} = \begin{bmatrix} \cos\phi_i & -\sin\phi_i \\ \sin\phi_i & \cos\phi_i \end{bmatrix} \begin{Bmatrix} \mathbf{u}_{\xi_i} \\ \mathbf{u}_{\eta_i} \end{Bmatrix} \tag{3.5}$$

which in a compact form can be expressed as

$$\mathbf{u} = \mathbf{A}_i \mathbf{u}'_i \tag{3.6}$$

where $\mathbf{u}$ is the unit vector expressed in terms of global coordinates, $\mathbf{u}'_i$ is the unit vector expressed in the local coordinate system and $\mathbf{A}_i$ represents the planar transformation matrix for body *i*, which defines the orientation of body-fixed coordinate system $\xi_i\eta_i$ with respect to the global coordinate system *xy*, being given by

$$\mathbf{A}_i = \begin{bmatrix} \cos\phi_i & -\sin\phi_i \\ \sin\phi_i & \cos\phi_i \end{bmatrix} \tag{3.7}$$

In the present work, each point in a rigid body is located by its constant position vector expressed in the body-fixed coordinate system. For instance, a point P_i can be described by the position vector $\mathbf{s}_i^P$ and by the global position of the body center of mass $\mathbf{r}_i$, resulting that

$$\mathbf{r}_i^P = \mathbf{r}_i + \mathbf{s}_i^P = \mathbf{r}_i + \mathbf{A}_i \mathbf{s}_i'^P \tag{3.8}$$

where $\mathbf{A}_i$ represents the transformation matrix given by Equation (3.7) and $\mathbf{s}_i'^P$ refers to the local components of point P_i. The location of point P_i with respect to body-fixed coordinate system is

$$\mathbf{s}_i'^P = \begin{Bmatrix} \xi_i^P & \eta_i^P \end{Bmatrix}^T \tag{3.9}$$

In the expanded form, Equation (3.8) is expressed as

$$x_i^P = x_i + \xi_i^P \cos\phi_i - \eta_i^P \sin\phi_i \tag{3.10}$$

$$y_i^P = y_i + \xi_i^P \sin\phi_i + \eta_i^P \cos\phi_i \tag{3.11}$$

It should be noted that

$$\mathbf{s}_i^P = \mathbf{A}_i \mathbf{s}_i'^P \tag{3.12}$$

is the relation between local and global components of the position of point P_i with respect to the body-fixed coordinate frame origin.

In what follows, the formulation of the most common types of kinematic constraints used in multibody systems associated with the application foreseen here will be presented, along with their contributions to the Jacobian matrix of the constraints and to the right-hand side of the velocity and acceleration constraint equations. These terms form the basis of the kinematic analysis of multibody systems. The kinematic analysis is of a preliminary nature and plays a key role in the understanding of the dynamics of moving bodies within a multibody system (Silva and Ambrósio, 2002).

Let the configuration of a multibody system be described by n absolute coordinates. Then a set of m algebraic kinematic independent holonomic constraints $\mathbf{\Phi}$ can be written as (Nikravesh, 1988; Roberson and Schwertassek, 1988)

$$\mathbf{\Phi}(\mathbf{q}, t) = \mathbf{0} \tag{3.13}$$

where $\mathbf{q}$ is the vector of generalized coordinates and t is the time variable.

The velocities and accelerations of the system components can be determined using the velocity and acceleration constraint equations. Thus, the first time derivative of Equation (3.13) provides the velocity constraint equations as

$$\mathbf{\Phi}_{\mathbf{q}}\dot{\mathbf{q}} \equiv -\mathbf{\Phi}_{t} = \boldsymbol{\upsilon} \tag{3.14}$$

where $\mathbf{\Phi}_{\mathbf{q}}$ is the Jacobian matrix of the constraint equations, that is, the matrix of the partial derivatives of $\mathbf{\Phi}$ with respect to $\mathbf{q}$, $\partial\mathbf{\Phi}/\partial\mathbf{q}$, $\dot{\mathbf{q}}$ represents the vector of generalized velocities and $\boldsymbol{\upsilon}$ denotes the right-hand side of velocity constraint equations, which contains the partial derivatives of $\mathbf{\Phi}$ with respect to time, $\partial\mathbf{\Phi}/\partial t$. Notice that only rheonomic constraints, typically associated with driving or guiding elements, contribute with non-zero entries to the vector $\boldsymbol{\upsilon}$ (Nikravesh, 1988).

A second differentiation of Equation (3.13) with respect to time leads to the acceleration constraint equations, yielding

$$\mathbf{\Phi}_{\mathbf{q}}\ddot{\mathbf{q}} \equiv -(\mathbf{\Phi}_{\mathbf{q}}\dot{\mathbf{q}})_{\mathbf{q}}\dot{\mathbf{q}} - 2\mathbf{\Phi}_{\mathbf{q}t}\dot{\mathbf{q}} - \mathbf{\Phi}_{tt} = \boldsymbol{\gamma} \tag{3.15}$$

where $\ddot{\mathbf{q}}$ is the vector of generalized acceleration and $\boldsymbol{\gamma}$ denotes the right-hand side of acceleration constraint equations, *i.e.*, the vector of quadratic velocity terms, which are exclusively functions of velocity, position and time. In the case of scleronomic constraints, that is, when $\boldsymbol{\Phi}$ is not explicitly dependent on the time, the terms $\boldsymbol{\Phi}_t$ in Equation (3.14) and $\boldsymbol{\Phi}_{\mathbf{q}t}$ and $\boldsymbol{\Phi}_{tt}$ in Equation (3.15) vanish.

The terms included in Equations (3.13) through (3.15) appear in a general form, that is, they do not reflect the type of dependent coordinates considered. Moreover, the constraint equations represented by Equation (3.13) are nonlinear in terms of $\mathbf{q}$ and are, usually, solved by employing the iterative Newton-Raphson method. In turn, Equations (3.14) and (3.15) are linear in terms of $\dot{\mathbf{q}}$ and $\ddot{\mathbf{q}}$, respectively, and can be solved by any method adopted for the solution of linear systems (Atkinson, 1989). The treatment of redundant constraints is out of the scope of this work. The interested reader in this topic is referred to the work by Wehage and Haug (1982) or to Arabyan and Wu (1998).

The kinematic analysis is the study of the motion of a multibody system, independently of the causes that produce it. Since in the kinematic analysis the forces are not considered, the motion of the system is specified by driving or guiding elements that govern the motion of certain degrees-of-freedom of the system during the analysis. The position, velocity and acceleration of the remaining elements of the system are defined by kinematic constraint equations that describe the system topology (Paul and Krajcinovic, 1970a; Paul and Krajcinovic, 1970b; Shigley and Uicker, 1995). It is clear that in the kinematic analysis, the number of driving and guiding constraints must be equal to the number of degrees-of-freedom of the multibody system.

The kinematic analysis of a multibody system can be carried by solving the set of Equations (3.13)-(3.15). The necessary steps to perform this type of analysis, sketched in Figure 3.6, can be summarized as follows (Flores, 2004)

1. Specify initial conditions for positions $\mathbf{q}^0$ and initialize the time t^0;
2. Evaluate the position constraint equations (3.13) and solve them for $\mathbf{q}$;
3. Evaluate the velocity constraint equations (3.14) and solve them for $\dot{\mathbf{q}}$;
4. Evaluate the acceleration constraint equations (3.15) and solve them for $\ddot{\mathbf{q}}$;
5. Increment the time. If the time is smaller than final time, go to step 2, otherwise stop the kinematic analysis.

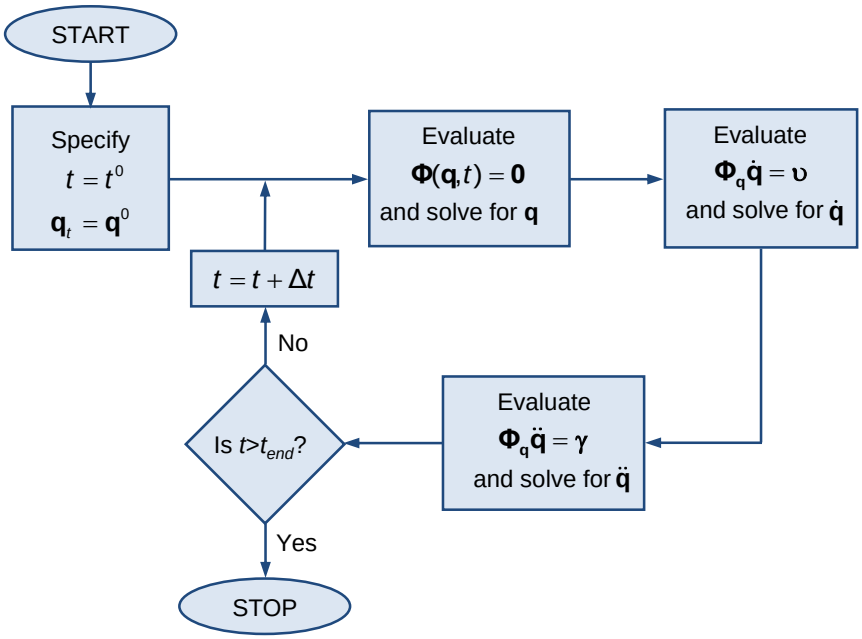

Figure 3.6 Flowchart of computational procedure for kinematic analysis of a multibody system.

Figure 3.7 shows two bodies *i* and *j* connected by a revolute or pin joint, which is one of the most common kinematic joints used in multibody models. A revolute joint constrains the relative translation of the bodies, allowing only the relative rotation.

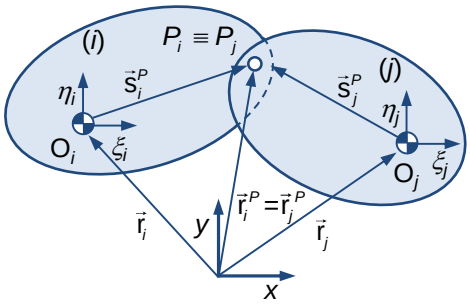

Figure 3.7 Revolute joint connecting bodies *i* and *j*.

The kinematic conditions for the revolute joint require that two different points, each one belonging to a different body, share the same position in space all the time. This means that the global position of the point P_i on body *i* is coincident with the global position of the point P_j on body *j*. Such condition is expressed by two algebraic equations that can be obtained from the following vector loop equation

$$\mathbf{r}_i + \mathbf{s}_i^P - \mathbf{r}_j - \mathbf{s}_j^P = \mathbf{0} \tag{3.16}$$

which can be rewritten as

$$\mathbf{\Phi}^{(r,2)} \equiv \mathbf{r}_i + \mathbf{A}_i \mathbf{s}_i'^P - \mathbf{r}_j - \mathbf{A}_j \mathbf{s}_j'^P = \mathbf{0} \tag{3.17}$$

where the superscripts *r* and 2 refer to a revolute joint constraint and the number of equations involved, respectively (Nikravesh, 1988).

In a more explicit form, Equation (3.17) can take the form of

$$\mathbf{\Phi}^{(r,2)} \equiv \begin{Bmatrix} x_i^P - x_j^P \\ y_i^P - y_j^P \end{Bmatrix} = \begin{Bmatrix} 0 \\ 0 \end{Bmatrix} \tag{3.18}$$

Expanding Equation (3.18) yields two constraint equations as

$$\mathbf{\Phi}^{(r,1\text{st})} \equiv x_i + \xi_i^P \cos\phi_i - \eta_i^P \sin\phi_i - x_j - \xi_j^P \cos\phi_j + \eta_j^P \sin\phi_j = 0 \tag{3.19}$$

$$\mathbf{\Phi}^{(r,2\text{nd})} \equiv y_i + \xi_i^P \sin\phi_i + \eta_i^P \cos\phi_i - y_j - \xi_j^P \sin\phi_j - \eta_j^P \cos\phi_j = 0 \tag{3.20}$$

Therefore, it can be stated that there is only one relative degree-of-freedom between two rigid bodies that are connected by a revolute joint. In other words, the two kinematic constraint equations (3.19) and (3.20) reduce the number of degrees-of-freedom of the multibody system by two.

In order to perform the kinematic analysis, it is necessary to evaluate the Jacobian matrix of the constraint equations for positions and the right-hand side of the velocity and acceleration constraint equations. Thus, the Jacobian matrix associated with the revolute joint is, by definition, the partial derivatives of Equations (3.19) and (3.20) with respect to generalized coordinates. For the revolute joint shown in Figure 3.7, the column vector of generalized coordinates is written as

$$\mathbf{q} = \begin{Bmatrix} x_i & y_i & \phi_i & x_j & y_j & \phi_j \end{Bmatrix}^T \tag{3.21}$$

Then, the Jacobian matrix is given by

$$\mathbf{\Phi}_{\mathbf{q}}^{(r,2)} = \begin{bmatrix} \dfrac{\partial \mathbf{\Phi}^{(r,1\text{st})}}{\partial x_i} & \dfrac{\partial \mathbf{\Phi}^{(r,1\text{st})}}{\partial y_i} & \dfrac{\partial \mathbf{\Phi}^{(r,1\text{st})}}{\partial \phi_i} & \dfrac{\partial \mathbf{\Phi}^{(r,1\text{st})}}{\partial x_j} & \dfrac{\partial \mathbf{\Phi}^{(r,1\text{st})}}{\partial y_j} & \dfrac{\partial \mathbf{\Phi}^{(r,1\text{st})}}{\partial \phi_j} \\ \dfrac{\partial \mathbf{\Phi}^{(r,2\text{nd})}}{\partial x_i} & \dfrac{\partial \mathbf{\Phi}^{(r,2\text{nd})}}{\partial y_i} & \dfrac{\partial \mathbf{\Phi}^{(r,2\text{nd})}}{\partial \phi_i} & \dfrac{\partial \mathbf{\Phi}^{(r,2\text{nd})}}{\partial x_j} & \dfrac{\partial \mathbf{\Phi}^{(r,2\text{nd})}}{\partial y_j} & \dfrac{\partial \mathbf{\Phi}^{(r,2\text{nd})}}{\partial \phi_j} \end{bmatrix} \tag{3.22}$$

The evaluation of the partial derivatives that appear in Equation (3.22) yield the corresponding values of the Jacobian terms as

$$\mathbf{\Phi}_{\mathbf{q}}^{(r,2)} = \begin{bmatrix} 1 & 0 & -\xi_i^P \sin\phi_i - \eta_i^P \cos\phi_i & -1 & 0 & \xi_i^P \sin\phi_i + \eta_i^P \cos\phi_i \\ 0 & 1 & \xi_i^P \cos\phi_i - \eta_i^P \sin\phi_i & 0 & -1 & -\xi_i^P \cos\phi_i + \eta_i^P \sin\phi_i \end{bmatrix} \tag{3.23}$$

Alternatively, Equation (3.23) can be written in an explicit form as

$$\mathbf{\Phi}_{\mathbf{q}}^{(r,2)} = \begin{bmatrix} 1 & 0 & -y_i^P + y_i & -1 & 0 & y_j^P - y_j \\ 0 & 1 & x_i^P - x_i & 0 & -1 & -x_j^P + x_j \end{bmatrix} \tag{3.24}$$

In turn, the right-hand side of the velocity constraint equations is given by

$$\boldsymbol{\upsilon}^{(r,2)} = -\mathbf{\Phi}_t = \mathbf{0} \tag{3.25}$$

or, alternatively

$$\boldsymbol{\upsilon}^{(r,2)} = -\mathbf{\Phi}_t = \begin{Bmatrix} \dfrac{\partial \mathbf{\Phi}^{(r,1\text{st})}}{\partial t} \\ \dfrac{\partial \mathbf{\Phi}^{(r,2\text{nd})}}{\partial t} \end{Bmatrix} = \begin{Bmatrix} 0 \\ 0 \end{Bmatrix} \tag{3.26}$$

In fact, Equation (3.25) represents a scleronomic constraint, that is, the revolute joint constraints do not depend explicitly on time. Consequently, the right-hand side of the acceleration constraint equations reduce to

$$\boldsymbol{\gamma}^{(r,2)} = -(\mathbf{\Phi}_{\mathbf{q}}\dot{\mathbf{q}})_{\mathbf{q}}\,\dot{\mathbf{q}} \tag{3.27}$$

which results in

$$\boldsymbol{\gamma}^{(r,2)} = \begin{bmatrix} (\xi_i^P \cos\phi_i - \eta_i^P \sin\phi_i)\dot{\phi}_i^2 - (\xi_j^P \cos\phi_j - \eta_j^P \sin\phi_j)\dot{\phi}_j^2 \\ (\xi_i^P \sin\phi_i + \eta_i^P \cos\phi_i)\dot{\phi}_i^2 - (\xi_j^P \sin\phi_j + \eta_j^P \cos\phi_j)\dot{\phi}_j^2 \end{bmatrix} \tag{3.28}$$

The kinematic constraint equations presented for the revolute joints are functions of the generalized coordinates of the system only, *i.e.*, they do not depend on time. Examples of kinematic constraints, besides the revolute joints, are the simple constraints, the ground constraints and the driving constraints (Nikravesh, 1988).

The guiding constraints are a type of rheonomic constraints that are frequently used in the formulation of biomechanical system, mainly in modeling and analysis of the human motion. The role of these constraints is to impose prescribed trajectories to certain points on the bodies, as it is the case of the human arm model depicted in Figure 3.8 (Meireles *et al.*, 2009). In general, this type of trajectories is obtained experimentally using a complete data acquisition system, being the data points expressed as functions of time variable (Silva, 2003).

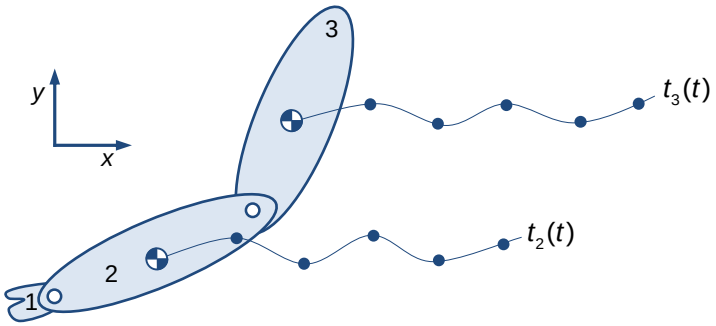

Figure 3.8 Human arm multibody model composed by three bodies: hand (1), forearm (2) and arm (3). The motions of forearm and arm are prescribed by the trajectories $t_2(t)$ and $t_3(t)$, respectively.

Considering, for instance, the trajectory of the center of mass of body 2, then three constraints can be written as

$$\mathbf{\Phi}^{(g,3)} \equiv \begin{Bmatrix} x_2 - t_2^x(t) \\ y_2 - t_2^y(t) \\ \phi_2 - t_2^\phi(t) \end{Bmatrix} = \mathbf{0} \tag{3.29}$$

where $t_2^k(t)$, (k=x, y, ϕ), denotes the trajectory coordinates of the body 2 center of mass.

The contributions of the guiding constraint equations (3.29) to the Jacobian matrix of the constraints and to the right-hand side of the velocity and acceleration constraints can be evaluated as follows, respectively

$$\mathbf{\Phi}_{\mathbf{q}}^{(g,3)} = \begin{bmatrix} \dfrac{\partial \mathbf{\Phi}^{(g,1st)}}{\partial x_2} & \dfrac{\partial \mathbf{\Phi}^{(g,1st)}}{\partial y_2} & \dfrac{\partial \mathbf{\Phi}^{(g,1st)}}{\partial \phi_2} \\ \dfrac{\partial \mathbf{\Phi}^{(g,2nd)}}{\partial x_2} & \dfrac{\partial \mathbf{\Phi}^{(g,2nd)}}{\partial y_2} & \dfrac{\partial \mathbf{\Phi}^{(g,2nd)}}{\partial \phi_2} \\ \dfrac{\partial \mathbf{\Phi}^{(g,3rd)}}{\partial x_2} & \dfrac{\partial \mathbf{\Phi}^{(g,2nd)}}{\partial y_2} & \dfrac{\partial \mathbf{\Phi}^{(g,3rd)}}{\partial \phi_2} \end{bmatrix} \tag{3.30}$$

$$\boldsymbol{\upsilon}^{(g,3)} = \left\{ \frac{\partial \boldsymbol{\Phi}^{(g,1st)}}{\partial t} \quad \frac{\partial \boldsymbol{\Phi}^{(g,2nd)}}{\partial t} \quad \frac{\partial \boldsymbol{\Phi}^{(g,3rd)}}{\partial t} \right\}^T \tag{3.31}$$

$$\boldsymbol{\gamma}^{(g,3)} = \left\{ \frac{\partial^2 \boldsymbol{\Phi}^{(g,1st)}}{\partial t^2} \quad \frac{\partial^2 \boldsymbol{\Phi}^{(g,2nd)}}{\partial t^2} \quad \frac{\partial^2 \boldsymbol{\Phi}^{(g,3rd)}}{\partial t^2} \right\}^T \tag{3.32}$$

Since the trajectory of body center of mass is typically discrete and obtained experimentally, in general, the data collected are used to derive the mathematical expressions by interpolating the coordinates in time. In the present work, this procedure is obtained by employing cubic splines interpolation, because higher order polynomials are known for exhibiting oscillations in the vicinity of curvature changes, whereas cubic splines provides much more smooth transitions (Chapra and Canale, 1988; Späth, 1995; Meireles *et al.*, 2009). Furthermore, the use of cubic spline is quite useful to ensure the continuity of the first and second derivatives, *i.e.*, velocity and acceleration, property that is very important in kinematic and dynamic analysis.

3.3 Equations of motions for constrained systems

The formulation of the equations of motion for constrained MBS adopted here follows closely the formulation presented by Nikravesh, in which the generalized absolute coordinates are used to describe the system configuration (Nikravesh, 1988). Thus, for a constrained MBS the kinematic constraints can be described by a set of holonomic algebraic equations (3.13). Differentiating Equation (3.13) with respect to time yield the velocity constraint equations (3.14) and after a second differentiation with respect to time the acceleration constraint equations (3.15) are obtained.

The translational and rotational equations of motion for a unconstrained multibody system made of rigid bodies are written as

$$\mathbf{M}\ddot{\mathbf{q}} = \mathbf{g} \tag{3.33}$$

where **M** is the global system mass matrix, containing the mass and moments of inertia of all bodies, and **g** is the generalized force vector that contains all external forces and moments applied on the system.

The forces applied over the multibody system components can be the result of springs, dampers, actuators or external forces. Figure 3.9 illustrates a biomechanical model where some of these forces are represented.

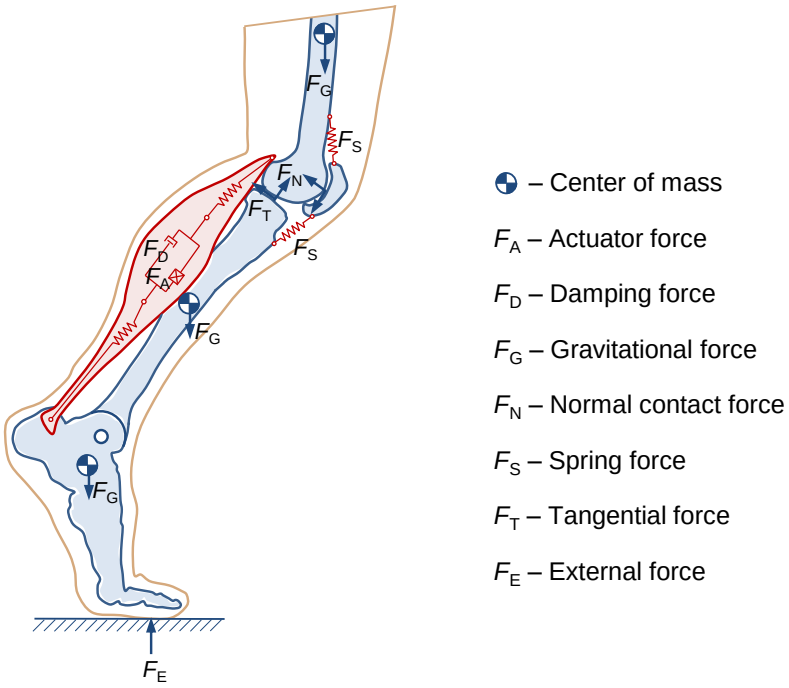

Figure 3.9 Different types of forces that can be present in a biomechanical multibody system.

External applied forces, of different nature and level of complexity, can act on a multibody system representing the interactions among the system components and between them and the surrounding environment. Gravitational forces, inertia forces, spring-damper-actuator forces, normal contact forces, tangential or frictional forces, external applied forces, forces due to elasticity of bodies, and thermal, electrical and magnetic forces are some of the actions over the system bodies that can be represented as external forces.

When a multibody system comprises kinematic constraints, the corresponding reaction forces and moments have to be included in the formulation. The forces and moments developed at the kinematic joints can be expressed in terms of the Jacobian matrix of the constraint equations and the vector of Lagrange multipliers as (Greenwood, 1965; Jálon and Bayo, 1994)

$$\mathbf{g}^{(\mathbf{c})} = -\mathbf{\Phi}_{\mathbf{q}}^{T}\boldsymbol{\lambda} \tag{3.34}$$

where $\boldsymbol{\lambda}$ is the vector that contains *m* unknown Lagrange multipliers associated with *m* holonomic constraints. The Lagrange multipliers are physically related to the reaction forces and moments between the bodies interconnected by kinematic joints.

Introducing now Equation (3.34) into Equation (3.33) yields

$$\mathbf{M}\ddot{\mathbf{q}} + \boldsymbol{\Phi}_{\mathbf{q}}^{T}\boldsymbol{\lambda} = \mathbf{g} \tag{3.35}$$

It is well known that in dynamic analysis, a unique solution of Equation (3.35) is obtained when the acceleration constraint equations are considered simultaneously with the differential equations of motion, for a proper set of initial conditions. Equation (3.15) is appended to Equation (3.35) and written in the Hessenberg matrix form as

$$\begin{bmatrix} \mathbf{M} & \boldsymbol{\Phi}_{\mathbf{q}}^{T} \\ \boldsymbol{\Phi}_{\mathbf{q}} & \mathbf{0} \end{bmatrix} \begin{Bmatrix} \ddot{\mathbf{q}} \\ \boldsymbol{\lambda} \end{Bmatrix} = \begin{Bmatrix} \mathbf{g} \\ \boldsymbol{\gamma} \end{Bmatrix} \tag{3.36}$$

Equation (3.36) is formed as a combination of the equations of motion and second time derivatives of the kinematic constraint equations, often referred to as a mixed set of differential and algebraic equations (DAE). This linear system of equations is solved for the variables $\ddot{\mathbf{q}}$ and $\boldsymbol{\lambda}$. Then, in each integration time step, the accelerations vector, $\ddot{\mathbf{q}}$, together with velocities vector, $\dot{\mathbf{q}}$, are integrated in order to obtain the system velocities and positions for the next time step. This procedure is repeated up to final time of analysis is reached. A set of initial conditions, positions and velocities, is required to start the dynamic simulation. Usually, the initial conditions are obtained from a previous kinematic simulation of the multibody system under analysis in order to ensure kinematic consistency for the initial positions and velocities. The subsequent initial conditions for each time step in the simulation are obtained in the usual way from the final conditions of the previous time step (Nikravesh, 2007).

It is clear that the system of the motion equations (3.36) does not use explicitly the position and velocity constraints, that is, Equations (3.13) and (3.14). For moderate or long simulation times, the original constraint equations start to be violated due to the numerical approximations on the integration process and/or to inaccurate initial conditions. Special procedures must be followed to avoid or minimize this effect. Several methods to solve this problem have been suggested and tested, being the most

common among them the augmented Lagrangian formulation (Bayo *et al.*, 1988), the coordinate partitioning method (Wehage and Haug, 1982) and the Baumgarte stabilization method (Baumgarte, 1972). An overview of the pros and cons of these methods is given by Neto and Ambrósio (2003).

In a simple way, the augmented Lagrangian formulation is based on Hamilton's principle and the constraint equations are taken into account using a penalty approach. This method consists of solving the system's equations of motion using an iterative process. The form of the constraint equations is similar to the Baumgarte approach, but it enables to handle redundant constraints in the process (Neto and Ambrósio, 2003).

In the coordinate partitioning method, the generalized coordinates are partitioned into independent and dependent sets. The numerical integration is carried out for independent generalized coordinates. Then, the constraint equations are solved for dependent generalized coordinates using the position and velocity constraint equations. The advantage of this method is that it satisfies all the constraints to the level of precision specified and maintains good error control. However, it suffers from poor numerical efficiency due to the requirement for the iterative solution for dependent generalized coordinates in the Newton-Raphson method. During integration, numerical problems may arise due to inadequate choice of independent and dependent coordinates that lead to poorly conditioned matrice (Arabyan and Wu, 1998).

Due to its simplicity and easiness for computational implementation, the Baumgarte stabilization method is probably the most popular and attractive technique to overcome the drawbacks of the standard resolution of the equations of motion. Baumgarte's method can be looked upon as an extension of feedback control theory. The principle of this method is to damp out the acceleration constraint violations by feeding back the violations of the position and velocity constraints. The choice of the feedback parameters depends on several factors, namely, the integrator used and the model of the multibody system (Flores *et al.*, 2011). However, this method does not solve all possible numerical instabilities such as, for instance, those that arise near kinematic singularities. Furthermore, the major drawback of the Baumgarte's method is the ambiguity in choosing feedback parameters. As pointed out by Baumgarte (1972), it seems that the choice of these coefficients usually involves a trial and error procedure.

In any case, it must be clearly noted that this method does not correct constraint violations but, simply, keeps then under control.

In the present work, the Baumgarte approach is used as stabilization method and, therefore, the fundamentals of this approach to control the violation of constraints are analized in the following paragraph. The Baumgarte stabilization method allows constraints to be slightly violated before corrective actions can take place, in order to force the violation to be reduced to a tolerant level. The objective of Baumgarte method is to replace the differential Equation (3.15) by the following equation

$$\ddot{\mathbf{\Phi}} + 2\alpha\dot{\mathbf{\Phi}} + \beta^2\mathbf{\Phi} = \mathbf{0} \tag{3.37}$$

which is a differential equation for a closed-loop system in terms of kinematic constraint equations in which the terms $2\alpha\dot{\mathbf{\Phi}}$ and $\beta^2\mathbf{\Phi}$ play the role of control terms. The principle of the method is based on the damping of acceleration of constraint violation by feeding back the position and velocity of constraint violations, as illustrated in Figure 3.10, which shows open-loop and closed-loop control systems.

In the open-loop systems $\mathbf{\Phi}$ and $\dot{\mathbf{\Phi}}$ do not converge to zero if any perturbation occurs and, therefore, the system is unstable. Thus, using the Baumgarte approach, the equations of motion for a system subjected to constraints are stated as follows

$$\begin{bmatrix} \mathbf{M} & \mathbf{\Phi}_\mathbf{q}^T \\ \mathbf{\Phi}_\mathbf{q} & \mathbf{0} \end{bmatrix} \begin{Bmatrix} \ddot{\mathbf{q}} \\ \boldsymbol{\lambda} \end{Bmatrix} = \begin{Bmatrix} \mathbf{g} \\ \boldsymbol{\gamma} - 2\alpha\dot{\mathbf{\Phi}} - \beta^2\mathbf{\Phi} \end{Bmatrix} \tag{3.38}$$

If α and β are chosen as positive constants, the stability of the general solution of Equation (3.38) is guaranteed. Baumgarte (1972) highlighted that the suitable choice of the parameters α and β is performed by numerical experiments. Hence, the Baumgarte method has some ambiguity in determining optimal feedback gains. Indeed, it seems that the value of the parameters is purely empiric, and there is no reliable method for selecting the coefficients α and β. The improper choice of these coefficients can lead to unacceptable results in the dynamics of the multibody systems (Nikravesh, 1984). The effect of the Baumgarte stabilization method on the dynamic response of a biomechanical system is presented in Section 3.5 throughout a demonstrative example of application. The reader interested in detailed information about the influence of the

Baumgarte stabilization method, and on the techniques to select the Baumgarte parameters, is referred the work by Flores and the co-authors (2011).

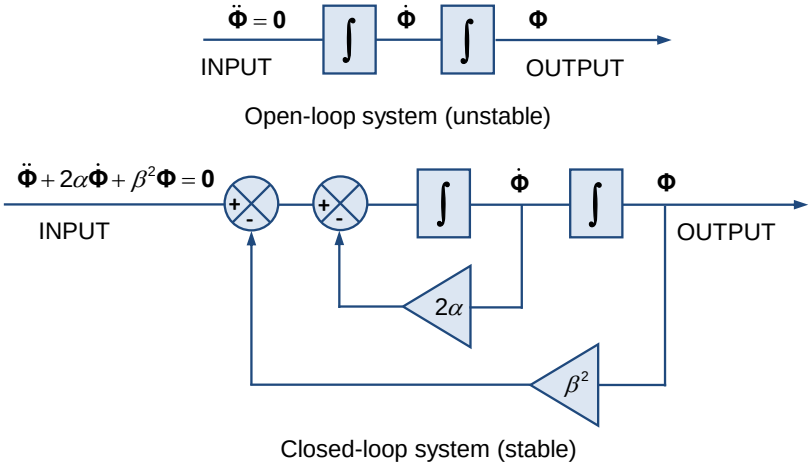

Figure 3.10 Open loop and closed loop control systems.

In addition to the three basic approaches presented above, many research papers have been published on the stabilization methods for the numerical integration the equations of motion of multibody systems. Yoon and the co-authors (1994) presented a direct correction method to eliminate the violation of the constraints in numerical simulation of constrained multibody systems. However, this method is formulated on the positions level only. Blajer (1995) considered the projection method to obtain the dynamic equations of motion for constrained multibody systems in the form of ordinary differential equations. Then, a standard solver is used to integrate the resulting system. Fisette and Vaneghem (1996), based on the coordinate partitioning method, used the LU-factorization of constraint Jacobian matrix to identify the dependent and independent coordinates. This aspect is of paramount importance since during the integration process, numerical problems may arise due to inadequate choice of the independent coordinates that lead to poorly conditioned matrices. This problem was also considered by Arabyan and Wu (1998) to study multibody mechanical systems with both holonomic and nonholonomic constraints. Weijia and the co-authors (2000) used the Taylor's expansion series to present a methodology to deal with the violation of the constraints. Neto and Ambrósio (2003) used different methodologies to handle the constraint violation correction for the integration of differential algebraic equations in the presence of redundant constraints. Tseng and the co-authors (2003) used the Maggi's equations with perturbed iteration to develop an efficient approach to

numerically solve constrained multibody systems. Nikravesh (1984) comparatively studied the direct integration of the equations of motion of multibody systems, the Baumgarte stabilization method and the coordinate partitioning method, and concluded that the implementation of the Baumgarte stabilization approach is twice as efficient as the integration of the mixed system.

3.4 Numerical solution of the equations of motion

In this Section, the main numerical aspects related to the numerical integration of the equations of motion of a multibody system are reviewed. The standard integration of the equations of motion, here called direct integration method (DIM), converts the n second-order differential equations of motion into $2n$ first-order differential equations. Then, a numerical integration scheme is used to solve the initial value problem (Shampine and Gordon, 1975; Gear, 1971b).

The $2n$ differential equations of motion are solved without considering the integration numerical errors and, consequently, during the simulation the propagation of these types of errors results in constraint violations. The two error sources that lead to constraint violations for any numerical integration step are truncation and round-off errors. Truncation or discretization errors are caused by the nature of the techniques employed to approximate values of a function. Round-off errors are due to the limited numbers of significant digits that can be retained by a computer. The truncation errors are composed of two parts: the first is a local truncation error that results from the application of the method over a single step, and the second is the propagated error that results from the approximation procedure applied in the previous step. The sum of the two is the total or global truncation errors (Chapra and Canale, 1988).

The commonly used numerical integration algorithms are useful in solving first-order differential equations that take the form (Gear, 1971b)

$$\dot{\mathbf{y}} = f(\mathbf{y}, t) \tag{3.39}$$

Thus, if there are n second-order differential equations, they are converted to $2n$ first-order equations by defining the $\mathbf{y}$ and $\dot{\mathbf{y}}$ vectors, which contain, respectively, the system positions and velocities and the system velocities and accelerations, as

$$\mathbf{y} = \begin{Bmatrix} \mathbf{q} \\ \dot{\mathbf{q}} \end{Bmatrix} \tag{3.40}$$

$$\dot{\mathbf{y}} = \begin{Bmatrix} \dot{\mathbf{q}} \\ \ddot{\mathbf{q}} \end{Bmatrix} \tag{3.41}$$

The reason for introducing these new vectors $\mathbf{y}$ and $\dot{\mathbf{y}}$ is that most numerical integration algorithms deal with first-order differential equations (Gear, 1971a; Shampine and Gordon, 1975). The following diagram can interpret the process of numerical integration at instant of time t

$$\dot{\mathbf{y}}(t) \xrightarrow{Integration} \mathbf{y}(t + \Delta t) \tag{3.42}$$

In other words, velocities and accelerations at instant t, after integration process, yield positions and velocities at next time step, $t=t+\Delta t$. Figure 3.11 presents a flowchart that shows the algorithm of direct integration method of the equations of motion. At $t=t^0$, the initial conditions on $\mathbf{q}^0$ and $\dot{\mathbf{q}}^0$ are required to start the integration process. These values cannot be specified arbitrarily, but must satisfy the Equations (3.13) and (3.35). The algorithm depicted in Figure 3.11 can be summarized in the following steps:

1. Start at instant of time t^0 with given initial conditions for positions $\mathbf{q}^0$ and velocities $\dot{\mathbf{q}}^0$;
2. Assemble the global mass matrix $\mathbf{M}$, evaluate the Jacobian matrix $\mathbf{\Phi_q}$, construct the constraint equations $\mathbf{\Phi}$, determine the right-hand side of the accelerations $\boldsymbol{\gamma}$ and calculate the force vector $\mathbf{g}$;
3. Solve the linear set of the equations of motion (3.38) for a constrained multibody system in order to obtain the accelerations $\ddot{\mathbf{q}}$ at instant t and the Lagrange multipliers $\boldsymbol{\lambda}$;
4. Assemble the vector $\dot{\mathbf{y}}_t$ containing the generalized velocities $\dot{\mathbf{q}}$ and accelerations $\ddot{\mathbf{q}}$ for instant of time t;
5. Integrate numerically the $\dot{\mathbf{q}}$ and $\ddot{\mathbf{q}}$ vectors for time step $t+\Delta t$ and obtain the new positions and velocities;
6. Update the time variable, go to step 2 and proceed with the process for a new time step, until the final time of analysis is reached.

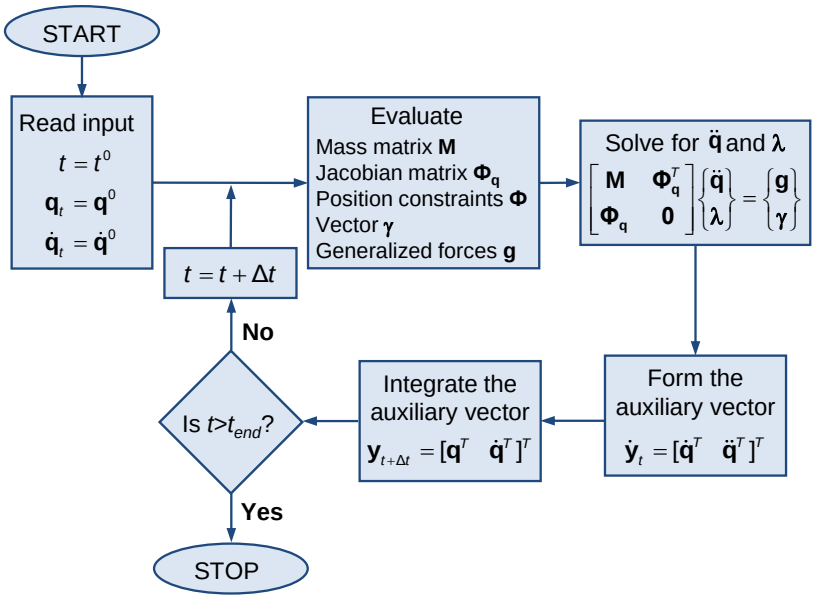

Figure 3.11 Flowchart of computational algorithm for dynamic analysis of multibody systems based on the direct integration method.

In what follows, the most widely used methods to the numerical integration of the equation of motion of multibody system are briefly described, namely Euler method, Rung-Kutta methods and Adams predictor-corrector methods. These explicit methods involve a step-by-step process in which a sequence of discrete points $t^0, t^1, t^2, ..., t^n$ is generated. The discrete points may have either constant or variable spacing defined as $h^i = t^{i+1} - t^i$, where h^i is the step size for any discrete point t^i. At each point t^i, the solution $y(t^i)$ is approximated by a number y^i. Since no numerical method is capable of finding $y(t^i)$ exactly, the global or total error at $t=t^i$ is given by

$$\varepsilon^i = \left| y(t^i) - y^i \right| \tag{3.43}$$

The integration methods are called single step methods when they only require information on the current time step to advance to the next time step. The Euler and Runge-Kutta methods are single-step methods. When information of the previous steps is used, the algorithm methods are called multi-step methods, as it is the case of Adams predictor-corrector schemes. The single-step methods are self-starting and they need a minimum amount of storage requirements. However, these methods require a larger number of function evaluations, for instance, four for the fourth-order Runge-Kutta method. Function evaluation is the name of the process by which, given t and y, the value of $\dot{y}$ is computed. The multi-step methods require a small amount of function evaluations, particularly if the time step is chosen so that the number of

predictor-corrector iterations per step is kept below two or three. Moreover, error estimates are easily provided and step size adjustments can be performed with no difficulties. The multi-step methods are not self-starting and require the help of a single-step scheme to start the integration process (Atkinson, 1989). Regardless of the numerical method used, the numerical task deals with the integration of an initial-value problem that can be written as (Shampine and Gordon, 1975)

$$\dot{y}_1 = f\left(y,t\right) \tag{3.44}$$

with the initial condition $y(t^0)=y^0$ and where y is the variable to be integrated and function $f(t,y)$ is defined by the computational sequence of the algorithm selected. Equation (3.44) has a solution $y(t)$. The initial value y^0 can be defined for any value of t^0, although it is often assumed that a transformation has been made so that $t^0=0$. This does not affect the solution or method used to approximate the solution.

The Euler integration method is one of the simplest integrators available. This approach may be sufficient in giving a very rough idea of the motion of multibody systems. This method solves differential equations in a single step as

$$y^{i+1} = y^i + hf\left(y^i,t\right) \tag{3.45}$$

where h is the integration step size $h=t^{i+1}-t^i$, for i a non-negative integer. This method implies that the next step of the state variable can be evaluated by using the current state variable. The intuitive basis of the Euler method is illustrated in Figure 3.12, in which the curve labeled $y=y(t)$ is the solution of the differential equation (3.44), which passes through point $P(t^0,y^0)$. It is desired to find the value of $y^1=y^0+\Delta y$ corresponding to $t=t^1$. In other words, the height $\overline{RQ}$ needs to be determined. Although the position of the curve at every point is not known, its slope is equal to $f(t,y)$, which is simply the geometric interpretation of the differential equation. Thus, the slope of the tangent at point P is $y^0=f(t^0,y^0)$, which can be computed since y^0 and t^0 are both known. If h is reasonable small, the tangent line $\overline{PS}$ should not deviate too much from the curve PQ, hence, the height $\overline{RS}$ (which by simple geometry is equal to $h\dot{y}^0$) should be an approximation to the required height $\overline{RQ}$. Therefore, a first approximation to Δy is given by the expression $\Delta y^1=RS=hf(t^0,y^0)$ (Shampine and Gordon, 1975; Atkinson, 1989).

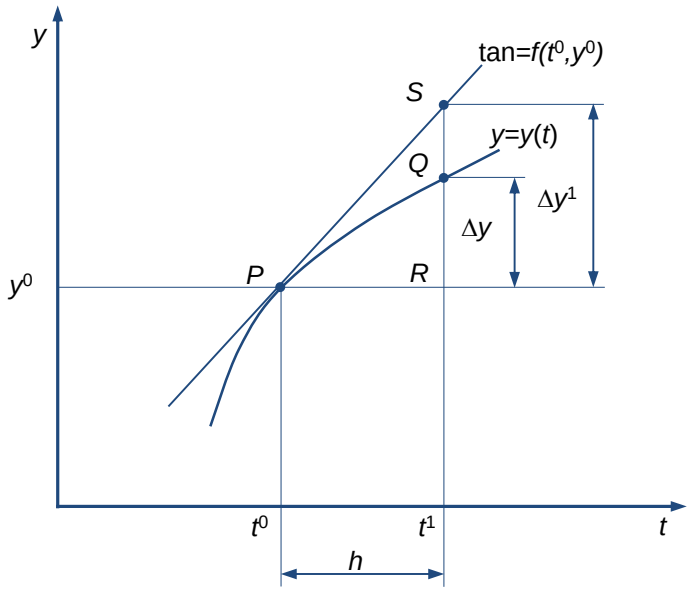

Figure 3.12 Geometric interpretation of the Euler integration method.

For larger time steps and for greater accuracy, the fourth-order Runge-Kutta integration method is most popular and widely used. This method is stable and, as a computer program, occupy relatively small amount of core storage. The fourth-order Runge-Kutta integration algorithm can be expressed by (Pina, 1995)

$$y^{i+1} = y^i + hg \tag{3.46}$$

where

$$g = \frac{1}{6}(f_1 + 2f_2 + 2f_3 + f_4) \tag{3.47}$$

$$f_1 = f(t^i, y^i) \tag{3.48}$$

$$f_2 = f(t^i + \frac{h}{2}, y^i + \frac{h}{2} f_1) \tag{3.49}$$

$$f_3 = f(t^i + \frac{h}{2}, y^i + \frac{h}{2} f_2) \tag{3.50}$$

$$f_4 = f(t^i + h, y^i + hf_3) \tag{3.51}$$

This method is explicit because all f_i depend only on previous values already calculated. This algorithm is easy to implement in the measure that it only requires function evaluations, and it is self-starting integrator scheme, which means that there is no need for any other algorithm or technique to start the integration process. Figure 3.13

illustrates the geometric interpretation of the fourth-order Runge-Kutta integration method. In this method four tangents are determined, being their average weighted according to Equations (3.47)-(3.51).

The standard fourth-order Runge-Kutta method does not provide an estimate of the local error, so that the user does not have way of knowing whether the time step being used is adequate. The local error of this method is of order h^5, which is relatively small even for larger time steps. The major drawback of this method is that the function $f(t,y)$ needs to be evaluated four times at each time step. This method is less efficient than the multi-steps such as the Adams predictor-correctors. On some problems, Runge-Kutta method requires almost twice as much computing time as other multi-steo methods (Conte and Boor, 1981).

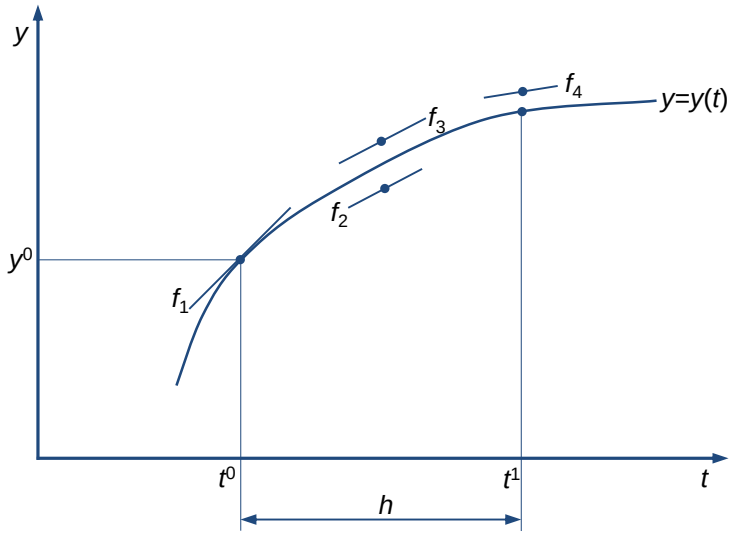

Figure 3.13 Geometric interpretation of the fourth-order Runge-Kutta method.

For the Euler and Runge-Kutta methods the next step value y^{i+1} is computed by using solely the current value y^i and time t^i, over a time range of $h=t^{i+1}-t^i$. Multi-step methods utilize information about the solution at more than one point. The aim of the multi-step methods is to automatically select the proper order and the proper time step size, which minimizes the amount of computer time required to achieve the specified accuracy for a given problem. The multi-step algorithms require only two function evaluation per step compared with four function evaluations with the fourth-order Runge-Kutta method, being, therefore, considerably faster. Predictor-corrector methods provide an automatic error estimate at each time step, thus allowing the algorithm to select an optimum value of h for a required accuracy. This type of approach exhibits

better performance with respect to the propagation of error that it can use time steps more than twice as large.

In Adams predictor-corrector methods an explicit method is used to predict a value of y^{i+1}, while an implicit method corrects that value. The implicit corrects appear to be more stable and accurate than the explicit predictors and are both chosen to be of equal order. The Adams-Bashforth predictor algorithm of fourth-order can be written as

$$y^{i+1} = y^i + \frac{h}{24}(55 f^i - 59 f^{i-1} + 37 f^{i-2} - 9 f^{i-3}) \tag{3.52}$$

where

$$f^i = f(t^i, y^i) \tag{3.53}$$

$$f^{i-j} = f(t^{i-j}, y^{i-j}), \quad (j = 1, 2, 3) \tag{3.54}$$

The corresponding Adams-Moulton corrector algorithm can be expressed by

$$y^{i+1} = y^i + \frac{h}{24}(9 f^{i+1} + 19 f^i - 5 f^{i-1} + f^{i-2}) \tag{3.55}$$

where

$$f^i = f(t^i, y^i) \tag{3.56}$$

$$f^{i-j} = f(t^{i-j}, y^{i-j}), \quad (j = 1, 2) \tag{3.57}$$

The major disadvantage of multi-step methods is that they are not self-starting. Thus, in the fourth-order Adams predictor-corrector method four successive values of function evaluation at equally spaced points before instant of time t^i must be known. These starting values must be obtained by some independent method, such as the Runge-Kutta method. On the other hand, Adams predictor-corrector algorithms are more complicated to program in the measure that they require special techniques for starting and for doubling and halving the time step, and they be subject to numerical instability (Conte and Boor, 1981; Pina, 1995; Flores and Ambrósio, 2010).

An alternative numerical schemes frequently adopted in multibody dynamics are based on the Newmark method (Newmark, 1959), also referred as the average acceleration method. This method constitutes a special category of the finite difference methods that has been widely used in solving the multi-DOF second-order differential equations that appear in structural dynamics (Alonso *et al.*, 2010; Tian *et al.*, 2011). The Newmark method is an implicit single-step integrator that is easy to implement and has good stability properties. Similarly to the multi-step methods, this implicit algorithm can be used in a predictor-corrector fashion, with fixed point iteration, although it is commonly introduced in the equations of motion of the system and solved through the Newton-Raphson iteration (Jálon and Bayo, 1994). It is important to mention that the implicit approaches are particularly suitable and convenient for real-time simulations (Cuadrado *et al.*, 2004). The interested reader in the details on the Newmark method is referred to the work by Newmak (1959) and Bathe (1982).

Finally, the choice of the integration time step is an important issue, since time steps too small lead to high computational time, and large time steps induce a reduced accuracy instabilities on the computation. Therefore, it is important to select a appropriate time step to obtain accurate results without unnecessarily increasing the computation time (Nikravesh, 2008a). In the present work, the integrators used are of the explicit type with both constant and variable time steps. The former are utilized for the simulations without contact events, while the later are considered when the simulations include contact or impact. The integrators with variable order and time step have all the ingredients for efficiency and accuracy (Flores and Ambrósio, 2010).

3.5 Demonstrative example of application

A human body model is here used as a numerical example to study the influence of the Baumgarte stabilization method on the control of the constraint violations. Figure 3.14 shows a schematic representation of this biomechanical model developed under the framework of multibody methodologies. The model is composed by seven rigid bodies, being six of them relative to the locomotor system, *i.e.*, the two lower-limbs, and one that represents the main upper body segments here denominated by HAT, acronym for

head, arms and trunk. In the present study only the skeletal structure is taken into account, being the effect of muscles, tendons and ligaments neglected.

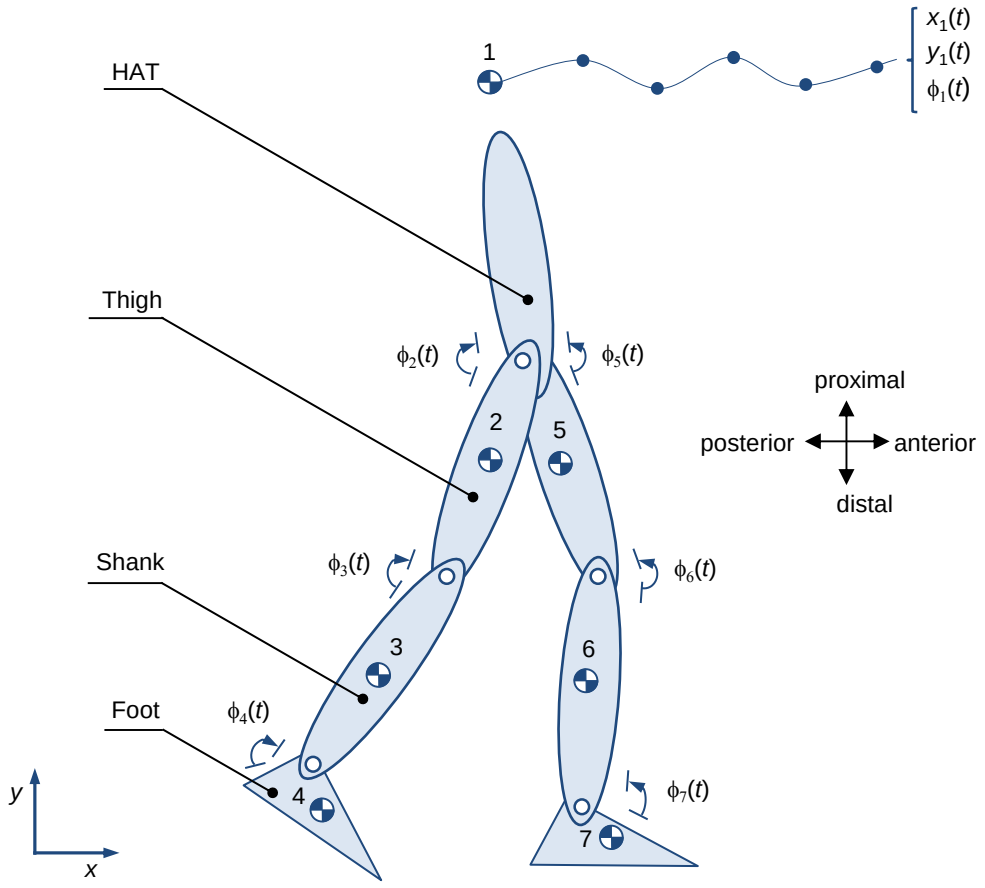

Figure 3.14 Biomechanical multibody model of a human body on the sagittal plane.

The anthropometric description of the seven anatomical segments considered and their corresponding body numbers are listed in Table 3.1 (Meireles *et al.*, 2009). In this biomechanical model, the anatomical segments are connected by six revolute joints, which results in twelve kinematic constraints in the system. These six revolute joints corresponds to the principal articular human joints, namely right hip, right knee, right ankle, left hip, left knee and left ankle. These six revolute joints reduce the DOF of the system to nine, which correspond to six rotations about revolute joints axis, plus two translations and one rotation of the main body (HAT). Therefore, nine guiding constraints are included to drive the system according to the DOF mention previously. Note that by guiding all degrees-of-freedom of the system the direct dynamic analysis has some equivalence to a kinematic analysis of the same system. Thus, the case studied here cannot be confused with the dynamic simulation by the same system solely driven by the internal and contact forces which leads to an unstable motion if not corrected.

Three guiding constraints are associated with the HAT body to guide the x, y and ϕ coordinates of its center of mass. Additionally, a guiding constraint is allocated to each relative DOF of the locomotor system in order to restrain the relative rotation of the adjacent bodies. The kinematic trajectories associated with the guiding constraints are obtained using cubic spline interpolation techniques. The motion data utilized to derive the mathematical expressions by interpolating the coordinates along time is based on the data published by Winter (2009). These data represent a time period of 0.957 seconds related to a human gait cycle of normal cadence. The first 0.4 seconds of simulation corresponds to the swing phase of gait cycle, and the remaining period of simulation corresponds to stance phase.

Table 3.1 Anthropometric data for each anatomical segment of the biomechanical human model.

Segment	Description	Length [m]	Proximal location of the center of mass [m]	Mass [kg]	Moment of inertia [kg.m^2]
1	HAT	0.2575	-0.0355	19.221	1.0392
2	Right Thigh	0.3141	0.1360	5.6700	0.0583
3	Right Shank	0.4081	0.1840	2.6365	0.0400
4	Right Foot	0.1221	0.0610	0.8221	0.0027
5	Left Thigh	0.3141	0.1360	5.6700	0.0583
6	Left Shank	0.4081	0.1840	2.6365	0.0400
7	Left Foot	0.1221	0.0610	0.8221	0.0027

Besides the kinematic constraints, external applied forces that act at the feet are also considered in this study as input data. These forces are included to simulate the reaction forces between the feet and the ground. The kinetic data presented in Winter (2009), namely the force magnitude and the coordinates of the point of application, is utilized in this study. In each instant of simulation, the components of the external applied forces, designated by F_x and F_y, are transferred to the center of mass of the foot. These transferred forces and moments are then added to the generalized force vector.

The rheonomic constraints, such as the guiding constraints, are not susceptible to be violated during a dynamic simulation, since they define explicitly the position of the bodies at each time step. In turn, the scleronomic constraints, such as the revolute joints, are usually subjected to constraint violations when moderate or long time simulations are performed. The first cause of constraints violations in multibody dynamics relies on the set of the initial conditions. In fact, the initial configuration given to the system can be inaccurate or not well-defined. These inconsistences lead to constraint violations

even during the first instant of the simulation, and tends to increase with the time. Hence, prior to run dynamic simulations is recommended to perform a previous kinematic analysis in order to correct the initial conditions of the system, namely the positions and velocities of the bodies (Silva and Ambrósio, 2002). In this study, a pre-kinematic analysis was performed with this purpose. Thus, the risk of having constraint violations due to the inaccuracy of the initial conditions is avoid or at least minimized.

The effect of the application of the Baumgarte stabilization method is demonstrated throughout this work using the developed biomechanical model. For this purpose, two forward dynamic simulations are performed using the fourth-order Runge-Kutta method as numerical integrator, being the time step equal to 0.00145 s. The first simulation corresponds to the direct integration method, which means that the stabilization method is not considered. In the second simulation, the Baumgarte stabilization method is used, being the Baumgarte parameters, α and β, both equal to 5. The results obtained for these two computational simulations are also compared with the data provided by Winter (2009). These results are plotted in Figure 3.15, where it is visible the effect of the Baumgarte stabilization method on the control of the violations of the position constraints of the four bodies, namely HAT, thigh, shank and foot.

From the analysis of Figure 3.15, it can be observed that when the direct integration method is used the violation of constraints grows significantly with time. This growth produces unacceptable results, even for a relatively short simulation, because of the inherent instability of the equations used and the rapid constraint violations that occur during the computation. This behavior can be related to the fact that the biomechanical model is an open kinematic chain being more susceptible to exhibit constraint violations than those constituted by closed loop systems (Nikravesh, 1988). In turn, when the Baumgarte method is utilized, the system response is clearly different, as it is illustrated in the plots of Figure 3.15. Furthermore, in this last case, the outcomes are close to the data published by Winter (2009).

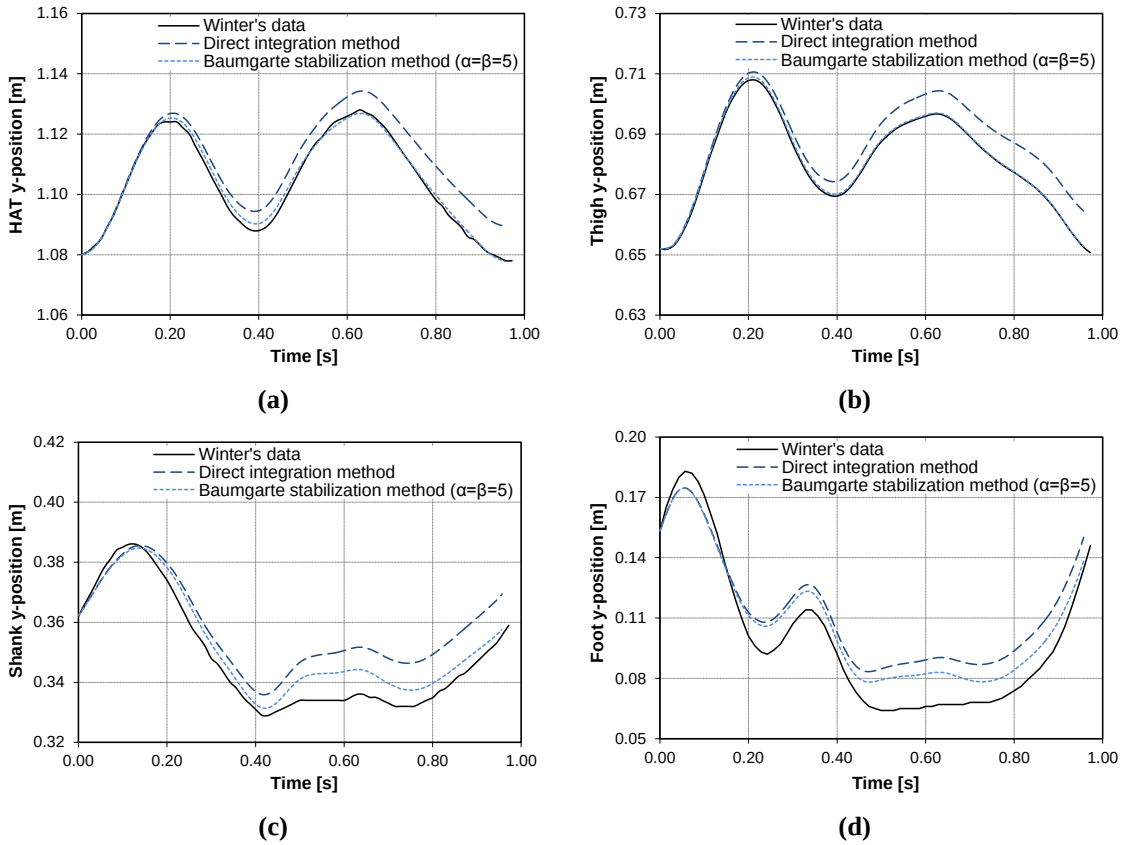

Figure 3.15 Influence of the Baumgarte parameters, α and β, on the y-position of the four bodies of the human body model: (a) HAT; (b) Thigh; (c) Shank; (d) Foot.

3.6 Summary and discussion

The fundamentals of the multibody formulation for the dynamics of biomechanical systems have been presented throughout this Chapter. Firstly, the concept of multibody system, made of interconnected bodies that undergo large displacements and rotations, was introduced, in which different examples, in biomechanics and other fields, were also presented.

The main types of coordinates that can be used in the formulation of the equations of motion of constrained multibody systems were analyzed, being their relative advantages and drawbacks also discussed. In this work, due to their simplicity and easiness for computational implementation, Cartesian coordinates were selected to describe the topology of rigid bodies in biomechanical multibody system. Furthermore, from the mathematical point of view, Cartesian coordinates are the supporting structure for all methodologies and dynamic analysis developed within the multibody systems concept. The kinematic constraint equations associated with revolute joints, as well as

those related to guiding constraints, were revised. In addition, their contributions to the Jacobian matrix of the constraints and to the right-hand side of velocity and acceleration constraint equations were presented. These kinematic constraints are the basic and fundamental ingredients to perform the kinematic analysis of biomechanical systems.

The Newton-Euler approach was employed to obtain the translational and rotational equations of motion of constrained multibody systems that was augmented with the constraint equations that results in the establishment of a mixed set of differential resulting to a set of differential and algebraic equations. The great merit of this formulation is that it is very straightforward in terms of assembling equations of motion and providing all reaction forces. In this process, the fundamental issues related to the numerical methods used to solve the equations of motion were briefly analyzed. In a simple way, the equations of motion for constrained multibody systems are expressed in the Hessenberg form. A set of initial conditions imposed on the positions and velocities is required to start the dynamic simulation. The selection of the appropriate initial conditions plays a crucial role in the prediction of the dynamic response of multibody systems. The subsequent initial conditions, for each time step in the simulation, are obtained from the final conditions of the previous time step. Then, from the initial values for positions and velocities, the equations of motion are solved for accelerations and Lagrange multipliers, using any available numerical algorithm for linear equations, for instance, the Gaussian elimination or the LU-factorization. The positions and velocities at the next time step are then obtained by integration of the velocity and acceleration vectors. This procedure is repeated until the final time of simulation is reached. The integration process can be performed using explicit methods, with constant step size or a predictor-corrector with both variable step and order.

In addition, several methods to avoid the constraint violations problem that occur during the numerical solution of the standard equations of motion were briefly described, namely the augmented Lagrangian formulation, the coordinate partitioning method and the Baumgarte stabilization method. Special attention was given to Baumgarte stabilization method, because this technique was adopted in this work to keep the constraint violations under control. Finally, a biomechanical human model was utilized as a demonstrative example of application to demonstrate the influence of the Baumgarte stabilization method on the dynamic response of the system.

References

Alonso, F.J., Cuadrado, J., Lugrís, U., Pintado, P. (2010) A compact smoothing-differentiation and projection approach for the kinematic data consistency of biomechanical systems. *Multibody System Dynamics*, 24(1), pp. 67-80.

Ambrósio, J.A., Nikravesh, P.E. (1992) Elasto-plastic deformations in multibody dynamics. *Nonlinear Dynamics*, 3(2), pp. 85-104.

Ambrósio, J., Neto, M.A., Leal, R.P. (2007) Optimization of a complex flexible multibody systems with composite materials. *Multibody System Dynamics*, 18(2), pp. 117-144.

Arabyan, A., Wu, F. (1998) An improved formulation for constrained mechanical systems. *Multibody Systems Dynamics*, 2(1), pp. 49-69.

Atkinson, K.A. (1989) *An introduction to numerical analysis*. John Wiley and Sons: New York (NY).

Barroso, M.P., Arezes, P.M., Costa, L.G., Sérgio Miguel, A. (2005) Anthropometric study of portuguese workers. *International Journal of Industrial Ergonomics*, 35(5), pp. 401-410.

Bathe, K.-J. (1982) *Finite element procedures in engineering analysis*. Prentice-Hall: Englewood-Cliffs (NJ).

Baumgarte, J. (1972) Stabilization of constraints and integrals of motion in dynamical systems. *Computer Methods in Applied Mechanics and Engineering*, 1(1), pp. 1-16.

Bayo, E., Jálon, J.G., Serna, A.A. (1988) Modified lagrangian formulation for the dynamic analysis of constrained mechanical systems. *Computer Methods in Applied Mechanics and Engineering*, 71(2), pp. 183-195.

Bei, Y., Fregly, B.J. (2004) Multibody dynamic simulation of knee contact mechanics. *Medical Engineering & Physics*, 26(9), pp. 777-789.

Blajer, W. (1995) An orthonormal tangent space method for constrained multibody systems. *Computer Methods in Applied Mechanics and Engineering*, 121(1-4), pp. 45-57.

Carvalho, M., Ambrósio, J. (2011) Development of generic road vehicle multibody models for crash analysis using an optimisation approach. *International Journal of Crashworthiness*, 16(5), pp. 537-556.

Castellucci, H.I., Arezes, P.M., Viviani, C.A. (2010) Mismatch between classroom furniture and anthropometric measures in Chilean schools. *Applied Ergonomics*, 41(4), pp. 563-568.

Chace, M.A. (1967) Analysis of the time-dependence of multi-freedom mechanical systems in relative coordinates. *Journal of Engineering for Industry*, 89, pp. 119-125.

Chapra, S.C., Canale, R.P. (1988) *Numerical methods for engineers*. McGraw-Hill: New York (NY).

Conte, S.D., Boor,C. (1981) *Elementary numerical analysis: An algorithmic approach*. McGraw-Hill: Singapore.

Cuadrado, J., Dopico, D., Gonzalez, M., Naya, M.A. (2004) A combined penalty and recursive real-time formulation for multibody dynamics. *Journal of Mechanical Design*, 126(4), pp. 602-608.

Cuadrado, J., Dopico, D., Naya, M.A., Gonzalez, M. (2004) Penalty, semi-recursive and hybrid methods for MBS real-time dynamics in the context of structural integrators. *Multibody System Dynamics*, 12(2), pp. 117-132.

Cuadrado, J., Pamies-Vila, R., Lugrís, U., Alonso, F.J. (2011) A force-based approach for joint efforts estimation during the double support phase of gait. *Procedia IUTAM*, 2(2), pp. 26-34.

Delp, S.L., Anderson, F.C., Arnold, A.S., Loan, P., Habib, A., John, C.T., Guendelman, E., Thelen, D.G. (2007) OpenSim: open-source software to create and analyze dynamic simulations of movement. *IEEE Transactions on Biomedical Engineering*, 54(11), pp. 1940-1950.

Delp, S.L., Loan, J.P., Hoy, M.G., Zajac, F.E., Topp, E.L., Rosen, J.M. (1990) An interactive graphics-based model of the lower extremity to study orthopaedic surgical procedures. *IEEE Transactions on Biomedical Engineering*, 37(8), pp. 757-767.

Dias, J.P., Pereira, M.S. (1995) Dynamics of flexible mechanical systems with contact-impact and plastic deformations. *Nonlinear Dynamics*, 8(4), pp. 491-512.

Dopico, D., Luaces, A., Gonzalez, M., Cuadrado, J. (2011) Dealing with multiple contacts in a human-in-the-loop application. *Multibody System Dynamics*, 25(2), pp. 167-183.

Eberhard, P., Schiehlen, W. (2006) Computational dynamics of multibody systems: History, formalisms, and applications. *Journal of Computational and Nonlinear Dynamics*, 1(1-3), pp. 3-12.

Ferreira, A. (2008) *Multibody model of the cervical spine and head for the simulation of traumatic and degenerative disorders.* MSc Thesis, Techincal University of Lisbon, Lisbon, Portugal.

Fintelman, D.M., den Braver, O., Schwab, A.L. (2011) A simple 2-dimensional model of speed skating which mimics observed forces and motions. In J. Ambrósio *et al.* (Eds.), *EUROMECH Colloquium 511 on Biomechanics of Human Motion* (20p.). Ponta Delgada, Azores, Portugal.

Fisette, P., Vaneghem, B. (1996) Numerical integration of multibody system dynamic equations using the coordinate method in an implicit Newmark scheme. *Computer Methods in Applied Mechanics and Engineering*, 135(1-2), pp. 85-105.

Flores, P. (2004) *Dynamic analysis of mechanical systems with imperfect kinematic joints.* PhD Thesis, University of Minho, Guimarães, Portugal.

Flores, P. (2009) Modeling and simulation of wear in revolute clearance joints in multibody systems. *Mechanism and Machine Theory,* 44(6), pp. 1211-1222.

Flores, P. (2010) *MUBODYNA - A FORTRAN program for dynamic analysis of planar multibody systems.* University of Minho, Guimarães, Portugal.

Flores, P., Ambrósio, J. (2010) On the contact detection for contact-impact analysis in multibody systems. *Multibody System Dynamics,* 24(1), pp. 103-122.

Flores, P., Ambrósio, J., Claro, J.C.P., Lankarani, H.M. (2008) *Kinematics and dynamics of multibody systems with imperfect joints: models and case studies - In Lecture Notes in Applied and Computational Mechanics* (34). Springer-Verlag: Berlin/Heidelberg, Germany.

Flores, P., Machado, M., Seabra, E., Silva, M.T. (2011) A parametric study on the Baumgarte stabilization method for forward dynamics of constrained multibody systems. *Journal of Computational and Nonlinear Dynamics,* 6(1), 011019, 9p.

Font-Llagunes, J.M., Pàmies-Vilà, R., Alonso, J., Lugrís, U. (2011) Simulation and design of an active orthosis for an incomplete spinal cord injured subject. *Procedia IUTAM,* 2(2), pp. 68-81.

García-Vallejo, D., Schiehlen, W. (2011) Parameter optimization of a neuro-musculo-skeletal model of human gait simulation. In J. Ambrósio *et al.* (Eds.), *EUROMECH Colloquium 511 on Biomechanics of Human Motion* (16p.). Ponta Delgada, Azores, Portugal.

Gear, C.W. (1971a) *Numerical initial value problems in ordinary differential equations.* Prentice-Hall: Englewood Cliffs (NJ).

Gear, C.W. (1971b) Simultaneous numerical solution of differential-algebraic equations. *IEEE Transactions on Circuit Theory,* 18(1), pp. 89-95.

Gerstmayr, J., Matikainen, M.K., Mikkola, A.M. (2008) A geometrically exact beam element based on the absolute nodal coordinate formulation. *Multibody System Dynamics,* 20(4), pp. 287-306.

Gonçalves, S.B., Silva, M.T., Martins, J.M., Neves, M.C. (2011) Advanced computer methods for pathological and non-pathological human movement analysis. In J. Ambrósio *et al.* (Eds.), *EUROMECH Colloquium 511 on Biomechanics of Human Motion* (22 p.). Ponta Delgada, Azores, Portugal.

Greenwood, D.T. (1965) *Principles of dynamics.* Prentice Hall: Englewood Cliffs (NJ).

Guess, T.M., Thiagarajan, G., Kia, M., Mishra, M. (2010) A subject specific multibody model of the knee with menisci. *Medical Engineering & Physics*, 32(5), pp. 505-515.

Haug, E.J. (1989) *Computer aided kinematics and dynamics of mechanical systems. Vol. 1: Basic Methods.* Allyn & Bacon: Needham Heights (MA).

Hoyos, D., Martínez, L. (1999) The effect of shock absorbing sports surfaces in jumping. *Sports Engineering*, 2(2), pp. 103-108.

Huston, R.L. (1990) *Multibody dynamics.* Butterworth-Heinemann: Boston (MA).

Jálon, J.G. (2007) Twenty-five years of natural coordinates. *Multibody System Dynamics*, 18(1), pp. 15-33.

Jálon, J.G., Bayo, E. (1994) *Kinematic and dynamic simulations of multibody systems: the real-time challenge.* Springer-Verlag: New York (NY).

Jiménez, J.M., Avello, A., García-Alonso, A., Jálon, J.G. (1990) COMPAMM - A simple and efficient code for kinematic and dynamic numerical simulation of 3-D multibody system with realistic graphics. In W. Schiehlen (Ed.), *Multibody systems handbook* (pp. 285-304). Springer-Verlag: Berlin, Germany.

Kecskeméthy, A., Masic, I., Tändl, M. (2009) Workspace fitting and control for a serial-robot motion simulator. In M. Ceccarelli (Ed.), *Proceedings of EUCOMES 08* (pp. 183-190). Springer: Heidelberg, Germany.

Kurz, T., Eberhard, P., Henninger, C., Schiehlen, W. (2010) From Neweul to Neweul-M^2: symbolical equations of motion for multibody system analysis and synthesis. *Multibody System Dynamics*, 24(1), pp. 25-41.

Li, L., Patil, S., Steklov, N., Bae, W., Temple-Wong, M., D'Lima, D.D., Sah, R.L., Fregly, B.J. (2011) Computational wear simulation of patellofemoral articular cartilage during in vitro testing. *Journal of Biomechanics*, 44(8), pp. 1507-1513.

Ma, D., Lankarani, H.M. (1997) A multibody/finite element analysis approach for modeling of crash dynamic responses. *Journal of Mechanical Design*, 119(3), pp. 382-387.

Machado, M., Flores, P., Ambrósio, J., Completo, A. (2011) Influence of the contact model on the dynamic response of the human knee joint. *Proceedings of the Institution of Mechanical Engineers, Part K: Journal of Multi-body Dynamics*, 225(4), pp. 344-358.

Machado, M., Flores, P., Claro, J.C.P., Ambrósio, J., Silva, M., Completo, A., Lankarani, H.M. (2010) Development of a planar multibody model of the human knee joint. *Nonlinear Dynamics*, 60(3), pp. 459-478.

Magnus, K. (1978) *Dynamics of multibody systems*. Springer-Verlag: Berlin, Germany.

Meireles, F., Machado, M., Silva, M.T., Flores, P. (2009) Dynamic modeling and analysis of human locomotion using multibody system methodologies. *International Journal of Computational Vision and Biomechanics,* 2(2), pp. 199-207.

Moreira, P., Silva, M., Flores, P. (2010) A biomechanical multibody foot model for forward dynamic analysis. *Proceedings of the 1st Joint International Conference on Multibody System Dynamics* (10p.). Lappeenranta, Finland.

Müller, A. (2009) Generic mobility of rigid body mechanisms. *Mechanism and Machine Theory,* 44(6), pp. 1240-1255.

Neto, M.A., Ambrósio, J. (2003) Stabilization methods for the integration of DAE in the presence of redundant constraints. *Multibody System Dynamics,* 10(1), pp. 81-105.

Newmark, N.M. (1959) A method of computation for structural dynamics. *Journal of the Engineering Mechanics Division,* 85(3), pp. 67-94.

Nikravesh, P.E. (1984) Some methods for dynamic analysis of constrained mechanical systems: A survey. In E. J. Haug (Ed.), *Computer-aided analysis and optimization of mechanical system dynamics* (pp. 351-368). Springer-Verlag: Berlin, Germany.

Nikravesh, P.E. (1988) *Computer-aided analysis of mechanical systems.* Prentice Hall: Englewood Cliffs (NJ).

Nikravesh, P.E. (2007) Initial condition correction in multibody dynamics. *Multibody System Dynamics,* 18(1), pp. 107-115.

Nikravesh, P.E. (2008a) *Planar multibody dynamics: formulation, programming, and applications.* CRC Press: London, United Kingdom.

Nikravesh, P.E. (2008b) Newtonian-based methodologies in multi-body dynamics. *Proceedings of the Institution of Mechanical Engineers, Part K: Journal of Multi-body Dynamics,* 222(4), pp. 277-288.

Orlandea, N., Chace, M.A., Calahan, D.A. (1977) A sparsity oriented approach to the dynamic analysis and design of mechanical systems - Part 1 and 2. *Journal of Engineering for Industry,* 99, pp. 773-784.

Pandy, M.G. (2001) Computer modeling and simulation of human movement. *Annual Review of Biomedical Engineering,* 3, pp. 245-273.

Paul, B., Krajcinovic, D. (1970a) Computer analysis of machines with planar motion: Part 1 - Kinematics. *Journal of Applied Mechanics,* 37(3), pp. 697-702.

Paul, B., Krajcinovic, D. (1970b) Computer analysis of machines with planar motion: Part 2 – Dynamics. *Journal of Applied Mechanics,* 37(3), pp. 703-712.

Pina, H. (1995) *Métodos numéricos.* McGraw-Hill: Lisbon, Portugal.

Pombo, J. (2004) *A multibody methodology for railway dynamics applications.* PhD Thesis, Technical University of Lisbon, Lisbon, Portugal.

Pombo, J., Ambrósio, J. (2008) Application of a wheel-rail contact model to railway dynamics in small radius curved tracks. *Multibody System Dynamics,* 19(1-2), pp. 91-114.

Rasmussen, J., Damsgaard, M., Christensen, S., Surma, E. (2002) Design optimization with respect to ergonomic properties. *Structural and Multidisciplinan Optimization,* 24(2), pp. 89-97.

Rasmussen, J., Damsgaard, M., Surma, E., Christensen, S.T., de Zee, M., Vondrak, V. (2003) AnyBody - a software system for ergonomic optimization. *Fifth World Congress on Structural and Multidisciplinary Optimization*, Venice, Italy.

Roberson, R.E., Schwertassek, R. (1988) *Dynamics of multibody systems.* Springer: Berlin, Germany.

Rulka, W. (1990) SIMPACK - A computer program for simulation of large motion multibody systems. In W. Schiehlen (Ed.), *Multibody systems handbook* (pp. 265-284). Springer-Verlag: Berlin, Germany.

Schiehlen, W. (1990a) Computational aspects in multibody system dynamics. *Computer Methods in Applied Mechanics and Engineering*, 90(1-3), pp. 569-582.

Schiehlen, W. (1990b) *Multibody systems handbook.* Springer-Verlag: Berlin, Germany.

Schiehlen, W. (2006) Computational dynamics: theory and applications of multibody systems. *European Journal of Mechanics A/Solids*, 25(4), pp. 566-594.

Schiehlen, W., Kreuzer, E. (1978) Symbolic computational derivation of equations of motion. In K. Magnus (Ed.), *Dynamics of Multibody Systems* (pp. 290-305). Springer: Berlin, Germany.

Seth, A., Sherman, M., Reinbolt, J.A., Delp, S.L. (2011) OpenSim: a musculoskeletal modeling and simulation framework for in silico investigations and exchange. *Procedia IUTAM,* 2(2), pp. 212–232.

Shabana, A.A. (1989) *Dynamics of multibody systems.* John Wiley & Sons: New York, (NY).

Shabana, A.A. (1997a) Definition of the slopes and absolute nodal coordinate formulation. *Multibody System Dynamics,* 1(3), pp. 339-348.

Shabana, A.A. (1997b) Flexible multibody dynamics: Review of past and recent developments. *Multibody System Dynamics,* 1(2), pp. 189-222.

Shampine, L., Gordon, M. (1975) *Computer solution of ordinary differential equations: The initial value problem.* Freeman: San Francisco (CA).

Sharp, R.S., Evangelou, S., Limebeer, D.J.N. (2004) Advances in the modelling of motorcycle dynamics. *Multibody System Dynamics*, 12(3), pp. 251-283.

Shigley, J.E., Uicker, J.J. (1995) *Theory of machines and mechanisms.* McGraw Hill: New York (NY).

Silva, M.T. (2003) *Human motion analysis using multibody dynamics and optimization tools.* PhD Thesis, Technical University of Lisbon, Lisbon, Portugal.

Silva, M.T., Ambrósio, J. (2002) Kinematic data consistency in the inverse dynamic analysis of biomechanical systems. *Multibody System Dynamics,* 8(2), pp. 219-239.

Silva, P.C., Silva, M.T., Martins, J.M. (2010) Evaluation of the contact forces developed in the lower limb/orthosis interface for comfort design. *Multibody System Dynamics,* 24(3), pp. 367-388.

Späth, H. (1995) *One dimensional spline interpolation algorithms.* AK Peters: Wellesley (MA).

Sugiyama, H., Suda, Y. (2009) Wheel/rail two-point contact geometry with back-of-flange contact. *Journal of Computational and Nonlinear Dynamics,* 4(1), 011010, 6p.

Tian, Q., Liu, C., Machado, M., Flores, P. (2011) A new model for dry and lubricated cylindrical joints with clearance in spatial flexible multibody systems. *Nonlinear Dynamics,* 64(1-2), pp. 25-47.

Tseng, F.-C., Ma Z-D, Z.-D., Hulbert, G.M. (2003) Efficient numerical solution of constrained multibody dynamics systems. *Computer Methods in Applied Mechanics and Engineering,* 192(3-4), pp. 439-472.

Wasfy, T.M., Noor, A.K. (2003) Computational strategies for flexible multibody systems. *Applied Mechanics Reviews,* 56(6), pp. 553-613.

Wehage, R.A., Haug, E.J. (1982) Generalized coordinate partitioning for dimension reduction in analysis of constrained systems. *Journal of Mechanical Design*, 104, pp. 247-255.

Weijia, Z., Zhenkuan, P., Yibing, W. (2000) An automatic constraint violation stabilization method for differential/algebraic equations of motion in multibody system dynamics. *Applied Mathematics and Mechanics,* 21(1), pp. 103-108.

Winter, D.A. (2009) *Biomechanics and motor control of human movement*. John Wiley & Sons: Hoboken (NJ).

Wittenburg, J. (1977) *Dynamics of systems of rigid bodies.* B.G. Teubner: Stuttgart, Germany.

Yoon, S., Howe, R.M., Greenwood, D.T. (1994) Geometric elimination of constraint violations in numerical simulation of lagrangian equations. *Journal of Mechanical Design,* 116(4), pp. 1058-1064.

Zhu, W.-H., Piedboeuf, J.-C., Gonthier, Y. (2006) A dynamics formulation of general constrained robots. *Multibody System Dynamics,* 16(1), pp. 37-54.

4

Contact modeling and analysis

4.1 *Methods to deal with contact problems* **4**-2
4.2 *Geometric detection of contact* **4**-5
4.3 *Elastic contact force models* **4**-13
4.4 *Dissipative contact force models* **4**-19
4.5 *Demonstrative example of application* **4**-28
4.6 *Summary and discussion* **4**-31
References **4**-32

The problem of contact is of paramount importance in the field of multibody dynamics because contact events can take place frequently and in many cases the function of multibody systems is based on them (Pfeiffer and Glocker, 1996; Tian *et al.*, 2009; Ambrósio and Veríssimo, 2009; Machado *et al.*, 2010; Choi *et al.*, 2010). The impact is a physical phenomenon characterized by its short duration, high force level, rapid energy dissipation and large changes in velocities of the bodies, which affects the motion characteristics and the dynamic response of the overall systems (Gilardi and Sharf, 2002). Contact has a longer duration and the intervenient bodies may change their relative configuration while it lasts. The contact modeling and analysis has received great attention over the past few decades and still remains an active field of investigation (Gonthier *et al.*, 2004; Sharf and Zhang, 2006). Indeed, proper representation of the contact phenomenon for multibody dynamics is still a big challenge, since it depends on many factors, such as the geometry of the contacting surfaces, the material properties of the contacting bodies and the constitutive law considered to represent the interaction among the different bodies that comprises the multibody systems (Flores and Ambrósio, 2010; Machado and Flores, 2011).

In this Chapter, the methodologies utilized in multibody dynamics to deal with contact problems are introduced. In addition, an overview of the existing techniques for geometric detection of contact events is also presented. The most common elastic and dissipative laws used to evaluate normal contact forces are revised. Finally, a slider crank mechanism experiencing two frictionless impacts with an external free sliding block is considered as demonstrative example of application.

4.1 Methods to deal with contact problems

Impact occurs in the collision of two or more bodies, which can be unconstrained or may belong to a multibody system (Flores *et al.*, 2006). An impact typically involves high force levels, rapid dissipation of energy, large accelerations, and very short duration (Gilardi and Sharf, 2002). These characteristics may have a great influence on the dynamic response of a system and, they must be considered on the design and analysis of mechanical and biological systems. The word contact is often utilized interchangeably with impact. The contact corresponds to the physical situation where two or more bodies come in touch with each other at some locations. Inherently, contact implies a continuous process which takes place over a finite time (Gilardi and Sharf, 2002). Some effects related to the impact phenomena are those of vibration propagation through the system, local elastic and plastic deformations at the contact zone and frictional energy dissipation (Haug *et al.*, 1986; Flickinger and Bowling, 2010).

In a broad sense, a contact mechanics problem can be analyzed by using either the finite element method or the multibody systems approach. On the one hand, there is no doubt that the finite element analysis is the most powerful and accurate method to solve contact problems (Ebrahimi and Eberhard, 2006; Liu *et al.*, 2007). On the other hand, the multibody systems formulation is the most efficient approach for the dynamic analysis of the gross motion of mechanical systems (Ebrahimi and Kövecses, 2010).

Regardless of the method utilized to describe contact problems of the colliding bodies, it is necessary to model and analyze the contact process. This involves two main steps, namely: (*i*) the contact detection and (*ii*) the evaluation of the contact forces, which are the result of collisions between bodies. The contact detection is an important issue in contact modeling of moving bodies, which deals with the determination of when, where and which points are in contact. The efficiency and accuracy of this step

depend on the complexity of the contacting surfaces, the number of potential colliding bodies (Tasora *et al.*, 2008) and the kinematics of the bodies (Hirschkorn *et al.*, 2006).

In the context of multibody dynamics, the evaluation of the contact forces can be performed by considering different approaches introduced over the last decades (Lankarani and Nikravesh, 1990; Glocker and Studer, 2005). Two distinct formulations can be applied for impact and contact situations, namely the discrete and continuous methods. The discrete approach considers an impact as an impulsive phenomenon of infinitesimal duration. Within this method, the system configuration is halted during impact, and an appropriate model is employed for relating the states of the system immediately before and immediately after the event (Bottasso and Trainelli, 2001). This approach is recommended for the description of prompt events of very short duration, that is, impact analysis. Furthermore, its extension to flexible systems as well as extension to more general cases involving multiple contacts and intermittent contact is quite complex (Gilardi and Sharf, 2002).

In turn, the continuous method relies upon the fact that the interaction forces act in a continuous manner during the contact event. In this approach, the local deformations and normal contact forces are treated as continuous events. The implementation of a continuous approach is simple and straightforward in contrast with the discrete method that requires the interruption of the numerical resolution of the equations of motion when an impact is detected (Bottasso and Trainelli, 2001). From the modeling methodology point of view, there are several different continuous methods able to model the contact response in multibody systems. As a rough classification, they can be divided into contact force based models and methods based on geometric constraints, each of them showing advantages and disadvantages for each particular application. In other words, there are two main formulations to model multibody systems with contact-impact events, namely the regularized models and non-smooth approaches (Pfeiffer and Glocker, 1996).

The regularized approaches, commonly referred as penalty or compliant methods, have been gaining significant importance in the context of multibody systems with contacts due to their computational simplicity and efficiency (Flores *et al.*, 2011). In these methods, there are no impulses at the instant of contact, therefore, there is no need for impulsive dynamics calculations and the contact loss can easily be determined from position and velocity data (Flores *et al.*, 2008). One of the main drawbacks associated

with the penalty methods is the difficulty to select contact parameters such as the equivalent stiffness or the degree of nonlinearity of the indentation, especially for complex contact scenarios and nonmetallic materials. Another limitation of this approach is the possible introduction of highly-frequency dynamics into the system, due to the presence of stiff springs in compliant surfaces. The compliant force models can be understood as if each contact region of the contacting bodies is covered with spring-damper elements scattered over their surfaces. The normal force, including elastic and damping, prevents indentation. The contact response produced by these force reaction terms is computed based on the indentation, material properties and surface geometries of the colliding bodies.

An alternative way to treat the contact-impact problems within multibody systems is to utilize the non-smooth dynamics approach, namely the Linear Complementarity Problem (LCP) (Pfeiffer and Glocker, 1996). Assuming that the contacting bodies are truly rigid, as opposed to locally deformable bodies as in the penalty approach, the complementarity formulation solves the contact dynamics problem by using unilateral constraints to compute contact impulses or forces to prevent indentation from occurring. The basic idea of complementarity in multibody systems can be stated as for a unilateral contact either relative kinematics is zero and the corresponding constraint forces are zero, or vice versa. Therefore, the product of these two groups of quantities is always zero. This leads to a complementarity problem and constitutes a rule which allows for the treatment of multibody systems with unilateral constraints (Glocker and Pfeiffer, 1993; Pang and Trinkle, 1996; Pfeiffer, 2003).

In summary, the different methods to deal with contact problems in multibody systems have inherently advantages and disadvantages for each particular application. None of the formulations briefly described above can *a-priori* be said to be superior compared to other for all applications. It is a fact that a specific multibody problem might be easier to describe by one formulation, but this does not yield a general predominance of this formulation in all situations. The interested reader in the details on the LCP approaches is referred to the works by Glocker and Pfeiffer (1993) and Pfeiffer and Glocker (1996).

4.2 Geometric detection of contact

From a mechanical point of view, contact detection is a two-step procedure that includes the identification of the coordinates of the potential contact points and the evaluation of the indentation of the two bodies. In a broad sense, the contact detection process is often referred to as collision detection and the associated computational algorithms rely on several factors, which can be grouped in six classes (Ericson, 2005):

(*i*) Geometric representation: The geometric representations used to describe the contact scenario and its objects have a direct influence on the algorithms applied.

(*ii*) Proximity queries: In the context of collision detection, a proximity query corresponds to any computation that produces information about the relative configuration or placement of objects. Thus, the computational effort is as greater as the query types and results are more detailed.

(*iii*) Environment simulation parameters: The simulation itself includes several parameters that affect the collision detection process. These include the number of contacting bodies, the position of the contacting bodies, if they are moving or not, and whether they are rigid or flexible.

(*iv*) Performance: In real-time simulations, a trade-off between time and space has to be establishing, being some features balanced to meet performance demands.

(*v*) Robustness: Not all applications require the same level of physical simulation. For example, a multibody model of the human knee joint requires much more sophistication from a collision detection algorithm than a bouncing ball system, since the geometry of the human knee joint is much more complex than a sphere.

(*vi*) Ease of implementation and use: Decisions regarding straightforward and simple implementation are crucial in the process of selection the approach to be taken, especially when there are deadlines to accomplish or some lack of resources.

All these issues affect the modeling process of a system with contact. However, the first three are the ones that influence most the dynamics of the system. Hence, these three factors will be described in the following Subsections (Lin and Gottschalk, 1998).

4.2.1 Geometric representation

There are several types of geometric representations that have been used for contact detection purposes. These representations can be distinguished by polygonal models and non-polygonal models, as Figure 4.1 illustrates.

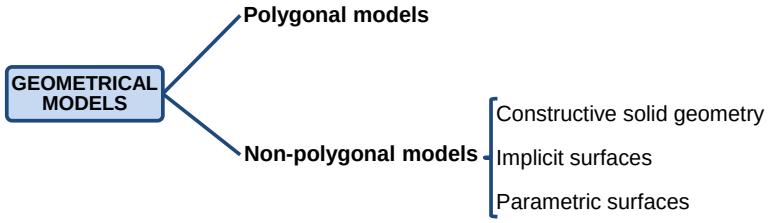

Figure 4.1 Taxonomy of geometric models (Lin and Gottschalk, 1998).

The polygonal models are frequently applied to model complex shapes due to their versatility and simpler representation. Polygonal representations may be unstructured (such as a polygonal soup), arranged as meshes, or form convex polytopes. The "polygonal soup" is the class of polygonal models more often utilized, because it is the output format used by default when geometry is exported from a 3-D modeling package (such as Autodesk® Maya®, Blender, etc.). Hippmann was one of the first authors proposing a contact detection algorithm based on polygonal models (Hippmann, 2004). This approach, named polygonal contact model (PCM), uses body surfaces described as polygon meshes and is a robust and well-known method for contact detection of complexly shaped bodies. The PCM has been utilized in many research studies on contact dynamics (Ebrahimi *et al.* 2005, Ebrahimi and Eberhard 2006). Dopico and co-authors (2011) proposed other contact detection method to be applied to machinery and vehicles simulators. This approach relies on to approximate the environments and the multibody models by using primitive objects: the complex CAD environments by triangular meshes and the multibody systems by spheres or boxes. Choi *et al.* (2010) used also triangular representations to compute the contact between freeform surfaces. This approach comprises two parts: a pre-search algorithm and a detailed search method.

The non-polygonal models fall into three main groups: constructive solid geometry (CSG), implicit methods and parametric functions, as Figure 4.1 depicts. Constructive solid geometry is a solid modeling technique that allows generating a complex geometry by using Boolean operators, such as union, intersection, and difference, to combine objects. These objects are called primitives and represent, generally, solids with simple shapes, such as spheres, cones, cylinders, cuboids, etc. Using a CSG representation it is easy to define arbitrary points as being either inside or outside the shape created by CSG, which is a very convenient property in collision detection procedures (Lin, 1993; Lin and Gottschalk, 1998). Examples of collision detection methods based on CSG representations are given in the works of Faverjon (1989), Cameron (1991), Keyser *et al.* (1999) and Su *et al.* (1999).

Implicit function defines the location of the points belonging to surface. With this type of representation, the boundaries of an object are well-defined as closed manifolds, and the evaluation whether a point belongs to the surface, or not, is an easy and trivial task, as in a CSG representation (Sigg, 2006). Implicit functions are often utilized as primitives in CSG systems. If the function is polynomial in x, y and z, then it is called algebraic (Lin and Gottschalk, 1998). A special case of algebraic surfaces are the quadrics, which can represent univocally cones, spheres, and cylinders. Lopes *et al.* (2011) proposed a mathematical framework for contact detection between quadric and superquadric surfaces based on their implicit formulations.

Parametric representations are a set of equations that map one or two parameters into Euclidean space. One parameter is utilized to define a curve. To describe a parametric surface two parameters are demanded, which are usually represented by the symbols u and v. With this approach, it is quite easy to generate a set of points belonging to a surface, because the Cartesian coordinates are explicit and independent functions of the parametric coordinates (Farin, 1995). It is worth noting that parametric representations are generally non-unique, so the same quantities may be expressed by a number of different parameterizations. Unlike implicit surfaces, parametric surfaces are not generally closed manifolds and hence, they do not represent a complete solid model, but rather a description of surface boundary. Parametric surfaces are easier to polygonalize and render as compared to the implicits (Lin and Gottschalk, 1998). With the parametric method, it is possible to define different types of surfaces that can range from very simple geometries, such as the spherical examples, to surfaces with high

degree of complexity using, for instance, NURBS, acronym for Non-Uniform Rational Basis Splines (Farin, 1995). NURBS are very popular in CAD/CAM field due to their suitable geometric properties that make them easier to operate on. It is worth noting that rational parametric surfaces (like NURBS and Bezier patches) are a proper subset of algebraic surfaces (Lin and Gottschalk, 1998). An example of application of using parametric surfaces for contact detection purposes is the work by Bei and Fregly (2004). In this study, Bei and Fregly (2004) utilize NURBS surfaces to describe the contact surfaces of the knee joint. Machado *et al.* (2010) use also parametric representations to define the boundaries of the contacting bodies on their general multibody code. Tasora and Righettini (2003) proposed a multibody method for simulation of sliding contact between freeform surfaces represented by parametric functions. This approach relies on geometric constraints that are defined by a tangential plane which moves between the contacting bodies, hence only a simple point-on-plane constraint had to be added to the equations of motion.

4.2.2 Proximity queries

Regarding the proximity queries, many applications on computer graphics or computer simulated environments need to determine spatial or proximity relationships between two geometric objects (Larsen *et al.*, 2000). The collision detection query is an example of a proximity query that determines the intersection between given objects. Table 4.1 listed the five most familiar and easily defined proximity measures, namely collision detection, minimum distance (also called separation distance), maximum distance (also referred as spanning distance), Hausdorff distance, and penetration depth. Furthermore, there are queries applicable to dynamic scenarios, such as finding when the next contact between two moving bodies will occur. This query is known as the estimated time of arrival or time of impact computation and is used to for instance, control the time step in a multibody simulation (Lin and Gottschalk, 1998; Gottschalk, 2000; Ericson, 2005).

The subject of contact detection is quite challenging and an actual problem in various areas such as, discrete element methods, robotic systems, multibody simulations, or video games engines and computer graphics. The diversity of application fields demands different approaches and specifications to deal with the contact detection problem. For instance, in computer graphics finding any one point in

common between the objects might be sufficient, since its main concern is usually to ensure a fast and reliable visualization. In contrast, in multibody simulations more detailed information is required in order to compute the reactions forces or impulses that result from the contact (van den Bergen, 2004). Throughout this work, two of the five queries listed in Table 4.1 are employed, namely the separation distance and the penetration depth. The separation distance query is used instead of the collision distance query since it is necessary to not only check whenever contact occurs, but also to identify the set of contacting points (*i.e.*, the contact manifold or the contact locus). In turn, the penetration depht query is applied in contact conditions to evaluate the contact indentation (van den Bergen, 2004; Lopes *et al.*, 2011).

Table 4.1 Five proximity queries (Gottschalk, 2000).

Query	Definition	Condition
Collision detection	Checks whether two objects overlap in space or their boundaries share at least one common point	$\mathrm{col}(P,Q) = P \cap Q$
Separation distance	Length of the shortest line segment joining two sets of points	$d_{sep}(P,Q) = \min_{p\in P} \min_{q\in Q} \lvert p-q \rvert$
Spanning distance	Maximum deviation of one set from the other	$d_{span}(P,Q) = \max_{p\in P} \max_{q\in Q} \lvert p-q \rvert$
Hausdorff distance	Maximum distance between the points of two sets	$d_{haus}(P,Q) = \max_{p\in P} \min_{q\in Q} \lvert p-q \rvert$
Penetration depth	Minimum distance needed to translate one set to make it disjoint from the other	$d_{pen}(P,Q) = \min \lVert \mathbf{v} \rVert$, *such that* $\min_{p\in P} \min_{q\in Q} \lvert \mathbf{p}-\mathbf{q}+\mathbf{v} \rvert > 0$

4.2.3 Environmental simulation parameters

As mentioned, the environmental simulation parameters have also effect on the contact detection process. An example of these parameters is the number of objects of the system. A larger number of contacting bodies may slow down significantly the performance of a contact detection algorithm, since the proximity queries have to be checked in every simulation step for each body. To overcome this problem, some computational approaches are utilized in order to reduce the number of pairs tested and, thus, to speed up the computational simulation. According to Hubbard (1993), these computational methods can be classified into two phases: the broad-phase and the narrow-phase. The broad-phase and narrow-phase methods are also referred as *n*-body processing and pair processing, respectively (Ericson, 2005; Kockara *et al.*, 2007). The broad-phase methods identifies smaller groups of objects that may be colliding and

quickly excludes those that definitely are not, either because they are far away from each other, or because other features inherent to the system or the application, *e.g.*, game rules. In contact mechanics, the broad-phase algorithms are generally utilized to check if the bodies are closely enough to be considered contact candidates (Tasora and Righettini, 2003). In these cases narrow-phase methods are employed, which test with more accuracy the subgroup of possible contacting pairs pointed out by the broad-phase algorithms. Narrow-phase approaches usually report more detailed information that is afterwards used to compute indentation and contact forces.

Spatial data structures are usually applied to formulate broad-phase and narrow-phase algorithms (Ericson, 2005; Kockara *et al.*, 2007). These structures fall into two classes: space partitioning and model partitioning. A space partitioning is a subdivision of space into convex regions called cells. Using such a structure several pairs of bodies can be quickly excluded from intersection testing, as it is only necessary to test the pairs of bodies that share a cell. The most commonly used space partitioning structures are the voxel grids, the octrees and *k*-d trees, and the binary space partitioning (BSP) trees. Figure 4.2 illustrates how to generate a BSP tree (van den Bergen, 2004).

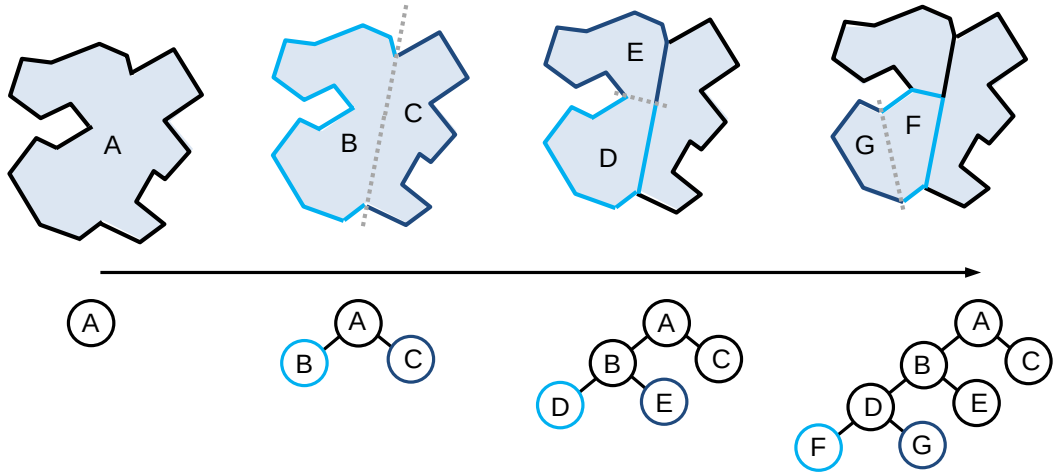

Figure 4.2 Four steps to generate a BSP tree (van den Bergen, 2004).

A model partitioning is often a better choice than space partitioning, because the model partitioning structures do not suffer from the problem of having multiple references to the same object. The basic strategy is to subdivide a set of objects into geometric coherent subsets and compute a bounding volume for each subset of objects. A bounding volume of a model is a primitive shape that encloses the model and should have the following properties: (*i*) a bounding volume should fit the model as tightly as possible in order to reduce the probability of a given object intersect the bounding

volume but not the model; (*ii*) overlap tests between bounding volumes should be computationally cheap; (*iii*) a bounding volume should be described using a relatively small amount of storage, which is preferably smaller than the storage used by the model; (*iv*) the cost of computing a bounding volume for a given model should be low (van den Bergen, 2004). The most used bounding volumes are: the bounding spheres, the axis-aligned bounding boxes (AABBs), the oriented bounding boxes (OBBs) and the discrete-orientation polytopes (*k*-DOPs). These volumes are illustrated in Figure 4.3. Nonetheless, there are some authors that utilized quadric and superquadric representations as bounding volumes. These geometric descriptions demand a greater computation effort than the bounding spheres, but are more accurate as they fit the model tighter than spheres (Lopes *et al.*, 2011; Portal *et al.*, 2009; Jia *et al.*, 2011). Examples of libraries and software packages developed for computing proximity queries are listed in Table 4.2. Some of these are based on bounding hierarchies, such as DEFORMCD, H-COLLIDE, IMMPACT, OPCODE, PQP, RAPID and SOLID.

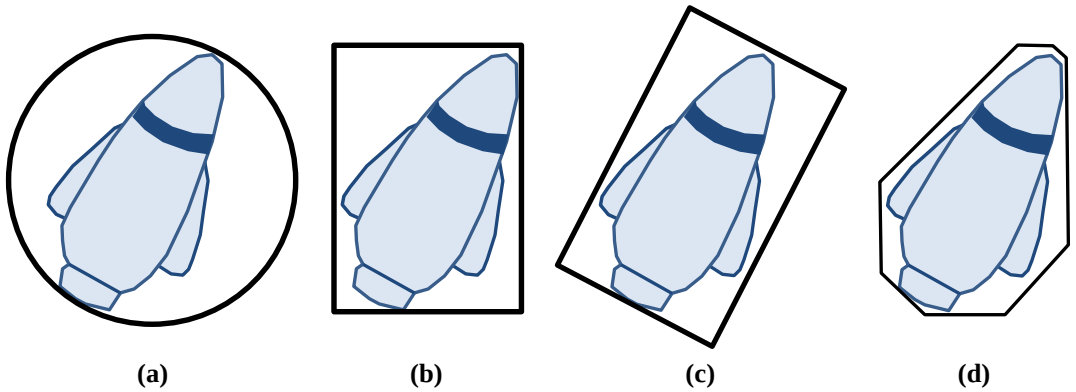

Figure 4.3 Bounding volumes: (a) Sphere; (b) AABB; (c) OBB; (d) 8-DOP.

With the intention to improve the computational efficiency of some algorithms of contact dynamics, some researchers utilize graphical processing units (GPUs) for fast image-space-based intersection techniques or as a co-processor for accelerating mathematics or geometry calculations, because GPUs have inherently more raw processing power than the main CPUs (Ericson, 2005). In multibody dynamics, some GPU-assisted algorithms have been used to perform large-scale simulations of ground vehicles running on sand, powder composites, and granular material flow (Tasora *et al.*, 2008; Tasora and Anitescu, 2010; Mazhar *et al.*, 2011; Negrut *et al.*, 2011).

Table 4.2 Software packages for collision detection and proximity query.

Authors	Library Description
Govindaraju *et al.* (2003)	CULLIDE: Interactive collision detection between complex models in large environments using graphics hardware.
Kim *et al.* (2002)	DEEP: Dual-space expansion for estimating penetration depth. This algorithm estimates the penetration depth between convex polytopes along with the associated penetration direction.
Sud *et al.* (2006)	DVD: Fast proximity computation among deformable models using discrete voronoi diagrams.
Tang and Manocha (2007)	DEFORMCD: Collision detection for deforming objects. For deforming objects, whose vertices are vibrating, AABB refitting solution is used for collision detection.
Gregory *et al.* (2000)	H-COLLIDE: Fast and accurate collision detection for haptic interaction. Within this approach, OBB trees are employed.
Cohen *et al.* (1995)	I-COLLIDE: Interactive and exact collision detection for large-scaled environments. This library only works for models which are convex polyhedra. But it exploits the special features of convex polytopes to very quickly determine contact status.
Wilson *et al.* (1999)	IMMPACT: Partitioning and Handling Massive Models for Interactive Collision Detection. Several types of bounding-volume hierarchies are utilized within this approach.
Terdiman (2001)	OPCODE: Optimized Collision Detection. This library works with general polygonal models and uses AABBs. It is memory efficient in comparison to RAPID, SOLID, or QuickCD.
Hoff III *et al.* (2001)	PIVOT: Proximity Information from Voronoi Techniques. It is a 2-D proximity engine that computes generalized proximity information between arbitrary objects.
Larsen *et al.* (2000)	PQP: Fast proximity queries with swept sphere volumes. This library supports collision detection, separation-distance computation or tolerance verification. It uses OBBs for collision queries and a hierarchy of swept-sphere volumes to perform distance queries.
Gottschalk *et al.* (1996)	RAPID: Robust and Accurate Polygon Interference Detection. This library works with polygonal soups and is based on OBBs.
Tang and Manocha (2010)	SELF-CCD: Continuous Collision Detection for Deforming Objects. It performs both inter- and intra-object collisions.
van den Bergen (2004)	SOLID: Software Library for Interference Detection. It supports the contact detection of multiple 3-D polygonal objects undergoing rigid motion. This library works with polygon soups and uses AABBs.
Ehmann (2000)	SWIFT: Speedy Walking Via Improved Feature Testing. It provides collision detection, distance computation, and contact determination between 3D polygonal objects undergoing rigid motion. This is faster, more robust and memory efficient than I-COLLIDE.
Ehmann (2001)	SWIFT++: Speedy Walking Via Improved Feature Testing for Non-convex Objects. It supports intersection detection, tolerance verification, distance computation, and contact determination of general 3-D polyhedral objects undergoing rigid motion. It uses the SWIFT to perform the computations between the bounding volumes.
Mirtich (1998)	V-Clip (*i.e.*, Voronoi Clip): Fast and Robust Polyhedral Collision Detection. This algorithm operates convex or nonconvex polyhedral. It supports distance computation, and also reports contact points.
Hudson *et al.* (1997)	V-COLLIDE: Accelerated Collision Detection for VRML. This is a collision detection library for large dynamic environments that joins the broad-phase algorithm of I-COLLIDE with the narrow-phase formulation of RAPID. It is designed to operate on large numbers of static or moving polygonal objects.

Single-phase formulations are also applied in contact detection problems. The effort of to implement broad-phase and narrow-phase approaches is only advantageous when its application represents an improvement in terms of computational efficiency and performance. Thus, single-phase methods are recommended wherever the contact simulation only requires a small number of contact calculations in each simulation step, such as a system with a few contacting bodies that are located nearby. The solution of this type of problems usually relies on the common-normal concept, which states that two points are the potential contact points if the normal vectors at these points are collinear to each other and perpendicular with the tangential plane of contact. The unknown variables of such problem are the coordinates of the potential contact points, which are reached by an iterative process when a set of geometric constraints is fulfilled. These constraints express collinearity and orthogonality conditions between the vectors defining the contacting surfaces at the contact points, namely the normal, tangent, binormal and distance vectors. As a result a system of nonlinear equations, obtained from equaling both normal vectors and from equaling the normal vector to the distance vector, is solved numerically. In general, there are two possible scenarios: (*i*) contact at a single point without indentation, and (*ii*) contact at a multiple points with indentation. The contact is detected when the minimum distance is lesser than or equal to zero and positive when surfaces are apart (Pombo *et al.*, 2007). The single-phase method for contact detection based on the common-normal concept is adopted throughout this work.

4.3 Elastic contact force models

The main purpose of this Section is to present some of the pure elastic contact force models used in the context of multibody system dynamics. The simplest contact force model is represented by a linear spring element, in which the spring embodies the elasticity of the contacting surfaces. This linear contact force model, also known as Hooke's law, can be expressed as (Shigley and Mischke, 1989)

$$F_N = k\delta \tag{4.1}$$

where k is the linear stiffness parameter and δ represents the relative indentation of the colliding bodies.

Figure 4.4 illustrates two externally colliding spheres with the same radius of 20 mm and the same mass of 0.092 kg. Both spheres have equal and opposite impact velocities of 0.15 m/s and a relative contact stiffness parameter equal to 5.5×10^{9} N/m$^{3/2}$. Figure 4.5 depicts the contact force-indentation relation given by Hooke's law for the two externally colliding spheres illustrated in Figure 4.4. The assumption of a linear relation between the relative indentation and the contact force is at best a rough approximation, because the contact force is affected by the shape, surface conditions and mechanical properties of the contacting bodies, all of which suggest a more complex relation.

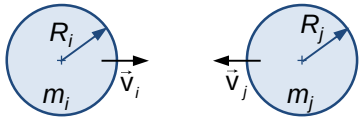

Figure 4.4 Schematic representation of two externally colliding spheres.

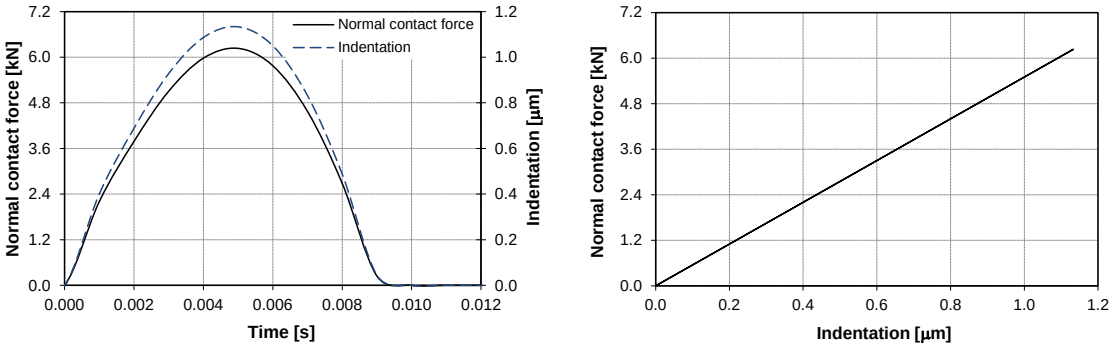

(a) **(b)**

Figure 4.5 Externally colliding spheres modeled by Hooke's contact law: (a) Normal contact force and indentation *versus* time; (b) Normal contact force-indentation relation.

The best known contact force model for representing the collision between two spheres of isotropic materials is due to Hertz (Hertz, 1881). The interested reader in the details on the Hertzian contact theory is referred to the works by Goldsmith (1960) and Johnson (1985). The Hertz law relates the normal contact force with a nonlinear power function of contact indentation and is expressed as (Hertz, 1881)

$$F_N = K\delta^n \tag{4.2}$$

where K is the generalized stiffness parameter, δ has the same meaning as defined above, and n is the nonlinear power exponent determined from material and geometric properties of the local region of the contacting bodies.

The contact stiffness parameter K is dependent on the material properties and shape of the contact surfaces. For instance, for two spheres of isotropic materials in contact, the contact stiffness parameter is a function of the radii of the sphere i and j and the material properties as (Goldsmith, 1960)

$$K = \frac{4}{3(\sigma_i + \sigma_j)} \sqrt{\frac{R_i R_j}{R_i + R_j}} \tag{4.3}$$

in which the material parameters σ_i and σ_j are given by

$$\sigma_k = \frac{1-\nu_k^2}{E_k}, \quad (k=i, j) \tag{4.4}$$

where the quantities ν_k and E_k are the Poisson's ratio and Young's modulus associated with each sphere. It is must be noted that, by definition, the radius is negative for concave surfaces and positive for convex surfaces. For contact between a sphere i and a plane j, the contact stiffness parameter depends on the radius of the sphere and the material properties of the contacting surfaces, being expressed as

$$K = \frac{4}{3(\sigma_i + \sigma_j)} \sqrt{R_i} \tag{4.5}$$

According to Hertz (1881), the power exponent n is equal to 3/2 for the case where there is a parabolic distribution of contact stresses. For different materials, the value of this exponent can be either higher or lower, leading to a convenient contact force expression which is based on experimental work, but that should not be confused with the Hertzian contact theory (Shivaswamy and Lankarani, 1997).

For the contact scenario illustrated in Figure 4.4 of two externally colliding spheres, Figure 4.6 shows the contact force, the indentation, the force-indentation relation and the phase portrait, obtained utilizing the Hertz contact law. The contact indentation and the indentation velocity are the variables used to plot the phase portrait. By observing Figures 4.6a and 4.6b, it should be highlighted that the contact force varies in a nonlinear and continuous manner and it starts from zero and returns to zero while always remains compressive. Figure 4.6c depicts the phase trajectory of the impact process, in which point A denotes the initial instant of impact with null

indentation and impact velocity equal to 0.3 m/s. The segment $\overline{AB}$ corresponds to the compression phase that ends at point *B*, where the maximum relative indentation is reached. Finally, the segment $\overline{BC}$ represents the restitution phase, which terminates with relative velocity equal to -0.3 m/s and null indentation. It is apparent that the Hertz contact law given by Equation (4.2) is limited to frictionless contacts with pure elastic deformations and does not include energy dissipation.

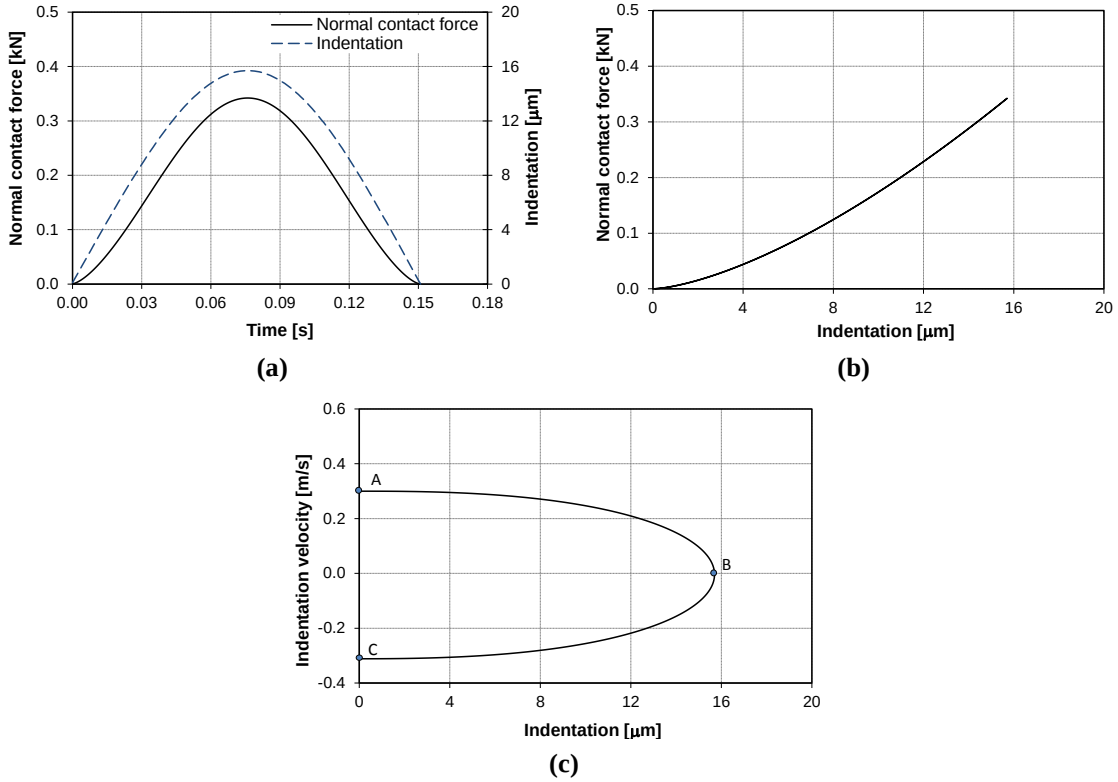

Figure 4.6 Externally colliding spheres modeled by Hertz contact law: (a) Normal contact force and indentation *versus* time; (b) Normal contact force-indentation relation; (c) Phase portrait.

According to Gonthier (2007), Hertz law should be utilized to model contact mechanics only when contacting geometries can be described by second-order polynomials. However, this theory can also be extended to be applied to bodies with smooth surfaces as long as the resulting contact area remains small with respect to the dimensions of the bodies. Even though the geometric boundary conditions may not be exactly fulfilled, the Hertzian assumption that the contact pressure distribution is elliptical will still apply, or at least provide a good approximation. Nevertheless, in some cases the dimensions of contact areas are significantly large regarding the size of the bodies, and in these conditions the assumption of elliptical pressure distribution is no longer valid. These situations happen when the contacting bodies present similar shapes, that is, are conformal.

When the contact area cannot be represented as a single contact point, the use of the elastic foundation approach is recommended (Johnson, 1985). This method, also referred as Winkler foundation, provides a simple approximation of the distribution of the contact pressure in conformal scenarios (Hippmann, 2004; Pérez-González *et al.*, 2008). Using the Winkler elastic foundation, the deformable part of the contacting bodies is modeled as a set of springs (*i.e.*, mattress of springs) spread over the contact surface, as illustrated in Figure 4.7. The springs represent the elastic layer and the thickness of the layer is composed by the thickness of one or both bodies, depending on whether one of the bodies is defined as rigid. The series of discrete and independent springs act only in the normal direction of the contact surface, being the shear force between the springs neglected (Põdra and Andersson, 1997). As a result, the elastic foundation model disregards the effect of a contact pressure on the relative indentation of neighboring locations. Figure 4.7 shows two contact scenarios that elucidate this problem. In Figure 4.7a, a spherical body collides with an elastic layer, producing a contact force F_N. The same spherical body is cut in order to give it straight edges. Then, the new configuration of the body is put again into contact with the elastic layer, being the resultant contact force F_N equal to the previous one, as depicted in Figure 4.7b. From Figure 4.7, it can be stated that this is a limitation of the elastic foundation model since the experienced displacement at one location is a function of the pressure applied at other locations (Mukras *et al.*, 2010). Nevertheless, despite this simplifying assumption violates the very nature of elastic contact problems, some benefits can be derived from its application, namely the computational efficiency and the possibility to analyze conformal contacts (Bei and Fregly, 2004).

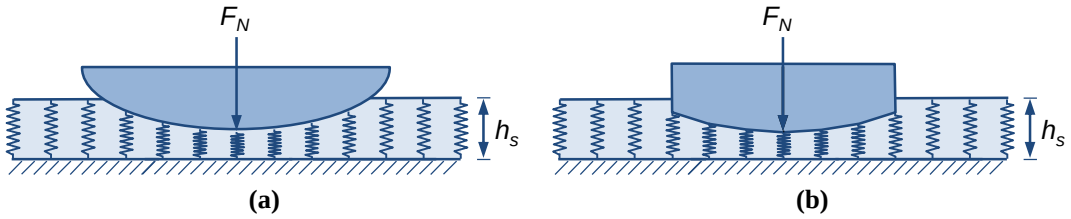

Figure 4.7 Elastic foundation model or Winkler foundation model.

The contact pressure for any spring *s* in the elastic foundation can be expressed as

$$p_s = \frac{E_W}{h_s}\delta_s \tag{4.6}$$

where p_s is the contact pressure, E_W is the Winkler modulus for the elastic layer, h_s is the thickness of the elastic layer and δ_s is the relative indentation of the spring *s*. When both bodies are deformable, E_W is a function of the Young's modulus and Poisson's ratio for the two bodies. The procedure used to determine the Winkler modulus E_W is discussed in detail by Johnson (1985) and by Põdra and Andersson (1997). For the case of only one of the bodies in contact is deformable, the Winkler modulus E_W can be given by

$$E_W = \frac{(1-\nu)E}{(1+\nu)(1-2\nu)} \tag{4.7}$$

where E and ν are the Young's modulus and Poisson's ratio of the deformable body. Thus, introducing now Equation (4.7) into Equation (4.6) yields

$$p_s = \frac{(1-\nu)E}{(1+\nu)(1-2\nu)}\frac{\delta_s}{h_s} \tag{4.8}$$

Different forms of the elastic foundation model can be used depending on the magnitude of surface indentations. Equation (4.8) can be utilized to calculate the pressure p_s of any spring element in contact scenarios where only small deformations are allowed, such as in artificial human articulations. It is important to mention that in cases where both bodies possess an elastic layer of the same material, then the two layers are treated as a single layer of combined thickness h_s. According to Bei and Fregly (2004), for larger deformations as in natural human articulations, the stiffness of the elastic layer increases with surface deformation due to geometric nonlinear behavior, so Equation (4.8) becomes

$$p_s = -\frac{(1-\nu)E}{(1+\nu)(1-2\nu)}\ln\left(1-\frac{\delta_s}{h_s}\right) \tag{4.9}$$

The total force supported by the elastic layer can be computed by summing the contact forces on all elements in the normal direction of the contact surface. Thus, the magnitude of the resultant force can be expressed as

$$F_N = \sum p_s A_s \tag{4.10}$$

where A_s is the element area projected into the normal direction (Mukras *et al.*,2010).

4.4 Dissipative contact force models

The Kelvin and Voigt approach is one of the first dissipative contact force models that combines a linear spring with a linear damper (Goldsmith, 1960). These two elements are associated in parallel and the contact force model can be written as

$$F_N = k\delta + D\dot{\delta} \tag{4.11}$$

in which the first term of the right-hand side is referred to as the linear elastic force component, which exhibits a Hooke type behavior, and the second term accounts for the energy loss during the contact process. In Equation (4.11), the parameter *D* represents the damping coefficient of the damper element and $\dot{\delta}$ represents the relative normal contact velocity. The remaining variables have the same meaning described in Section 4.3. Besides its simplicity and some weaknesses, the Kelvin and Voigt model has been used by a wide number of researchers.

The linear Kelvin and Voigt force model may not be very accurate since it does not represent the overall nonlinear nature of an impact, and a number of weaknesses restrict its application, mainly for high impact velocities. Dubowsky *et al.* (1987) suggested that the elastic and damping force components must be expressed as nonlinear functions of the relative indentation and impact velocity. Furthermore, the fact that the contact force at the beginning of the contact is not continuous due to the existence of the damping component is also a limitation of the Kelvin and Voigt contact force model. This particular issue is not realistic because when the contact begins, both elastic and damping force components must be null. Moreover, at the end of the restitution phase, the indentation is null, the relative contact velocity is negative and, consequently, the resulting contact force is also negative, as Figure 4.8a illustrates. This situation does not make sense from the physical point of view, in the measure that the bodies can not attract each other. Another drawback of the Kelvin and Voigt model is that its damping force component is active with the same damping coefficient during the entire impact time interval. This results in a uniform dissipation during the compression and restitution phases, which is not fully consistent with reality (Marhefka and Orin, 1999; Gilardi and Sharf, 2002).

Hunt and Crossley (1975) have argued that the damping coefficient in the case of vibroimpact should be proportional to a power of the spring force. These authors also

showed that the linear Kelvin and Voigt approach does not represent the physical nature of the energy transferred during the contact process. Therefore, Hunt and Crossley (1975) represent the contact force by the purely elastic Hertz's law combined with a nonlinear viscoelastic element, as depicted in Figure 4.8b.

Figure 4.8 Schematic diagram of a normal contact force-indentation relation for: (a) Spring-dashpot model (e.g., Kelvin and Voight law); (b) Nonlinear damping model (e.g., Hunt and Crossley law).

The Hunt and Crossley contact force law can be expressed as

$$F_N = K\delta^n + \chi\delta^n\dot{\delta} \tag{4.12}$$

where the parameter χ is called hysteresis damping factor that can be written as

$$\chi = \frac{3(1-c_r)}{2}\frac{K}{\dot{\delta}^{(-)}} \tag{4.13}$$

in which K is the contact stiffness parameter, c_r denotes the coefficient of restitution and $\dot{\delta}^{(-)}$ represents the initial impact velocity. The expression for the Hunt and Crossley contact force model can be written as

$$F_N = K\delta^n\left[1+\frac{3(1-c_r)}{2}\frac{\dot{\delta}}{\dot{\delta}^{(-)}}\right] \tag{4.14}$$

Although the Hunt and Crossley approach is only valid for direct central, it has been used by many researchers because of its simplicity and to be straightforward to implement (Anderson *et al.*, 2009; Moreira *et al.*, 2010; Silva *et al.*, 2010). For instance, Guess *et al.* (2010) employed the Hunt and Crossley formulation to successfully model the interaction between tibia, femur and menisci in a global three-dimensional multibody knee model.

The use of the Hunt and Crossley contact law to evaluate the normal contact forces produced during the impact of two externally colliding spheres implies the

outcomes depicted in Figure 4.9, where the contact force, the indentation, the force-indentation relation and the phase portrait are presented. The impact scenario considered here is the same utilized in Section 4.3 to describe the elastic models, which is illustrated in Figure 4.4. A contact stiffness parameter of 5.5×10^{9} N/m$^{3/2}$ and a coefficient of restitution equal 0.7 have been considered for the calculations.

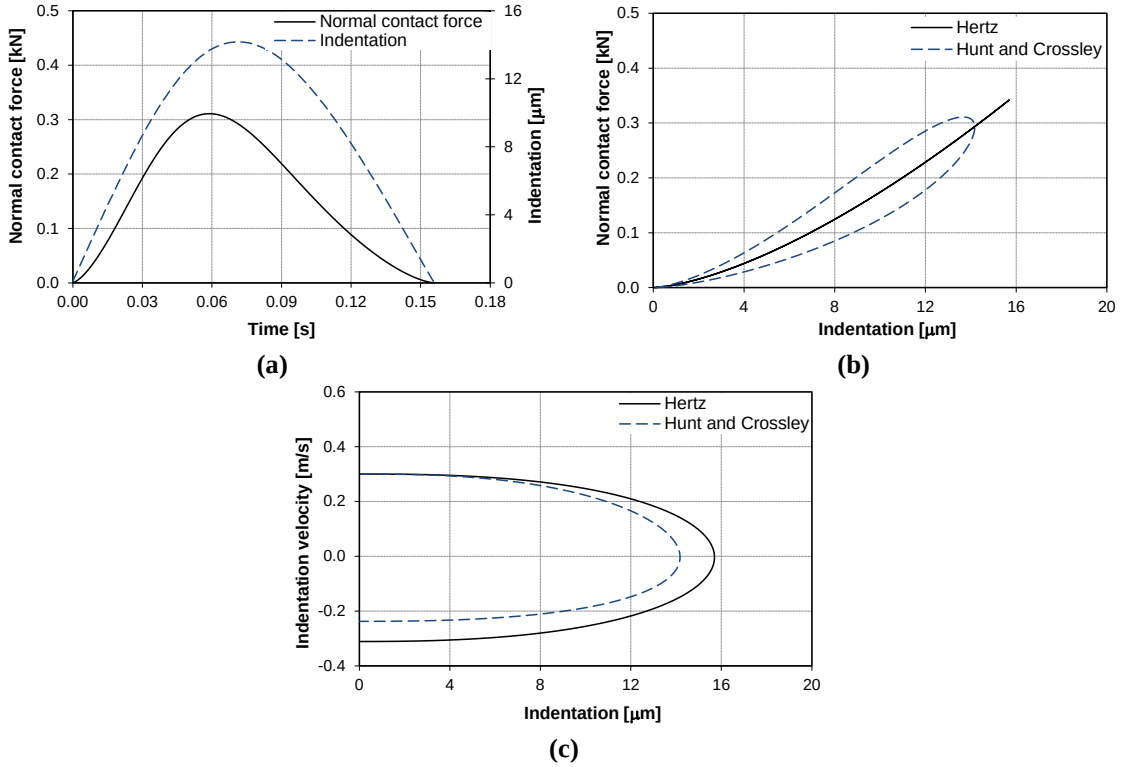

Figure 4.9 Externally colliding spheres modeled by Hunt and Crossley force law: (a) Normal contact force and indentation *versus* time; (b) Normal force-indentation relation; (c) Phase portrait.

From the plots of Figure 4.9a, it can be observed that the compression and restitution phases of the contact process are not equal due to the differences in the energy dissipation that occurs during these two phases. This fact is clear and visible in the non-symmetrical nature of the contact force curve. The energy dissipated during the contact process is related to material damping of the contacting bodies that is associated with the hysteresis loop of the force-indentation curve, shown in Figure 4.9b. Figure 4.9 shows the continuous nature of the contact forces, which build up from zero upon impact and smoothly return to zero upon separation. By comparing the plots of Figures 4.9b and 4.9c, the main differences between the Hertz approach and the Hunt and Crossley model are easily discerned.

A different formulation to account for the energy loss in contact-impact events that has the coefficient of restitution as main parameter was presented by Herbert and

McWhannell (1977). In this model, the authors combined the dynamic equations of motion of the impacting bodies with the Hunt and Crossley contact force model, being the hysteresis damping factor written as

$$\chi = \frac{6(1-c_r)}{[(2c_r-1)^2+3]}\frac{K}{\dot{\delta}^{(-)}} \tag{4.15}$$

and the corresponding contact force expression is given by

$$F_N = K\delta^n\left[1+\frac{6(1-c_r)}{[(2c_r-1)^2+3]}\frac{\dot{\delta}}{\dot{\delta}^{(-)}}\right] \tag{4.16}$$

Lee and Wang (1983) proposed another hysteresis damping factor that is quite similar to the one presented by Hunt and Crossley. Their main concern was to satisfy the expected hysteresis boundary conditions, that is, zero damping force at zero and maximum relative indentation of contact. Lee and Wang developed their work in the context of dynamic modeling and analysis of mechanisms with intermittent motion, being the hysteresis damping factor given by

$$\chi = \frac{3(1-c_r)}{4}\frac{K}{\dot{\delta}^{(-)}} \tag{4.17}$$

which results in an expression for the contact force written as

$$F_N = K\delta^n\left[1+\frac{3(1-c_r)}{4}\frac{\dot{\delta}}{\dot{\delta}^{(-)}}\right] \tag{4.18}$$

Figure 4.10 shows the force-indentation diagram and the phase portrait for the two externally colliding spheres illustrated in Figure 4.4, when the Hertz, Hunt and Crossley, Herbert and McWhannell, and Lee and Wang contact force laws are utilized. Figure 4.10 depicts that the Lee and Wang approach, among the dissipative models, is the one that produces the highest magnitude of impact force due to the fact that this model allows a lower dissipation of energy during the impact, as displays the smallest area of the hysteresis loop. It can also be observed that the Herbert and McWhannell law dissipates a higher amount of energy, visible in the larger hysteresis loop of Figure 4.10a, and also in the lower post-impact velocity seen in Figure 4.10b. In turn, the Hunt

and Crossley model gives a contact response in-between the other two dissipative models, but closer to the Herbert and McWhannell approach.

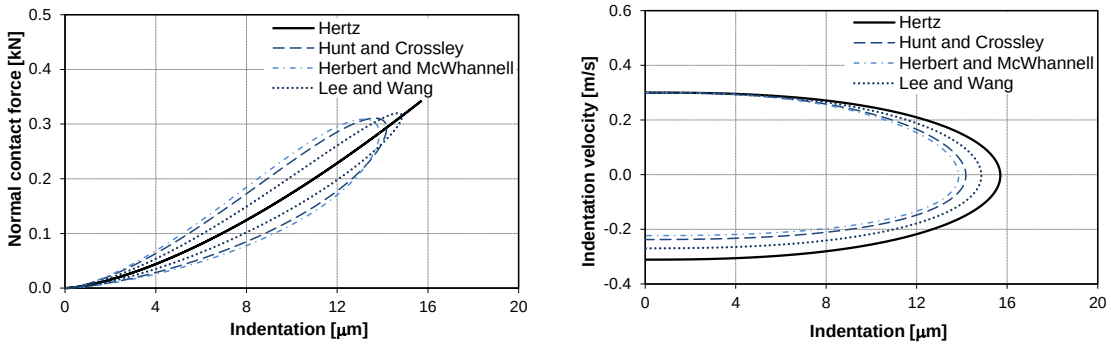

Figure 4.10 Externally colliding spheres modeled by Hertz, Hunt and Crossley, Herbert and McWhannell, and Lee and Wang contact force laws: (a) Normal contact force-indentation relation; (b) Phase portrait.

One of the most popular contact force models used in multibody systems was proposed by Lankarani and Nikravesh (1990). In their study, Lankarani and Nikravesh obtained an expression for the hysteresis damping factor by associating the kinetic energy loss of the impacting bodies with the energy dissipated in the system due to internal damping. According to these authors, considering the kinetic energies before and after impact, the amount of energy loss, ΔE, can be expressed as a function of the coefficient of restitution, c_r, and initial impact velocity, $\dot{\delta}^{(-)}$, as

$$\Delta E = \frac{1}{2} m \dot{\delta}^{(-)^2} (1 - c_r^2) \tag{4.19}$$

where m is the equivalent mass. The energy loss can also be evaluated by the integration of the contact force around the hysteresis loop. Thus, assuming that the damping force characteristics during the compression and restitution phases are the same, the energy loss due to the internal damping can be expressed as (Lankarani and Nikravesh, 1990)

$$\Delta E \simeq \frac{2}{3} \frac{\chi}{K} m \dot{\delta}^{(-)^3} \tag{4.20}$$

Thus, after substituting Equation (4.19) in Equation (4.20) an expression for the hysteresis damping factor is obtained as

$$\chi = \frac{3(1 - c_r^2)}{4} \frac{K}{\dot{\delta}^{(-)}} \tag{4.21}$$

which is a quadratic function of the coefficient of restitution. Introducing now Equation (4.21) into Equation (4.12) results the continuous contact force model due to Lankarani and Nikravesh written as

$$F_N = K\delta^n \left[1 + \frac{3(1-c_r^2)}{4} \frac{\dot{\delta}}{\dot{\delta}^{(-)}} \right] \tag{4.22}$$

This contact force model is satisfactory for general mechanical contacts, in particular for the cases in which the energy dissipated during the contact is relatively small when compared to the maximum absorbed elastic energy.

The contact force models presented above, known as point contact models, are adequate for the cases where the area of contact is small when compared to the dimensions of the contacting bodies, that is, the contact is considered to occur at a single point. In the situations of large contact areas, such as those associated with non-conformal contacts, other models are required. In line with this concern, Gonthier and his co-workers (2004) developed a volumetric contact force model for multibody dynamics in which the hysteresis damping factor is given by

$$\chi = \frac{d}{c_r} \frac{K}{\dot{\delta}^{(-)}} \tag{4.23}$$

where the dimensionless factor *d* is defined as

$$\frac{1 + d/c_r}{1-d} = e^{d\left(1 + 1/c_r\right)} \tag{4.24}$$

which can be approximated by

$$d \approx 1 - c_r{}^2 \tag{4.25}$$

and, finally, the Gonthier *et al.* (2004) force model can be written as

$$F_N = K\delta^n \left[1 + \frac{1-c_r^2}{c_r} \frac{\dot{\delta}}{\dot{\delta}^{(-)}} \right] \tag{4.26}$$

It should be mentioned that this approach gives the exact solution of the dynamic contact problem when Equation (4.24) is considered, in contrast with the contact force models presented above that are approximate solutions developed with base on different simplifications and assumptions. Moreover, by analyzing Equation (4.26), it can be concluded that for a perfectly elastic contact, *i.e.*, c_r=1, the hysteresis damping factor assumes a zero value, while for a purely inelastic contact, *i.e.*, c_r=0, the hysteresis damping factor is infinite, which is reasonable from the physical point of view. This analysis is not true for the hysteresis damping factors given by Equations (4.13), (4.15), (4.17) and (4.21), in which this parameter does not assume an infinite value for null coefficient of restitution, as it would be expected. Moreover, the Gonthier *et al.* approach provides accurate contact responses for the complete range of coefficient of restitution, *i.e.*, in elastic or inelastic contacting conditions.

More recently, Zhiying and Qishao (2006) described a contact force in which the hysteresis damping factor is given by

$$\chi = \frac{3(1-c_r^2)e^{2(1-c_r)}}{4}\frac{K}{\dot{\delta}^{(-)}} \tag{4.27}$$

and the force is expressed as

$$F_N = K\delta^n\left[1+\frac{3(1-c_r^2)e^{2(1-c_r)}}{4}\frac{\dot{\delta}}{\dot{\delta}^{(-)}}\right] \tag{4.28}$$

The work done by Zhiying and Qishao (2006) was developed in the context of impact analysis with the aim of seeking a mathematical relation between the coefficient of restitution, the contact parameters and the energy dissipated in the contact process.

Flores *et al.* (2011) described another contact force model, which was developed under the foundation of the Hertz contact theory, together with a hysteresis damping parameter. In the work by Flores *et al.* (2011), an expression for the hysteresis damping factor was derived by evaluating the kinetic energy dissipated in the system due to internal damping, likewise in the work by Lankarani and Nikravesh (1990). On one hand, the kinetic energy loss can be expressed as a function of the coefficient of restitution and initial impact velocity and is given by Equation (4.19). On the other hand, the energy dissipated during the contact process can be determined by integrating

the contact force around the hysteresis loop. Flores *et al.* (2011) considered an equation for the dissipated energy different from Equation (4.20) proposed by Lankarani and Nikravesh (1990). These authors used a single degree-of-freedom system to model the contact event and expressed the energy dissipated due to the internal damping as

$$\Delta E = \frac{1}{4}\chi(1-c_r)\dot{\delta}^{(-)}\delta_{max}^{\frac{5}{2}} \tag{4.29}$$

where δ_{max} refers to the maximum indentation. Substituting Equation (4.29) in Equation (4.19), which expresses the kinetic energy as a function of the coefficient of restitution and initial impact velocity, and taking into account the linear momentum balance, yields the following expression for the hysteresis damping factor as

$$\chi = \frac{8(1-c_r)}{5c_r}\frac{K}{\dot{\delta}^{(-)}} \tag{4.30}$$

and, hence the contact force model is expressed as

$$F_N = K\delta^n\left[1+\frac{8(1-c_r)}{5c_r}\frac{\dot{\delta}}{\dot{\delta}^{(-)}}\right] \tag{4.31}$$

Figure 4.11 depicts the force-indentation relation and the phase portrait for the two impacting spheres illustrated in Figure 4.4, when the contact is model with the Hertz, Hunt and Crossley, Lankarani and Nikravesh, Gonthier *et al.*, Zhiying and Qishao, and Flores *et al.* formulations. From Figure 4.11 it can be observed that the outcomes of the Hunt and Crossley approach and Lankarani and Nikravesh force model do not differ in a significant manner. This fact is not surprising because these two models were developed taking into account similar simplifying premises. In addition, the results obtained with the Gonthier *et al.*, Zhiying and Qishao, and Flores *et al.* force models present a quite close evolution, in which the compression and restitution phases of the contact process are not equal to each other due to the differences in the energy dissipation between these two phases. This fact is quite visible by observing the non-symmetrical nature of the contact force-indentation plots.

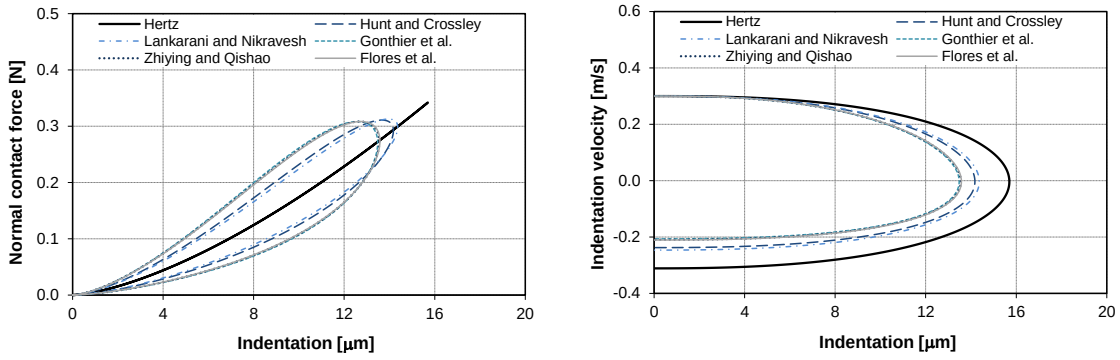

Figure 4.11 Externally colliding spheres modeled by Hertz, Hunt and Crossley, Lankarani and Nikravesh, Gonthier *et al.*, Zhiying and Qishao, and Flores *et al.* force models: (a) Normal contact force-indentation relation; (b) Phase portrait.

With the purpose to better understand what are the differences between the dissipative contact force models presented above, let the evolution of the hysteresis damping factor be analyzed for the entire range of the coefficient of restitution, as Figure 4.12 illustrates. In order to keep the analysis simple, the contact stiffness parameter and the initial impact velocity are equal to each other and equal to unity. By observing the plots of Figure 4.12, it can be concluded that the contact force models exhibit a similar behavior for high values of coefficient of restitution. Furthermore, the Hunt and Crossley, Herbert and McWhannell, Lee and Wang, and Lankarani and Nikravesh formulations do not perform adequately for low values of the coefficient of restitution. The Lee and Wang approach is the one that dissipates the less amount of energy during the contact process. In turn, the Zhiying and Qishao contact force model presents a superior response mainly for low values of the coefficient of restitution. The force approaches due to Gonthier *et al.* and Flores *et al.* have a similar behavior and for low values of the coefficient of restitution the hysteresis damping factor increases asymptotically with the decrease of the coefficient of restitution, which means that they can perform well for perfectly inelastic contacts. From Figure 4.12 it can be observed that for moderate and high values of the coefficient of restitution, *i.e.*, for coefficients of restitution higher than 0.5, the Gonthier *et al.*, the Zhiying and Qishao, and the Flores *et al.* force models present very close responses.

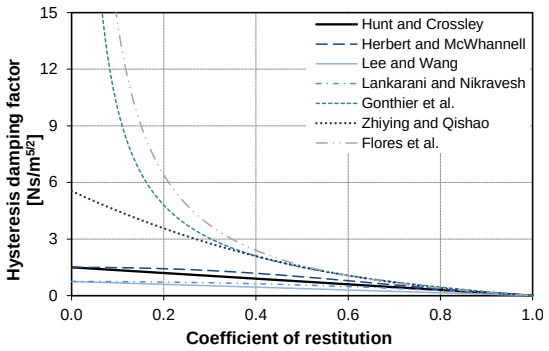

Figure 4.12 Evolution of the hysteresis damping factor as function of the coefficient of restitution.

4.5 Demonstrative example of application

In order to better understand the consequences of the use of different contact force laws, a slider crank mechanism experiencing two frictionless impacts with an external free sliding block is considered (Machado and Flores, 2011). Figure 4.13 shows a generic configuration of the system which consists of five rigid bodies representing the slider-crank mechanism and the free sliding block. The body numbers and their corresponding coordinate systems are also shown in Figure 4.13. The system is kinematically constrained by three revolute joints and one translational joint, being therefore a multibody model of two degrees-of-freedom. The set of data considered to build the model used to perform the dynamic simulations is listed in Table 4.3.

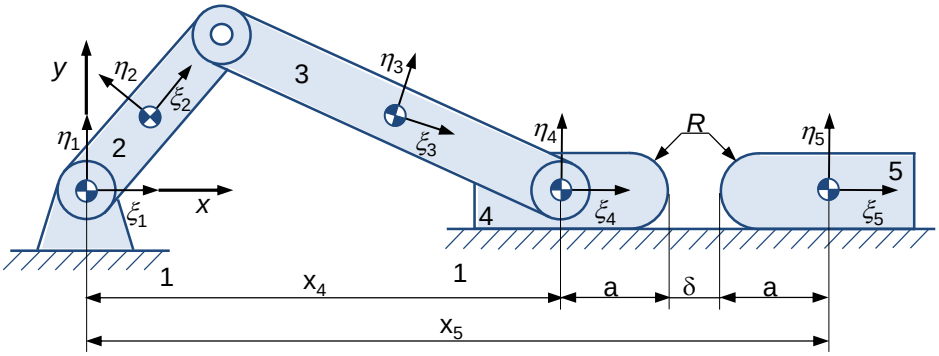

Figure 4.13 Multibody system composed by a slider-crank mechanism and a free sliding block.

Table 4.3 Geometric and inertial properties of the slider-crank mechanism and the free sliding block.

Body	Description	Length [m]	Mass [kg]	Moment of inertia [kg.m^2]
2	Crank	0.153	0.038	7.4×10^{-5}
3	Connecting rod	0.306	0.076	5.9×10^{-5}
4	Slider	-	0.038	1.8×10^{-6}
5	Free block	-	0.190	2.7×10^{-5}

The slider-crank mechanism is initialized with a crank angular velocity of 150 rad/s counter clockwise. At the start of the dynamic analysis, the crank and connecting-rod links are aligned in the *x* direction that corresponds to the dead point. Initially, the free sliding block is driven at a constant linear velocity equal to 15 m/s to the left. The initial position of the sliding block is located at *x* coordinate equal to 0.914 m. This multibody system is acted upon by gravitational force only which is taken as acting in the negative *y* direction.

The contact surfaces of the sliding bodies have spherical shapes with radius equal to 8.5 mm and the contact stiffness parameter is evaluated as 9.5×10^9 N/m$^{3/2}$. The value of the restitution coefficient used in the simulations is equal to 0.7. The geometric condition that allows for the evaluation of the relative indentation between the sliding bodies can be written as

$$\delta = x_5 - x_4 - 2a \tag{4.32}$$

where x_5 and x_4 represent the *x* coordinate of the sliding bodies and the dimension *a*, shown in Figure 4.13, is equal to 16.93 mm.

In the present study, the performance of this multibody system is quantified by the plots of the position of the free sliding block and the velocity of the constrained slider. In addition, the force-indentation relation for the two impacts is also plotted and analyzed. For this purpose, seven different contact force laws are utilized, namely Hunt and Crossley, Herbert and McWhannell, Lee and Wang, Lankarani and Nikravesh, Gonthier *et al.*, Zhiying and Qishao, Flores *et al.* models.

The time history of the position of the free sliding block and the velocity of the constrained slider are represented in the plots of Figure 4.14. Two impacts between the sliders that occur during the dynamic simulation are visible by the discontinuities of those plots. By analyzing the curves plotted in Figure 4.14, it can be observed that the contact force model proposed by Lee and Wang produces impacts with higher rebounds, due to the smaller amount of energy dissipated in the two contact events. Furthermore, it is noteworthy that the Gonthier *et al.*, Zhiying and Qishao, and Flores *et al.* force models exhibit similar behaviors, for which rebounds are smaller when compared with the other formulations. This phenomenon is quite visible in both position and velocity diagrams of Figure 4.14. Finally, the Lankarani and Nikravesh, Hunt and Crossley, and

Herbert and McWhannell models present an intermediate response, and the Herbert and McWhannell force law the most dissipative one among these last three approaches.

Figure 4.15 shows the force-indentation plots for the two impacts between the slider bodies. Again, it is observed that the Lee and Wang model is the one that dissipates less energy, as it is visible by the smaller hysteresis loop. In turn, the Gonthier *et al.*, Zhiying and Qishao, and Flores *et al.* force models dissipate more energy, exhibiting larger hysteresis loops. As a consequence, the rebounding velocity is lower when compared to the other force models. This analysis is valid for both impacts, as it can be seen in Figures 4.15a and 4.15b. The same conclusion can be achieved for the Lankarani and Nikravesh, Hunt and Crossley, and Herbert and McWhannell approaches. In short, the contact force models can be grouped into two main classes, one for the higher dissipative approaches that comprises the Gonthier *et al.*, Zhiying and Qishao, and Flores *et al.* force models, and another one for the remaining formulations.

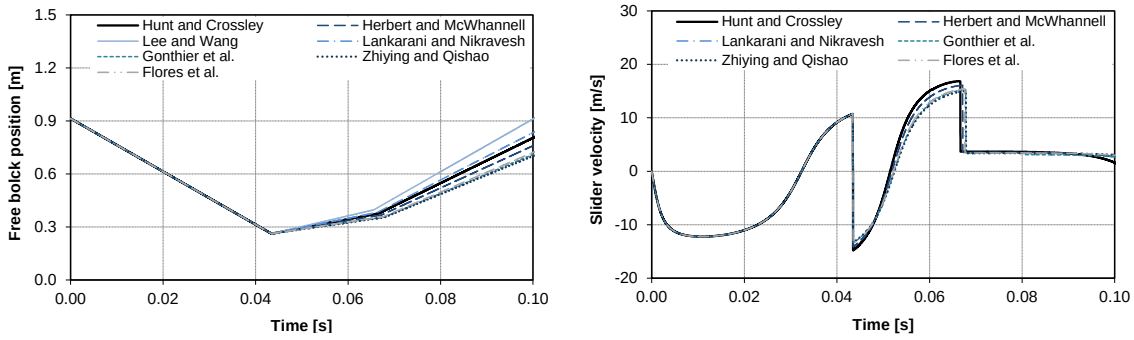

(a) **(b)**

Figure 4.14 (a) Position of the free sliding block; (b) Velocity of the constrained slider.

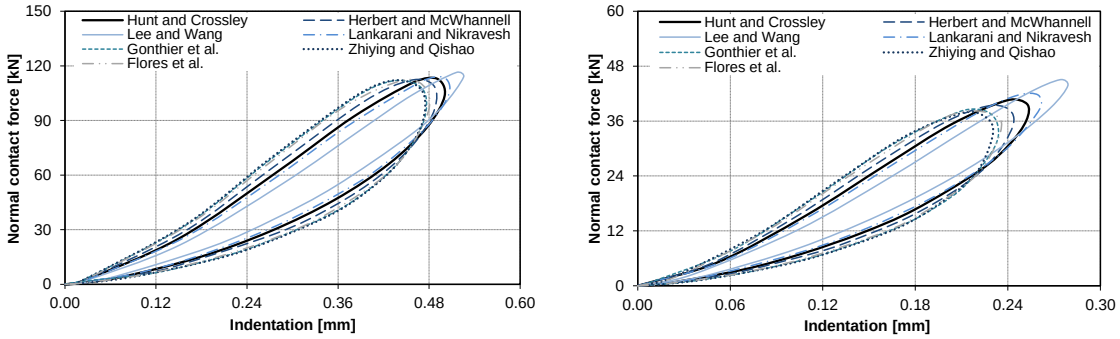

(a) **(b)**

Figure 4.15 Normal contact force-indentation relation for the two impacts: (a) First impact; (b) Second impact.

4.6 Summary and discussion

The contact modeling in multibody systems can be divided in contact detection and contact response. The contact detection is a two-step procedure that includes the identification of the spatial coordinates of the potential contact points and the evaluation of the indentation of the two bodies. In turn, the contact response consists of evaluating the contact force based on the state variables of the system. The dynamic response of the system is obtained by simply including updated forces into the equations of motion.

The contact detection is a common problem to several areas from mechanical engineering to computer graphics. Thus, several software packages and computational methods have been developed for contact detection purposes. In general, these algorithms rely on six features: (*i*) geometric representation, (*ii*) proximity queries, (*iii*) environment simulation parameters, (*iv*) performance, (*v*) robustness, and (*vi*) easiness of implementation and use. The geometric representation corresponds to the mathematical method utilized to define the geometry of the contact scenario and the colliding objects, which can be accomplished by using polygonal models or non-polygonal models, such as CSG approaches, implicit or parametric functions. In turn, a proximity query consists of a computation that produces information about the relative configuration or placement of objects. Some examples of proximity queries are: collision detection, minimum distance, maximum distance, Hausdorff distance, and penetration depth. Environmental simulation parameters affect also the contact detection process, such as the number of contacting bodies which may slow down significantly the performance of a contact detection algorithm. To speed up the simulation, advanced computational methods are used, which are classified as broad-phase and the narrow-phase approaches. The broad-phase methods identifies smaller groups of objects that may be colliding and quickly excludes those that definitely are not. Then, narrow-phase methods are employed, which ones test with more accuracy the subgroup of possible contacting pairs pointed out by the broad-phase algorithms. There are also single-phase formulations that are used when the contact simulation only requires a small number of contact calculations in each simulation step. These single-phase solutions usually rely on the common-normal concept.

The process of evaluating contact forces plays a key role in multibody dynamics. Therefore, the contact forces must be computed by using appropriate constitutive laws that take into account material properties of the contacting surfaces, geometric

characteristics of the impacting surfaces and, eventually, the impact velocity. In this Chapter, several compliant contact force models were revised from elastic to dissipative formulations. Firstly, three elastic contact force models were presented, namely the Hooke's law, the Hertz's law and the Winkler or elastic foundation model. A similarity of these three force formulations is that they do not account for the energy dissipation during the contact process. The major difference of the Hertz model in relation to Hooke law relies on its physical meaning represented by its nonlinearity.

The dissipative formulations described in this work are based on the foundation of the Hertzian contact theory, which is augmented with a hysteresis damping term that reflects the loss of energy that occurs during the contact process. The hysteresis damping term distinguishes the contact response of the different dissipative force models. For high values of the coefficient of restitution, the contact force models exhibit similar behaviors, namely when the coefficient is close to unity, *i.e.*, in almost elastic contacts. In contrast, for moderate or low coefficients of restitution, the Gonthier *et al.*, Zhiying and Qishao, and Flores *et al.* approaches present a superior performance, when compared to other models. In these three models, the increase in damping reduces the indentation because there is less energy to store in the contact process.

A slider-crank mechanism including a contact-impact block was considered as example of application to demonstrate the similarities of and differences between the investigated contact force models. The computational results proved that the contact force model significantly influences the impacting rebound and the rebounding velocity, since these variables are greater the lower the energy dissipated.

References

Ambrósio, J., Veríssimo, P. (2009) Improved bushing models for general multibody systems and vehicle dynamics. *Multibody System Dynamics*, 22(4), pp. 341-365.

Anderson, R.W.G., Long, A.D., Serre, T. (2009) Phenomenological continuous contact-impact modelling for multibody simulations of pedestrian-vehicle contact interactions based on experimental data. *Nonlinear Dynamics*, 58(1), pp. 199-208.

Bei, Y., Fregly, B.J. (2004) Multibody dynamic simulation of knee contact mechanics. *Medical Engineering & Physics*, 26(9), pp. 777-789.

Bottasso, C.L., Trainelli, L. (2001) Implementation of effective procedures for unilateral contact modeling in multibody dynamics. *Mechanics Research Communications*, 28(3), pp. 233-246.

Cameron, S. (1991) Efficient bounds in constructive solid geometry. *IEEE Computer Graphics & Applications*, 11(3), pp. 68-74.

Choi, J., Ryu, H.S., Kim, C.W., Choi, J.H. (2010) An efficient and robust contact algorithm for a compliant contact force model between bodies of complex geometry. *Multibody System Dynamics*, 23(1), pp. 99-120.

Cohen, J.D., Lin, M.C., Manocha, D., Ponamgi, M.K. (1995) I-COLLIDE: An interactive and exact collision detection system for large-scale environments. *Proceedings of the 1995 Symposium on Interactive 3D graphics* (pp. 189-196), Monterey (CA).

Dopico, D., Luaces, A., Gonzalez, M., Cuadrado, J. (2011) Dealing with multiple contacts in a human-in-the-loop application. *Multibody System Dynamics*, 25(2), pp. 167-183.

Dubowsky, S., Deck, J.F., Costello, H. (1987) The dynamic modeling of flexible spatial machine systems with clearance connections. *Journal of Mechanisms, Transmissions, and Automation in Design*, 109(1), pp. 87-94.

Ebrahimi, S., Hippmann, G., Eberhard, P. (2005) Extension of polygonal contact model for flexible multibody systems. *International Journal of Applied Mathematics and Mechanics*, 1, pp. 33-50.

Ebrahimi, S., Eberhard, P. (2006) A linear complementarity formulation on position level for frictionless impact of planar deformable bodies. *ZAMM - Journal of Applied Mathematics and Mechanics*, 86(10), pp. 807-817.

Ebrahimi, S., Kövecses, J. (2010) Unit homogenization for estimation of inertial parameters of multibody mechanical systems. *Mechanism and Machine Theory*, 45(3), pp. 438-453.

Ehmann, S. (2000) *SWIFT Speedy walking via improved feature testing*. (URL: http://gamma.cs.unc.edu/SWIFT/, accessed on January 31st 2012).

Ehmann, S. (2001) *SWIFT++ Speedy walking via improved feature testing for non-convex objects*. (URL: http://gamma.cs.unc.edu/SWIFT++/, accessed on January 31st 2012).

Ericson, C. (2005) *Real-time collision detection*. Morgan Kaufmann Publishers: San Francisco (CA).

Farin, G.E. (1995) *NURBS curves and surfaces: from projective geometry to practical use*. AK Peters: Wellesley (MA).

Faverjon, B. (1989) Hierarchical object models for efficient anti-collision algorithms. *Proceedings of the 1989 IEEE International Conference on Robotics & Automation*, 1, pp. 333-340.

Flickinger, D.M., Bowling, A. (2010) Simultaneous oblique impacts and contacts in multibody systems with friction. *Multibody System Dynamics*, 23(3), pp. 249-261.

Flores, P., Ambrósio, J. (2010) On the contact detection for contact-impact analysis in multibody systems. *Multibody System Dynamics*, 24(1), pp. 103-122.

Flores, P., Ambrósio, J., Claro, J.C.P., Lankarani, H.M. (2006) Influence of the contact-impact force model on the dynamic response of multibody systems. *Proceedings of the Institution of Mechanical Engineers, Part-K Journal of Multi-body Dynamics*, 220(1), pp. 21-34.

Flores, P., Ambrósio, J., Claro, J.C.P., Lankarani, H.M. (2008) *Kinematics and dynamics of multibody systems with imperfect joints: models and case studies - In Lecture Notes in Applied and Computational Mechanics* (34). Springer-Verlag: Berlin/Heidelberg, Germany.

Flores, P., Machado, M., Silva, M.T., Martins, J.M. (2011) On the continuous contact force models for soft materials in multibody dynamics. *Multibody System Dynamics*, 25(3), pp. 357-375.

Gilardi, G., Sharf, I. (2002) Literature survey of contact dynamics modeling. *Mechanism and Machine Theory*, 37(10), pp. 1213-1239.

Glocker, C., Pfeiffer, F. (1993) Complementarity problems in multibody systems with planar friction. *Archive of Applied Mechanics*, 63(7), pp. 452-463.

Glocker, C., Studer, C. (2005) Formulation and preparation for numerical evaluation of linear complementary systems in dynamics. *Multibody System Dynamics*, 13(4), pp. 447-463.

Goldsmith, W. (1960) *Impact - The theory and physical behaviour of colliding solids*. Edward Arnold: London, England.

Gonthier, Y. (2007) *Contact dynamics modelling for robotic task simulation*. PhD Thesis, University of Waterloo, Ontario, Canada.

Gonthier, Y., McPhee, J., Lange, C., Piedboeuf, J.-C. (2004) A regularized contact model with asymmetric damping and dwell-time dependent friction. *Multibody System Dynamics*, 11(3), pp. 209-233.

Govindaraju, N.K., Redon, S., Lin, M.C., Manocha, D. (2003) CULLIDE: Interactive collision detection between complex models in large environments using graphics hardware. In M. Doggett *et al.* (Eds.), *Proceedings of the ACM SIGGRAPH/EUROGRAPHICS conference on Graphics hardware*, The Eurographics Association: San Diego (CA).

Gottschalk, S. (2000) *Collision queries using oriented bounding boxes*. PhD Thesis, University of North Carolina, Chapel Hill (NC).

Gottschalk, S., Lin, M.C., Manocha, D. (1996) OBBTree: A hierarchical structure for rapid interference detection. *Computer Graphics*, 30, pp. 171-180.

Gregory, A., Lin, M.C., Gottschalk, S., Taylor, R. (2000) Fast and accurate collision detection for haptic interaction using a three degree-of-freedom force-feedback device. *Computational Geometry*, 15(1-3), pp. 69-89.

Guess, T.M., Thiagarajan, G., Kia, M., Mishra, M. (2010) A subject specific multibody model of the knee with menisci. *Medical Engineering & Physics*, 32(5), pp. 505-515.

Haug, E.J., Wu, S.C., Yang S.M. (1986) Dynamics of mechanical systems with coulomb friction, stiction, impact and constraint addition deletion - I Theory. *Mechanism and Machine Theory*, 21(5), pp. 401-406.

Herbert, R.G., McWhannell, D.C. (1977) Shape and frequency composition of pulses from an impact pair. *Journal of Engineering for Industry*, 99(3), pp. 513-518.

Hertz, H. (1881) Über die Berührung fester elastischer Körper. *Journal für die reine und angewandte Mathematik*, 92, pp. 156-171.

Hippmann, G. (2004) An algorithm for compliant contact between complexly shaped bodies. *Multibody System Dynamics*, 12(4), pp. 345-362.

Hirschkorn, M., McPhee, J., Birkett, S. (2006) Dynamic modeling and experimental testing of a piano action mechanism. *Journal of Computational and Nonlinear Dynamics*, 1(1), pp. 47-55.

Hoff III, K.E., Zaferakis, A., Lin, M.C., Manocha, D. (2001) Fast and simple 2D geometric proximity queries using graphics hardware. *Proceedings of the 2001 Symposium on Interactive 3D graphics* (pp. 145-148), New York (NY).

Hubbard, P.M. (1993) Interactive collision detection. *Proceedings of the 1993 IEEE Symposium on Research Frontiers in Virtual Reality* (pp. 24-31), San Jose (CA).

Hudson, T.C., Lin, M.C., Cohen, J., Gottschalk, S., Manocha, D. (1997) V-COLLIDE: accelerated collision detection for VRML. *Proceedings of the Second Symposium on Virtual Reality Modeling Language* (pp. 119-125), Monterey (CA).

Hunt, K.H., Crossley, F.R.E. (1975) Coefficient of restitution interpreted as damping in vibroimpact. *Journal of Applied Mechanics*, 42(2), pp. 440-445.

Jia, X., Choi, Y-K., Mourrain, B., Wang, W. (2011) An algebraic approach to continuous collision detection for ellipsoids. *Computer Aided Geometric Design*, 28(3), pp. 164-176.

Johnson, K.L. (1985) Contact mechanics. Cambridge University Press: Cambridge, United Kingdom.

Keyser, J., Krishnan, S., Manocha, D. (1999) Efficient and accurate B-rep generation of low degree sculptured solids using exact arithmetic: I-representations. *Computer Aided Geometric Design*, 16(9), pp. 841-859.

Kim, Y.J., Lin, M.C., Manocha, D. (2002) DEEP: Dual-space expansion for estimating penetration depth between convex polytopes. *Proceedings of the 2002 IEEE International Conference on Robotics & Automation* (pp. 921-926), Washington (DC).

Kockara, S., Halic, T., Iqbal, K. (2007) Collision detection: A survey. *Proceedings of the 2007 IEEE International Conference on Systems, Man and Cybernetics* (pp. 4046-4051), Montreal, Canada.

Lankarani, H.M., Nikravesh, P.E. (1990) A contact force model with hysteresis damping for impact analysis of multibody systems. *Journal of Mechanical Design*, 112(3), pp. 369-376.

Larsen, E., Gottschalk, S., Lin, M.C., Manocha, D. (2000) Fast distance queries with rectangular swept sphere volumes. *Proceedings of the 2000 IEEE International Conference on Robotics & Automation*, 4, pp. 3719-3726.

Lee, T.W., Wang, A.C. (1983) On the dynamics of intermittent-motion mechanisms. Part 1 - Dynamic model and response. *Journal of Mechanisms, Transmissions, and Automation in Design*, 105, pp. 534-540.

Lin, M. (1993) *Efficient collision detection for animation and robotics*. PhD Thesis, University of California, Berkeley (CA).

Lin, M., Gottschalk, S. (1998) Collision detection between geometric models: A survey. *Proceedings of IMA Conference on Mathematics of Surfaces*, Birmingham, United Kingdom, pp. 602-608.

Liu, C.-S., Zhang, K., Yang, R. (2007) The FEM analysis and approximate model for cylindrical joints with clearances. *Mechanism and Machine Theory*, 42(2), pp. 183-197.

Lopes, D. S., Silva, M.T., Ambrósio, J.A., Flores, P. (2011) A mathematical framework for rigid contact detection between quadric and superquadric surfaces. *Multibody System Dynamics*, 24(3), pp. 103-122.

Machado, M., Flores, P. (2011) A novel continuous contact force model for multibody dynamics. *Proceedings of the ASME 2011 International Design Engineering Technology Conferences & Computers and Information in Engineering Conference* (10p.), Washington (DC).

Machado, M., Flores, P., Claro, J.C.P., Ambrósio, J., Silva, M., Completo, A., Lankarani, H.M. (2010) Development of a planar multibody model of the human knee joint. *Nonlinear Dynamics*, 60(3), pp. 459-478.

Marhefka, D.W., Orin, D.E. (1999) A compliant contact model with nonlinear damping for simulation of robotic systems. *IEEE Transactions on Systems, Man, and Cybernetics, Part A: Systems and Humans*, 29(6), pp. 566-572.

Mazhar, H., Heyn, T., Negrut, D. (2011) A scalable parallel method for large collision detection problems. *Multibody System Dynamics*, 26(1), pp. 37-55.

Mirtich, B. (1998) V-Clip: Fast and robust polyhedral collision detection. *ACM Transactions on Graphics*, 17(3), pp. 177-208.

Moreira, P., Silva. M., Flores, P. (2010) A biomechanical multibody foot model for forward dynamic analysis. *Proceedings of the 1st Joint International Conference on Multibody Dynamics* (10p.), Lappeenranta, Finland.

Mukras, S., Mauntler, A., Kim, N.H., Schmitz, T.L., Sawyer, W.G. (2010) Evaluation of contact force and elastic foundation models for wear analysis of multibody systems. *Proceedings of the ASME 2010 International Design Engineering Technology Conferences* (14p.), Montreal, Canada.

Negrut, D., Tasora, A., Mazhar, H., Heun, T., Hahn, P. (2011) Leveraging parallel computing in multibody dynamics. *Multibody System Dynamics*, 27(1), pp. 95-117.

Pang, J.S., Trinkle, J.C. (1996) Complementarity formulations and existence of solutions of dynamic multi-rigid-body contact problems with Coulomb friction. *Mathematical Programming*, 73(2), pp. 199-226.

Pérez-González, A., Fenollosa-Esteve, C., Sancho-Bru, J.L., Sánchez-Marín, F.T., Vergara, M., Rodríguez-Cervantes, P.J. (2008) A modified elastic foundation contact model for application in 3D models of the prosthetic knee. *Medical Engineering & Physics*, 30(3), pp. 387-398.

Pfeiffer, F. (2003) The idea of complementarity in multibody dynamics. *Archive of Applied Mechanics*, 72(11-12), pp. 807-816.

Pfeiffer, F., Glocker, C. (1996) *Multibody dynamics with unilateral constraints*. John Wiley and Sons: New York (NY).

Põdra, P., Andersson, S. (1997) Wear simulation with the Winkler surface model. *Wear*, 207(1), pp. 79-85.

Pombo, J., Ambrósio, J., Silva, M. (2007) A new wheel-rail contact model for railway dynamics. *Vehicle System Dynamics*, 45(2), pp. 165-189.

Portal, R.J.F., Dias, J.M.P., Sousa, L.A.G. (2009) Contact detection between convex superquadric surfaces on multibody dynamics. In K. Arczewski, J. Frączek, M. Wojtyra (Eds.), *Proceedings of the Multibody Dynamics 2009, ECCOMAS Thematic Conference* (14p.), Warsaw, Poland.

Sharf, I., Zhang, Y. (2006) A contact force solution for non-colliding contact dynamics simulation. *Multibody System Dynamics*, 16(3), pp. 263-290.

Shigley, J.E., Mischke, C.R. (1989) *Mechanical engineering design*. McGraw-Hill: New York (NY).

Shivaswamy, S., Lankarani, H.M. (1997) Impact analysis of plate using quasi-static approach. *Journal of Mechanical Design*, 119(3), pp. 376-381.

Sigg, C. (2006) *Representation and rendering of implicit surfaces*. PhD Thesis. Eidgenössische Technische Hochschule Zürich, Zurich, Switzerland.

Silva, P., Silva, M., Martins, J. (2010) Sensitivity analysis of the parameters used to calculate the interface forces between lower limb and orthosis. *Proceedings of the 1st Joint International Conference on Multibody Dynamics* (9p.), Lappeenranta, Finland.

Su, C-J., Lin, F., Ye, L. (1999) A new collision detection method for CSG-represented objects in virtual manufacturing. *Computers in Industry*, 40(1), pp. 1-13.

Sud, A., Govindaraju, N., Gayle, R. Kabul, I., Manocha, D. (2006) Fast proximity computation among deformable models using discrete voronoi diagrams. *ACM Transactions on Graphics*, 25(3), pp. 1144-1153.

Tang, M., Manocha, D. (2007) *DeformCD: Collision detection for deformable models*. (URL: http://gamma.cs.unc.edu/DEFORMCD/index.html, accessed on January 31st 2012).

Tang, M., Manocha, D. (2010) *Self-CCD: Continuous collision detection for deforming objects* (URL: http://gamma.cs.unc.edu/SELFCD/download.html, accessed on January 31st 2012).

Tasora, A., Righettini, P. (2003) Sliding contact between freeform surfaces. *Multibody System Dynamics*, 10(3), pp. 239-262.

Tasora, A., Negrut, D., Anitescu, A. (2008) Large-scale parallel multi-body dynamics with frictional contact on the graphical processing unit. *Proceedings of the Institution of Mechanical Engineers, Part-K Journal of Multi-body Dynamics*, 222(4), pp. 315-326.

Tasora, A., Anitescu, M. (2010) A convex complementary approach for simulating large granular flows. *Journal of Computational and Nonlinear Dynamics*, 5(3), 031004, 7p.

Terdiman, P. (2001) *Memory-optimized bounding-volume hierarchies*. (URL: http://www.codercorner.com/Opcode.pdf, accessed on January 31st 2012).

Tian, Q., Zhang, Y., Chen, L., Flores, P. (2009) Dynamics of spatial flexible multibody systems with clearance and lubricated spherical joints. *Computers and Structures*, 87(13-14), pp. 913-929.

van den Bergen, G.J.A. (2004) *Collision detection in interactive 3D environments*. Morgan Kaufmann: San Francisco (CA).

Wilson, A., Larsen, E., Manocha, D., Lin, M.C. (1999) Partitioning and handling massive models for interactive collision detection. *Computer Graphics Forum*, 18(3), pp. 319-330.

Zhiying, Q., Qishao, L. (2006) Analysis of impact process based on restitution coefficient. *Journal of Dynamics and Control*, 4, pp. 294-298.